

AD-A087390

TRW DEFENSE AND SPACE SYSTEMS GROUP REDONDO BEACH CA

F/G 10/3

USCS II. BATTERY ANOMALY INVESTIGATION SATELLITES 9437 AND 9438--ETC

APR 80 P BAUER, C LURIE

TRW-32824-AR-019-01

SD-TR-80-33

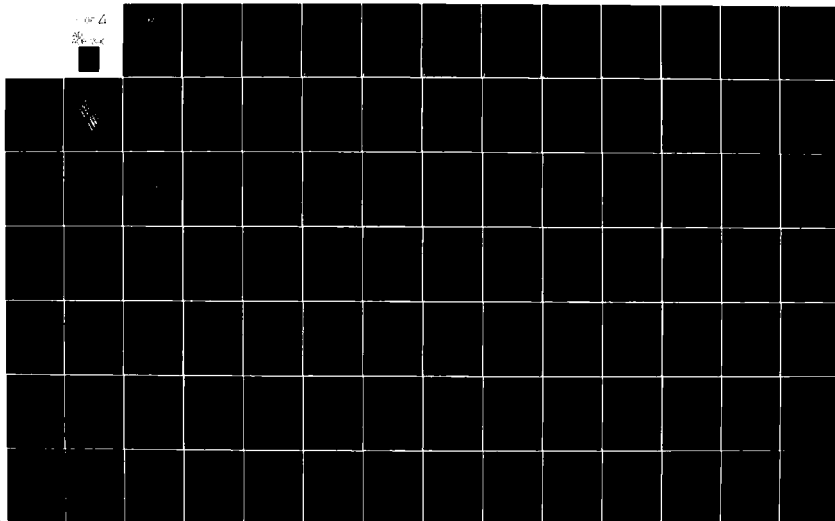
F04701-77-C-0118

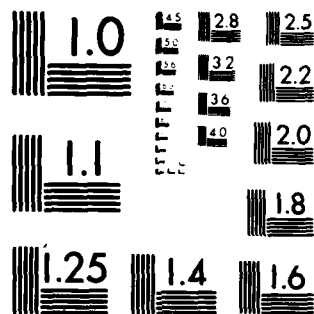
NL

UNCLASSIFIED

1 of 4

2/2/80





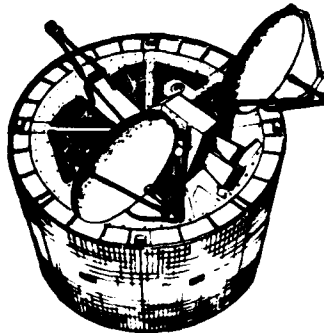
MICROCOPY RESOLUTION TEST CHART
NATIONAL BUREAU OF STANDARDS-1963-A

SD-TR-80-33

LEVEL

II

2



DSCS II

**BATTERY ANOMALY INVESTIGATION
SATELLITES 9437 AND 9438**

TRW DEFENSE AND SPACE SYSTEMS GROUP
ONE SPACE PARK
REDONDO BEACH, CALIFORNIA 90278
REPORT NO. 32824-AR-019-01

APRIL 1980

DTIC
ELECTRONIC
S AUG 0 1 1980 **D**
E

FINAL REPORT

APPROVED FOR PUBLIC RELEASE

DISTRIBUTION UNLIMITED

THIS DOCUMENT IS BEST QUALITY PRACTICABLE.
THE COPY FURNISHED TO DDC CONTAINED A
SIGNIFICANT NUMBER OF PAGES WHICH DO NOT
REPRODUCE LEGIBLY.

Prepared for

DEPARTMENT OF THE AIR FORCE HEADQUARTERS
SPACE DIVISION (AFSC)

CDRL Sequence Number B009
Contract FO4701-77-C-0118

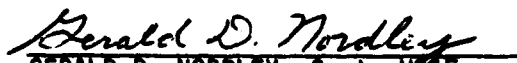
DDC FILE COPY


80 7 25 122

This report was prepared by the TRW Defense and Space Systems Group, Redondo Beach, CA 90278, under Contract F04701-77-C-0118 with the Headquarters, Air Force Space Division, Deputy for Space Communications Systems, P.O. Box 92960, Worldway Postal Center, Los Angeles, CA 90009. It was reviewed and approved for TRW Defense and Space Systems Group by R. H. Alborn, Manager, DSCS II Orbital Operations. Capt. Gerald D. Nordley was the project engineer.

This report has been reviewed by the Office of Public Affairs (PAS) and is releasable to the National Technical Information Service (NTIS). At NTIS, it will be available to the general public, including foreign nations.

This technical report has been reviewed and is approved for publication. Publication of this report does not constitute Air Force approval of the report's findings or conclusions. It is published only for the exchange and stimulation of ideas.


GERALD D. NORDLEY, Capt, USAF
Project Engineer


JAMES H. BELT, Major, USAF
Director of Engineering, DSCS II
Deputy for Space Comm Systems

FOR THE COMMANDER


JAMES E. FREYTAG, Colonel, USAF
System Program Director, DSCS II
Deputy for Space Comm Systems

DISCLAIMER NOTICE

**THIS DOCUMENT IS BEST QUALITY
PRACTICABLE. THE COPY FURNISHED
TO DTIC CONTAINED A SIGNIFICANT
NUMBER OF PAGES WHICH DO NOT
REPRODUCE LEGIBLY.**

UNCLASSIFIED

(19) TH-12-33

SECURITY CLASSIFICATION OF THIS PAGE (When Data Entered)

REPORT DOCUMENTATION PAGE		READ INSTRUCTIONS BEFORE COMPLETING FORM
1. REPORT NUMBER (18) SD-TR-80-33 ? where	2. GOVT ACCESSION NO. AD-A087390	3. RECIPIENT'S CATALOG NUMBER
4. TITLE (and Subtitle) (6) DSCS II. Battery Anomaly Investigation Satellites 9437 and 9438, Final Report		5. TYPE OF REPORT & PERIOD COVERED (9) Final Rpt.
7. AUTHOR(s) P. Bauer C. Lurie (12) 325		6. PERFORMING ORG. REPORT NUMBER (14) TRW-32824-AR-019-01
9. PERFORMING ORGANIZATION NAME AND ADDRESS TRW Defense and Space Systems Group One Space Park Redondo Beach, California		8. CONTRACT OR GRANT NUMBER(s) (15) F04701-77-C-0118
11. CONTROLLING OFFICE NAME AND ADDRESS Department of the Air Force Headquarters Space Division (AFSC). Post Office Box 92960 Worldway Postal Center, Los Angeles, CA 90009		10. PROGRAM ELEMENT, PROJECT, TASK AREA & WORK UNIT NUMBERS (11) 25 APR 80
14. MONITORING AGENCY NAME & ADDRESS (if different from Controlling Office) (10) Paul / Bauer Charles / Lurie		12. REPORT DATE 25 April 1980
16. DISTRIBUTION STATEMENT (of this Report) APPROVED FOR PUBLIC RELEASE; UNLIMITED DISTRIBUTION		13. NUMBER OF PAGES 318
17. DISTRIBUTION STATEMENT (of the abstract entered in Block 20, if different from Report)		15. SECURITY CLASS. (of this report) Unclassified
18. SUPPLEMENTARY NOTES		15a. DECLASSIFICATION/DOWNGRADING SCHEDULE
19. KEY WORDS (Continue on reverse side if necessary and identify by block number) DSCS II, Nickel Cadmium Batteries, Battery Cell Anomaly		
20. ABSTRACT (Continue on reverse side if necessary and identify by block number) This report presents a description of the anomalous behavior of the electric power subsystems of DSCS II Satellites 9437 and 9438, and of the investigations conducted to determine the cause of the anomalies. These investigations include ground test simulations using flight-configuration batteries, component level testing, and analyses of components and systems. The investigations are described and the results discussed. The study concludes that the anomalous behavior was the result of battery cell short circuiting. The cause of the short circuiting is identified as excessive		

overcharge, its cause and the corrective actions taken are discussed.


Accession For	
NTIS GRA&I	<input checked="checked" type="checkbox"/>
DDC TAB	<input type="checkbox"/>
Unannounced	<input type="checkbox"/>
Justification	
By _____	
Distribution/	
Availability Codes	
Dist.	Avail and/or special
A	23

DSCS II
BATTERY ANOMALY INVESTIGATION
SATELLITES 9437 AND 9438
FINAL REPORT


32824-AR-019-01
25 APRIL 1980

Prepared By
Paul Bauer
Charles Lurie

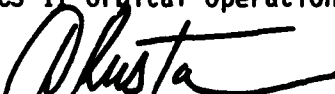
APPROVED BY:


R. H. Alborn, Manager
DSCS II Orbital Operations

APPROVED BY:


F. R. Cartier
Project Manager
DSCS II

APPROVED BY:


D. W. Rusta, Manager
Power Sources
Engineering Department

Prepared for
Department of the Air Force Headquarters
Space Division (AFSC)
CDRL Sequence Number B009
Contract F04701-77-C-0118

TRW Defense and Space Systems Group
One Space Park
Redondo Beach, California 90278

CONTENTS

	Page
1. SUMMARY AND CONCLUSIONS	1-1
1.1 Scope	1-1
1.2 Anomaly Description	1-1
1.3 Anomaly Investigations	1-1
1.4 Conclusions	1-1
2. BACKGROUND	2-1
2.1 Power Subsystem	2-1
2.2 Orbital Chronology Prior to Identifying the Anomaly	2-1
3. ANOMALY OBSERVATIONS	3-1
3.1 Satellite 9437	3-1
3.1.1 State of the Batteries Prior to the Anomaly Observation	3-1
3.1.2 Anomalous Behavior	3-1
3.2 Satellite 9438	3-6
3.2.1 State of the Batteries Prior to the Anomaly Observation	3-6
3.2.2 Anomalous Behavior	3-6
4. ANOMALY INVESTIGATIONS	4-1
4.1 Scope	4-1
4.2 Postulated Causes of the Anomaly	4-1
4.3 Cell Short Circuits	4-2
4.3.1 Evidence in Support of the Existence of Short-Circuited Cells	4-2
4.3.2 Causes of Battery Cell Short-Circuit Failure	4-6
4.4 Variations in Cell Characteristics	4-12
4.4.1 Gulton versus General Electric Cells	4-12
4.4.2 Destructive Physical Analysis (DPA)	4-14

CONTENTS (CONTINUED)

	Page
4.5 Investigations Resulting in the Elimination of Other Plausible Causes of Failure	4-16
4.5.1 Thermal Characteristics	4-17
4.5.2 Charge Control Failure	4-17
4.5.3 Battery Heater Switch Operation	4-17
5. CORRECTIVE ACTION	5-1
5.1 Satellites 9437 and 9438	5-1
5.1.1 Control of Load Sharing	5-1
5.1.2 Control of Recharge Fraction and Recharge Rate	5-1
5.2 Satellites 9441 and 9442	5-2
5.3 Satellite 9443 and all Subsequent Spacecraft	5-3
APPENDICES	
1 POWER SUBSYSTEM DESIGN DESCRIPTION	A1-1
2 BRANCH CURRENT ANOMALY	A2-1
3 FLIGHT 7/8 AND 11/12 GROUND TEST SIMULATIONS	A3-1
4 TWO-BATTERY LOAD SHARING TEST SIMULATIONS	A4-1
5 DESTRUCTIVE PHYSICAL ANALYSIS	A5-1
6 SSTS FAILURE MODES AND EFFECTS ANALYSIS	A6-1
7 SPACECRAFT THERMAL CONTROL	A7-1
8 BATTERY CONTROL NETWORK DESIGN FOR DSCS II FLIGHTS 13-16	A8-1

ILLUSTRATIONS

		Page
2-1	DSCS II 12 Ah Battery	2-2
3-1	Satellite 9437, 10 to 11 September 1978, 27-Hour Automonitor Showing Battery 3 Anomalous Behavior	3-3
3-2	Satellite 9437 - 26 September 1978 - Eclipse Battery Load Sharing	3-5
3-3	Satellite 9438 - 7 September 1978 - Exerpt from 50-Hour Monitor Showing Battery 3 Anomalous Behavior	
3-4	Satellite 9438 Minimum Bus Voltage, Eclipse Season Three (September 1978)	3-11
4-1	Battery S/N 3-6 - Season 3, Cycle 3 - Short Circuit Event - Battery Data	4-3
4-2	Battery S/N 3-6 - Season 3, Cycle 9 - Short Circuit Event - Cell Data	4-4
4-3	Offset of Apparent SSTS Switch Point Simulated in Test with a Battery Containing a Shorted Cell	4-6
4-4	Battery S/N 3-6 - Preshort Signature - Cells 15 and 16	4-10
4-5	Overcharge Voltage versus Overcharge Current	4-12
5-1	Revised Charge Control Circuit	5-4

TABLES

	Page
2-1 Satellite 9437 Chronology Prior to the Anomaly Observation	2-2
2-2 Satellite 9438 Chronology Prior to the Anomaly Observation	2-5
2-3 Reconditioning Discharge Capacities (Ah)	2-8
3-1 Initial Battery 3 Anomaly Observation	3-1
3-2 Battery 2 Anomaly Showing Voltage Decrease and Current Increase on Trickle Charge	3-4
4-1 Overcharge Testing of Positive Plates (Visual Results)	4-15
5-1 Battery Heat Rejection Capability	5-6

1. SUMMARY AND CONCLUSIONS

1.1 SCOPE

This report contains a description of the anomalous behavior of the Electric Power Subsystems of DSCS II Satellites 9437 and 9438, and of the investigations conducted to determine the cause of the anomalies.

1.2 ANOMALY DESCRIPTION

During the third eclipse season beginning in September 1978, indications of anomalous behavior were observed in both satellites:

- a) Unbalanced battery currents on both charge and discharge
- b) Battery overtemperature and overtemperature disconnect
- c) Switch from full charge to trickle charge at temperatures apparently outside the switching tolerance range
- d) Branch current anomalies, i.e., the measured currents in the several branches of the power subsystem, did not add up to the measured total
- e) Apparent battery heater switching outside the temperature tolerance range of the heater thermostats.

1.3 ANOMALY INVESTIGATIONS

An extensive series of investigations was conducted to determine the causes of the various anomalies. These investigations included ground test simulations using flight-configuration batteries, component level testing, and analyses of components and systems.

1.4 CONCLUSIONS

The following conclusions have been reached:

- a) Two batteries on Satellite 9437 and one on Satellite 9438, each contain one short-circuited cell. In each case the shorted cell is located near the midpoint of the cell stack.
- b) The cause of the cell short-circuiting has been identified as excessive overcharge during post-eclipse recharge, pulse-overcharging in auto mode, or both.
- c) In the absence of existing damage, similar failures can be avoided, or their rate of incidence greatly decreased, in existing satellites, by modification of on-orbit charging procedures. Several proposals have been advanced for the

redesign of charge control circuitry on future spacecraft for preventing cell short-circuiting by maintaining more positive control of peak overcharge currents. A circuit design has been selected and implemented.

- d) Several causes of excessive overcharge in Satellites 9437 and 9438 have been postulated, i.e.:
 - 1) Changes in operating temperatures
 - 2) Lot to lot cell behavior changes
 - 3) Changes in cell type without a corresponding change in charge control settings.
- e) The mechanism of cell failure has not been identified. Advanced methods of cell disassembly and destructive analysis have produced useful information. Efforts to identify the mechanism are continuing.
- f) Battery overtemperature is a direct result of cell short-circuit failure (which increases overcharge current), heat dissipation, and temperature.
- g) Apparent out-of-tolerance switch-to-trickle temperatures are a direct result of short-circuit cell failures. Temperature gradients induced by shorted cells are responsible for a false indication of temperature at the switching point. Solid-state temperature switch operation is normal.
- h) Apparent power subsystem branch current anomalies are a direct result of the current monitor design. Currents beyond the sensor design range caused a misinterpretation of telemetered data. Current sensor and telemetry operation is normal.

2. BACKGROUND

2.1 POWER SUBSYSTEM

The DSCS II power subsystem is of the unregulated bus direct energy transfer (DET) type, delivering power directly from the illuminated solar arrays to the load without any intervening loss elements other than the distribution cabling. Part of the power delivered by the solar array is accepted by the loads and the remainder is available for battery charging. Three sealed 22-cell nickel cadmium batteries are connected in parallel to the primary bus through independent control circuits. Figure 2-1 is an isometric drawing of the battery showing the positions of major battery parts. Appendix 1 contains a simplified functional block diagram and tutorial material necessary for a clear understanding of the operation of the electrical power subsystem.

2.2 ORBITAL CHRONOLOGY PRIOR TO IDENTIFYING THE ANOMALY

Satellites 9437 and 9438 were launched on 12 May 1977. Detailed satellite timelines showing the significant activities performed prior to identification of the anomaly are presented in Tables 2-1 and 2-2. Automatic (Auto), manual full, trickle and minitrickle charge modes were successfully demonstrated during the first 2 weeks of satellite operation. The batteries were maintained in the minitrickle charge mode until the start of reconditioning at the end of August 1977. One reconditioning cycle was performed prior to the first eclipse season. Reconditioning discharge capacities are presented in Table 2-3. These results are considered nominal and define a baseline. After reconditioning, the batteries were commanded to the auto charge mode until the first eclipse season which began on 5 September 1977. Battery performance was nominal and batteries were commanded to the minitrickle charge mode soon after the eclipse season ended. The Preseason 2 reconditioning was conducted during February 1978. The batteries were reconditioned twice prior to the start of the second eclipse season on 3 March 78.

Reconditioning discharge capacities are presented in Table 2-3. The general loss of capacity during the second reconditioning discharge is a result of the shallow nature of the discharge imposed by the manual termination at 23 volts.

Table 2-1. Satellite 9437 Chronology Prior to the Anomaly Observation

Date (1977)	Time (Z)	Event
12 May	1427:01.661	Liftoff
	1558	Telemetry Acquisition
	2055:32.9	Separation
28 Aug	1655-1710	Start Battery Reconditioning, Battery No. 1 + Recondition Discharge
1 Sep	2200-2215	Complete Battery Reconditioning, Battery No. 3 + Minitrickle Charge Mode
5 Sep	1655-1710	Batteries to Auto Charge Mode
21 Oct	1650-1655	Batteries to Minitrickle Charge Mode
Date (1978)	Time (Z)	Event
5 Feb	0100-0115	Start Battery Reconditioning, Battery 1 to Recondition Discharge Mode
6 Feb	0305-0605	Battery 1 to Trickle Charge Mode
	0800-0815	Battery 1 to Auto Charge, Battery 2 to Recondition Discharge Mode
	1255-1310	Battery 1 to Minitrickle Charge Mode
7 Feb	1100-1240	Battery 2 to Trickle Charge Mode
	1555-1610	Battery 2 to Auto Charge Mode, Battery 3 to Recondition Discharge Mode
	2250-2325	Battery 2 to Minitrickle Charge Mode
8 Feb	1800-2100	Battery 3 to Trickle Charge Mode
		Battery 3 to Auto Charge Mode
		Battery 3 to Minitrickle Charge Mode
24 Feb	0000-0015	Battery 1 to Recondition Discharge Mode
25 Feb	0030-0200	Battery 1 to Trickle Charge Mode
	0615-0630	Battery 1 to Auto Charge Mode
		Battery 2 to Recondition Discharge Mode
25 Feb	1015-1030	Battery 1 to Minitrickle Charge Mode
26 Feb	0610-0900	Battery 2 to Trickle Charge Mode

Table 2-1. Satellite 9437 Chronology Prior to the Anomaly Observation
(Continued)

Date (1978)	Time (Z)	Event
26 Feb	1215-1230	Battery 2 to Auto Charge Mode Battery 3 to Recondition Discharge Mode
	1630-1645	Battery 2 to Minitrickle Charge Mode
27 Feb	1200-1500	Battery 3 to Trickle Charge Mode
	1740-1750	Battery 3 to Auto Charge Mode
	2155-2205	Battery 3 to Minitrickle Charge Mode
2 Mar	0450-0525	Batteries to Auto Charge Mode
17 Apr	2115-2150	Batteries to Minitrickle Charge Mode
6 Aug	2350-0005	Battery 1 to Recondition Discharge Mode
7 Aug	1825-1840	Battery 1 to Auto Full Charge Mode
7 Aug	2240-2250	Battery 1 to Minitrickle Charge Mode
8 Aug	0715-0730	Battery 2 to Recondition Discharge Mode
9 Aug	0540-0550	Battery 2 to Trickle Charge Mode
9 Aug	0845-0855	Battery 2 to Auto Full Charge Mode
9 Aug	1505-1540	Battery 2 to Minitrickle Charge Mode Battery 1 to Recondition Discharge Mode
9 Aug	2230-2240	Battery 3 to Recondition Discharge Mode
10 Aug	1135-1140	Battery 1 to Trickle Charge Mode
10 Aug	1350-1400	Battery 1 to Auto Full Charge Mode
10 Aug	1615-1915	Battery 3 to Trickle Charge Mode
10 Aug	1759	Battery 1 to Minitrickle Charge Mode
10 Aug	2200	Battery 3 to Auto Full Charge Mode
11 Aug	0150-0200	Battery 3 to Minitrickle Charge Mode
11 Aug	2200	Batteries to Trickle Charge Mode
15 Aug	9150-0200	Battery 1 to Recondition Discharge Mode
16 Aug	0210-0305	Battery 1 to Trickle Charge Mode
16 Aug	0640-0715	Battery 1 to Auto Full Charge Mode
16 Aug	1220-1255	Battery 1 to Trickle Charge Mode
23 Aug	0005-0020	Battery 2 to Recondition Discharge Mode
23 Aug	0955-1010	Battery 3 to Recondition Discharge Mode

Table 2-1. Satellite 9437 Chronology Prior to the Anomaly Observation
(Continued)

Date (1978)	Time (Z)	Event
24 Aug	0115-0125	Battery 2 to Trickle Charge Mode
24 Aug	0605-0615	Battery 2 to Auto Full Charge Mode
24 Aug	1035-1200	Battery 3 to Trickle Charge Mode
		Battery 2 to Trickle Charge Mode
24 Aug	1410-1420	Battery 3 to Auto Full Charge Mode
24 Aug	2000-2010	Battery 3 to Trickle Charge Mode
1 Sep	1050-1105	Batteries to Auto Charge Mode
2 Sep	0450-0540	Lunar Eclipse Monitor
2 Sep	1015-1145	Lunar Eclipse Monitor
3 Sep	1605-1620	Battery 3 Temperature noted at 88°F During Auto Trickle Mode
10 Sep	2250	27-hour Battery Monitor
12 Sep	0610-0615	Battery 3 to Trickle Charge Mode
15 Sep	0005	12-hour Eclipse Load Share and Recharge Monitor
22 Sep	1335	Battery 2 Found in Minitrickle Due to 95°F Overtemp Switch Closure
22 Sep	1340-1350	Battery 2 to Trickle Charge Mode
22 Sep	1500-1510	Begin Manual Control of Batteries 1 and 2 During Recharge Cycle

Table 2-2. Satellite 9438 Chronology Prior to the Anomaly Observation

Date (1977)	Time (Z)	Event
12 May	1427:01 661	Liftoff
	1558	Telemetry Acquisition
	2106:44.7	Separation
28 Aug	1350-1405	Start Battery Reconditioning, Battery No. 1 + Recondition Discharge
1 Sep	1855-1910	Complete Battery Reconditioning, Battery No. 3 + Minitrickle Charge Mode
4 Sep	0345-0400	Batteries to Auto Charge Mode
22 Oct	0310-0345	Batteries to Minitrickle Charge Mode
Date (1978)	Time (Z)	Event
5 Feb	0710-0730	Start Battery Reconditioning, Battery 1 to Recondition Discharge
6 Feb	0800-1100	Battery 1 to Trickle Charge Mode
	1345-1400	Battery 1 to Auto Charge Mode
		Battery 2 to Recondition Discharge
	1835-1850	Battery 1 to Minitrickle Charge Mode
7 Feb	1420-1510	Battery 2 to Trickle Charge Mode
	1815-1830	Battery 2 to Auto Charge Mode
	2015-2030	Battery 3 to Recondition Discharge Mode
	2245-2255	Battery 2 to Minitrickle Charge Mode
	2130-0030	Battery 3 to Trickle Charge Mode
9 Feb	0230-0245	Battery 3 to Auto Charge Mode
		Battery 3 to Minitrickle Charge Mode
24 Feb	0535-0550	Battery 1 to Recondition Discharge Mode
25 Feb	0600-0900	Battery 1 to Trickle Charge Mode
	1105-1115	Battery 1 to Auto Charge Mode
		Battery 2 to Recondition Discharge Mode
	1535-1545	Battery 1 to Minitrickle Charge Mode

Table 2-2. Satellite 9438 Chronology Prior to the Anomaly Observation
(Continued)

Date (1978)	Time (Z)	Event
26 Feb	0930-1300	Battery 2 to Trickle Charge Mode
	1545-1555	Battery 2 to Auto Charge Mode
		Battery 3 to Recondition Discharge Mode
27 Feb	2030-2040	Battery 2 to Minitrickle Charge Mode
	1545-1738	Battery 3 to Trickle Charge Mode
	2115-2225	Battery 3 to Auto Charge Mode
28 Feb	0150-0200	Battery 3 to Minitrickle Charge Mode
2 Mar	1250-1305	Batteries to Auto Charge Mode
18 Apr	0440-0455	Batteries to Minitrickle Charge Mode
7 Aug	1645-1700	Battery 1 to Recondition Discharge Mode
8 Aug	1450-1510	Battery 1 to Trickle Charge Mode
8 Aug	1645-1910	Battery 1 to Auto Full Charge Mode
8 Aug	2200-2210	Battery 1 to Minitrickle Charge Mode
8 Aug	2245-2300	Battery 2 to Recondition Discharge
9 Aug	1920-2020	Battery 2 to Trickle Charge Mode
9 Aug	2310	Battery 2 to Auto Full Charge Mode
10 Aug	0300-0310	Battery 2 to Minitrickle Charge Mode
10 Aug	0600-0635	Battery 3 to Recondition Discharge Mode
11 Aug	0350-0400	Battery 3 to Trickle Charge Mode
11 Aug	0620-0920	Battery 3 to Auto Full Charge Mode
11 Aug	1100-1230	Battery 3 to Minitrickle Charge Mode, A0 Spin Axis Maneuver, NCA Update
11 Aug	2320	Batteries to Trickle Charge Mode
25 Aug	1435-1450	Battery 1 to Recondition Discharge Mode
26 Aug	0055-0130	Battery 2 to Recondition Discharge Mode
26 Aug	1405-1655	Battery 1 to Trickle Charge Mode
26 Aug	1910-1945	Battery 1 to Auto Full charge Mode
26 Aug	2100-2115	Battery 3 to Recondition Discharge Mode

Table 2-2. Satellite 9438 Chronology Prior to the Anomaly Observation
(Continued)

Date (1978)	Time (Z)	Event
27 Aug	0000-0030	Battery 2 to Trickle Charge Mode
27 Aug	0250-0300	Battery 2 to Auto Full Charge Mode
27 Aug	0730-0740	Battery 2 to Trickle Charge Mode
27 Aug	2030-2230	Battery 3 to Trickle Charge Mode
28 Aug	0130-0140	Battery 3 to Auto Full Charge Mode
28 Aug	0700-0710	Battery 3 to Trickle Charge Mode
3 Sep	1305-1320	Batteries to Auto Charge Mode
4 Sep	0450	Battery 3 Found in Minitrickle Due to 90°F Overtemp switch closure
7 Sep	1000	50-Hour Battery Monitor
9 Sep	1820-1830	Battery 3 to Trickle Charge Mode
15 Sep	1140	12-Hour Eclipse Load Share and Recharge Monitor
20 Sep	1035-1045	Battery 3 to Recondition Discharge Mode
21 Sep	0035-0110	Batteries 1 and 2 to Minitrickle, then Trickle Charge Mode
21 Sep	1100-1230	Batteries 1 and 2 to Auto Charge Mode
21 Sep	1345-1355	Battery 3 to Minitrickle Charge Mode
21 Sep	1940-0010	Battery 3 to Trickle, then Auto Full Charge
22 Sep	1000-1810	Batteries to Auto Full Charge
23 Sep	0530	Battery 3 to Minitrickle Charge Mode
23 Sep	1125-1140	Begin Manual Control of Battery 1 and 2 During Recharge Cycle

Table 2-3. Reconditioning Discharge Capacities (Ah)

Satellite	Battery	Preseason 1	Preseason 2	Preseason 3
9437	1	18.1	17.3, 16.4	9.0, 12.5, 15.2
	2	18.2	17.0, 16.4	13.2, 15.6
	3	N/A	17.2, 16.4	9.0, 15.1
9438	1	17.6	17.3, 16.3	13.3, 15.7
	2	17.5	15.9, 16.6	11.4, 14.0
	3	17.5	17.4, 16.6	13.5, 15.2

The first cycle capacity of Battery 2, Satellite 9438, was low and suggests that cell degradation may have begun during the first eclipse season. Battery performance during the second eclipse season appeared to be normal.

The Preseason 3 reconditioning was conducted during the early part of August 1978. All battery capacities were low, and multiple reconditionings were run in an effort to restore the lost capacity. Reconditioning discharge capacities are presented in Table 2-3. Review of these data indicates that significant degradation had occurred during the second eclipse season.

3. ANOMALY OBSERVATIONS

3.1 SATELLITE 9437

3.1.1 State of the Batteries Prior to the Anomaly Observation

Satellite 9437 batteries were reconditioned in early August in preparation for the autumnal equinox season (Season 3) beginning 4 September 1978. The batteries all exhibited low capacity during the first reconditioning discharge. Multiple cycles were run in an attempt to restore capacity. Reconditioning discharge data are presented in Table 2-3. These data suggest that significant degradation had occurred during the second eclipse season.

On 1 September 1978 the three battery charge controllers were placed in the auto mode in preparation for the lunar eclipses of 2 September 1978 at 0457 Z and 1023 Z. They were left in the auto mode in anticipation of the start of the equinox eclipse season on 4 September 1978.

3.1.2 Anomalous Behavior

The first observation of an anomaly occurred on 3 September 1978 during a monitoring pass at 1605 Z. Battery No. 3 voltage was low and its trickle charge current and temperature high. Voltage, current, and temperature data for the anomalous 1605 Z pass and a typical prior pass at 0615 Z are shown in Table 3-1.

Table 3-1. Initial Battery 3 Anomaly Observation

Battery No.	0615 Z Pass			1605 Z Pass		
	Voltage (V)	Current (A)	Temperatures (°F)	Voltage (V)	Current (A)	Temperatures (°F)
1	30.52	0.33	81	30.52	0.29	82
2	30.54	0.36	73	30.67	0.32	71
3	30.67	0.31	74	29.44	0.47	88

For diagnostic purposes, the satellite was monitored continuously for a period of 27 hours, beginning at approximately 2253 Z on 10 September. All batteries were in the auto charge mode. This period included a satellite eclipse. Monitoring observations are summarized in Figure 3-1.

Several further indications of anomalous behavior were seen during this monitoring pass:

- a) Although the three batteries were under automatic control, (auto mode) a severe current imbalance occurred during discharge. Battery 3 failed to carry its share of the discharge load current, and accepted more than its share of charging current.
- b) Battery 3 temperatures rose more rapidly at end-of-charge than those of Batteries 1 and 2. This is consistent with excessive charging current.
- c) The sum of the three battery discharge telemetry currents did not equal the main bus current telemetry data. The magnitude of the error was too great to be explained by tolerances in the current sensors. Subsequent investigation showed that the high discharge currents carried by Battery 1 were beyond the current sensor design range and that the apparent anomaly was an interpretation error only (see Appendix 2 for details).
- d) The solid state temperature switch (SSTS), which is designed to operate at 77°F, appeared to be operating at an indicated temperature of 80 to 81° on Battery 3, and 79 to 80°F on Battery 1. This was found to be due to temperature gradients in the battery rather than a SSTS malfunction.

From the above observations it was concluded that Battery 3 was exhibiting symptoms which could lead to rapid deterioration due to over-temperature operation, and on 12 September 78 it was switched to manual trickle charge at 0610 Z.

An additional 12-hour monitoring pass on 15 September 1978 showed that Batteries 1 and 2 were sharing the loads adequately and appeared to be normal in behavior. This normal behavior continued through 21 September 1978.

On 22 September 1978, a routine monitoring pass showed the Battery 2 controls to be in the minitrickle state, indicating that at some time prior to the observation the Battery 2 overtemperature circuit, designed to

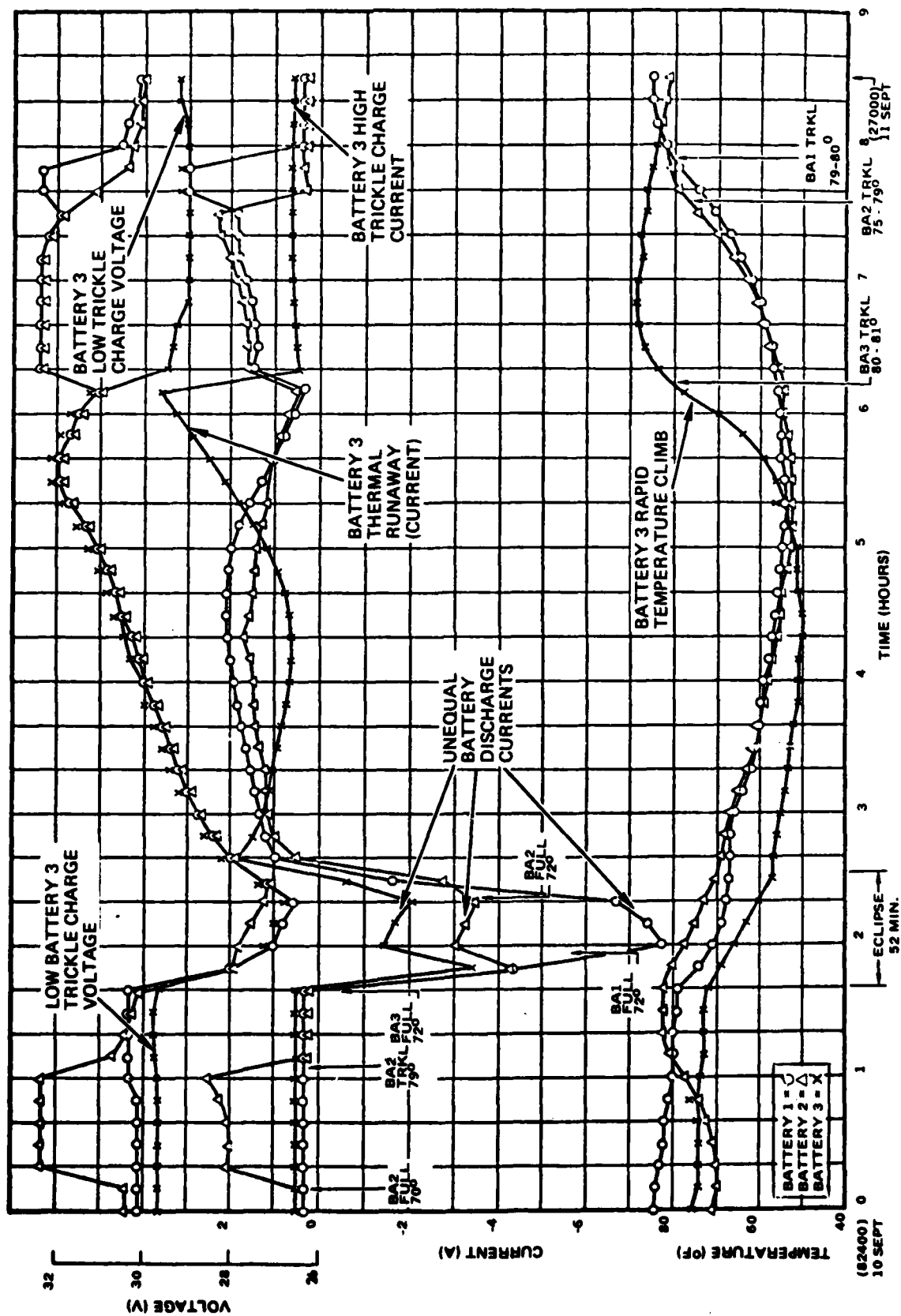


Figure 3-1. Satellite 9437, 10 to 11 September 1978, 27-Hour Automonitor Showing Battery 3 Anomalous Behavior

operate at 95°F, had been activated. Battery 2 was subsequently commanded to manual trickle charge. Observations made with all batteries on trickle charge showed that Battery 2 was exhibiting symptoms similar to those observed on Battery 3, i.e., low voltage and high trickle charging current. The temperature of Battery 2 was low; however, this was judged of no significance, since the battery had been in minitrickle state for an unknown period, and had had time to cool. Comparative data for 21 September 1978 and 22 September 1978 are shown in Table 3-2.

Table 3-2. Battery 2 Anomaly Showing Voltage Decrease and Current Increase on Trickle Charge

Battery No.	21 September (1830 Z) Pass			22 September (1335 Z) Pass		
	Voltage (V)	Current (A)	Temperature (°F)	Voltage (V)	Current (A)	Temperature (°F)
1	30.11	0.37	80	30.24	0.37	78
2	30.12	0.39	73	29.17	0.55	59
3*	29.85	0.43	63	29.99	0.43	61

* Battery 3 data reflects a prior failure.

Throughout the remainder of the eclipse season the batteries were operated as follows:

- Battery 3 was maintained in the manual trickle charge mode
- Batteries 1 and 2 were in auto charge during eclipse and first recharge. They were then switched to manual trickle charge until just prior to the next eclipse.

Severe imbalances in battery discharge currents continued, as shown in Figure 3-2. (Telemetry data falling outside the current sensor design range has been corrected.)

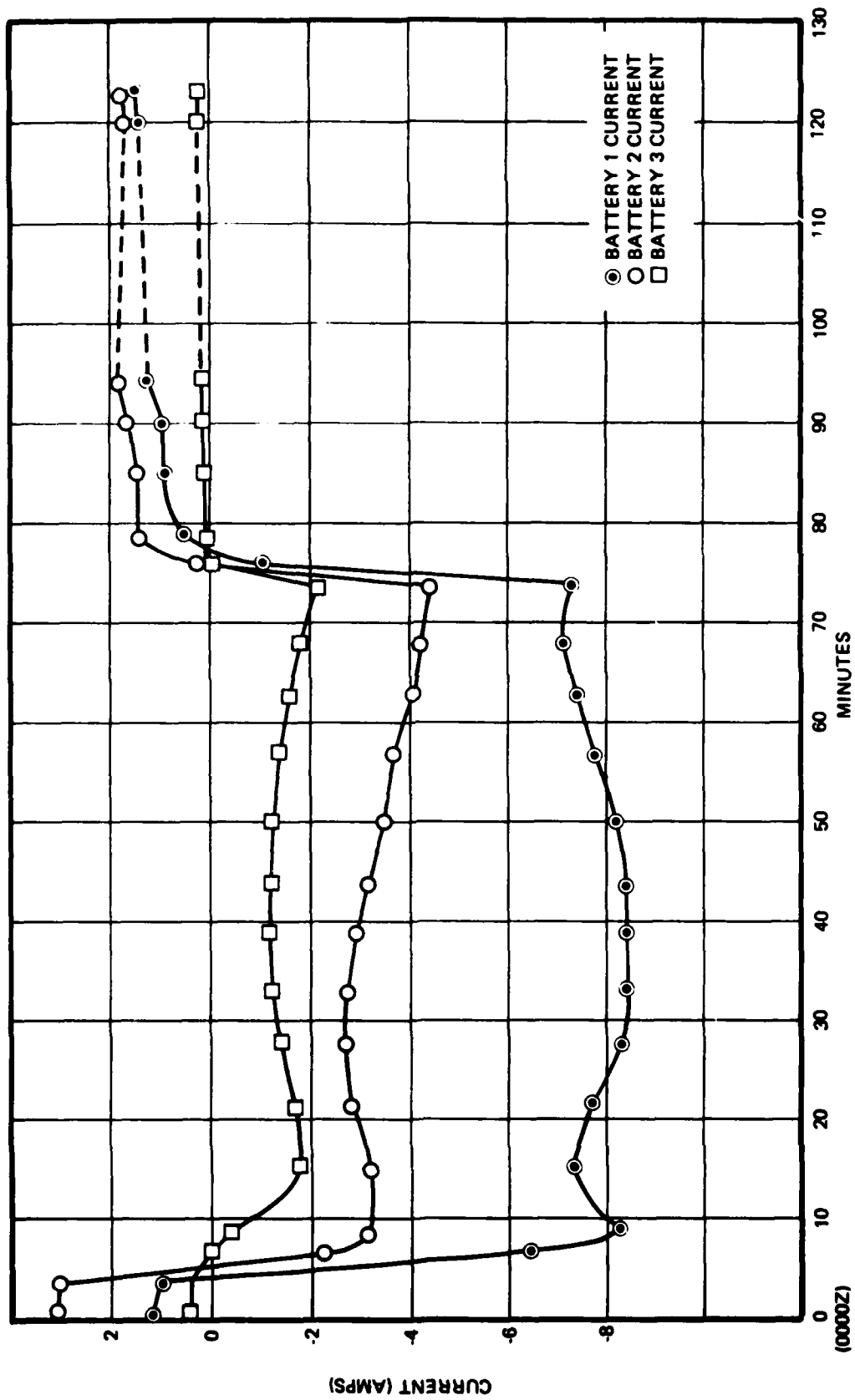


Figure 3-2. Satellite 9437 - 26 September 1978 - Eclipse 24 - Battery Load Sharing

Post-eclipse reconditioning attempts failed to restore nominal performance of Batteries 2 and 3. After placing the three batteries in the minitrickle state for the solstice season, Batteries 2 and 3 continued to exhibit low temperature and high current behavior when compared with Battery 1.

3.2 SATELLITE 9438

3.2.1 State of the Batteries Prior to Anomaly Observation

Satellite 9438 batteries were reconditioned in early August in preparation for the autumnal equinox season (Season 3) beginning 4 September 1978. The batteries all exhibited low capacity during the first reconditioning discharge. Two cycles were run in an attempt to restore capacity. Reconditioning discharge data is presented in Table 2-3. These data indicate that significant degradation had occurred during the second eclipse season.

3.2.2 Anomalous Behavior

The third eclipse season began on 4 September 1978. The batteries were placed in the auto charge mode at approximately 1350 Z on 3 September 1978. During a routine pass at 0450 Z, 4 September 1978 prior to the first eclipse of the season, Battery 3 was found to be in minitrickle. It was concluded that in the intervening period the 95°F overtemperature circuit had activated and had automatically switched to minitrickle.

At 0818 Z, the battery was placed in manual trickle and after reaching a temperature of 53°F in auto charge. After an extended period of trickle charging on 4 September 1978, battery characteristics were:

Battery	Voltage (V)	Current (A)	Temperature (°F)
1	31.18	0.15	78
2	30.64	0.29	72
3	28.97	0.55	92

Battery 3 was placed in manual trickle at this time.

For diagnostic purposes Satellite 9438 was continuously observed for a period of 50 hours, beginning at 1000 Z on 7 September 1978. Figure 3-3 is an excerpt of this test period, showing current and temperature imbalances similar to those observed in Satellite 9437.

At the end of the 50-hour monitor period, with the batteries in the trickle charge mode, the parameters were as follows:

Battery	Voltage (V)	Current (A)	Temperature (°F)
1	30.23	0.34	77
2	29.95	0.37	83
3	29.11	0.51	83

The above indicates that Batteries 1 and 2 are almost equivalent, and that Battery 3 is degraded or has a shorted cell.

On 9 September 1978, Battery 3 was switched to trickle charge. On 15 September 1978, an extended monitoring pass (12 hours) showed that Batteries 1 and 2 were sharing the loads well, but that high overcharge currents were being drawn. These were sufficient to cause the main bus to fall out of limiting regulation after it had reached this point.

On 20 - 21 September 1978, Battery 3 was subjected to a reconditioning discharge cycle. During reconditioning, the battery capacity was a normal 14.8 ampere-hours. No discontinuities were observed in the discharge curve. However, the plateau voltage was depressed and consistent with the presence of one shorted cell.

After recondition termination, Battery 3 was switched to minitrickle until Batteries 1 and 2 were fully charged. The three batteries were then switched to trickle charge mode. When Battery 3 reached a voltage of 28.5 V, and a temperature of 48°F, it was switched to the auto charge mode and allowed to recharge. Bus limiting was reached in 3 hours. Overcharge currents as high as 4.5 amperes were observed, followed by a rapid

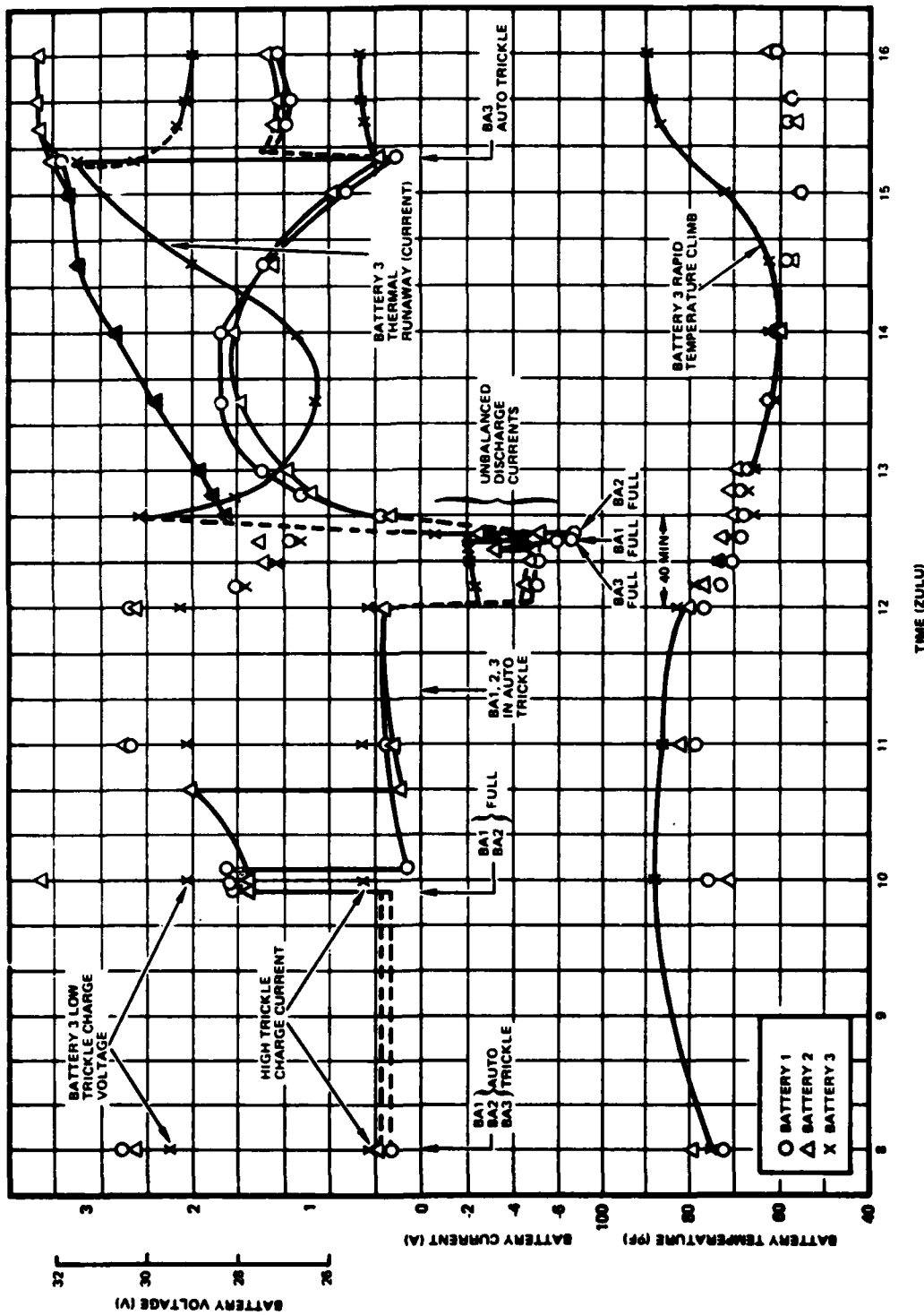


Figure 3-3. Satellite 9438 - 7 September 1978 - Excerpt from 50-Hour Monitor Showing Battery 3 Anomalous Behavior

temperature rise, and an automatic switch to trickle charge. Battery 3 was commanded to the minitrickle charge mode at a temperature of 98°F.

Batteries 1 and 2 load shared approximately equally while Battery 3 supported a much smaller part of the load. Load sharing at eclipse end was approximately:

Battery 1 = 40 percent (auto-full)
Battery 2 = 39 percent (auto-full)
Battery 3 = 21 percent (auto full)

On 7 October 1978 attempts were made to recondition Battery 3. After two cycles the third recondition discharge characteristic had not measurably improved (approximately 0.3 volt rise in the voltage plateau). Load sharing tests (in auto-full) after the reconditioning also showed no significant improvement:

Battery 1 = 40 percent
Battery 2 = 38 percent
Battery 3 = 22 percent

As a result, starting on 14 October 1978 and for the remainder of the eclipse season, the batteries were command-controlled as follows:

- Battery 3 was maintained in the manual trickle charge mode
- Batteries 1 and 2 were in auto charge during eclipse and first recharge. They were then switched to manual trickle charge until just prior to the next eclipse.

On 17 October 1978, the batteries were put in the manual trickle charge mode for the last two days of the season eclipse with the following load sharing:

Battery 1 = 38 percent
Battery 2 = 36 percent
Battery 3 = 26 percent

Post-eclipse season, minitrickle charge battery parameters as of 7 November 1978 were as follows:

Battery	Voltage (V)	Current (A)	Temperature (°F)
1	30.36	0.15	57
2	30.23	0.13	53
3	29.80	0.20	55

Figure 3-4 depicts the variation of end-of-eclipse bus voltage during the third eclipse season of Satellite 9438. Other than the discontinuities resulting from the attempts to recondition Battery 3, it appears that the minimum bus voltage for the season was approximately 25.6 volts.

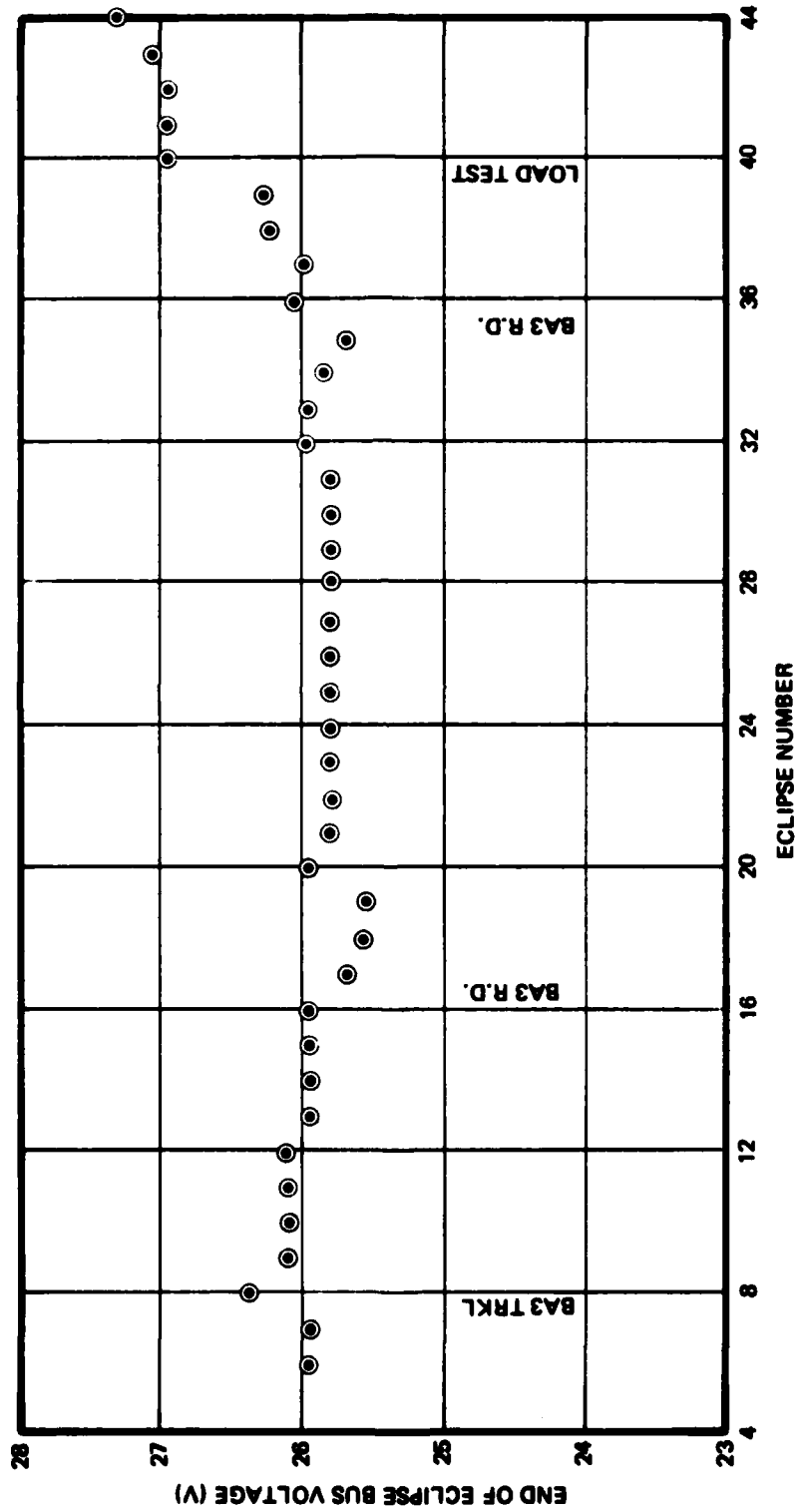


Figure 3-4. Satellite 9438 Minimum Bus Voltage, Eclipse Season Three (September 1973)

4. ANOMALY INVESTIGATIONS

4.1 SCOPE

An extensive series of investigations was conducted to determine the causes of the various anomalies. These investigations included: ground test simulations using flight-configuration batteries, component level testing, analyses of components and systems. Copies of relevant anomaly investigation reports are included in the appendices and referenced in the following text.

4.2 POSTULATED CAUSES OF THE ANOMALY

Several possible causes of the battery anomalies were considered during the course of these investigations:

- a) Accelerated degradation of battery characteristics, e.g., premature cell degradation due to overstressing during charge and overcharge.
- b) Changed cell characteristics, e.g., the existence of a cell voltage-charge control system mismatch causing higher than anticipated charging currents.
- c) Anomalous cell quality, e.g., a cell manufacturing problem making the cells used in these batteries more susceptible to early failure than previous cells.
- d) Battery charge control circuit failures, e.g., a drift in the SSTS switching temperature, or failure of the SSTS or the K1 relay to switch.
- e) A deterioration in the thermal characteristics of the satellite/battery causing the battery overtemperature.

Because of the similarities in the behavior of the batteries in Satellites 9437 and 9438, a single investigation was conducted.

The remainder of this section discusses the above hypotheses in terms of data telemetered from the satellites and data acquired during ground test investigations.

These analyses provided a preponderance of evidence indicating that cell short circuit events occurred in batteries in Satellites 9437 and 9438. The evidence in support of this conclusion is discussed in Section 4.3.1.

4.3 CELL SHORT CIRCUITS

4.3.1 Evidence in Support of the Existence of Short-Circuited Cells

Evidence in support of the short circuited cell hypothesis is voluminous and includes:

- Flight simulation tests
- Flight voltage data
- SSTS operating temperature offset data
- Flight current imbalance data

These areas are summarized below and detailed in the appendices referenced in each summary.

4.3.1.1 Flight Simulation Tests (Appendix 3)

A laboratory test was conducted in which one flight-configuration battery was subjected to a simulation of cycling conditions observed on Satellites 9437 and 9438 and another to the anticipated conditions of Satellites 9441 and 9442. The 9437/9438 simulation used a bus voltage limit of 32.4 V. The 9441/9442 simulation used a lower voltage limit of 31.8 V. During this test, Battery S/N 3-6, which was tested under Satellite 9437/9438 conditions, developed a permanently short-circuited cell during Cycle 9 of Season 3 (in-flight failures occurred between Cycles 1 and 20 of Season 3 in Satellites 9437 and 9438). It was also observed that permanent cell short-circuits were preceded by a period of anomalous operation and, upon occasion, by self-clearing short circuits. The onset of a short-circuit is clearly seen as an abrupt drop in cell voltage to zero volts, and is confirmed (in centrally located cells) by a rapid rise in temperature of the RT2 thermistor which is centrally located on one of the two cell blocks (see Figure 2-1). This rapid temperature rise results from internal heat dissipation due to self-discharge of the shorted cell through the internal short-circuit (as shown in Figures 4-1 and 4-2).

4.3.1.2 Voltage Data (Tables 3-1, 3-2, 3-3 and 3-5)

Inspection of the voltage data reveals that the defective battery voltages are lower than those of the normal batteries by slightly less than

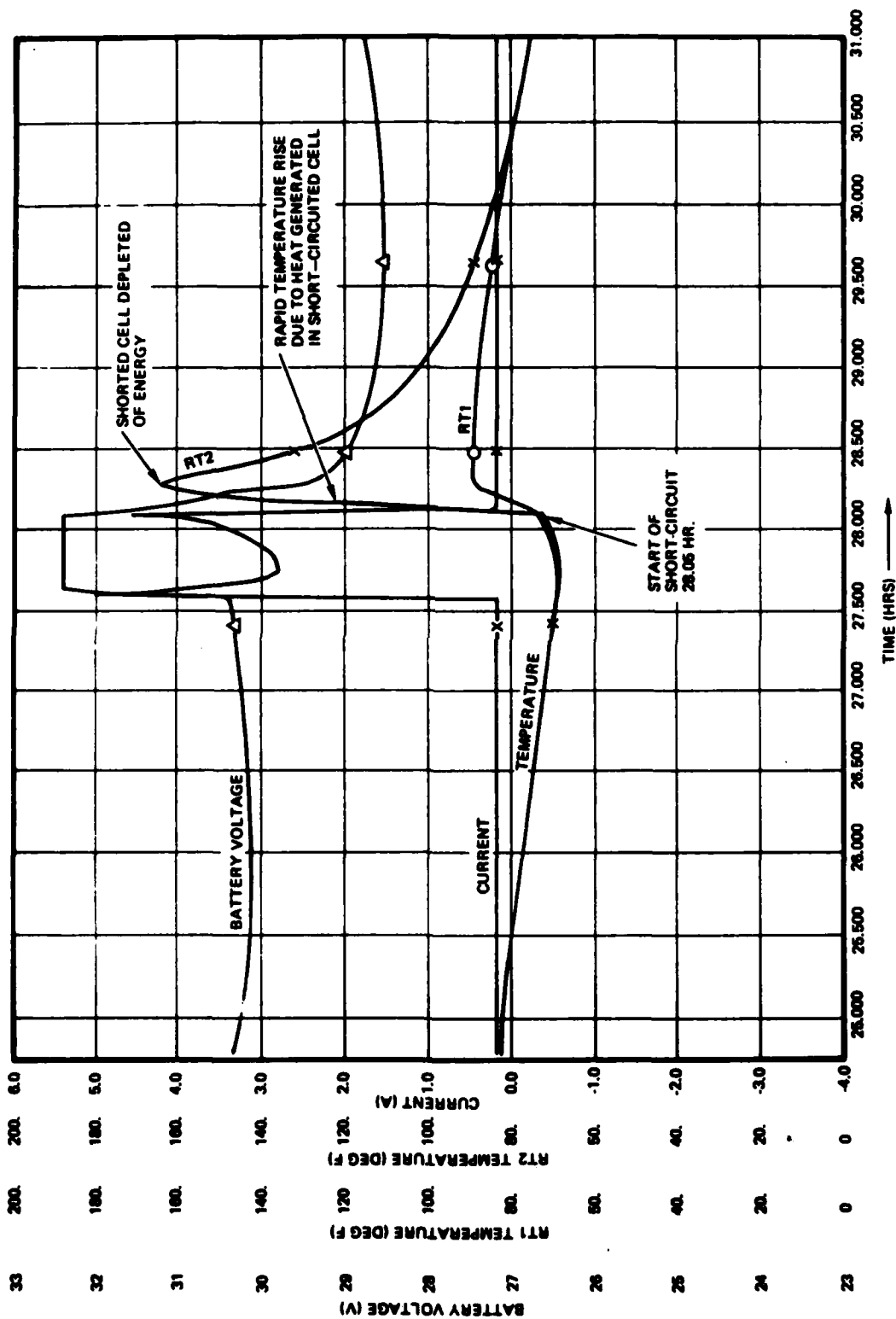


Figure 4-1. Battery S/N 3-6 - Season 3, Cycle 3 - Short Circuit Event -
Battery Data

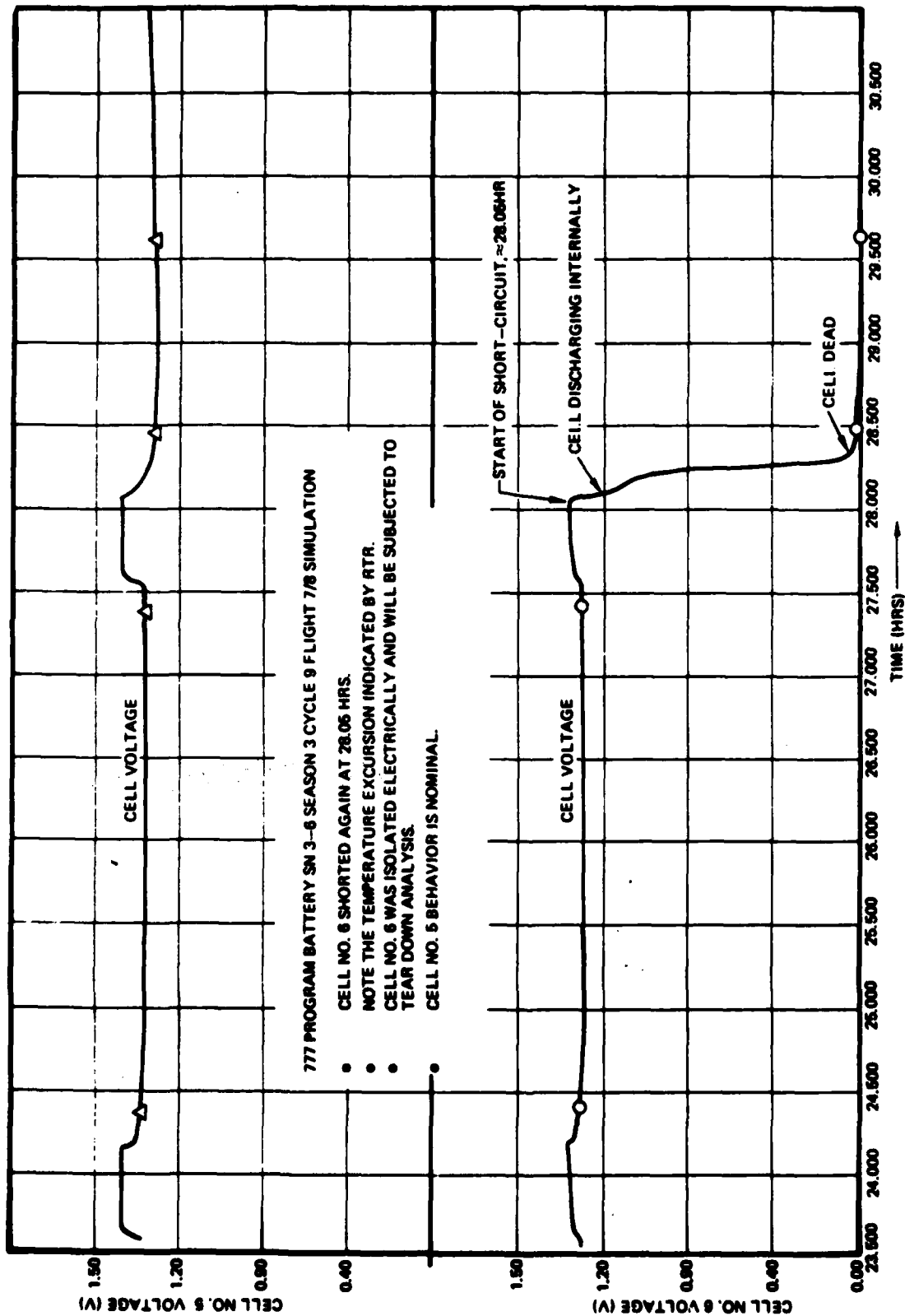


Figure 4-2. Battery S/N 3-6 - Season 3, Cycle 9 - Short Circuit Event - Cell Data

the voltage of one cell. The charging current of the low-voltage battery is slightly higher than that of the normal-voltage battery. This is consistent with the presence of a short-circuited cell in the low-voltage battery. The higher current caused by the lower battery voltage increases the voltage drop across the unfailed cells of the battery, offsetting, in part, the loss of the one-cell-voltage. This higher current is also consistent with the depressed voltages observed generally. These voltage losses are not recoverable by reconditioning.

4.3.1.3 SSTS Operating Temperature Offset

Further confirmation of the cell short-circuit hypothesis is found in the analysis of an apparent shift in the operating temperature of the SSTS. Since an analysis of the performance of the SSTS failed to find an explanation of the observed shift in operating temperature, it was hypothesized that the shift might be due to a temperature gradient in the battery between the points at which the SSTS and the telemetry sensor measure battery temperature. This kind of temperature gradient will not occur if the heat dissipation in the two cell blocks of the battery is symmetrically distributed. If the following assumptions are made, such a temperature gradient would be possible:

- a) One of the two cell blocks is assumed to contain a short-circuited cell.
- b) A short-circuited cell dissipates no heat either on charge or discharge.
- c) The short-circuited cell is located in the vicinity of the SSTS thermistor where it acts as a heat sink, preventing the SSTS sensor from heating up as rapidly as the corresponding point on the other cell block, where the telemetry temperature sensor is mounted. Under these circumstances, the SSTS will appear to switch at an indicated temperature higher than its normal setting.
- d) The short-circuited cell is located on the other cell block in the vicinity of the telemetry thermistor, acting as a heat sink to keep the telemetry temperature sensor cooler than the SSTS sensor. Under these circumstances the SSTS will appear to switch at a lower than normal temperature.

A series of laboratory tests was conducted in which a battery containing a short-circuited cell was charged and overcharged at varying rates, so as to produce varying rates of temperature increase. Figure 4-3

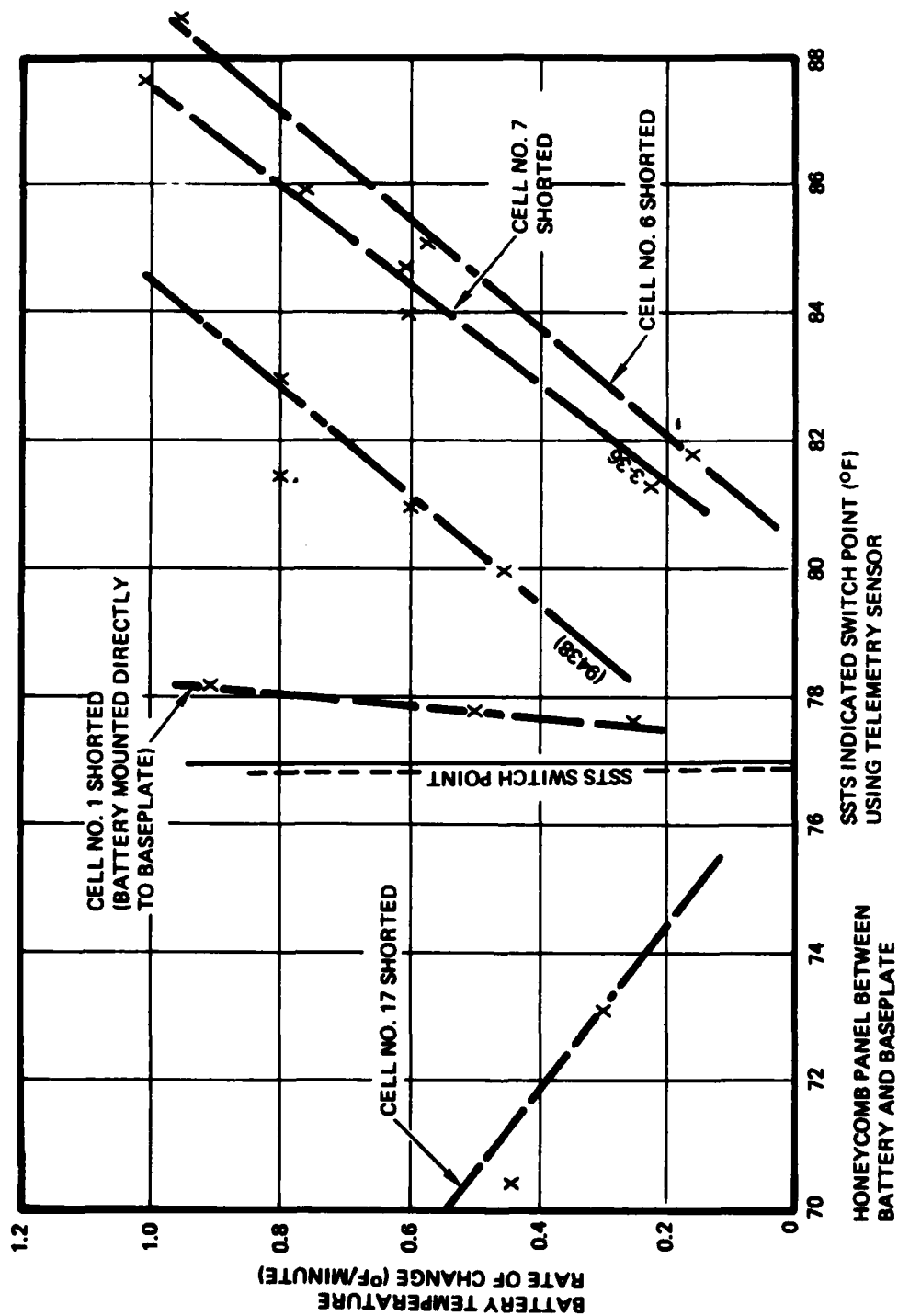


Figure 4-3. Offset of Apparent SSTS Switch Point Simulated in Test with a Battery Containing a Shorted Cell

shows a plot of the telemetry temperature indication at the moment of SSTS switching as a function of the rate of temperature change for several locations of short-circuited cell in the battery package. For comparison purposes a similar plot for Battery 3 of Satellite 9438 is also shown.

The similarity of the observed satellite phenomena and the test results is evidence in favor of the original assumptions, i.e.:

- a) The battery contains a short-circuited cell. It is located in the cell block on which the SSTS is mounted
- b) The short-circuited cell is located at or near the middle of the cell block.

4.3.1.4 Current Imbalances

Current imbalances, both on charge and on discharge are consistent with the hypothesis of a short-circuited cell in one or more batteries of a three-battery system. They are also consistent with the depressed voltages observed and will occur to some degree whenever there is an imbalance in the states of charge of three undegraded batteries.

A test was conducted to determine the effect of a shorted cell in one of two batteries operating in parallel. A test was conducted to determine the effect of a shorted cell in one of two batteries operating in parallel. Load sharing was evaluated for configurations in which the one-cell discrepancy was compensated by 0, 1, or 2 diodes. Diode compensation modified load sharing in a straightforward and predictable manner. Using 2 diodes (0.5 - 0.6 volts each) to compensate for the single cell difference (~1.2 V) resulted in an average load sharing of 51/49 percent whereas the uncompensated load sharing was 72/28 percent. The results of this test are reported in detail in Appendix 4.

Because only two parallel batteries were used, rather than three, this test must be considered a qualitative confirmation of the shorted cell hypothesis.

4.3.2 Causes of Battery Cell Short-Circuit Failure

Having established with reasonable certainty that the observed phenomena were a result of the occurrence of internal short-circuits in one or more battery cells, an effort was made to determine the causes of the short-circuits.

The following are plausible causes of a high short-circuit incidence in the Satellite 9437/9438 batteries:

- a) A deterioration of the quality of one or more lots of cells or internal cell components
- b) A change in the cell characteristics or in the characteristics of the charge control electronics which causes excessive overcharge stresses to be applied to the cells during the charging process.

Several parallel investigations are currently being conducted, including cell and battery cycling tests, and destructive physical analyses of selected cells. These tests are partially complete as of December 1979. Thus, only partial results are reported herein.

In summary, an examination of the tests which have been conducted indicates that while differences in cell quality from lot to lot have been observed, there is no indication of a connection between the observed differences and a tendency toward increased frequency of occurrence of short-circuited cells.

The results of battery-level cycling tests, on the other hand, suggest strongly that the frequency of occurrence of short-circuits is a direct function of the degree of stress applied to the battery cells by the charge controls.

4.3.2.1 Battery-Level Cycling Tests (Appendix 3)

Comparative tests on two identical batteries show that a reduction in the overcharge voltage (main bus voltage limit) reduces the rate of failures.

Two essentially identical flight-quality batteries (S/N 3-3 and 3-6) were cycled in an attempt to evaluate the effect of a reduced overcharge stress on the rate of failure of the cells.

S/N 3-6 was cycled in as close as possible an approximation of the actual conditions observed in the Satellites 9437 and 9438 batteries. Bus voltage limit was set at 32.4 volts and the SSTS at 77°F (switch-to-trickle).

S/N 3-3 was cycled in the same manner except that the bus voltage limit was set at 31.8 volts and the SSTS at 71°F (switch-to-trickle).

Under these conditions the peak overcharge currents drawn by S/N 3-3 were less than one third those drawn by S/N 3-6. Both batteries displayed a trend toward increasing peak overcharge currents in successive eclipse seasons.

The results of these cycling tests show that S/N 3-3 has shown no anomalous behavior for six successive eclipse seasons.

S/N 3-6 has shown two cell short-circuits occurring in the third season, one of which remained permanent, and one of which apparently cleared itself. Two additional cells exhibited symptoms which appeared to be precursors of a short-circuit. These preshort symptoms are a downward shift of the cell voltage from the average population level, an irregularity in the cell voltage waveform in the initial stages of charge, and a low ramp rise in voltage during the overcharge pulses (see Figure 4-4), instead of the normal rapid exponential rise. One of these cells failed 14 days later. It is not clear at this time whether or not this symptom occurs generally, nor has a method of detecting it in space been devised.

Actual short-circuits showed two clear-cut symptoms: a sudden falloff in cell (and battery) voltage, and a rapid rise in temperature of the battery temperature sensor (if any) nearest the shorted cell. This latter effect was caused by the internal heat dissipation occurring as the cell discharged rapidly through its internal short-circuit.

After completion of the third season, the four defective cells were removed from Battery S/N 3-6 and replaced with new cells. The test was modified to assess the practicability of recharging the battery on trickle charge, and the extent to which cell damage continues to appear after a more benign charging mode is used on an already overstressed battery.

Results obtained during Seasons 4 to 6 are presented in Appendix 3.

Two additional cell anomalies were observed during Battery S/N 3-6, Season 5 operation. However, in both instances the cells exhibited preshort signatures during Season 3. The presence of the signature prior to the change in charge mode is interpreted as evidence that the damage had occurred before the switch to the more benign trickle charge mode. There are no indications of anomalies initiated subsequent to the switch to trickle charge.

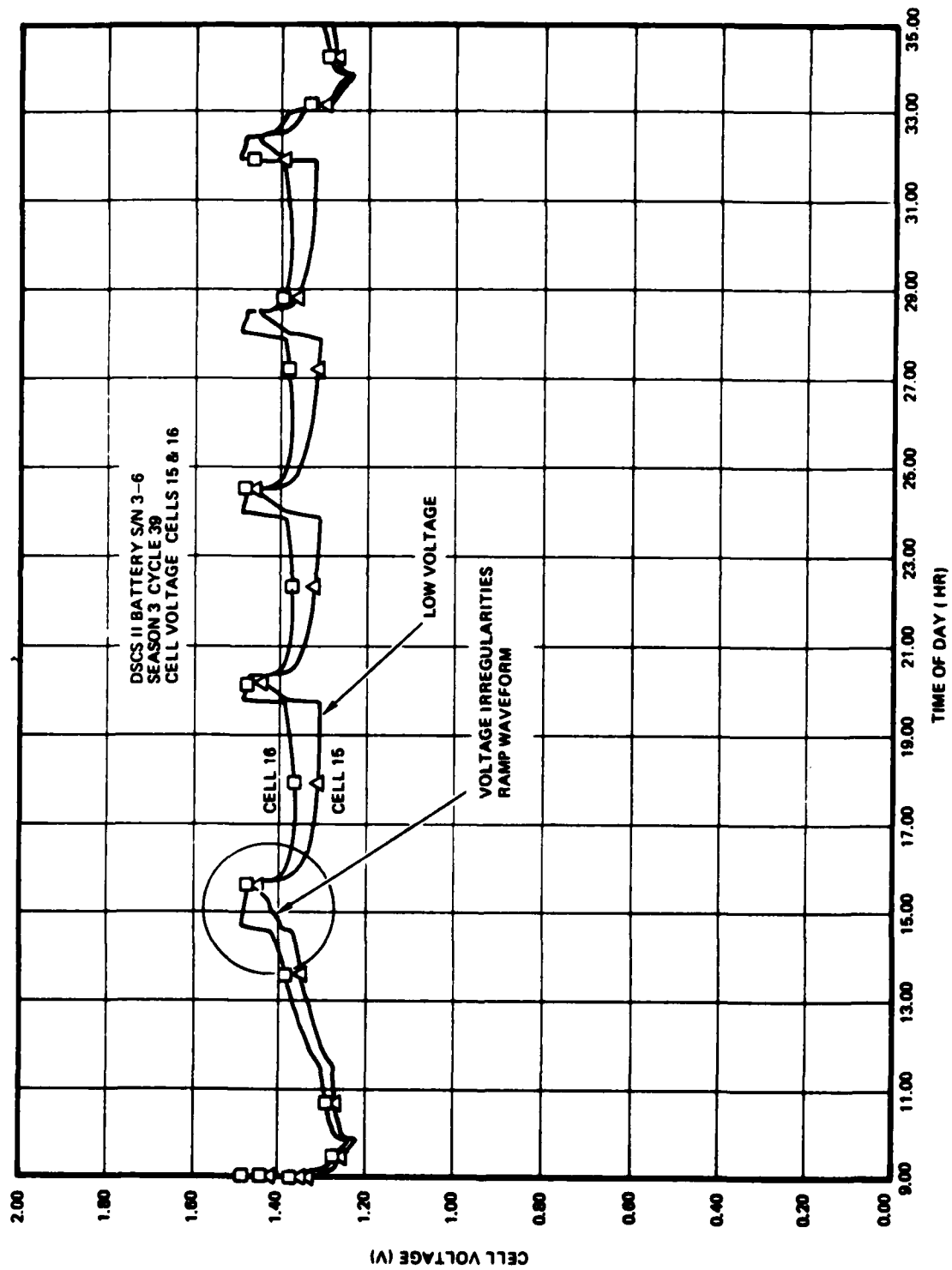


Figure 4-4. Battery S/N 3-6 - Preshort Signature - Cells 15 and 16

The clear disparity between S/N 3-6 and S/N 3-3 test results indicates a direct relationship between overcharge stress and failure incidence.

4.3.2.2 Cell-Level Pulse Overcharge Tests

Two sets of pulse overcharge tests were performed at different levels of overcharge current and time.

Test A - Overcharge at C/6 for 0.333 hour
Trickle charge at C/100 for 0.667 hour

Total input: 0.81 ampere-hour

Test B - Overcharge at C/3.75 for 0.5 hour
Open circuit for 0.5 hour

Total input: 2.0 ampere-hours

Results of these pulse overcharge tests are:

Test A - After 1500 pulses, no indication of cell damage or anomalous behavior was seen

Test B - After 1760 cycles, one cell short-circuit was found. The test was continued to 2760 cycles, without additional failures

No significant conclusions could be drawn from these tests regarding response to the relative severity of the test conditions. The failed cell has been subjected to destructive analysis. DPA procedures and results are reported in Appendix 5.

4.4 VARIATIONS IN CELL CHARACTERISTICS

4.4.1 Gulton versus General Electric Cells

The possibility exists that changes in cell characteristics from earlier to later spacecraft batteries may have contributed to the development of high overcharge currents and consequent excessive stresses in the cells.

The battery cells in use at the time the system was designed were manufactured by Gulton Industries, using electrodes manufactured by SAFT, France. The cells used in Satellites 9437 and 9438 were manufactured entirely by the General Electric Co. Figure 4-5 shows steady-state overcharge characteristics for Gulton cells manufactured during a period

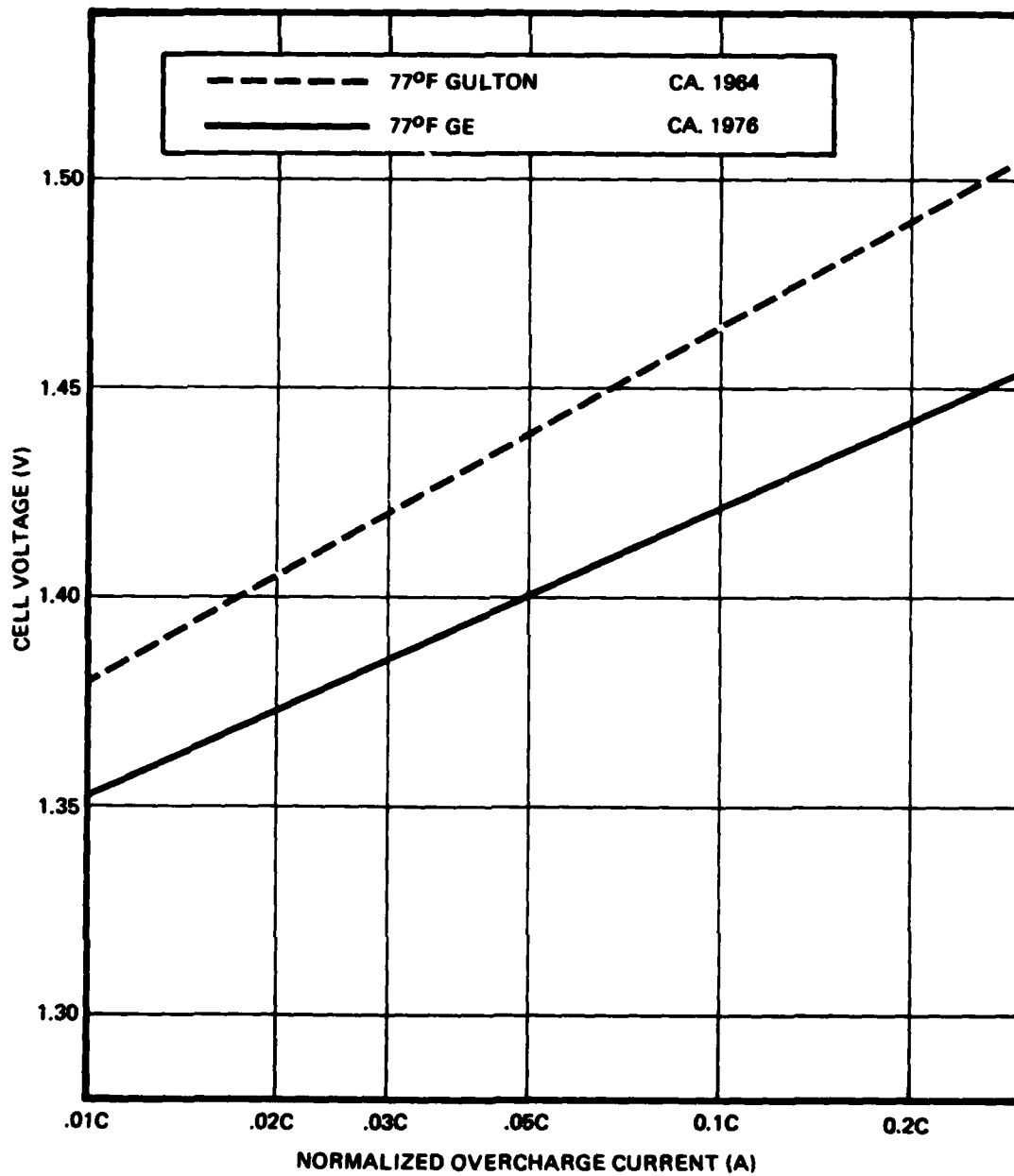


Figure 4-5. Overcharge Voltage versus Overcharge Current

approximately corresponding to the subsystem design and for General Electric cells manufactured during a period approximately corresponding to the purchase of Satellite 9437 and 9438 cells.

The difference between the Gulton and General Electric data (Figure 4-5) indicates that the General Electric cells will draw higher steady-state overcharge currents. The observation that Satellites 9437 and 9438 exhibited higher overcharge currents than previous satellites (containing Gulton cells) is consistent with the data.

However, determination of a specific cause is complicated by several factors:

- a) Peak overcharge currents during battery charge and overcharge pulses are transient phenomena; their relationship to the steady state overcharge current is not well defined.
- b) Differences in operating temperatures of the batteries of earlier satellites from those of Satellites 9437 and 9438 resulted in colder operation of the earlier batteries, and therefore lower peak overcharge currents.

The final result of the above analysis is that the primary cause of the higher overcharge current is not definitely known, if it is indeed higher. A combination of one or more of the following causes may be responsible.

- a) A change from the Gulton to the General Electric cell without a corresponding change in the main bus limit and other charge control parameters
- b) Higher battery operating temperatures in Satellites 9437 and 9438.

4.4.2 Destructive Physical Analysis (DPA) (Appendix 5)

The possibility was considered that a change might have occurred in the quality or structure of the electrode which might make it susceptible to short-circuiting. Two types of tests were performed:

- Destructive physical analysis (DPA) of electrodes selected from various cell lots was performed after long-term storage
- DPA of electrodes selected from various cell lots was performed after the cells were cycled.

DPA studies presently in progress suggest that the primary cause of the cell short-circuits may be related to penetration of the separator by dendrite-like masses of negative plate material.

4.4.2.1 DPA After Long-Term Storage

Several cell lots (including Lot 1, from which the anomalous Satellite 9437/9438 batteries were made) were subjected to destructive physical analysis. A number of observable features were found, including raised black spots, black outcroppings, disruptions in the sintered surface, and bumps. Lot No. 1 showed a higher than usual incidence of raised black spots.

While any or all of the described features could conceivably cause a predisposition to short-circuiting, there is as yet no evidence of such a causal relationship.

4.4.2.2 DPA After Cycling of Electrodes

Electrodes from different cell lots were assembled into experimental packages and cycled under a variety of conditions. The electrodes were examined after cycling to determine the degree of deterioration. Results are summarized in Table 4-1.

Lot 1, which was used in the Satellites 9437/9438 batteries, showed a greater degree of blistering (separation of layers of the sintered electrode from the main electrode mass) than did other lots, which suggests that a weakness in the structure of the sinter may have contributed to the short-circuiting.

However, the conditions of the tests were different from actual cell operating conditions and it is not possible at present to correlate cell performance and test results.

Differences between test and cell conditions are as follows:

- a) The test electrodes are completely submerged in electrolyte, whereas cells are operated with very small amounts of free electrolyte
- b) In actual use electrodes are restrained under compression within the cell, whereas in the tests, the electrodes are totally unrestrained.

Table 4-1. Overcharge Testing of Positive Plates (Visual Results)

Test No. PC-1			
<u>Flights 7 and 8</u>		<u>Flights 11 and 12</u>	
Lot 1	Lot 2	Lot 5	Lot 6
Heavy blisters and shedding	Some blistering in black spots only	Scattered blistering	No visible damage
Test No. PC-2 (Including some plates with visual defects)			
<u>Flights 7 and 8</u>		<u>DSP Plate</u>	
Lot 1	Lot 2	Lot 2	Lot 3
Heavy blisters changed	Bumps not visible	No visible damage	Heavy blistering
Test No. PC-3			
<u>Flights 11 and 12</u>		<u>DSP, from stored cells</u>	
Lot 1	Lot 2	Lot 1	Lot 2
3/4 Plates blistered	1/4 Plates blistered	2/2 Plates badly blistered	2/2 Plates severely blistering and shedding
Test No. CC-1 (GE Overcharge Test)			
<u>Flights 11 and 12</u>		<u>DSP, from stored cells</u>	
Lot 1	Lot 2	Lot 1	Lot 2
3/4 Plates blistered	No visible damage	Dry cell no visible damage	No visible damage

Experience gained with similar tests indicates that the blistering observed in these tests is rarely seen in normal operating cells after cycling under similar electrical test conditions.

4.4.2.3 DPA of a Shorted Cell

In an attempt to determine the mechanism by which short-circuits occur, one cell which had short-circuited in the course of high-stress pulse-overcharge testing was examined by means of a new dissection method. It was hoped that this method would provide additional insight into the shorting process.

The examination was unable to isolate the source of the original short-circuit, which had burned clear at the time of the short. The permanent short-circuit found at the time of the examination is believed to have occurred by the following process:

- a) A short-circuit occurred at or near the center of the electrode stack
- b) The cell discharged through the short-circuit, releasing its stored energy in a small area at the short-circuit, creating very high temperatures at this point
- c) The original short-circuit burned clear
- d) The high temperatures penetrated the electrodes, destroying the separators between the short-circuited electrodes and others adjacent to them in the cell stack, damaging the opposing faces of the electrodes
- e) A second short-circuit occurred between one of the original short-circuited electrodes and an opposing polarity electrode at the electrode surface opposite to that at which the original short-circuit occurred
- f) Insufficient energy was left in the cell to burn the second short-circuit clear, and it remained.

4.5 INVESTIGATIONS RESULTING IN THE ELIMINATION OF OTHER PLAUSIBLE CAUSES OF FAILURE

Prior to fixing upon the presence of short-circuited cells in the batteries, other hypotheses were sought as plausible explanations of the observed phenomena. Among these were:

- a) A possible failure of the thermal control system to maintain battery temperatures

- b) A failure of the charge controls to switch to trickle charge at the proper temperature, due either to failure of the SSTS or the K1 relay control circuit
- c) A failure of the heater switch to control battery temperature properly.

Investigations of each of the above possible causes were conducted with negative results. In each case the observed phenomena were not explainable in terms of a credible failure mechanism.

4.5.1 Thermal Characteristics

The possibility of deterioration in the thermal characteristics of the spacecraft was examined. No discernible variation in temperature other than batteries was observed. A detailed analysis, the results of which are reported in Appendix 7, led to the conclusion that no such thermal deterioration occurred. An analysis was also performed to determine the impact of increasing the radiator area of Battery 3 to reduce its temperature. This was temporarily abandoned when other battery short-circuits were observed.

4.5.2 Charge Control Failure

The possibility that a defective SSTS might have failed to open the K1 relay, or that a drift in SSTS operating temperature might have delayed operation of the K1 relay was considered. Several investigations were performed.

A complete failure modes and effects analysis was conducted on the SSTS, and may be found in Appendix 6. The result of this analysis was that there was no credible component failure or degradation mode which could reproduce the observed combination of the phenomena. A review was conducted of orbital data, which failed to find any instance of failure of the K1 relays to cycle.

4.5.3 Battery Heater Switch Operation

Analysis of the heater switch operation revealed that the apparently anomalous switching temperatures represent "normal" switch behavior given the thermal gradients across and within the battery during the period of anomalous performance.

The battery heater thermostats are snap-action switches actuated by a temperature-sensitive, bi-metallic disc. Anomalous heating and cooling rates can cause the thermostatic switch to close electrically but not snap mechanically into the closed position. The absence of the snap-action can result in a return to the previous position at a temperature different than anticipated. This behavior represents the response of a normal switch to an unanticipated thermal pattern.

Thus, the apparent shifts in the temperature settings are problems of interpretation of telemetry data and not thermal switch malfunction.

5. CORRECTIVE ACTION

5.1 SATELLITES 9437 AND 9438

Corrective action for Satellites 9437 and 9438 has taken the form of ground command control of the battery charge and discharge functions so as to minimize the stresses imposed upon the batteries.

5.1.1 Control of Load Sharing

The design of the power system permits the batteries to be discharged through three paths:

- A direct connection to the main power distribution bus (direct discharge)
- connection to the bus through a single diode (trickle charge mode)
- connection to the bus through two series-connected diodes (minitrickle mode)

Where one or more of the batteries has a shorted cell, and consequently a lower discharge voltage, it is possible to balance the load sharing by connecting the defective battery directly to the distribution bus, and the higher voltage good battery to the bus through one or two series-connected diodes. Under most circumstances this is sufficient to bring the system into satisfactory load-current balance.

Further control of the load sharing may be achieved by time-sharing the discharge, i.e., by allowing a battery to discharge at high rate directly to the bus for a period of time less than the total eclipse period, and then reducing its contribution by switching it to minitrickle, thereby forcing it to discharge through two diodes.

5.1.2 Control of Recharge Fraction and Recharge Rate

Several methods are available for the control of recharge fraction and recharge rate:

- a) Switch the battery to full charge and monitor until a rise in battery temperature signals that the end-of-charge is approaching; switch to trickle charge

- b) Switch the battery to full charge and integrate the charge current input until the ampere-hour input equals from 108 percent to 115 percent of the ampere-hour output on the prior discharge; switch to trickle charge.
- c) Command the bus to the high voltage limit of 33.4 volts and allow the battery to charge at the trickle rate determined by this bus voltage and the trickle charging resistance.

Of the three methods of recharge control, Method b is the least attractive, since it requires monitoring of the satellite during the entire charge period, so that the current can be integrated. Method a permits computation of the estimated time at which the batteries will return to the full-charge level, at which point a monitoring pass can be scheduled. However, since the batteries are imbalanced in discharge and charge rates, the three batteries will not reach full charge at the same time, and the length of the monitoring pass is extended, although shorter than that of Method b.

Method c requires no monitoring of recharge at all, but presents the risk that the batteries may not return to the fully charged state at the end of each daylight period of the eclipse season. However, it is possible to detect this by a fall in end-of-discharge voltage, and to restore full charge by reverting to Method a or Method b for a single orbit. In practice, however, Method c has provided adequate charge and it has not been found necessary to revert to Method a or b.

All of the above methods of load sharing and charging controls have been used at times in the latter part of Season 3, and in Season 4, as well as during aunar eclipse. Method c is now being used routinely in most eclipse orbits.

5.2 SATELLITES 9441 AND 9442

The "normal" main bus voltage limit was changed from 32.4 ± 0.2 Vdc to 31.8 ± 0.2 Vdc. This was accomplished by readjusting three potentiometers in each power control unit (PCU) accessible from outside the PCU. It was not necessary to open the PCU. After this was done, the "high" main bus voltage correspondingly changed from 33.4 ± 0.2 Vdc to 32.8 ± 0.2 Vdc. This change reduced the overcharge current into the battery by reducing the applied voltage.

The battery solid state thermal switch (SSTS) full/trickle switch points were changed from 70/77 to 64/71°F. This requires readjusting one potentiometer on each battery SSTS assembly, accessible without disassembly of the battery. This change reduces the duration and peak level of the overcharge current and consequent overcharge stress.

The radiator area under Battery 3 was increased from 90 square inches to 108 square inches. This provides the same radiating area as Batteries 1 and 2. This was accomplished by peeling back a controlled amount of thermal blanket insulation. This change also reduces battery operating temperature and, consequently, overcharge current and stress. Because of the difference in internal heat flow to Battery 3 (as compared with Batteries 1 and 2), Battery 3 tends to operate cooler than either Battery 1 or 2 during the solstice season.

5.3 SATELLITE 9443 AND ALL SUBSEQUENT SPACECRAFT

In this version of corrective action, the charge control circuitry has been redesigned to permit the use of charging modes more compatible with the General Electric cells. The new circuits provide greater flexibility of operation, including the capability to charge the batteries without excessive stressing of the cells in spite of the existence of a shorted cell. The following changes were made:

- a) The lower commandable bus voltage limit was reduced from 32.4 to 31.6 V
- b) The upper commandable voltage limit was raised from 33.4 to 33.8 V
- c) A 3.1 ohm resistance was inserted into the full charge path of the charge control circuit, with the capability of being bypassed by command if desired
- d) The trickle charge resistor was increased from 7 to 20 ohms
- e) The minitrickle resistor was eliminated. If the battery reaches the 95°F disconnect temperature, it is disconnected from the charging line altogether, although it may still be discharged through two series-connected diodes
- f) The SSTS operating temperature was reduced from 77 to 71°F
- g) The Battery 3 radiator mirror area was increased from 90 to 108 square inches.

Figure 5-1 is a block diagram of the revised charge control circuit, which provides a greater degree of flexibility than does the original charge control. Three charging modes are now available:

- Direct charge from the main bus
- Charge through a 3.1 ohm current-limiting resistor
- Charge through a 20 ohm minitrickle charging resistor.

Each of these charging modes may be used either with the low bus voltage of 31.6 V or with the high bus voltage of 33.8 V.

The resistance values and voltages were selected as a result of a detailed boundary conditions analysis, in which the effects of bus voltage, current, resistance, battery voltage and temperature were studied parametrically to determine a set of safe operating regions for batteries with 22 normal cells, and with 21 operational cells and one shorted cell. This report will be found in Appendix 8.

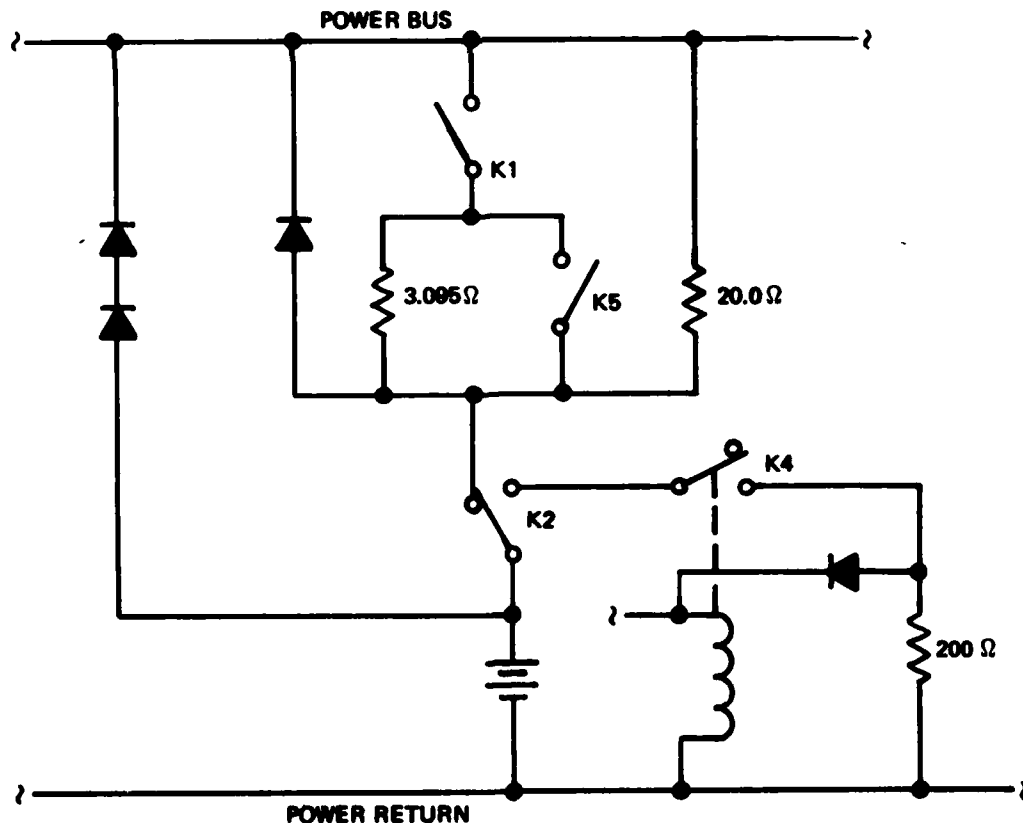


Figure 5-1. Revised Charge Control Circuit

The direct connection relay (K5) has been included in the change to provide additional flexibility in meeting unusual conditions which could occur during a satellite mission. The additional capability and flexibility provided by the K5 relay are as follows:

- a) Rapid recharge capability before and/or after a lunar eclipse which occurs between two successive earth eclipses
- b) More effective management of discharge load sharing with unequal batteries by providing a selectable direct connection path to the main bus
- c) Effective use of the low bus voltage setting to accomplish recharge of batteries if overall system considerations required operation of the satellite at the low bus voltage setting
- d) Increased ability to accommodate unexpected long term increases in battery voltage.

To make use of these capabilities, a lower bus voltage must be selected which is compatible with a direct connection between the battery and the main bus during charging and overcharging periods. This bus voltage has been selected to be in an acceptable overcharge operating region for a 22-cell battery with K5 closed, although it results in a smaller recharge taper current at end-of-mission, the acceptability of which has not been fully demonstrated by long-term operation. The selected value of 31.6 V also provides acceptable overcharge control of a battery with a shorted cell with K5 relay open.

One additional factor which influenced this selection was the power budget situation for end-of-mission winter solstice. The solar array margin under worst case predictions for winter solstice is approximately 10 watts for a 33.8 V bus. The existence of the commandable bus voltage of 31.6 V allows the margin to be increased to approximately 35 watts to accommodate limited load faults which may have occurred during the 5 year mission. Maintenance of the batteries under these conditions could be accomplished by selected periods of auto mode charging during the period when the bus is at the low value. In summer solstice high bus operation is preferable since this is the point when the solar array output is maximum.

The SSTS switch-to-trickle temperature has been reduced to 71°F in order to limit overcharge currents in the battery to below the desired 1.6 amps.

The thermal radiator under Battery 3 has been increased in size to 108 square inches to equalize the heat rejection capability for all three batteries. Table 5-1 shows the Flight 13-16 battery heat rejection capability during equinox season.

Table 5-1. Battery Heat Rejection Capability

Battery No.	Predicted Heat Rejection Capability (Watts)					
	Beginning-of-Mission			End-of-Mission		
	50°F	70°F	90°F	50°F	70°F	90°F
A	2.5	12.4	23.0	0.7	10.6	21.3
B	4.0	13.2	23.1	2.4	11.6	21.5
C	3.0	13.0	23.9	1.2	11.2	22.1

APPENDIX 1

POWER SUBSYSTEM DESIGN DESCRIPTION

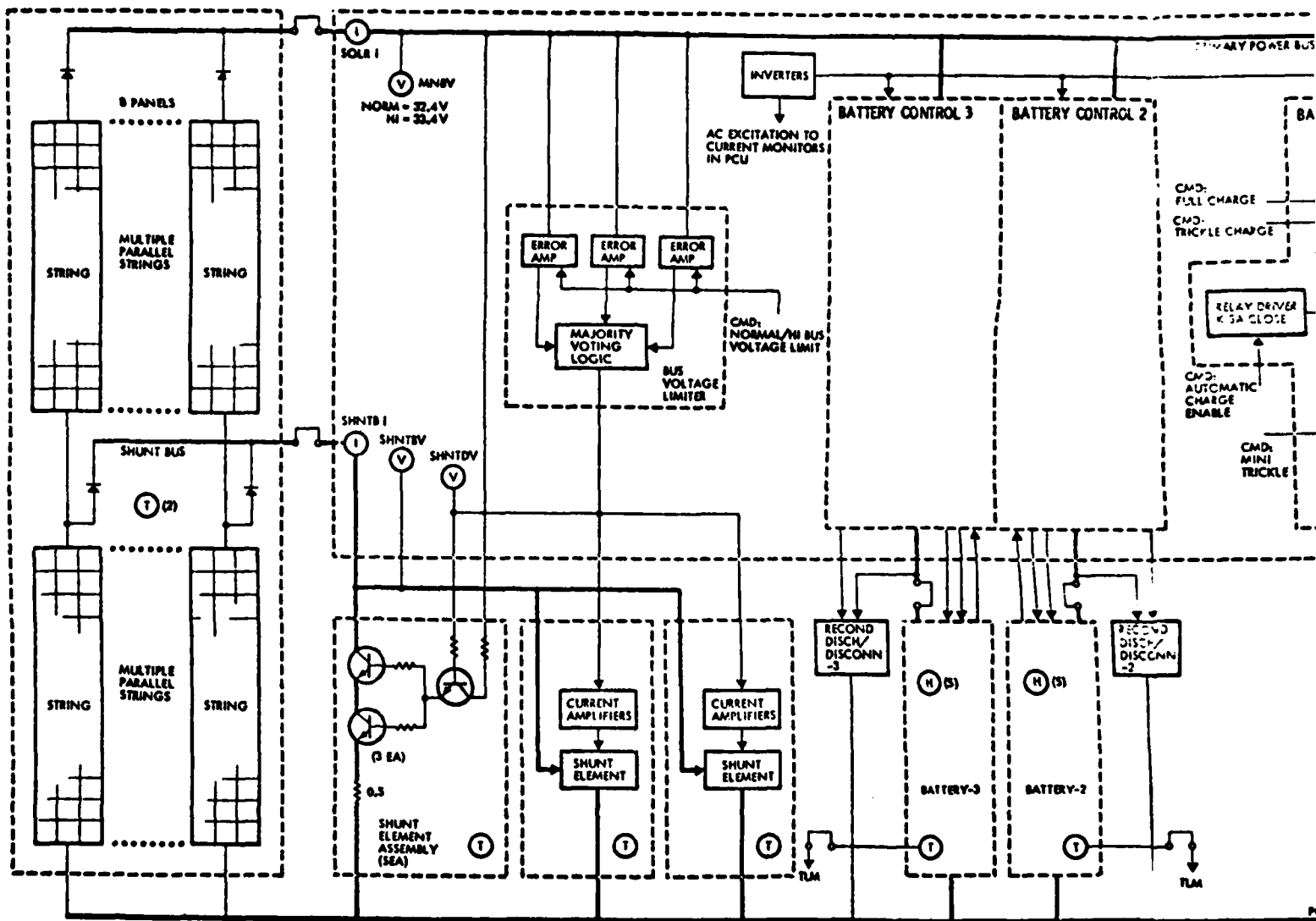
1. POWER SUBSYSTEM

This section provides tutorial material necessary for a clear understanding of the operation of the electric power subsystem and its interactions with other subsystems and its environment. It is intended for use by those previously unfamiliar with the DSCS II power subsystem.

The DSCS II power subsystem is of the unregulated bus direct energy transfer (DET) type, delivering power directly from illuminated solar arrays to the load without intervening loss elements other than distribution cabling. Figure A1-1 shows a simplified functional block diagram of the power subsystem.

Of the total power delivered by the solar array, part is accepted by the loads, and the remainder is available for battery charging through the battery controls. If the power delivered by the solar array exceeds that which can be used by both the loads and the charging batteries (as evidenced by a rise in bus voltage above a preset limit), the bus voltage limiting circuitry turns on the shunt, and varies its conductivity to maintain the bus voltage at the limiting value. If the bus voltage falls below the limiting value, the shunt is turned off.

If, at any time, the load power demand exceeds the output power of the solar array (due either to a load increase or to eclipsing of the spacecraft), the battery controls reconfigure the power subsystem for battery discharge, and the loads are supplied by the batteries or are shared between the batteries and solar array.



1

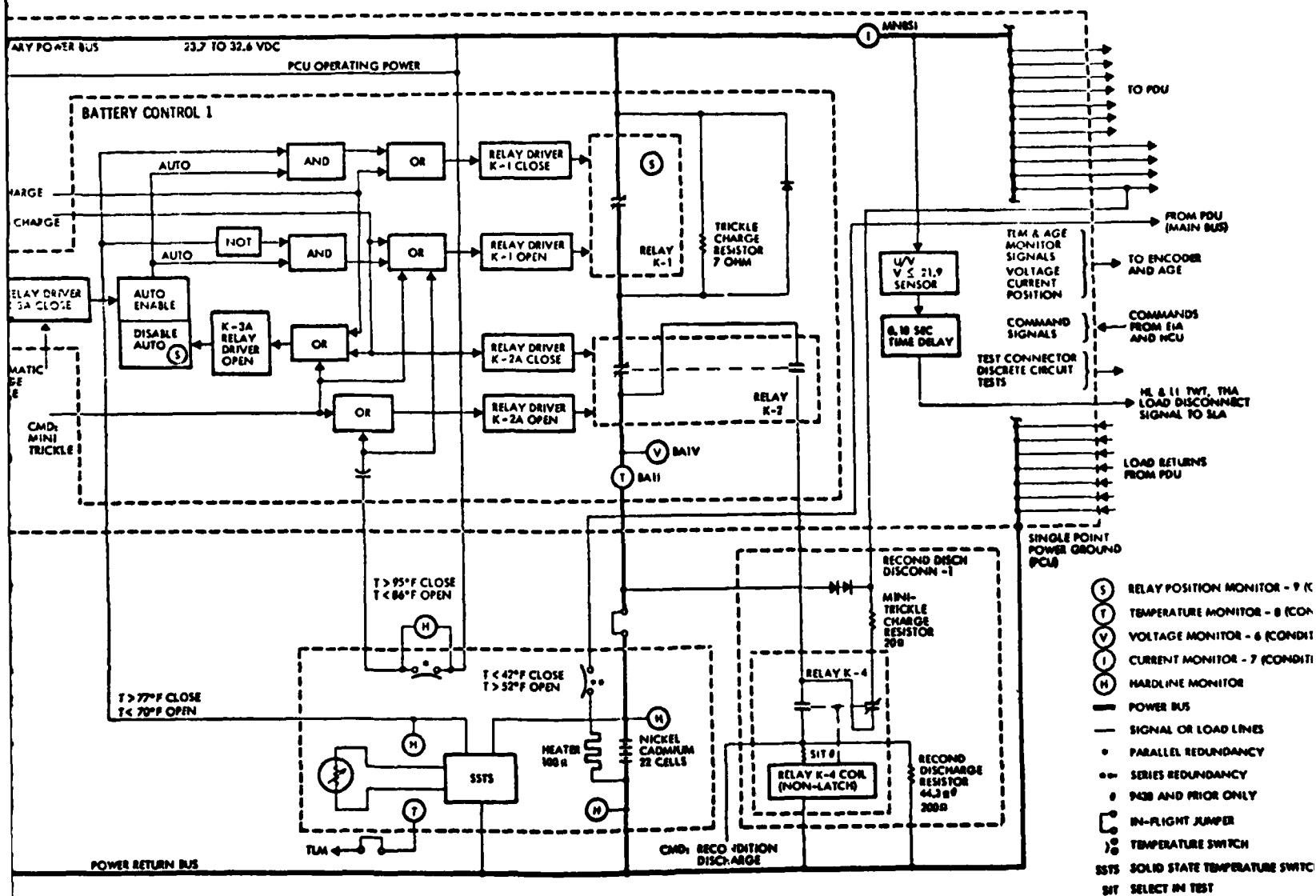


Figure A1-1. Primary Block I

REVISION A
31 OCTOBER 1977

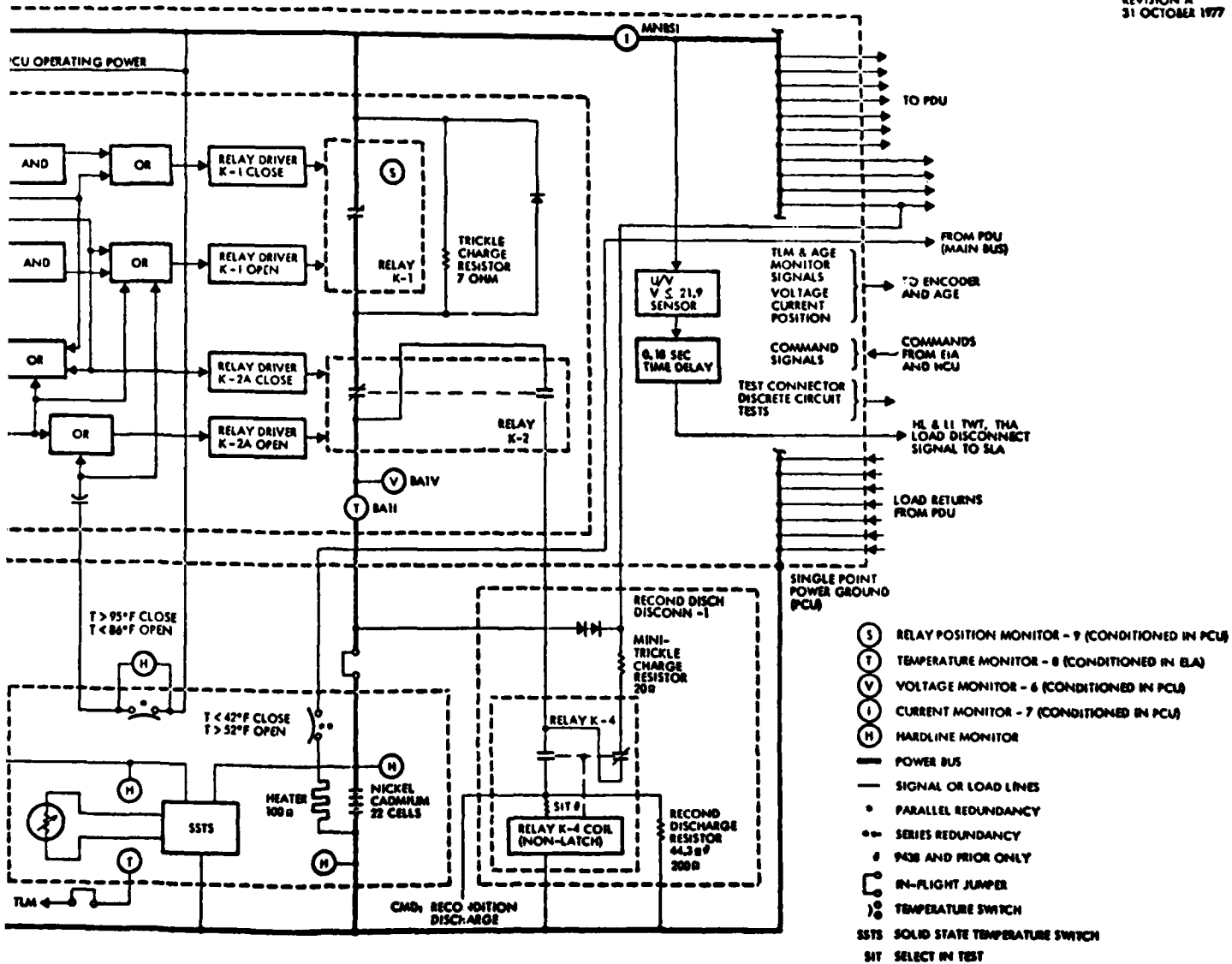


Figure A1-1. Primary Power Block Diagram

2. BATTERY

2.1 DESCRIPTION

Three 12 Ah sealed cell nickel-cadmium batteries are connected in parallel to the primary bus through independent control circuits. They provide power to the electrical loads when the loads exceed solar array output capability, during launch, prior to separation and spinup, and during earth and lunar eclipses. They also assist in smoothing distribution bus transients.

Each battery assembly consists of the following major components shown in Figure A1-2.

- a) Twenty-two series-connected cells in an aluminum restraining structure.
- b) A solid-state temperature switch (SSTS) which provides a two-state output signal to the power control unit (PCU). This is used as the primary battery charge control sensor.
- c) Two parallel mechanical thermal switches which provide a backup control signal to the PCU in the event of battery over-temperature. If the battery temperature exceeds $95 \pm 3^\circ\text{F}$, the K2 relay opens, placing the battery in a minitrickle charge mode which allows it to cool to normal levels.
- d) Heater strips, rated at 98 ohms, are mounted in the battery baseplates and are controlled by two-series connected mechanical thermal switches set to turn the heaters on at $42 \pm 3^\circ\text{F}$, and off at $52 \pm 3^\circ\text{F}$. The heaters operate at slightly over 10 watts at the bus voltage limit of 32.4 V.

2.2 BATTERY HEAT DISSIPATION AND EFFICIENCY

Batteries, like all electrochemical storage devices, generate heat during operation. This heat has two sources: IR loss, at a rate equal to the product of the current and voltage drop; thermodynamic heat, at a rate equal to the product of the current, the entropy change, and the absolute temperature. In the case of the nickel-cadmium cell, the IR losses and the thermodynamic heat are additive on discharge, and are subtractive on charge. The net result is that on discharge, the cell dissipates more heat than can be accounted for by the product of current and voltage drop, whereas on charge, the heat generated is far less. In some circumstances,

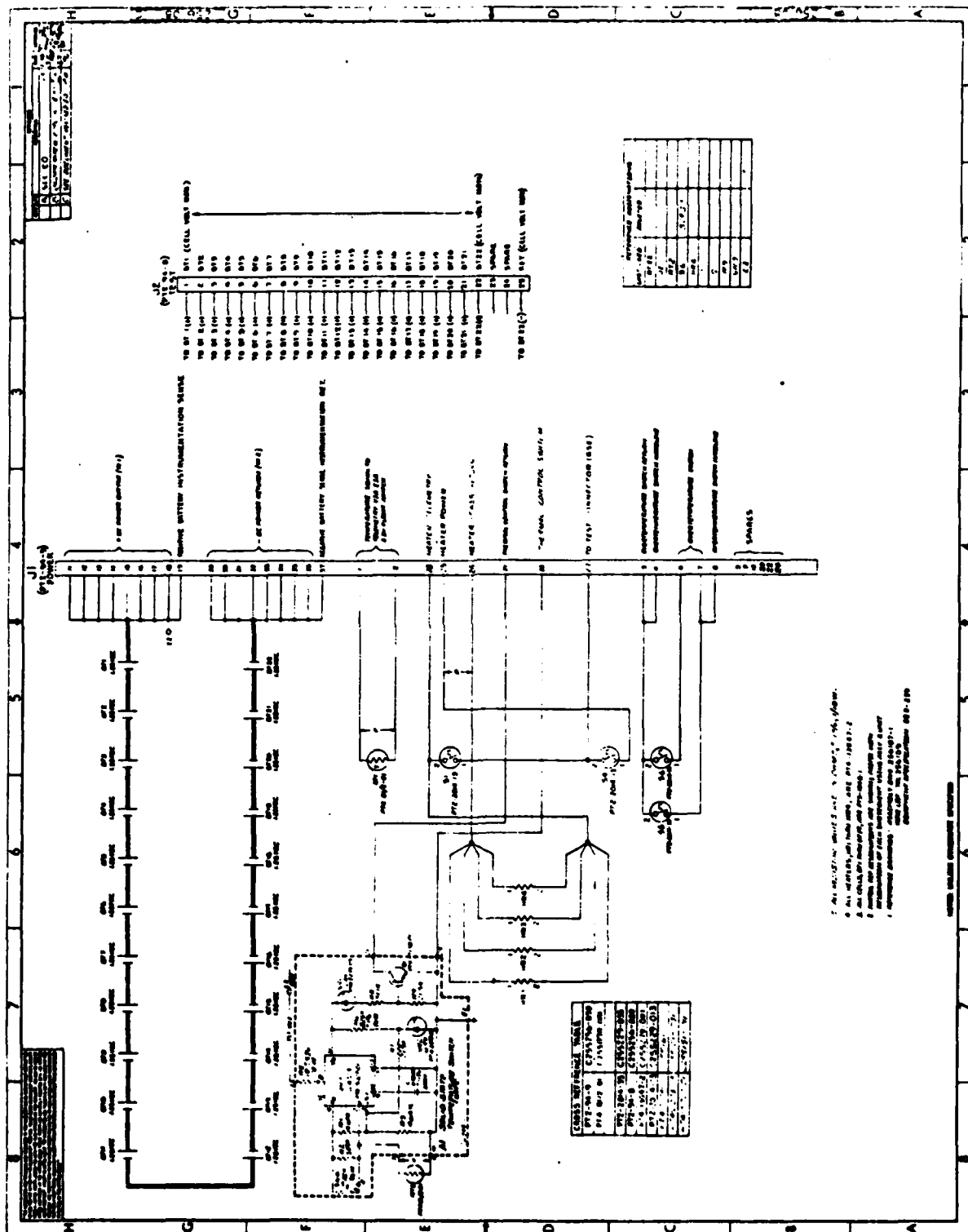


Figure A1-2. Battery Schematic Diagram

the batteries may absorb heat from their surroundings, growing cooler as they are charged. The nickel-cadmium cell is thus described as being endothermic on charge.

If charging power is forced through a sealed nickel-cadmium cell which is fully charged, a chemical overcharge reaction different from the normal charge-discharge reaction occurs which results in the total over-charge being dissipated in the cell as heat.

The ampere-hour efficiency on charge may be viewed as the ratio of the current being used in the charging reaction to the total charge current being forced through the cell, the remainder being used in overcharge reaction. On discharge, the ampere-hour efficiency of the nickel-cadmium cell is unity, or 100 percent.

Ampere-hour charging efficiency varies as a function of the state-of-charge of the cell or battery, approaching unity when the cell is nearly discharged, and up to a state-of-charge of about 80 percent of the total capacity of the cell. Beyond this point, the rate of the overcharge reaction becomes significant, and the efficiency falls exponentially until, at a state-of-charge approaching 100 percent, the overcharge reaction consumes virtually all of the current through the cell, and the charge efficiency is zero.

Ampere-hour efficiency also varies nonlinearly as a function of charging current and temperature, increasing with increasing current, and decreasing with increasing temperature.

2.3 BATTERY TRICKLE CHARGE AND SELF-DISCHARGE

Nickel-cadmium cells standing charged on open-circuit tend to self-discharge, losing part of their stored energy. The rate of loss increases with increasing temperature. To prevent this, nickel-cadmium batteries are usually maintained on trickle charge, a small charging current whose magnitude may vary from $C/100$ to $C/40$ (depending upon temperature), where C is the rated capacity of the cell in ampere-hours.

3. BATTERY CONTROLS

3.1 DESCRIPTION

Each of the three batteries is connected to the main power distribution bus through an independent set of controls whose functions are the control of battery charge and discharge, protection of the battery from catastrophic destruction in the event of internal battery failures or failures of the control circuitry, and provision for reconditioning of the battery so as to extend its longevity at high performance. Figure A1-2 shows a simplified diagram of the battery and its control circuitry. Figure A1-3 and Table A1-1 summarize the logic relationships for battery control operation.

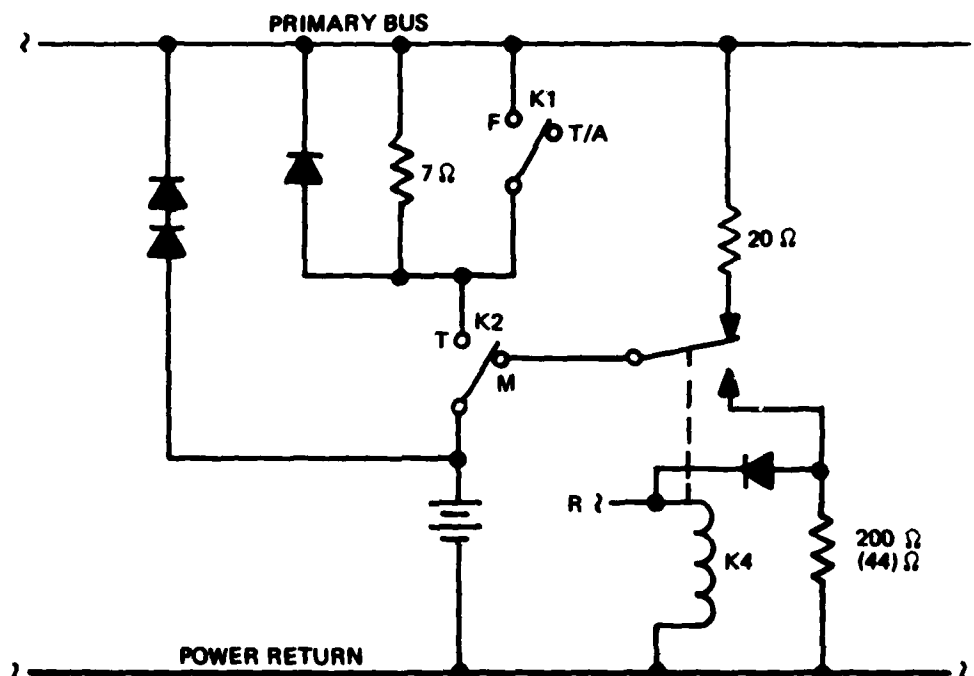
Several different functions are implemented. These are:

- a) Main Bus Voltage Limiting - As current is forced into a secondary battery to recharge it, an opposing electromotive force (voltage) is generated in the battery, increasing with battery state of charge. This increases the voltage required to drive the current into the battery. If the charging voltage of the battery is limited, the increasing opposing electromotive force results in a decrease in the current which the battery will accept at the limited voltage. This is the taper charging region of the charge control scheme, which occurs during the voltage limited portion of the charge cycle.

Because of the internal heat generated in the battery at the end of charge, and the negative temperature coefficient of the back-electromotive force, a simple voltage limiting scheme loses control of the battery after a period of time, and the battery enters the thermal runaway mode. Figure A1-4 illustrates the taper charging and thermal runaway conditions.

- b) In the DSCS II Satellite, when the battery temperature reaches 77°F, the battery is assumed to be in thermal runaway, and relay K1 is opened, interposing a resistance between the main power distribution bus and the battery, and limiting battery charging current to a value between 0.25 and 0.35 amperes. This terminates the thermal runaway process by allowing the battery to cool.

When the temperature of the battery falls to 70°F, the SSTS causes the K1 relay to close, reconnects the battery to the main distribution bus, and restores the battery to the high current charging mode. The battery then limit-cycles between



K1 RELAY: F = FULL CHARGE, MANUAL COMMAND; OR
AUTO MODE WITH SSTs <84°F (70°F)

T/A = TRICKLE CHARGE, MANUAL COMMAND; OR
AUTO MODE WITH SSTs >71°F (77°F)

K2 RELAY: T = TRICKLE CHARGE, MANUAL COMMAND
M = MINITRICKLE CHARGE, MANUAL COMMAND OR
BATTERY OVER-TEMPERATURE SWITCH >95°F

K4 RELAY: R = RECONDITIONING DISCHARGE, MANUAL COMMAND.

Figure A1-3. Battery Control 9437-9442

Table A1-1. Battery Control Logic Equation

Relay K1

Open = Trickle Charge/Diode Discharge
 Close = Full Charge/Direct Discharge

$$K1 \text{ (Open)} = [(T_{Batt} > 77 \text{ degrees F}) \cdot (\text{Automatic-Enable})] \\ + [\underline{\text{CMD}}: \text{Trickle Charge}] + [\underline{\text{CMD}}: \text{Minitrickle}] \\ + [T_{Batt} > 95 \text{ degrees F}]^*$$

$$K1 \text{ (Close)} = [(T_{Batt} < 70 \text{ degrees F}) \cdot (\text{Automatic-Enable})] \\ + [\underline{\text{CMD}}: \text{Full Charge}]$$

Relay K2

Open = Minitrickle Charge/Series Diode Discharge
 Close = Trickle Charge/Diode Discharge

$$K2 \text{ (Open)} = [T_{Batt} > 95 \text{ degrees F}]^* + [\underline{\text{CMD}}: \text{Minitrickle}]$$

$$K2 \text{ (Close)} = [\underline{\text{CMD}}: \text{Trickle Charge}]$$

Relay K3

Open = Automatic-Disable
 Close = Automatic-Enable

$$K3 \text{ (Open)} = [\underline{\text{CMD}}: \text{Trickle Charge}] + [\underline{\text{CMD}}: \text{Full Charge}] \\ + [\underline{\text{CMD}}: \text{Minitrickle}]$$

$$K3 \text{ (Close)} = [\underline{\text{CMD}}: \text{Automatic-Enable}]$$

Relay K4

Open = Minitrickle Charge
 Close = Recondition Discharge

$$K4 \text{ (Open)} = [K2 \text{ (Close)}] + (V_{Batt} < \sim 2 \text{ to } 7V)^{**}$$

$$K4 \text{ (Close)} = [(\underline{\text{CMD}}: \text{Recondition Discharge})] \cdot (V_{Batt} > \sim 2 \text{ to } 7 \text{ volts}).^{**}$$

(K2 Open)

* AC coupled
 ** 20V, 9438 and prior only.

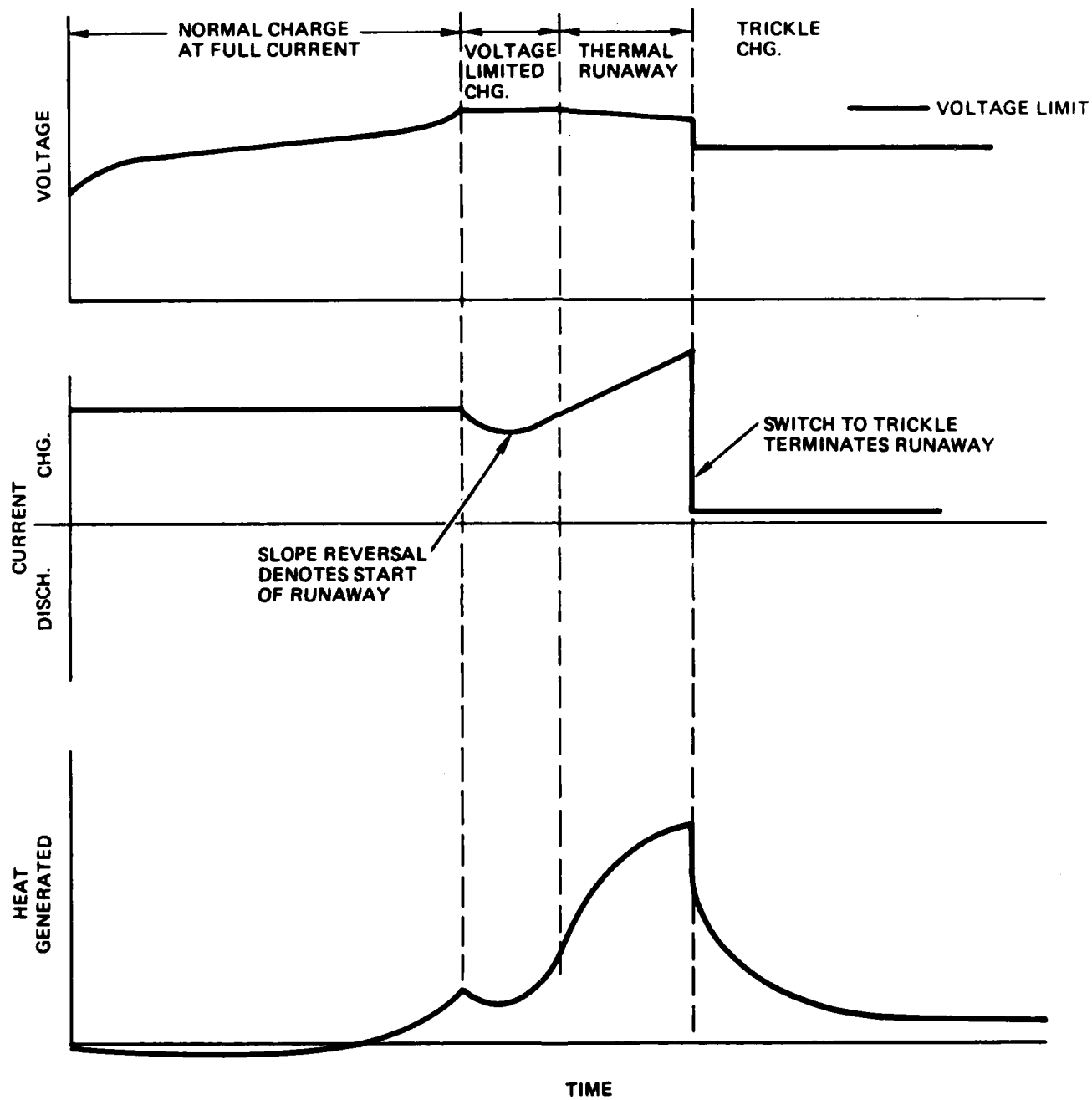


Figure A1-4. Taper Charge - Thermal Runaway Illustration

70° and 77°F (measured at the SSTS) as long as the solar arrays remain illuminated. Internal battery temperatures may reach considerably higher levels due to two factors:

- 1) Resistance to heat flow from interior to exterior
- 2) Delays in the generation of sensible heat due to temporary storage of the heat energy as chemical energy. This causes battery temperature to overshoot, i.e., climb above the SSTS trip point.

Should the spacecraft enter the eclipse period while the K1 relay of any battery is open, that battery will discharge through the discharge diode until the relay closes.

- c) Overtemperature Battery Disconnect (Minitrickle Mode) - Should the battery temperature exceed 95°F, as measured by the battery overtemperature thermostatic switches, the K2 relay opens, placing the battery in the minitrickle mode. The battery charge current is limited by a larger resistor to a very small current. Battery discharge can occur only through two series-connected diodes. The minitrickle mode is designed to permit partial use of the battery in the event of a failure in the primary charge control circuitry.
- d) Battery Reconditioning - If the K2 relay is placed in the minitrickle position, and the K4 relay is closed, the battery is discharged through the reconditioning resistor for the purpose of restoring the battery to its original condition by deep discharge and recharge.

3.3 BATTERY AND BATTERY CONTROL INTERACTIONS

Because of the independence of the battery control channels, and because they are connected in parallel, imbalances in current distribution between the batteries both on charge and on discharge are inherent in the design of this power subsystem. These are best illustrated by Figure A1-5, which is the output of a computer model* of the power subsystem of a DSCS II spacecraft in the normal midequinox operating mode. From top to bottom, this figure shows the currents of Batteries 1, 2, and 3, and the total current through the three batteries.

At the left-hand side of the chart, at 32 hours (during the second orbit of the run), two of the three batteries show the end of a typical

*A computer model is used because of the fine data resolution and clarity of presentation.

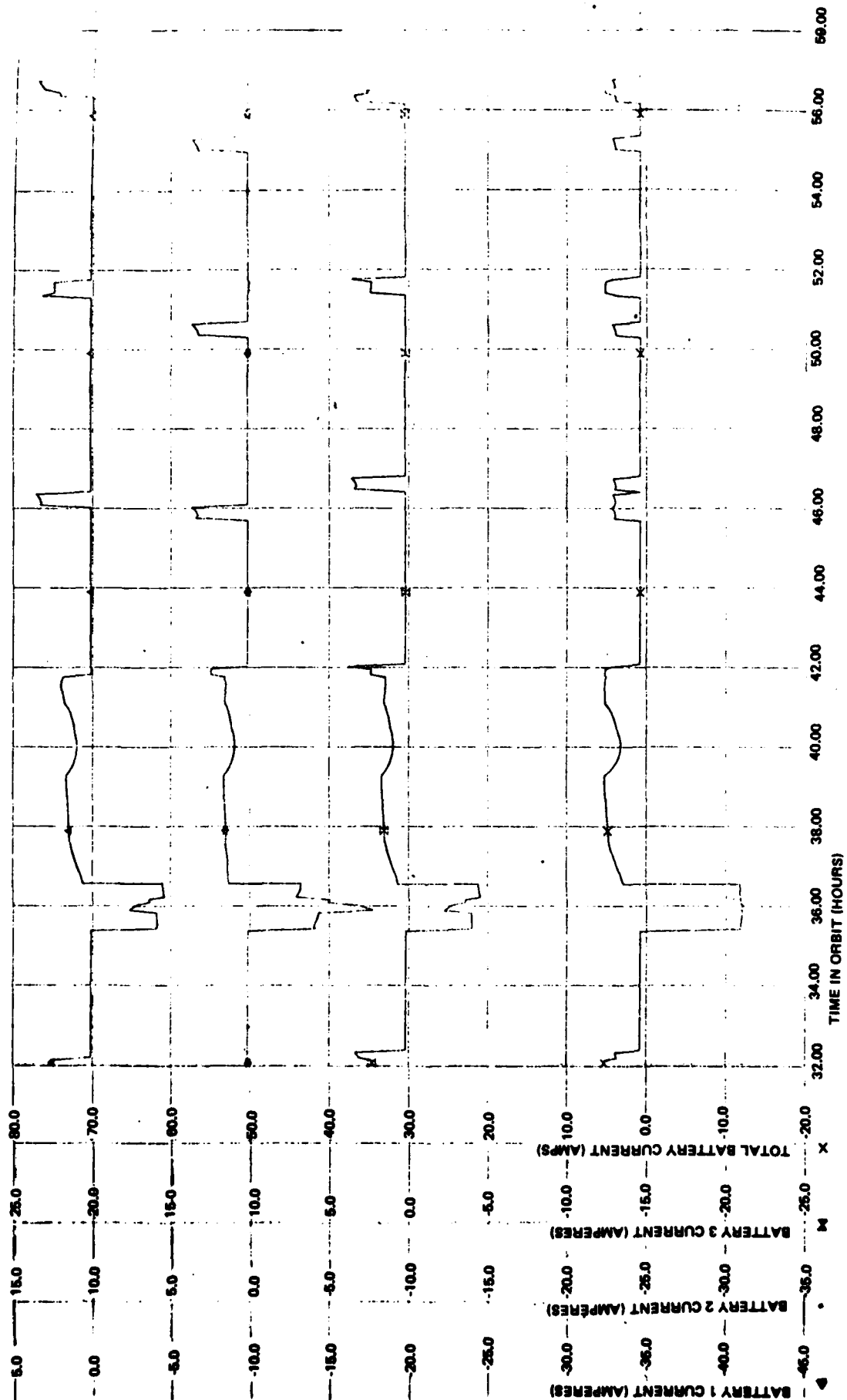


Figure A1-6. Battery Charge Control Interactions

pulse-charging signature, after which the three batteries enter into eclipse with the K1 relay open, drawing approximately equal discharge currents. Just prior to 36 hours, the Channel 2 K1 relay closes, eliminating the diode from the Battery 2 discharge path. Battery 2 discharge current increases (in the negative direction), and since the load requirements are constant, the discharge currents of Batteries 2 and 3 decrease accordingly. Because Battery 2 is being depleted more rapidly than the others, its current output falls from the initial surge, accompanied by a rise in the output of Batteries 1 and 3. After a few minutes, Batteries 1 and 3 K1 relays close simultaneously (within the resolution of the computer model) causing a decrease in Battery 2 current, and a sharp rise in Battery 2 and 3 currents. The eclipse ends shortly thereafter.

The three batteries share charging current at the end of eclipse. Battery 2, which was more extensively depleted than the others, initially accepted slightly more charge than the others. Just after 39 hours, the main bus voltage reached the voltage limit, causing the shunt to operate reducing the total current available for charging the batteries. As the batteries increase in state-of-charge, the current accepted by each of the three batteries decreases, until, at approximately 40 hours, decreased battery charging efficiency and increased battery temperature cause a reversal of this effect, and the battery currents begin to rise slowly. At approximately 41 hours, the shunt has ceased to operate and the batteries are charging at full solar array rate, sharing current equally.

The heat generated during high rate overcharging at end of charge increases battery temperature. Shortly before 42 hours, the SSTS causes the Battery K1 relay to open, placing a resistance into the Battery 1 charging path, and decreasing Battery 1 current to the trickle level. The available solar array current is then diverted to batteries 2 and 3, which show a rise in charge current. At 42 hours, the Battery 2 K1 relay opens, and all the charging current available is diverted to Battery 3. This surge of current causes Battery 3 to heat, and the K1 relay to open quickly, leaving the three batteries on trickle charge.

For the remainder of the daylight period of the orbit, each of the batteries cycles independently between full charge to trickle charge. Where the relays operate simultaneously, signatures similar to those

described above are found. Where relay operation is not simultaneous, the full available charging current is forced into a single battery.

APPENDIX 2

BRANCH CURRENT ANOMALY

APPENDIX 2
BRANCH CURRENT ANOMALY

The current sensors used in Satellites 9437 and 9438 power subsystem are of the biased saturable reactor type, having an output voltage versus current characteristic as shown in Figure A2-1. The design operating range of the sensor is from -7 amperes (discharge) to +3 amperes (charge). At discharge currents beyond -7 amperes, however the output voltage of the sensor is not single-valued and can be interpreted as either of two current values. The imbalance in battery currents caused by the existence of short-circuited cells caused a misinterpretation of the current sensor output. A 1 V (50 telemetry counts) output was interpreted as -5 amperes when it actually should have been interpreted as -9 amperes.

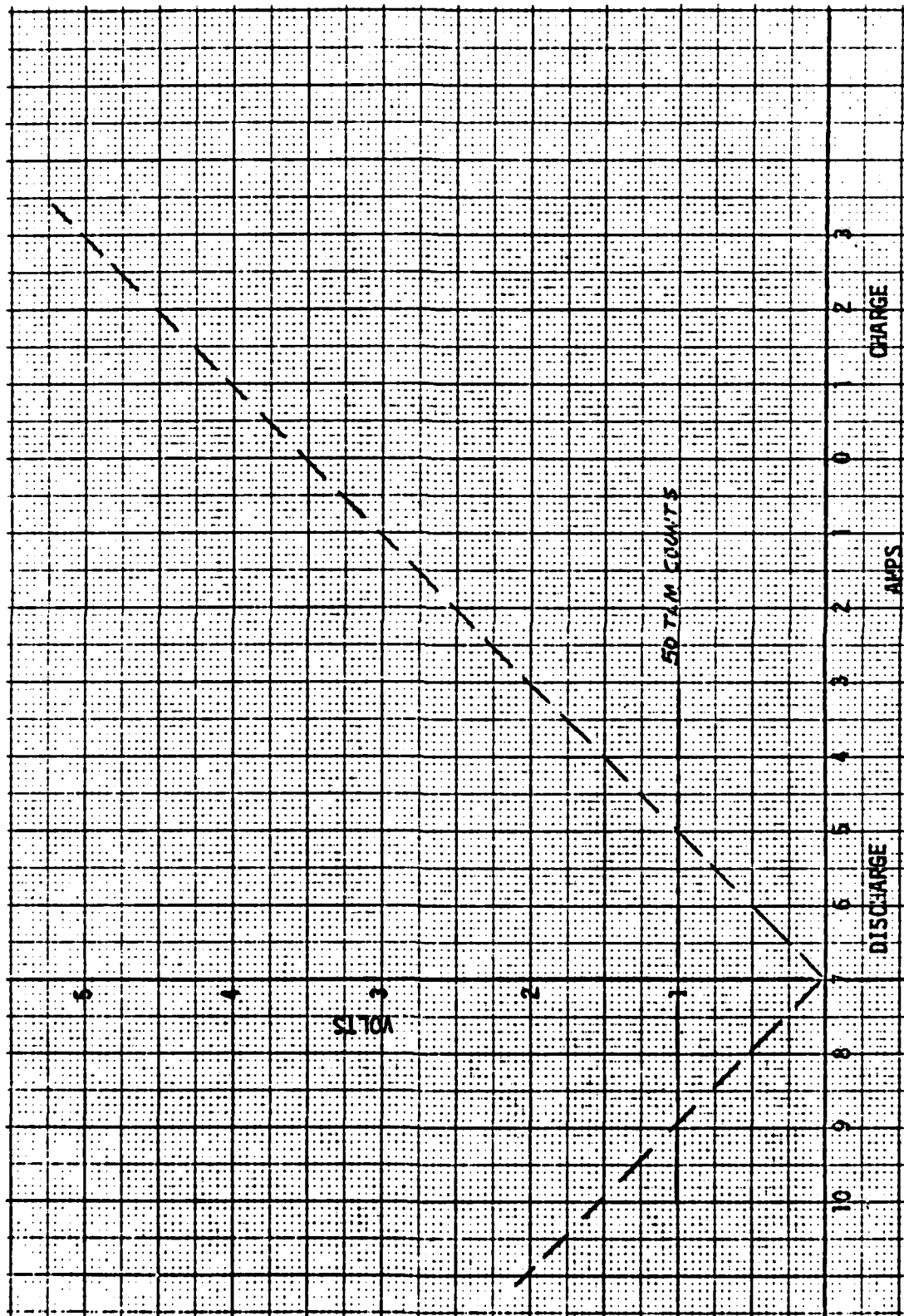


Figure A2-1. Battery Current Monitor Characteristic Curve

APPENDIX 3

FLIGHT 7/8 AND 11/12 GROUND TEST SIMULATIONS

Bailey

TRW
DEFENSE AND SPACE SYSTEMS GROUP
ONE SPACE PARK - REDONDO BEACH - CALIFORNIA 90770

INTEROFFICE CORRESPONDENCE

DSCS-C3-485
79-8725.2-069

TO: C. Sollo

cc: Distribution

DATE: 30 March 1979

SUBJECT: Test Plan - Three-Season Simulation of
DSCS II F7/8 and F11/12 Batteries

cl
FROM: C. Lurie
BLDG M1 MAIL STA. 1406 EXT. 50771

The test plan describing the three-season simulation of Flights 7/8 (Battery S/N 3-6) and Flights 11/12 (Battery S/N 3-3) batteries is attached. The test was started in January 1979, and is in progress.

CL:bj
Attachment

Distribution: E. Kipp B. Alborn
 L. Mack E. Ames
 P. Ritterman J. Durschinger
 D. Rusta *DR* N. North
 W. Scott A. Schoenfeld
 C. Stanley *CS* DSCS-II Data Center

Test Plan

Three-Season Simulation of DSCS II F7/8 and F11/12 Batteries

1.0 Scope

This plan describes a three-eclipse-season simulation of Flights 7/8 and Flights F11/12 batteries using batteries S/N 3-6 and S/N 3-3, P/N 256107-3X.

2.0 Test Equipment and Configuration

Each battery shall be mounted on a thermoelectric heat exchanger as indicated in Figure 1. Baseplate temperatures shall be maintained at $40 \pm 3^{\circ}\text{F}$ throughout the test. An aluminum honeycomb panel shall be placed between the battery and heat exchanger. Fiberglass shims shall be placed between the honeycomb panel and baseplate to simulate the orbital battery temperature profile observed during Flights 7 and 8. The battery shall be covered with fiberglass insulation and a plexiglass cover to isolate it from the ambient environment.

The electrical test configuration is shown in Figure 2. All battery discharges shall be into a constant power load of 110 ± 10 watts which simulates a two-out-of-three battery operation. Discharge duration shall vary in accordance with the simulated synchronous orbit eclipse charge/discharge profile shown in Table 1.

3.0 Procedure

3.1 Pretest Characterization

3.1.1 Visual Inspection

The battery shall be checked for physical damage.

3.1.2 Functional Bench Test

The Functional Bench Test shall be conducted in accordance with DR-14C-03, Rev. E.

3.2 Eclipse Season Cycling

The test batteries shall be subjected to three consecutive eclipse seasons consisting of charge/discharge cycles defined in Table 1.

All eclipse season battery discharges shall be into a constant power load of 110 ± 10 watts.

3.2 Eclipse Season Cycling cont'd.

The battery charge shall consist of:

- A constant current, one ampere charge, for a period of time equal to 3.6 times the discharge time, followed by
- A four ampere maximum charge rate to a battery voltage limit of 31.8 ± 0.2 volts for battery S/N 3-3 and 32.4 ± 0.2 volts for battery S/N 3-6.

The charge current shall be permitted to taper when the battery voltage reaches the voltage limit. Each battery shall be automatically switched between trickle charge and full charge on the basis of temperature. Charge rates and temperature switch points are given in Table 2.

3.3 Solstice Season Reconditioning

The batteries shall be reconditioned after completion of each eclipse season.

Battery S/N 3-3 shall be discharged into a 200-ohm load until the battery voltage reaches 12 volts.

Battery S/N 3-6 shall be discharged into a 44-ohm load until the battery voltage reaches 20 volts. S/N 3-6 shall be subjected to two consecutive reconditioning cycles.

Following the reconditioning both batteries shall be recharged at four amperes and maintained on trickle charge until the start of the next eclipse season.

The solstice period shall be limited to only the time required to perform battery reconditioning.

3.4 Post-Test Characterization

A Functional Bench Test shall be conducted in accordance with DR-14C-03, Rev. E.

4.0 Test Data Monitoring and Recording

Battery performance and test conditions shall be monitored continuously by the battery laboratory Digital Data Acquisition System (DDAS) at the following time intervals:

<u>Test Mode</u>	<u>Data Sampling Rate</u>
Battery Charge	Within one minute of start and completion plus every 10 minutes during charge.
Battery Discharge	Within one minute of start and completion plus every five minutes during discharge except for reconditioning discharge where the data shall be recorded every hour.

Battery test parameters are listed in Table 3. All parameters shall be monitored by the DDAS and stored on magnetic tape at the time intervals noted above.

The data shall also be printed on the line printer to facilitate real time assessment of the results by the responsible personnel.

5.0 Schedule

Figure 3 is a major task schedule in bar chart form.

Table 1

Duration of charge and discharge periods for each cycle of the eclipse season.

CYCLE NUMBER		24 Hour Cycle		
		Charge Time		Discharge Time
		Hours	Minutes	Minutes
1	45	23	40	20
2	44	23	32	28
3	43	23	25	35
4	42	23	20	40
5	41	23	17	43
6	40	23	13	47
7	39	23	10	50
8	38	23	07	53
9	37	23	04	56
10	36	23	02	58
11	35	23	00	60
12	34	22	58	62
13	33	22	56	64
14	32	22	58	66
15	31	22	53	67
16	30	22	52	68
17	29	22	51	69
18	28	22	50	70
19	27	22	50	70
20	26	22	49	71
21	25	22	49	71
22, 23	24	22	48	72

Table 2
Charge Control Parameters

Battery S/N	Bus Voltage (V)	Trickle Charge Rate (A)	SSTS Switch Points (°F)	Full Charge Rate (A)
3-3	31.8	0.175	64/71	4.0
3-6	32.4	0.250	70/77	4.0

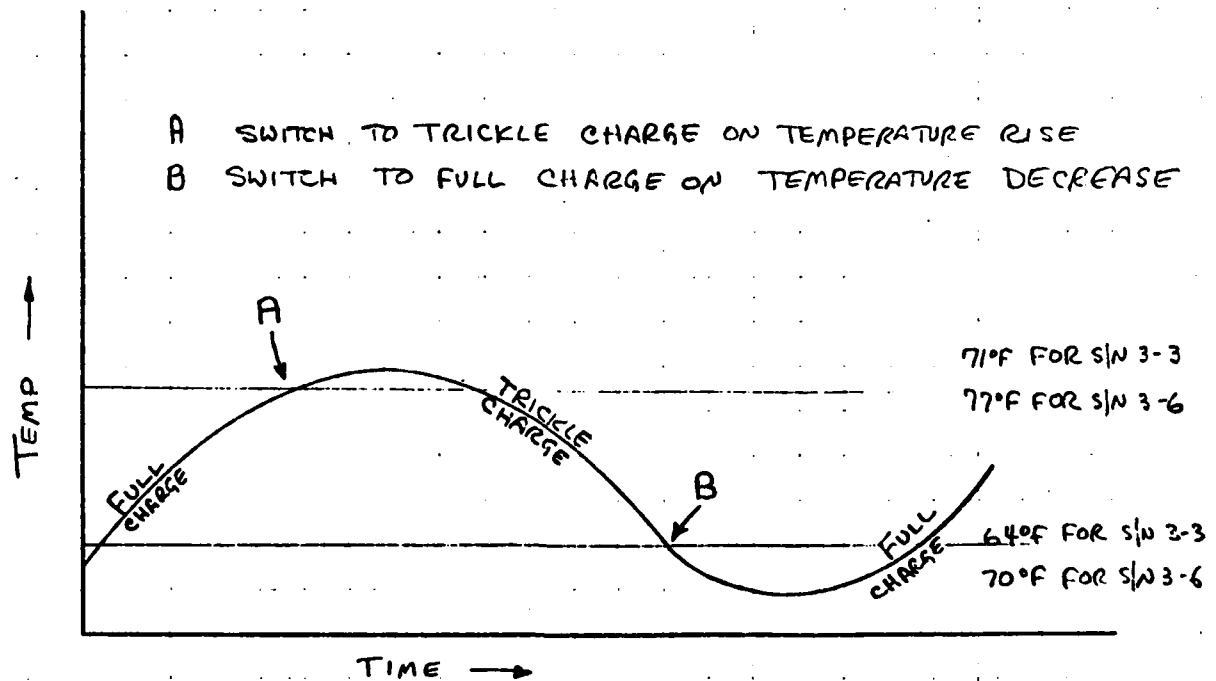


Table 3

Battery Test Parameters to be monitored and recorded during test

Parameter	Number of Parameters
Cell Voltage	22
Battery Voltage	1
Battery Current	1
Battery Temperatures RT1, RT2	2
Battery Heat Sink Temperature	2
Cycle Time	1
Battery End-of-Discharge Voltage	1

FIG 1

BATTERY / BASEPLATE CONFIGURATION

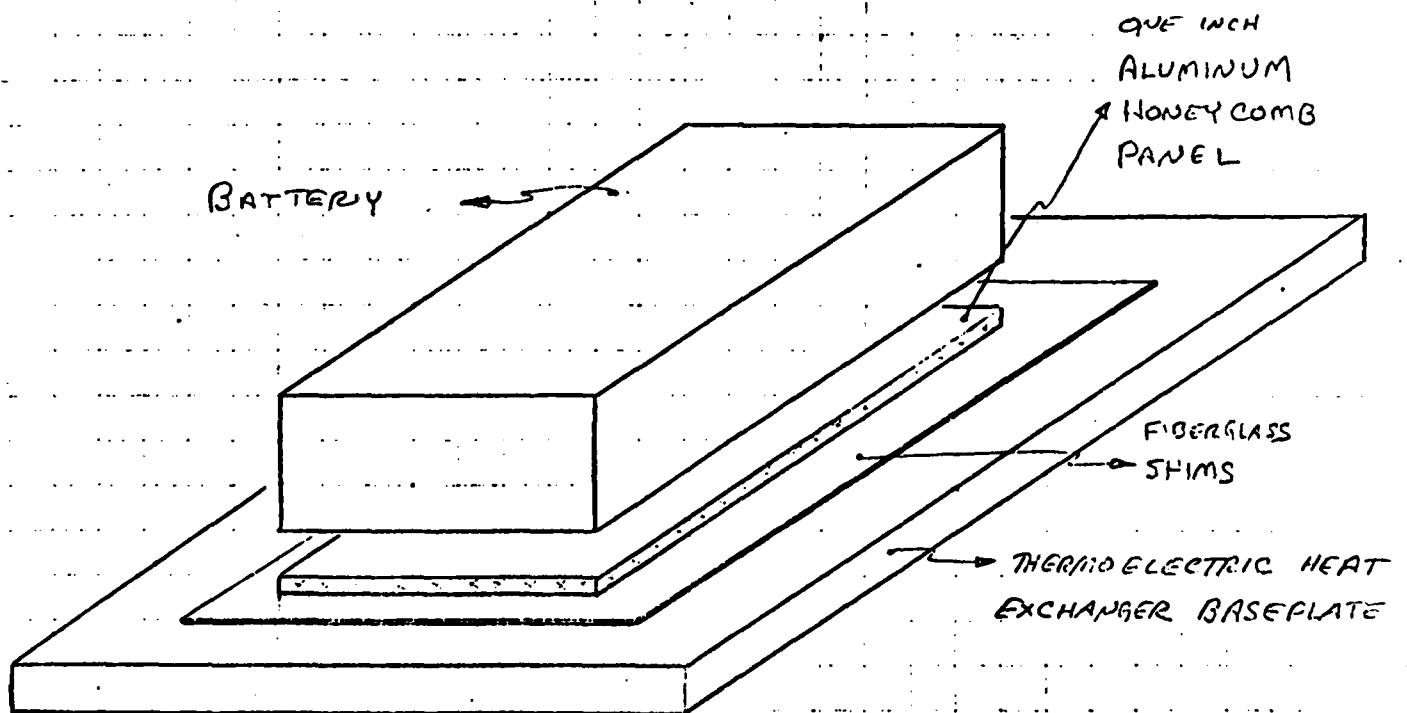


FIG 2

TEST CONFIGURATION

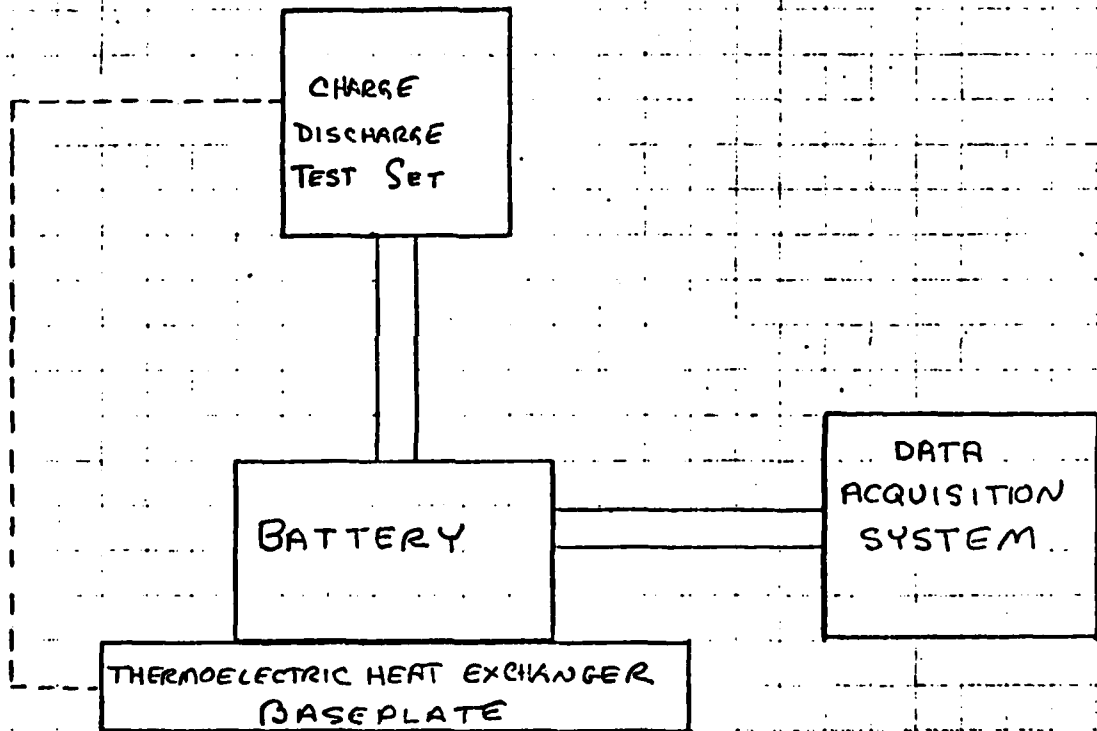







Fig 3

TEST PLAN SCHEDULE
THREE - SEASON SIMULATION OF DCS II F7/8; F11/12 BATTERIES

		W E E K S																					
No.	TASK DESCRIPTION	2	4	6	8	10	12	14	16	18	20	22	24	26	28	30	32	34	36	38	40		
1	PREPARE TEST PLAN																						
2	PERFORM DISCHARGE/RECHARGE CYCLES FOR ONE ECLIPSE SEASON; RECORD DATA;																						
3	PERFORM DISCHARGE/RECHARGE CYCLES FOR SECOND ECLIPSE SEASON; RECORD DATA; PREPARE INTERIM REPORT																						
4	PERFORM DISCHARGE/RECHARGE CYCLES FOR THIRD ECLIPSE SEASON; RECORD DATA																						
5	PREPARE AND PUBLISH FINAL REPORT WITH TESTS, ANALYSES; DOCUMENT CONCLUSIONS AND RECOMMENDATIONS																						

TENTATIVE START DATE : NOV. 1978

INTEROFFICE CORRESPONDENCE

DSCS-C3-481
79-8725.2-056

TO: D. Rusta

CC: Distribution

DATE: 28 March 1979

SUBJECT: 777 Battery Interim Report - Flight 7, 8, 11, 12
Simulation - Season 1 and 2

FROM: C. Lurie
BLDG M1 MAIL STA. 1406 EXT. 50771

The attached figures summarize the performance of 777 batteries S/N 3-3 and S/N 3-6 for Seasons 1 and 2, and the reconditioning for Season 3.

Figure Identification

Battery S/N	3-3		3-6		SUBJECT
Season	1	2	1	2	
Figure Number	1	5	9	13	Typical Midseason Temp., Voltage, Current Profile
	2	6	10	14	Reconditioning Discharge Profile
	3	7	11	15	Minimum Full Charge Fall-Off Current Trend
	4	8	12	16	End-of-Discharge Voltage Trend
	17		18		Peak Overcharge Current Trend

Reconditioning Discharge

The Battery Reconditioning Discharge Profiles give evidence of a second plateau phenomenon. The discharge profile for S/N 3-3, Season 3 (Figure 6) also shows a distinct linear region prior to a sharp end-of-discharge drop-off. Preliminary inspection of the test data suggests that the shape of the curve is real. The primary test data is being reviewed.

Minimum Full Charge Fall-Off Current Trend

The minimum full charge fall-off current is defined as the minimum current observed after the initial switching to maximum charge rate and prior to the increase due to heating. These currents are plotted vs. cycle number to demonstrate any trend. As can be seen from the figures the data is plotted twice.

D. Rusta

-2-

DSCS-C3-481
79-8725.2-056
28 March 1979

Reconditioning Discharge cont'd.

The upper plot utilizes raw data. The magnitude of the scatter and excursions is of interest. Inspection of the test data revealed considerable variation of the temperatures at the current minima. Analysis of the current-temperature data revealed a linear relationship for a given test configuration. The slope of the current-temperature line was used as a normalization factor as indicated below:

$$I_{T_0} = \frac{\Delta I}{\Delta T} (T_0 - T_i) + I_{T_i}$$

Where: I_{T_0} is the observed current normalized to T_i

T_0 is the median test temperature

T_i is the observed temperature

I_{T_i} is the current at T_i

$\frac{\Delta I}{\Delta T}$ is the slope of the current-temperature line

The temperature-normalized data is plotted in the lower portion of the figures. The plots are smoothed considerably and may be more meaningful in terms of the fall-off current minima vs. cycle number trend. The discontinuities occurring at the beginning of the seasons correspond to changes in the test set-up.

Peak Overcharge Current Trend

The peak overcharge current is defined as the peak current observed following the minimum full charge fall-off current of the previous paragraph. Several early-cycle data points could not be plotted. The primary test data is being reviewed for the cycles in question.

CL:bj

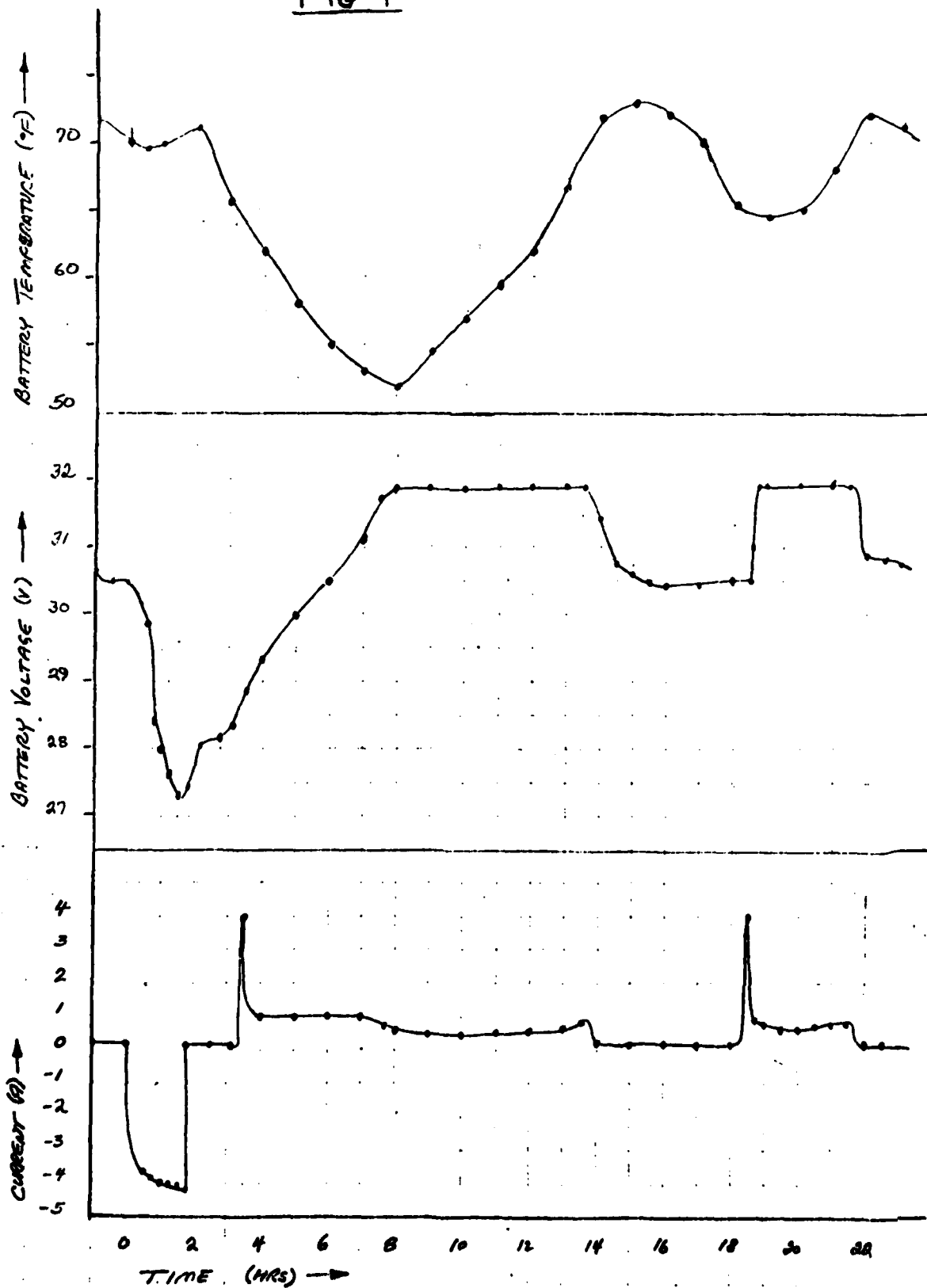
Attachment

Distribution: B. Alborn
E. Ames
J. Durschinger
E. Kipp
N. North

P. Ritterman
A. Schoenfeld
W. Scott
C. Sollo
C. Stanley
D. Rusta *DR*
Data Center

777 BATTERY
SN 3-3 TEST #7753 SEASON 1 CYCLE 20

FIG 1



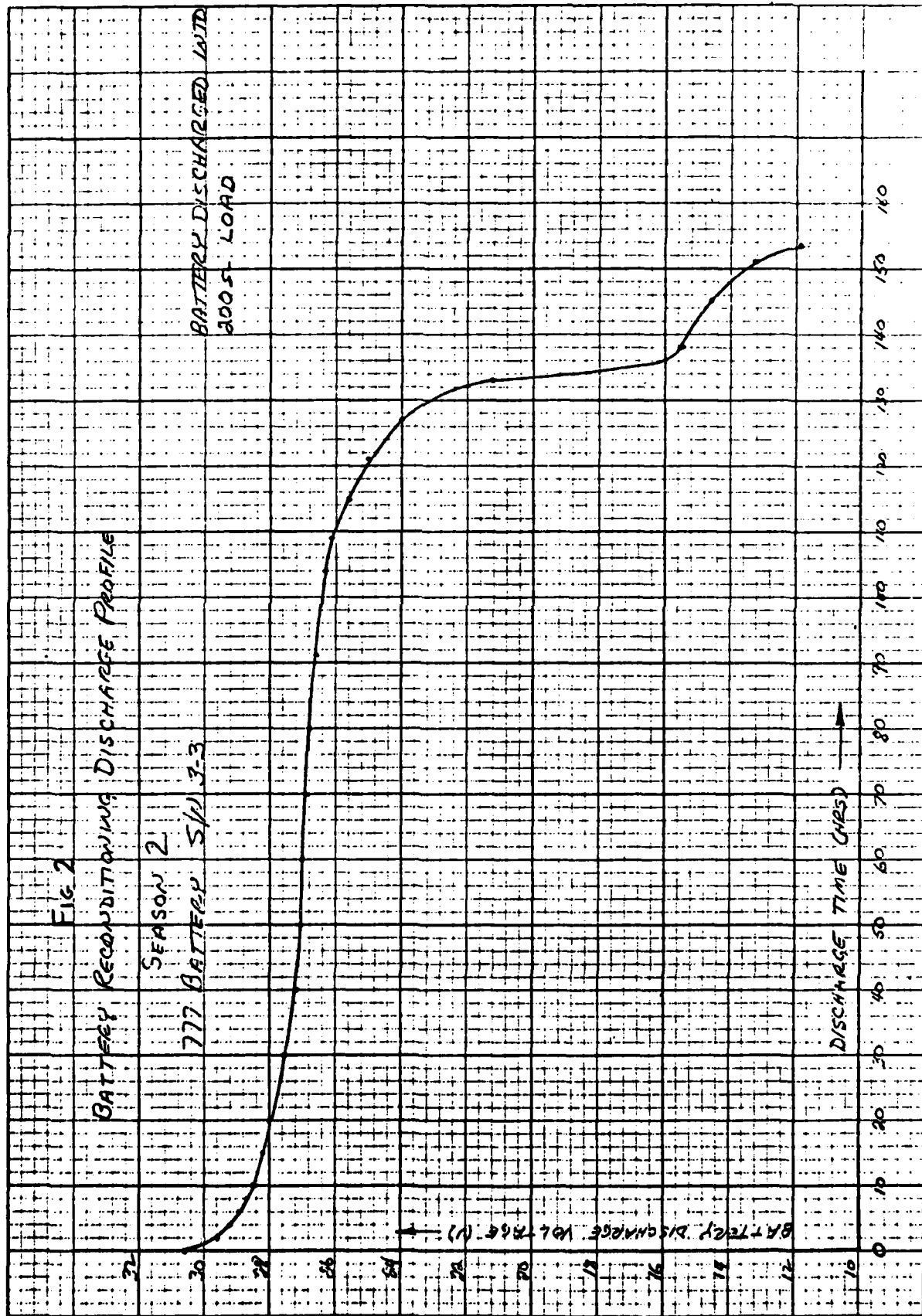


FIG 3

777 BATTERY S/N 8-3
MINIMUM FULL CHARGE FALL-OFF CURRENT
VS
CYCLE NUMBER

SEASON 1

RAW DATA

MIN FULL CHG FALL-OFF (I)

700
600
500
400
300
200

MIN FULL CHG FALL-OFF (I)

700
600
500
400
300
200

ABOVE DATA NORMALIZED
TO THE MEDIAN TEMPERATURE
(55°F)

2 4 6 8 10 12 14 16 18 20 22 24 26 28 30 32 34 36 38 40 42 44 46

CYCLE No. →

Q 2-23-79

Fig 4
BATTERY END-OF-DISCHARGE VOLTAGE
VS
CYCLE NUMBER

M7 BATTERY s/n 3-3
SESSION 1

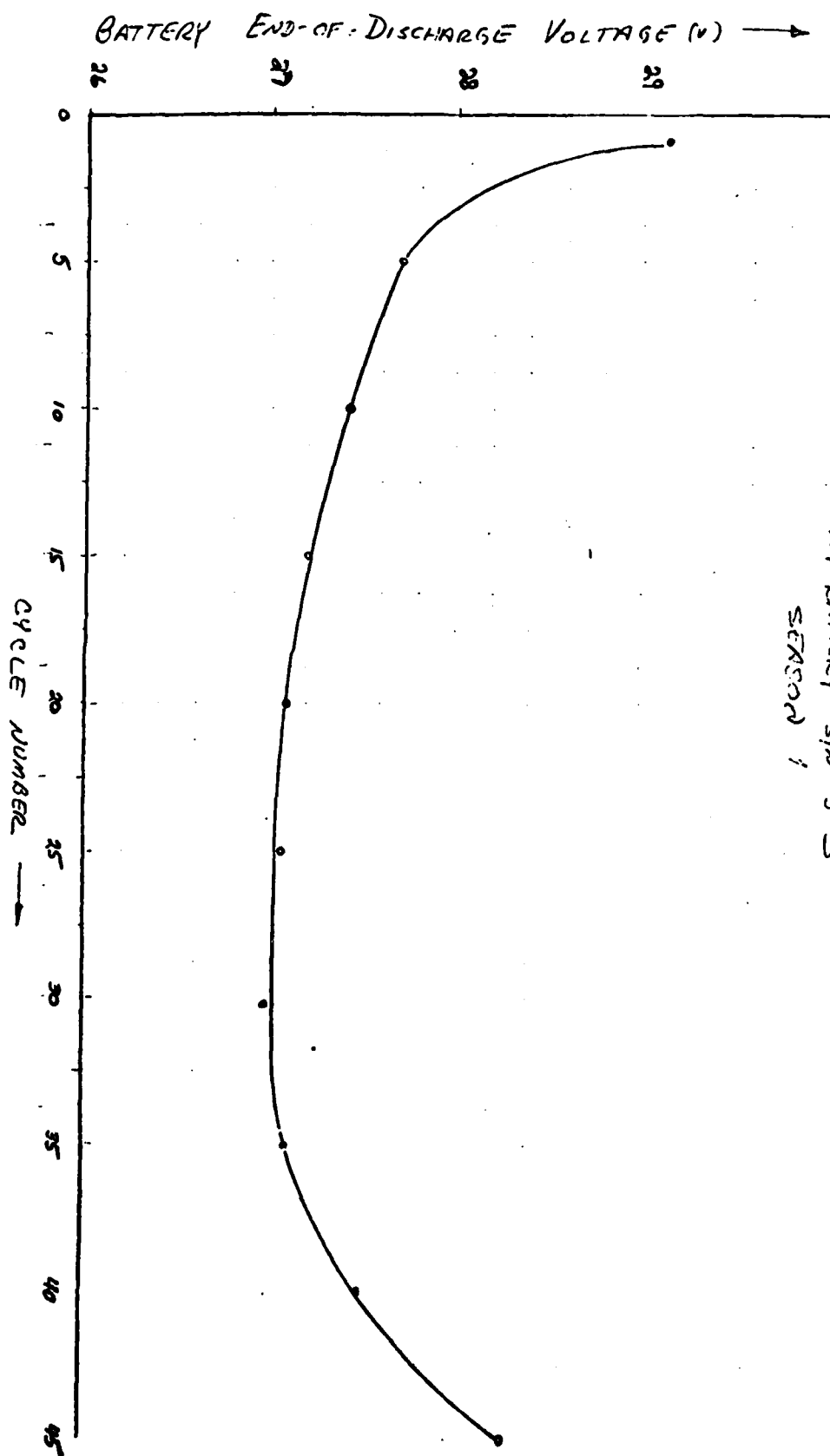
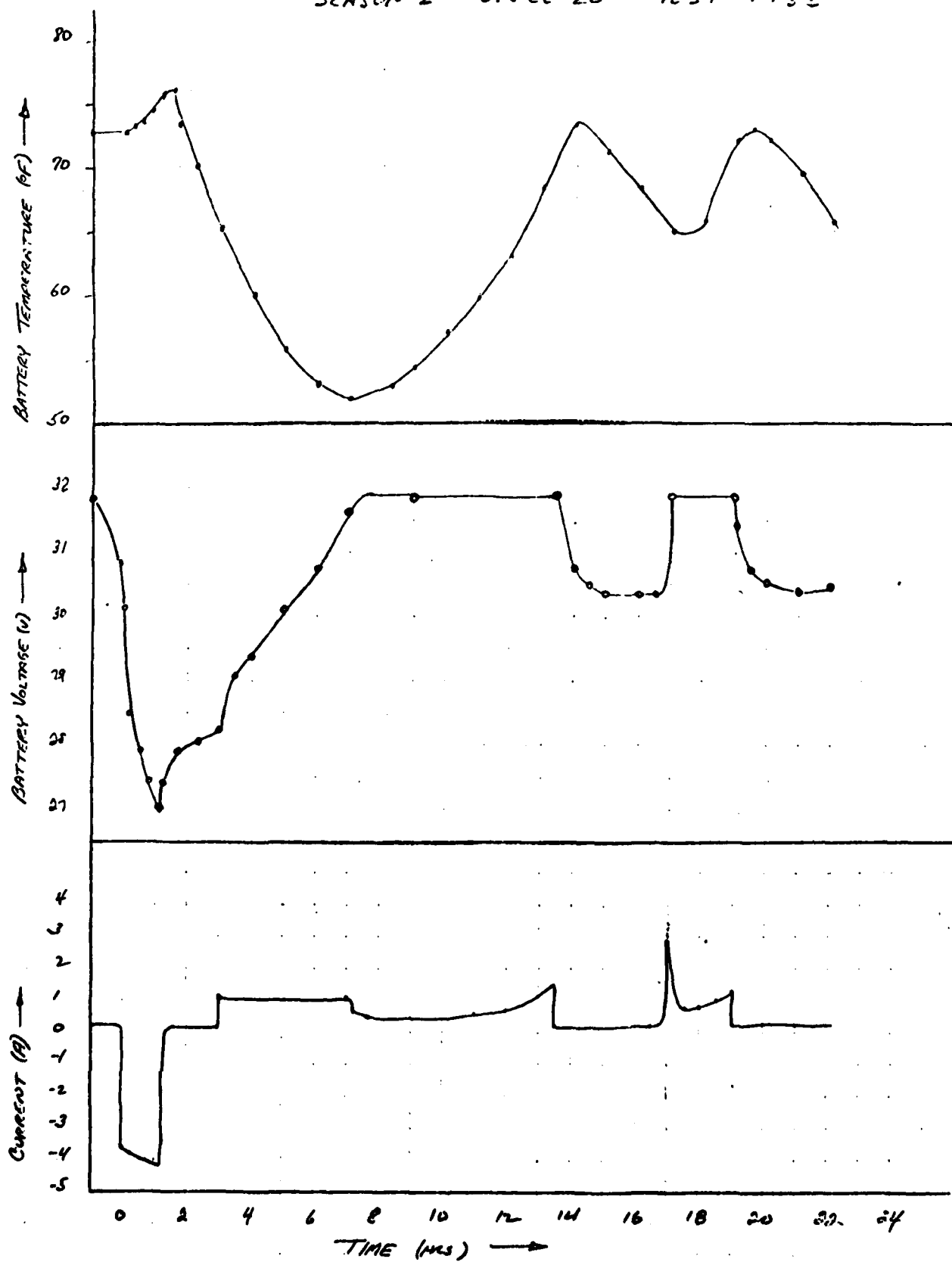


FIG 5

777 BATTERY S/N 2-3
SEASON 2 CYCLE 20 TEST #7732



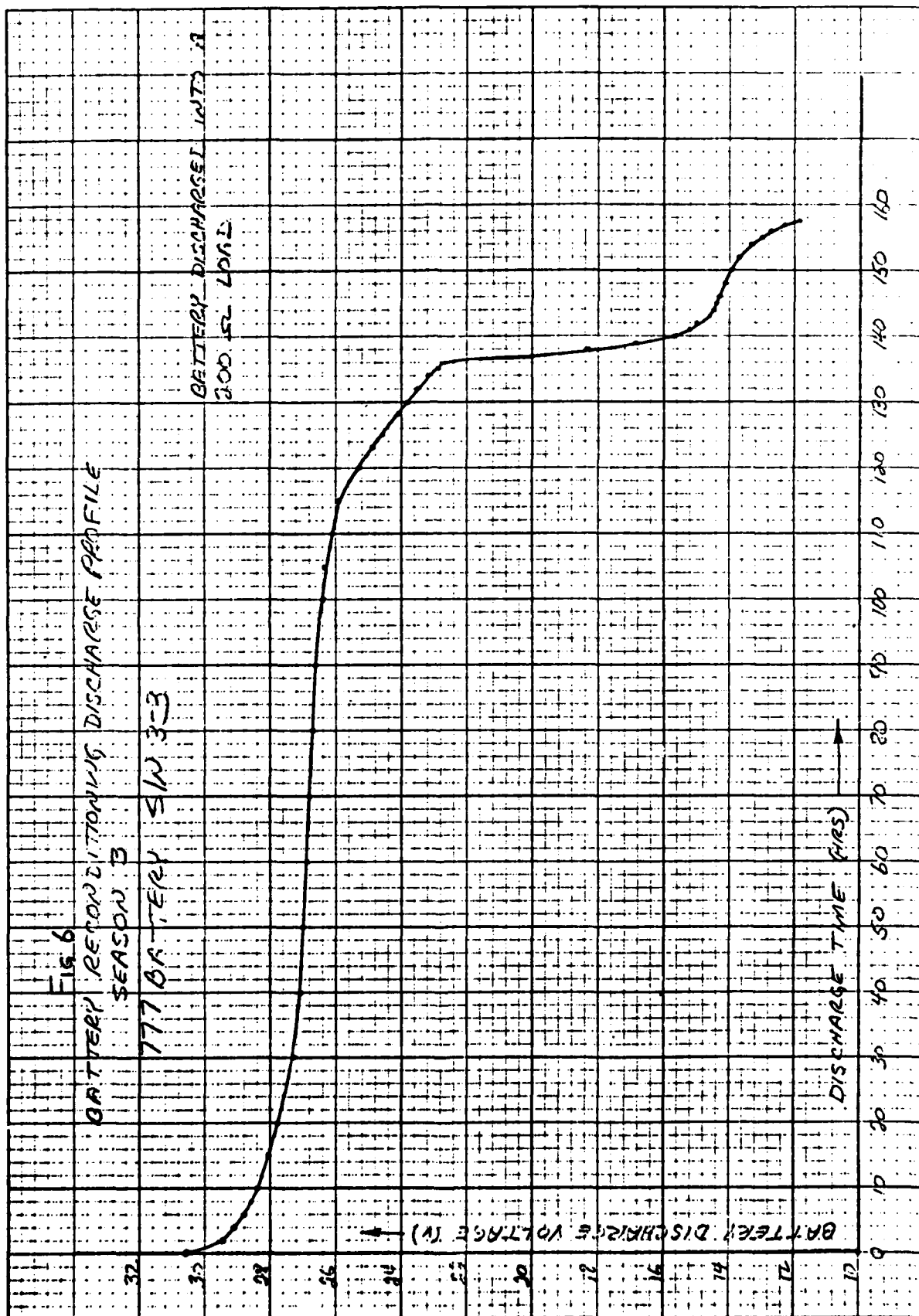
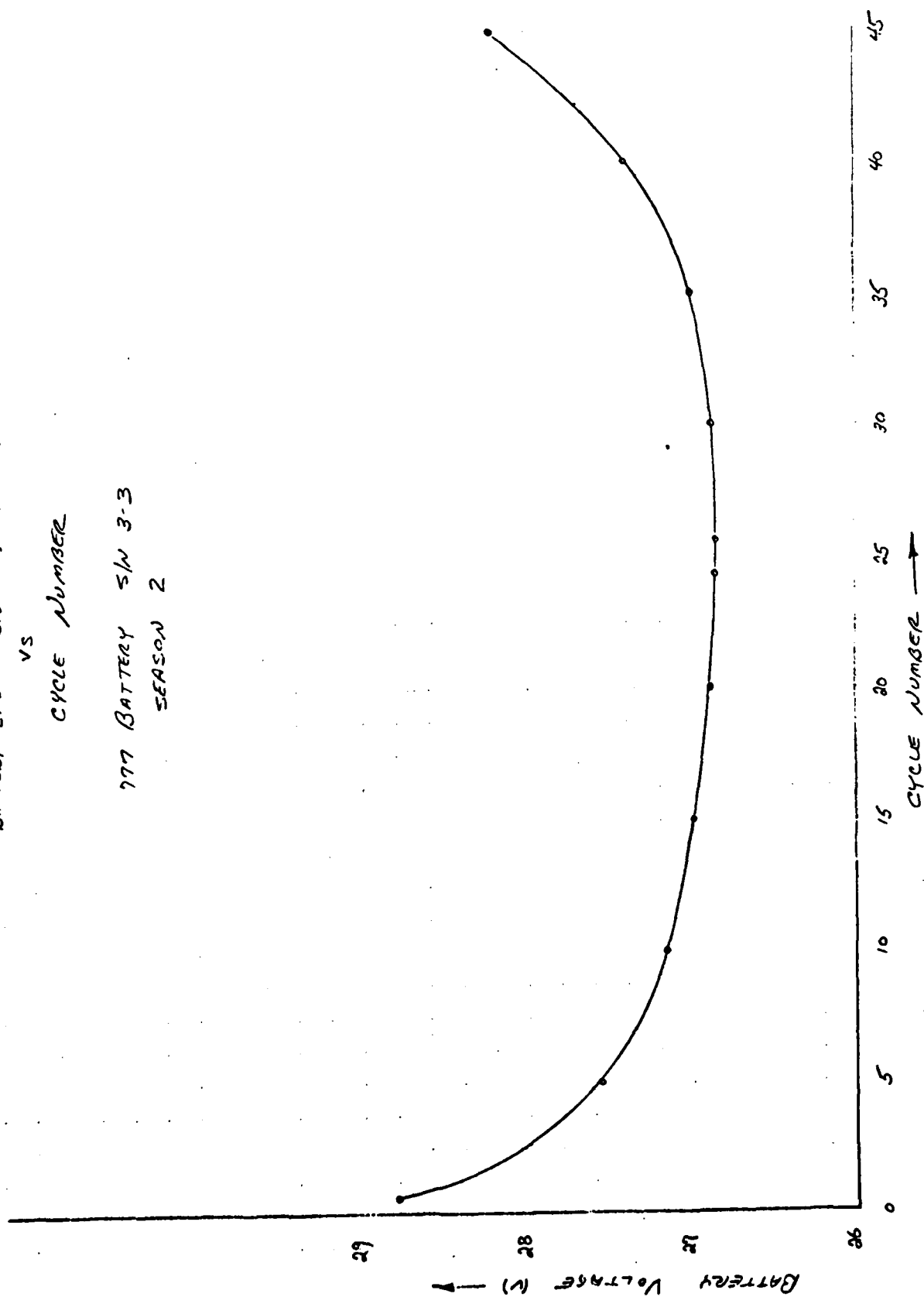


FIG
BATTERY END F-DISCHARGE VOLTAGE
VS
CYCLE NUMBER
777 BATTERY S/W 3-3
SEASON 2



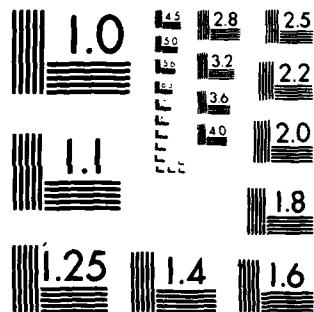
UNCLASSIFIED

TRW DEFENSE AND SPACE SYSTEMS GROUP REDONDO BEACH CA F/6 10/3
USCS II, BATTERY ANOMALY INVESTIGATION SATELLITES 9437 AND 9438-ETC
APR 80 P BAUER, C LURIE F04701-77-C-0118
TRW-32824-A-019-01 SD-TR-A0-33

SD-TR-80-33

2 OF 4
 2025-01-24 14:40

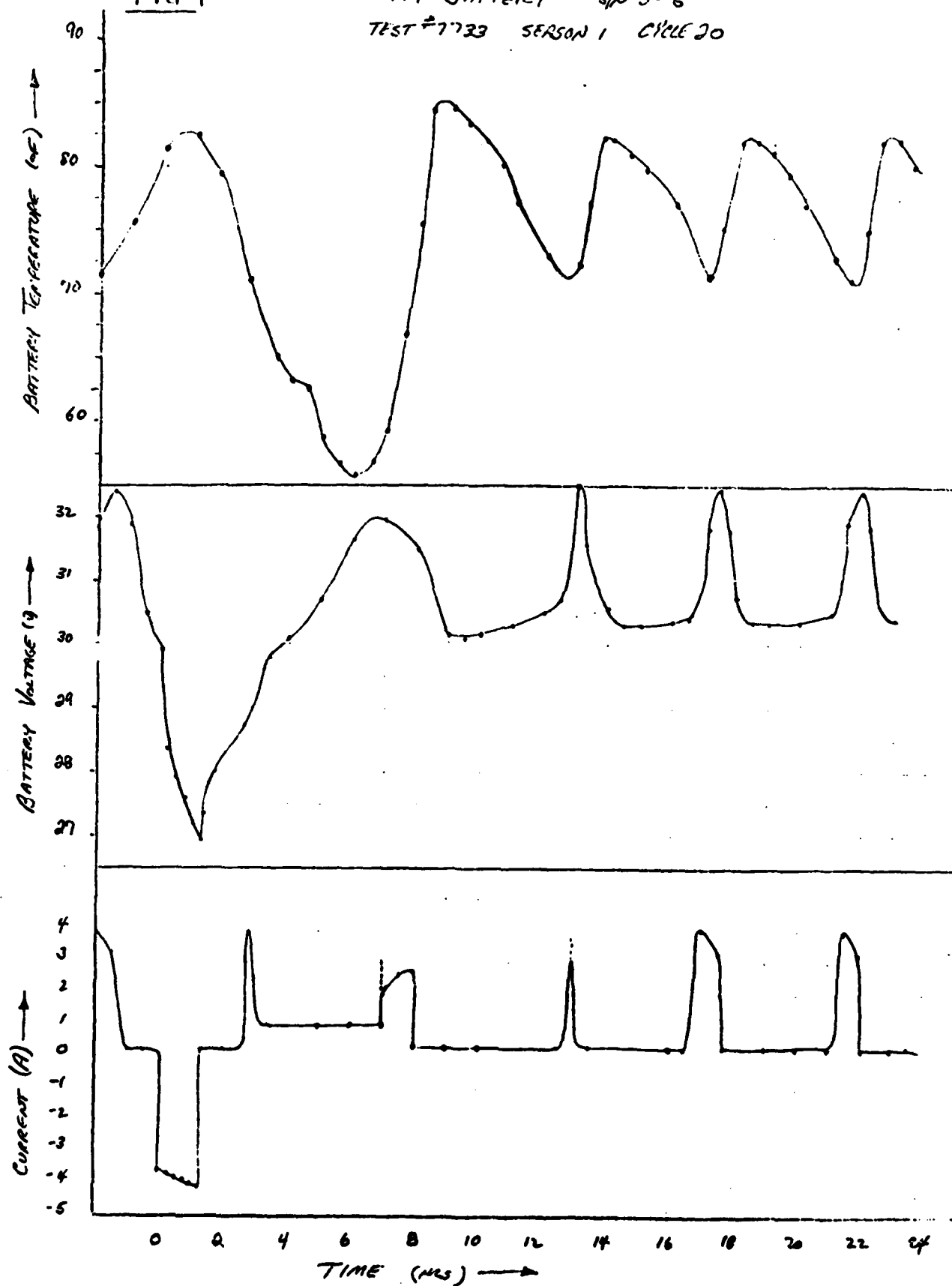
AG



MICROCOPY RESOLUTION TEST CHART
NATIONAL BUREAU OF STANDARDS-1963-A

FIG 9

777 BATTERY s/w 3-6
TEST #7733 SEASON 1 CYCLE 20



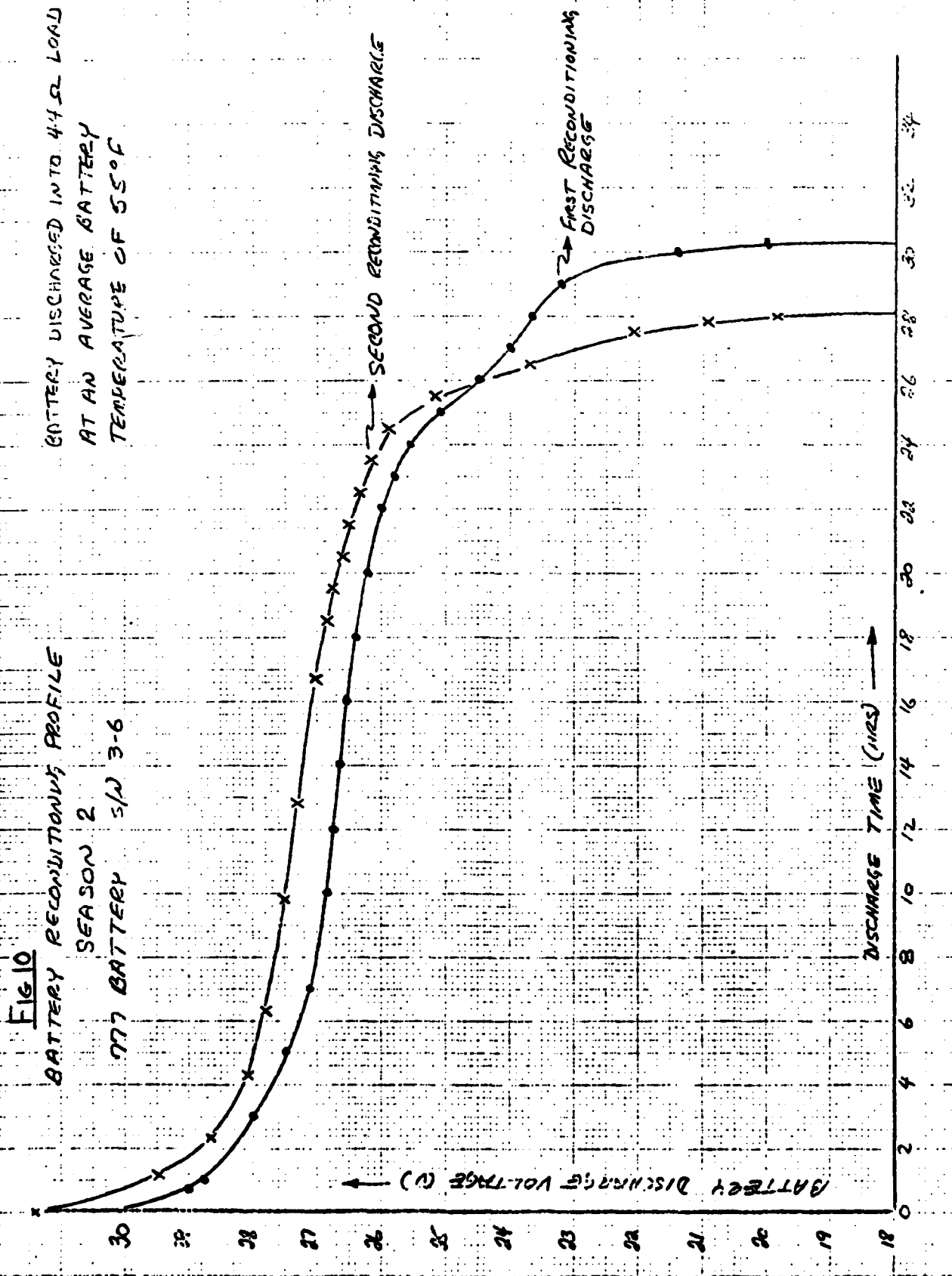


Fig 11

777 BATTERY SN 3-6
MINIMUM FULL CHARGE FALL-OFF CURRENT
VS
CYCLE NUMBER
SEASON 1

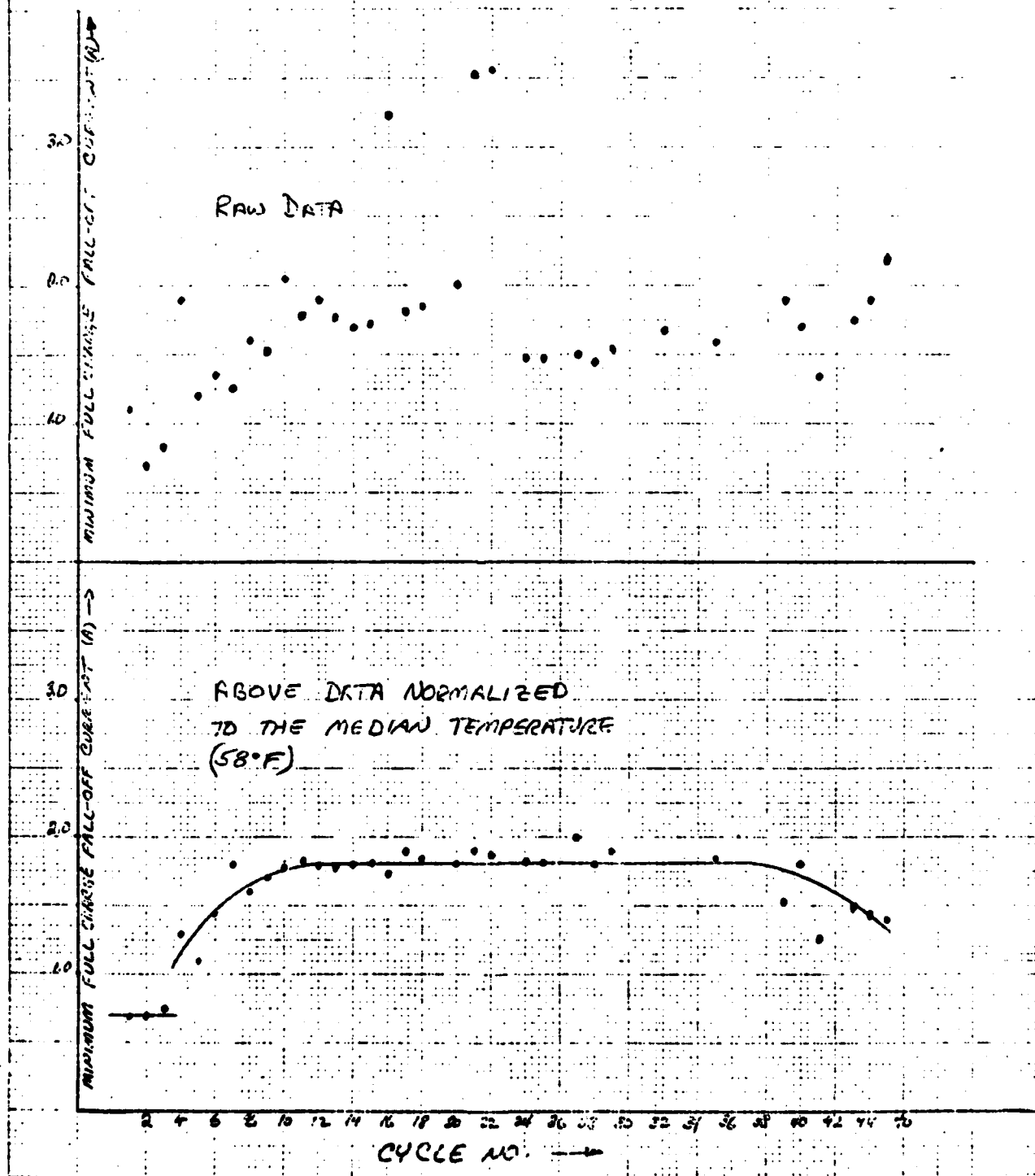


FIG 12
 BATTERY END-OF-DISCHARGE VOLTAGE
 VS
 CYCLE NUMBER

777 BATTERY SN 3-6
 SEASON 1

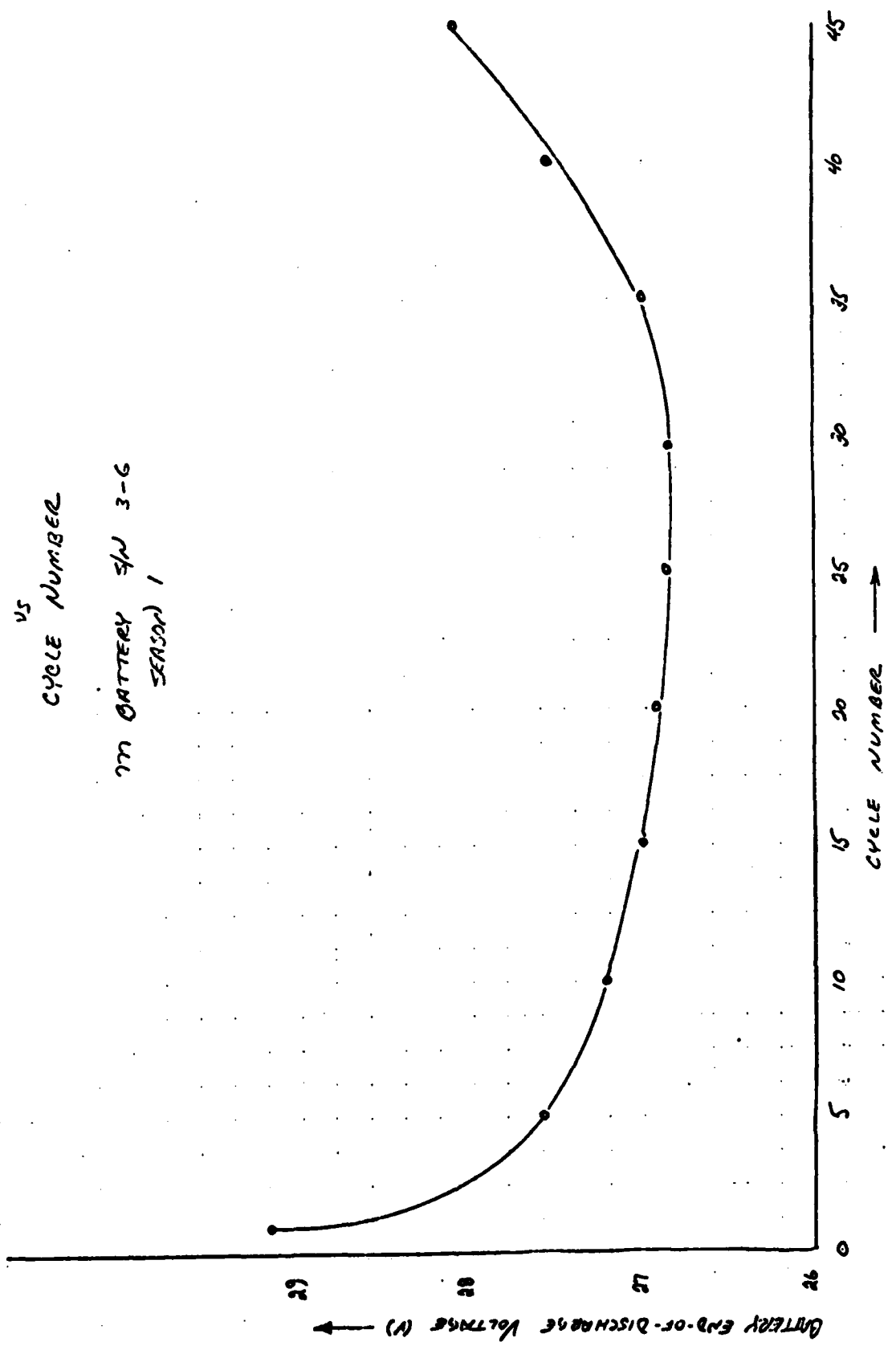


Fig 13

777 BATTERY S/N 8-6
TEST #7733 SEASON 2 CYCLE 20

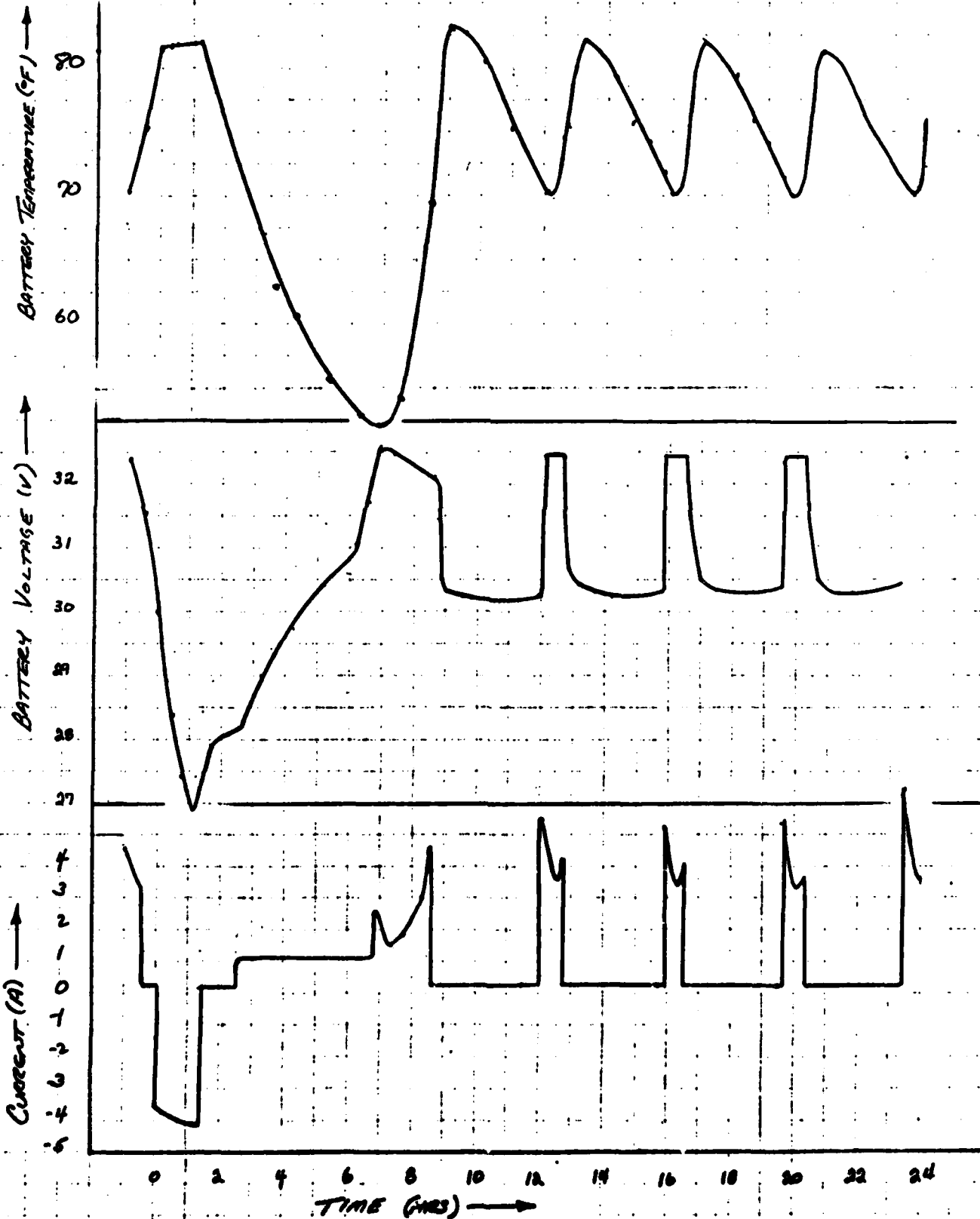
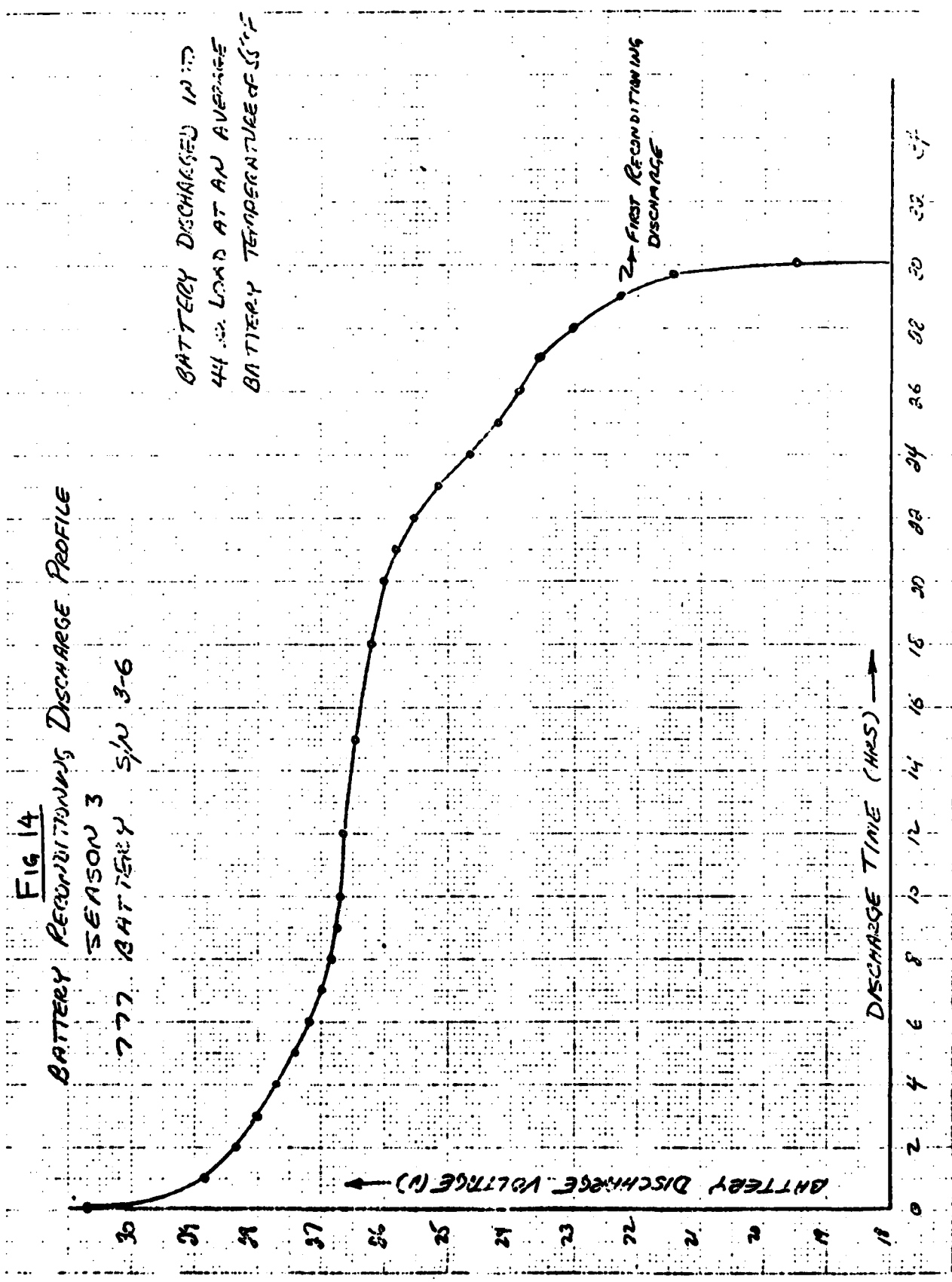


FIG 14
 BATTERY RECONDITIONING DISCHARGE PROFILE
 SEASON 3
 777 BATTERY S/N 3-6



BATTERY DISCHARGED IN 120
 44 W. LOAD AT AN AVERAGE
 BATTERY TEMPERATURE OF 55°F

THE

777 BATTERY SN 3-6
MINIMUM FULL CHARGE FALL-OFF CURRENT
VS
CYCLE NUMBER
SEASON 2

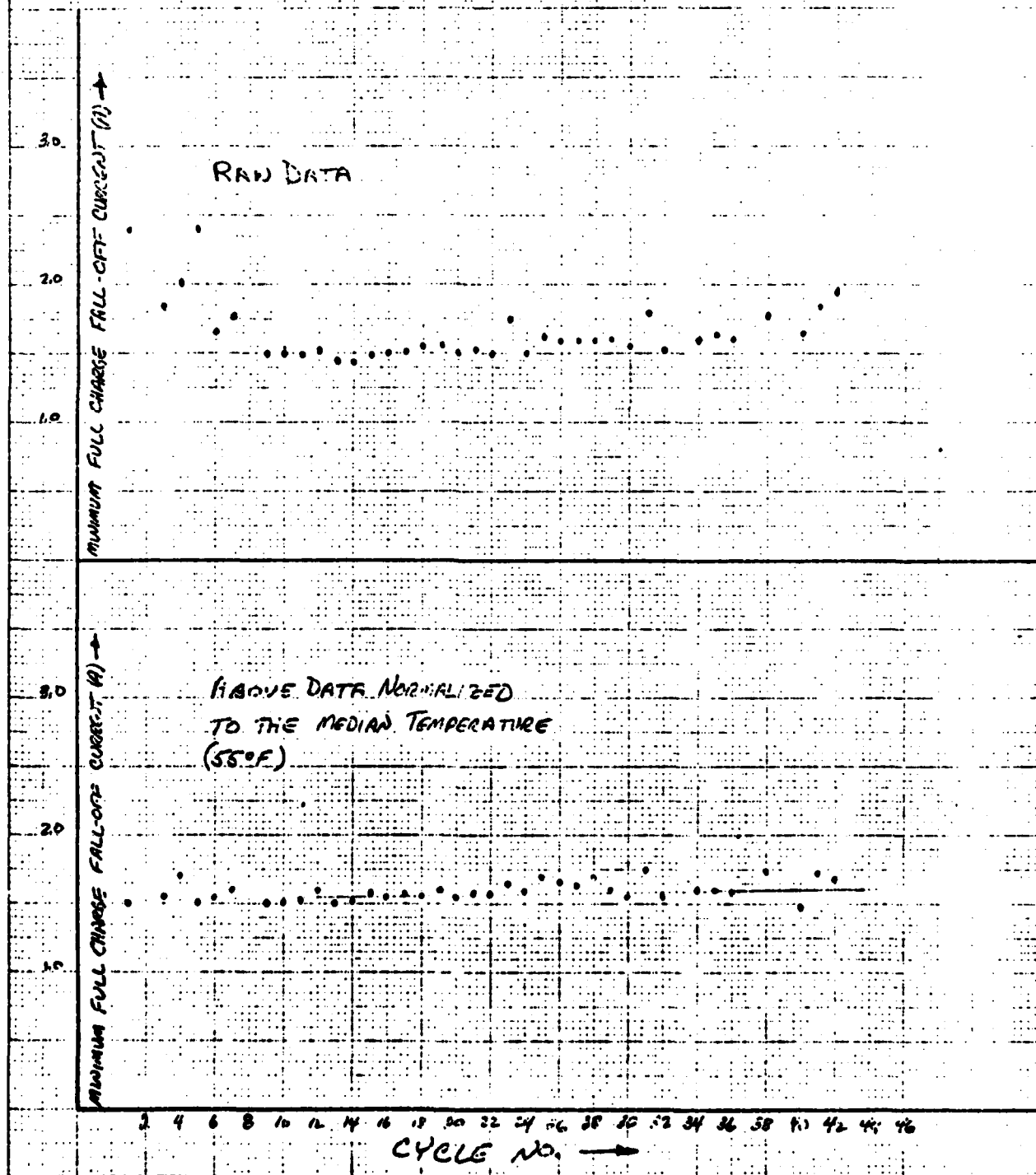


FIG 16
BATTERY END-OF-DISCHARGE VOLTAGE
VS
CYCLE NUMBER

777 BATTERY S/N 3-6
SEASON 2

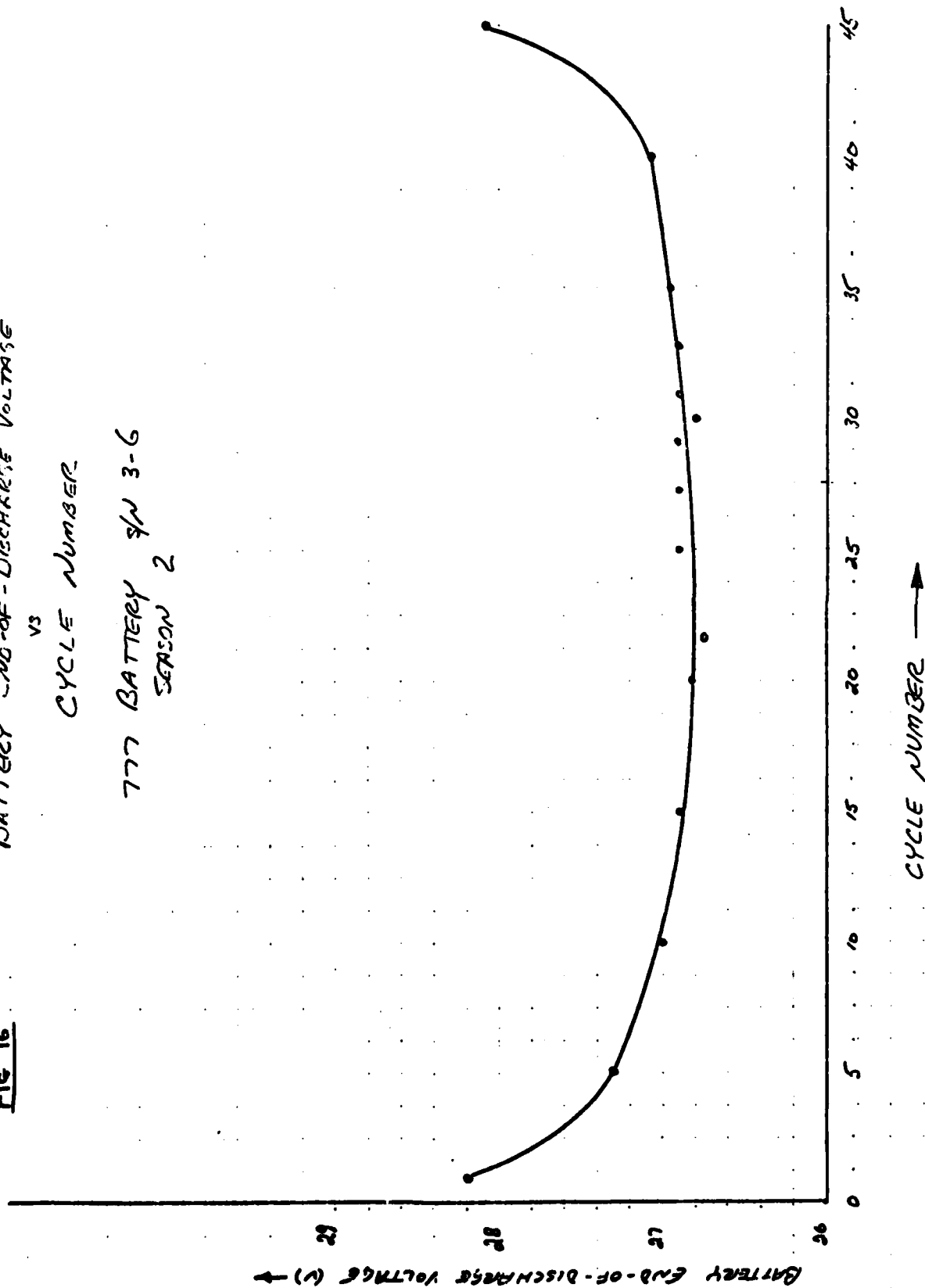


Fig 18

PEAK OVERCHARGE CURRENT w/ CYCLE NUMBER
777 BATTERY 5/12 3-6

SEASON 2
SEASON 1

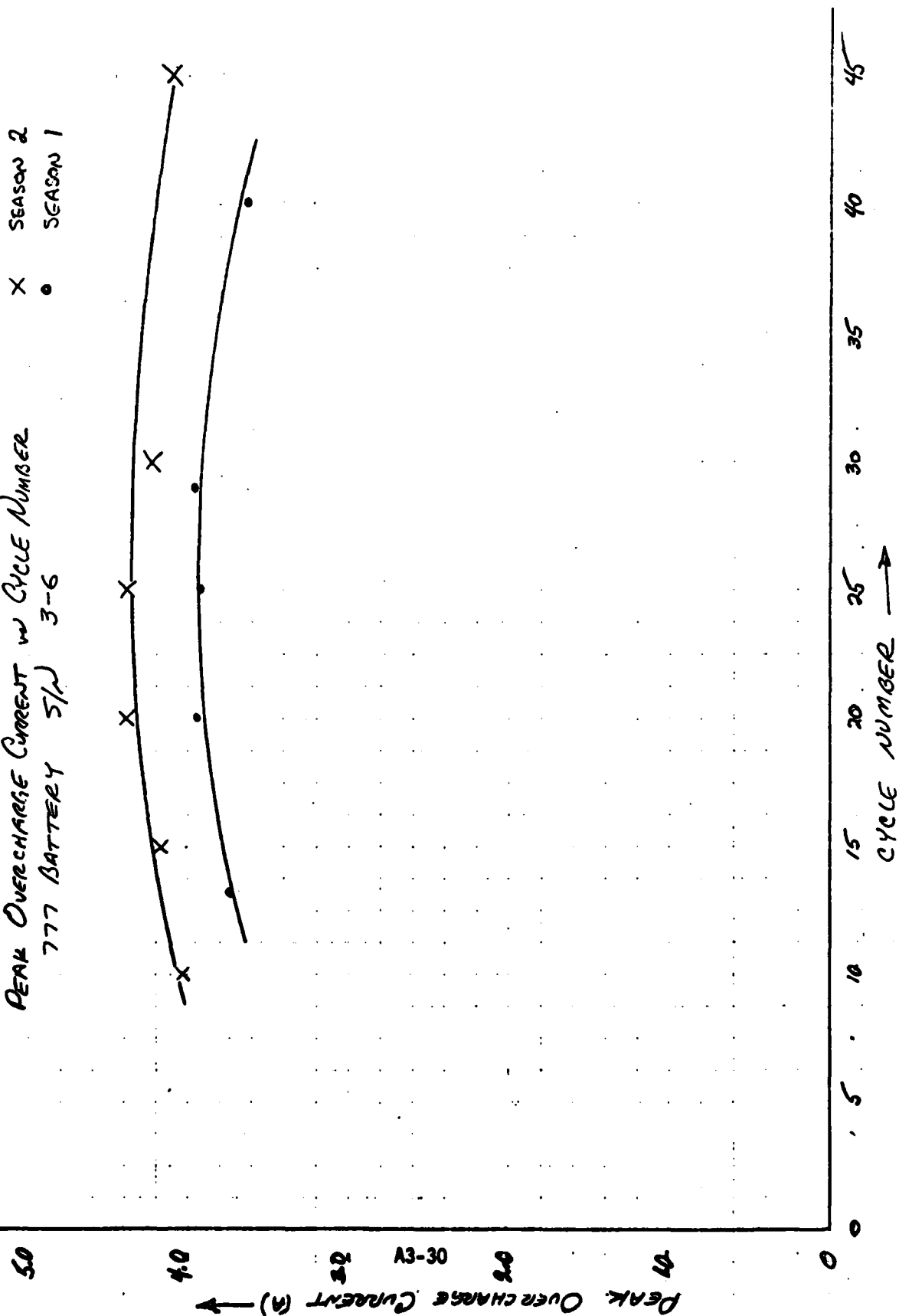
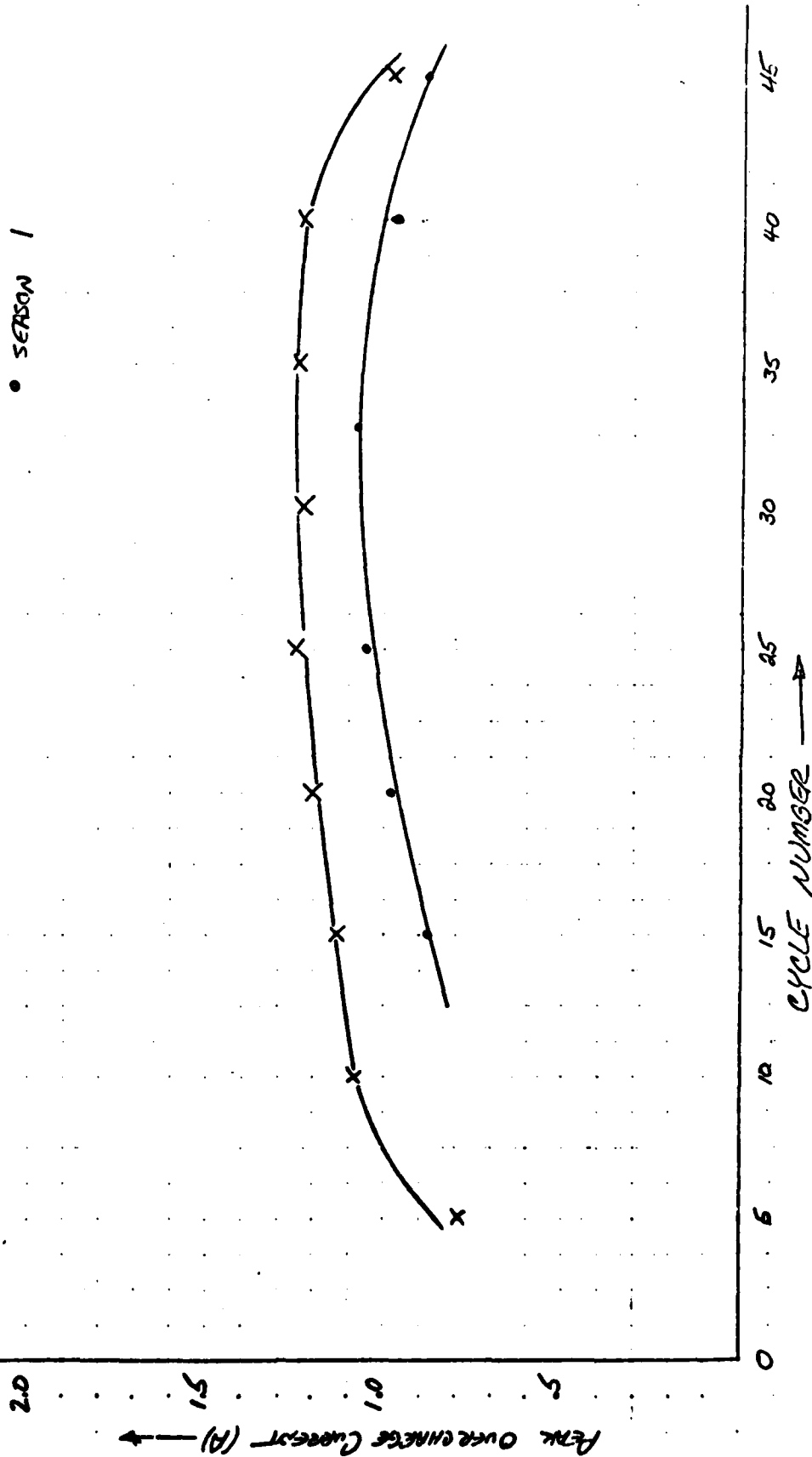


Fig 17

PEAK OVERCHARGE CURRENT vs CYCLE NUMBER
777 BATTERY S/N 3-3

X SEASON 2
• SEASON 1



INTEROFFICE CORRESPONDENCE

DSCS-03-498
79-8725.2-110

TO: C. Sollo

cc: Distribution

DATE: 23 May 1979

SUBJECT: 777 Battery Interim Report - F7/8, F11/12
Simulation - Season 3

FROM: C. Lurie
HLDG: M1 **MAIL STA:** 1406 **EXT:** 507

1.0 Summary and Recommendations

The F7/8 Season 3 simulation run with Battery S/N 3-6 produced two cell short circuits and two cells whose performance suggests impending shorts. No anomalies were observed during the F11/12 Season 3 simulation run with Battery S/N 3-3.

Inspection of Battery S/N 3-6 cell-level data suggests that cells may give warning of impending short circuit failure in terms of suppressed cell voltage and anomalous overcharge pulse waveforms. Both cells which shorted in Battery S/N 3-6 developed partial shorts which cleared prior to being removed from the battery circuit. One of these cells developed a permanent short prior to isolation.

Data describing the short circuits and general Season 3 battery performance are summarized by the figures listed in Table 1.

Several similarities are noted between the ground test and flight shorts.

<u>Attribute</u>	<u>Flight</u>	<u>Ground</u>
Cell P/N	8E005	8E005
Cell Mfg. Lot No.	1	1
Season	3	3
Eclipse	0-20	9
Short Location	Central Cell (By Analysis)	Central Cell (Cell No. 6)

Table 1
Figure Identification

Figure Number		Subject
S/N 3-3	S/N 3-6	
1	2	Typical Midseason Temperature, Voltage, Current Profile - Season 3, Cycle 20
3	4	Typical Midseason Temperature, Voltage, Current Profile - Season 2, Cycle 20
5	6	Typical Midseason Temperature, Voltage, Current Profile - Season 1, Cycle 20
7	8, 9	Battery Reconditioning Discharge Profile - Prescason 4
10	11	Minimum Full Charge Fall-Off Current Trend - Season 3
12	13	Battery End-of-Discharge Voltage Trend - Seasons 1, 2, 3
14	15	Peak Overcharge Current Trend - Seasons 1, 2, 3
	16-19	Cell No. 6 Short Circuit
	20	OCV Decay on Charged Stand following the Cell 6 Short
	21-25	Cell No. 15 Short Circuit

Analysis of the flight and ground test data led to the conclusion that the F7/8 charge regime contributes to cell short failures and should not be continued. The backup mode, i.e., high bus trickle charge, is therefore being evaluated as the prime mode.

Continuation of the F7/8 ground test battery simulation is recommended to support this change.

The F7/8 Season 4 simulation should utilize high bus trickle charge as the primary charge mode. Because the history of the F7/8 simulation battery (S/N 3-6) closely matches that of the flight battery the ground test data can provide valuable guidance for operational decisions.

Continuation of the F11/12 simulation is recommended as a design verification and is of special interest because the stresses imposed by its charge regime are intermediate between the F7/8 primary and backup modes.

2.0 Discussion of Season Three Battery Performance

2.1 Typical Midseason Temperature, Voltage, Current Profile (Figures 1-6)

Figures 1-6 depict typical midseason temperature, voltage, and current profiles for batteries S/N 3-3 and S/N 3-6 during seasons 1-3.

The low battery voltages recorded for Battery S/N 3-6 during Season 3 are caused by the loss of the three cells that were bypassed because of shorting or anomalous behavior.

2.2 Battery Reconditioning Discharge

The reconditioning discharge profile observed for S/N 3-3, following Season 3, is shown in Figure 7. The flat portion of the curve between 129 and 145 hours and sharp inflection at 145 hours were also observed during the reconditioning discharge following Season 2. The reconditioning discharge following Season 1 did not exhibit these features. The 19.3 Ah reconditioning discharge capacity obtained after Season 3 agrees well with the 19.8 Ah and 19.2 Ah capacities obtained after Seasons 2 and 1 respectively.

The reconditioning discharge profiles observed for S/N 3-6, following Season 3, are shown in Figures 8 and 9. Operational difficulties caused the discharges to be terminated at 22 volts instead of the planned 19 volts. The observed capacities of 14.5 and 14.4 Ah for the first and second discharges are therefore biased low and are not directly comparable to the corresponding Season 2 values of 17.3 and 18.0 Ah. However, if the Season 2 curves are integrated only to a point equivalent to the Season 3 cut-off voltage, first and second discharge capacities of 14.7 and 15.0 Ah are obtained. These values are in acceptable agreement with Season 3 capacities.

2.3 Minimum Full Charge Fall-Off Current Trend

The minimum current observed after the initial switching to maximum charge rate and prior to the increase due to heating is plotted vs. cycle number in Figure 10 (S/N 3-3) and Figure 11 (S/N 3-6).

The convention of plotting both raw and temperature-normalized data used previously (DSCS-C3-481, 28 March 79) is continued.

During the second half of the season the normalized Battery S/N 3-6 data showed more scatter than had been observed previously. No explanation is immediately available but inspection of the raw data reveals a steady and rapid increase in the minimum fall-off current during this period.

2.4 Battery End-of-Discharge Voltage Trend

Battery end-of-discharge voltage is plotted vs. cycle number in Figure 12 (S/N 3-3) and Figure 13 (S/N 3-6) for Seasons 1, 2 and 3. The season-to-season agreement is excellent and no trend is apparent.

2.5 Peak Overcharge Current Trend

The peak overcharge current observed following the minimum full charge fall-off current is plotted vs. cycle number in Figure 14 (S/N 3-3) and Figure 15 (S/N 3-6) for Seasons 1, 2, and 3.

The S/N 3-3 data (Figure 14) indicates that the Season 1 peak currents are about 0.2A lower than those of Seasons 2 and 3. The agreement between the Season 2 and 3 data is excellent. The S/N 3-6 data (Figure 15) appears to follow the same trend. However, the scatter is far greater than observed for the S/N 3-3 data. The increased scatter is probably related to the more dynamic nature of the F7/8 (S/N 3-6) charge regime.

3.0 Cell Short Circuit Failures (Battery S/N 3-6)

During Season 3, Battery S/N 3-6 produced two cell short circuits, and two cells whose performance suggests impending shorts. The shorts and associated events are discussed below.

3.1 Cell Number 6, Short Circuit

Relevant cell and battery data are presented in Figures 16-19.

Cell No. 6 first shorted at 15.55 hours. The time is confirmed by three observations:

- 1) A battery voltage inflection occurred at 15.55 hours (Figure 16)
- 2) Temperature sensor RT2, mounted adjacent to Cell No. 6, indicated a temperature excursion starting at 15.60 hours (Figure 16).
- 3) The Cell No. 6 cell voltage dropped off its overcharge plateau prematurely at 15.55 hours (Figure 17).

Inspection of the subsequent data indicates that the short cleared itself within minutes.

Cell No. 6 shorted again at 28.05 hours. Voltage and temperature observations were similar to the initial short. The short persisted for several hours; Cell No. 6 was isolated electrically prior to the next cycle.

3.2 OCV Decay

Battery S/N 3-6 was put on open circuit stand after completing the Season 3, Cycle 9 charge. The OCV decay on charged stand is presented in Figure 20. Analysis of the data indicated that two cells, Cell No. 4 and Cell No. 15, had OCV's more than three standard deviations less than the mean of the remaining 19 cells. Cells 4 and

15 are plotted individually.

3.3 Cell No. 4, Anomalous Behavior

Cell No. 4 was electrically isolated during Cycle No. 10. This action was based on two observations:

- The Cell No. 4 overcharge pulses exhibited subtle but real shape changes that are believed to be associated with impending shorts.
- The Cell No. 4 voltage was running 50-100MV lower than the remaining cells.

3.4 Cell Number 15, Short Circuit

Relevant cell and battery data are presented in Figures 21-24. Cell No. 15 shorted during the charge following the first reconditioning discharge after Season 3. The short occurred at 17.60 hours and is confirmed by inflections in the battery voltage and temperature (Figure 21) and cell voltage plots (Figure 22). The cell voltage dropped to zero and remained there for more than one hour. The voltage then rose slowly for about 14 hours at which time the short was substantially cleared.

An overcharge pulse occurred between 55.65 and 58.00 hours (Figures 23). The voltage responses of Cell No. 15 and a nominal cell, Cell No. 20, are presented in Figure 24. The response of Cell No. 15 is anomalous and suggests that it was not accepting charge normally.

Cell No. 15 was bypassed at 63.9 hours. The zero voltage after this time indicates only that the data acquisition system is no longer monitoring the cell. Immediately after being electrically isolated from the remaining battery cells, Cell No. 15 was discharged into a 10-ohm resistor to a 0.0 volt cut-off. The results are presented in Figure 25. The discharged capacity is 6 Ah. The cell had received a total of 40 Ah of charge (16 Ah before the short and 14 Ah after). This is equivalent to a charge efficiency of 43%, assuming zero state-of-charge immediately after the short. The efficiency of an unshorted cell should be approximately twice this value. The inefficiency provides an estimate of the magnitude of the short.

As can be seen from Figure 25 the voltage recovery, after removal of the 10-ohm resistor, was irregular and slow.

3.5 Cell Short Warning Signs

Inspection of cell voltage data prior to short circuit failure suggests that the cell voltage may signal an impending short in three ways.

(1) Cell Voltage Distribution

If the voltage of a cell, which had been part of the normal population, falls significantly below the population, the cell should be suspect.

(2) Voltage Response to the Initial Charge Pulse

The voltage response of cells with impending shorts appears to exhibit an irregular feature near the beginning of the initial charge pulse.

(3) Voltage Response to Overcharge Pulses

A cell with an impending short climbs to the maximum voltage slowly resulting in a ramp waveform.

A normal cell responds by climbing quickly to a maximum voltage and either remaining at that voltage or falling off slightly (due to overcharge heating).

Figure 26 shows the voltage response waveform of Cells 6 and 15, Battery S/N 3-6, during Cycle 7 of Season 3. Cell No. 15 appears normal. Cell No. 6 exhibits the three warning signs identified above. Cell No. 6 developed a short and failed two days later during Cycle 9.

Although Cell No. 15's waveform and working voltages appear normal during Cycle 7 and again during Cycle 9 its OCV decay rate was anomalous during the post-Cycle 9 stand (Paragraph 3.2). Figure 27 shows the voltage response waveforms of Cells 15 and 16, Battery S/N 3-6, during Cycle 33 of Season 3. Once again the three warning signs are present. Cell No. 15 developed a short and failed 14 days later during the charge following the first reconditioning discharge after completion of Season 3.

The absence of similar cell level data analysis for other systems makes it impossible to comment on the generality of these warning signs but it appears that these warning signs should be considered precursors of short circuit failure for the F7/8 battery configuration.

3.6 Teardown Analysis

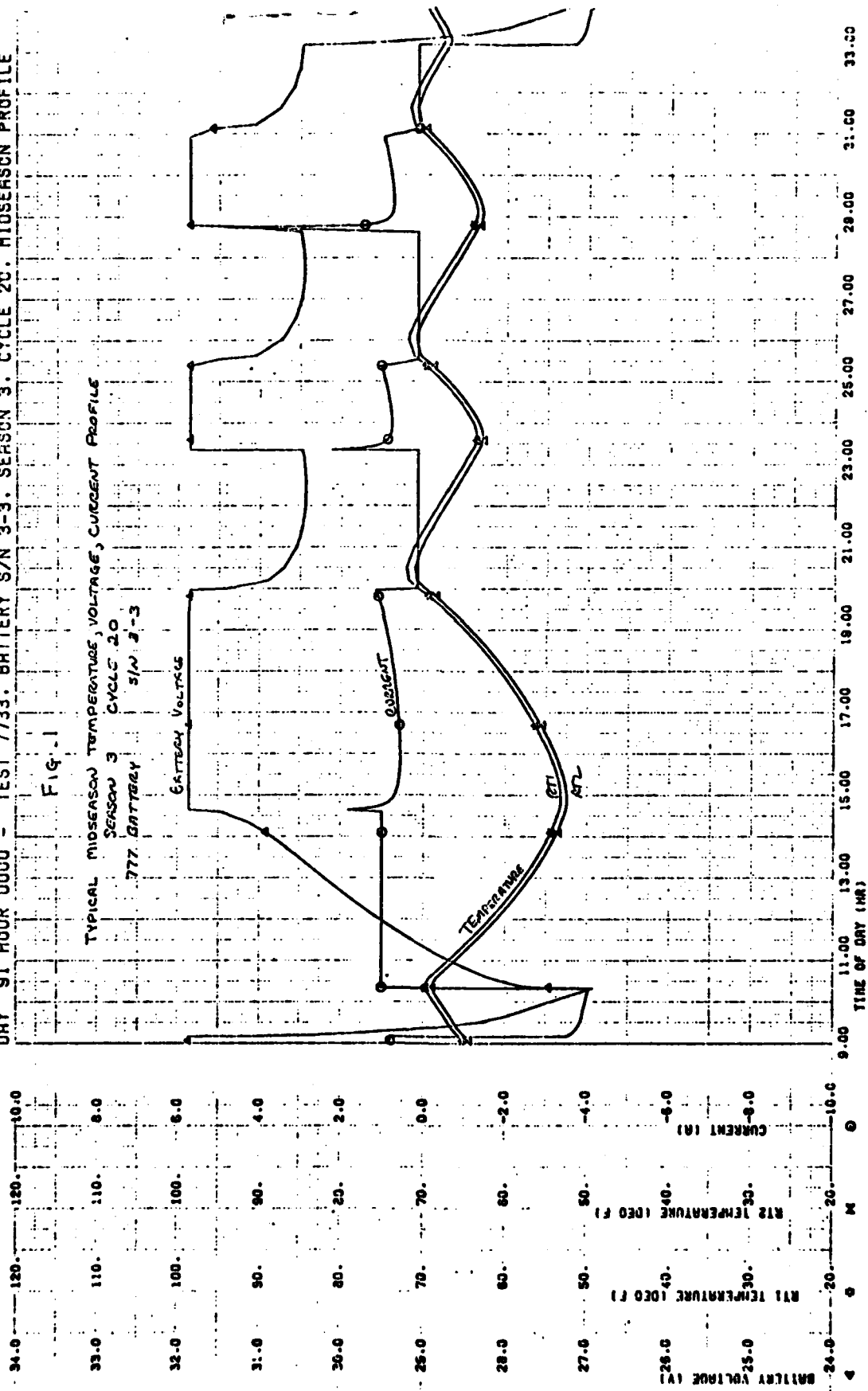
DPA shall be performed on Cells 4, 6, 8, and 15.

Cell No. 8 qualifies for teardown because of low voltage only.

DAY 91 HOUR 0000 - TEST 7733. BATTERY S/N 3-3. SEASON 3. CYCLE 20. MIDSEASON PROFILE

Fig. 1

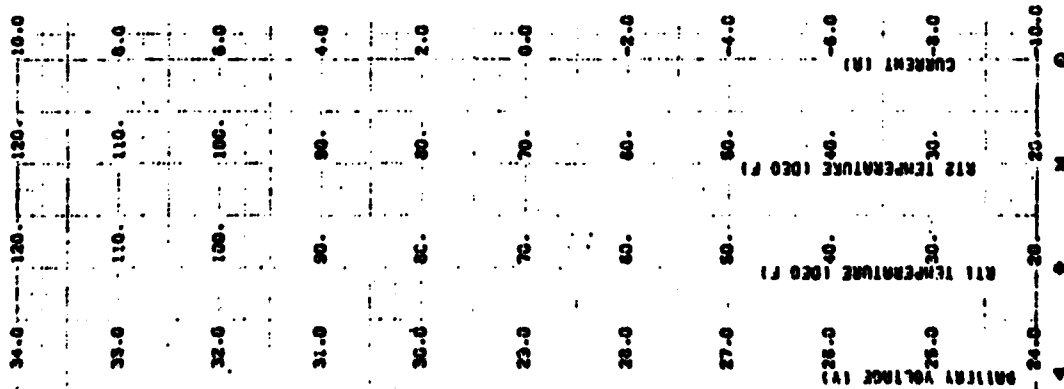
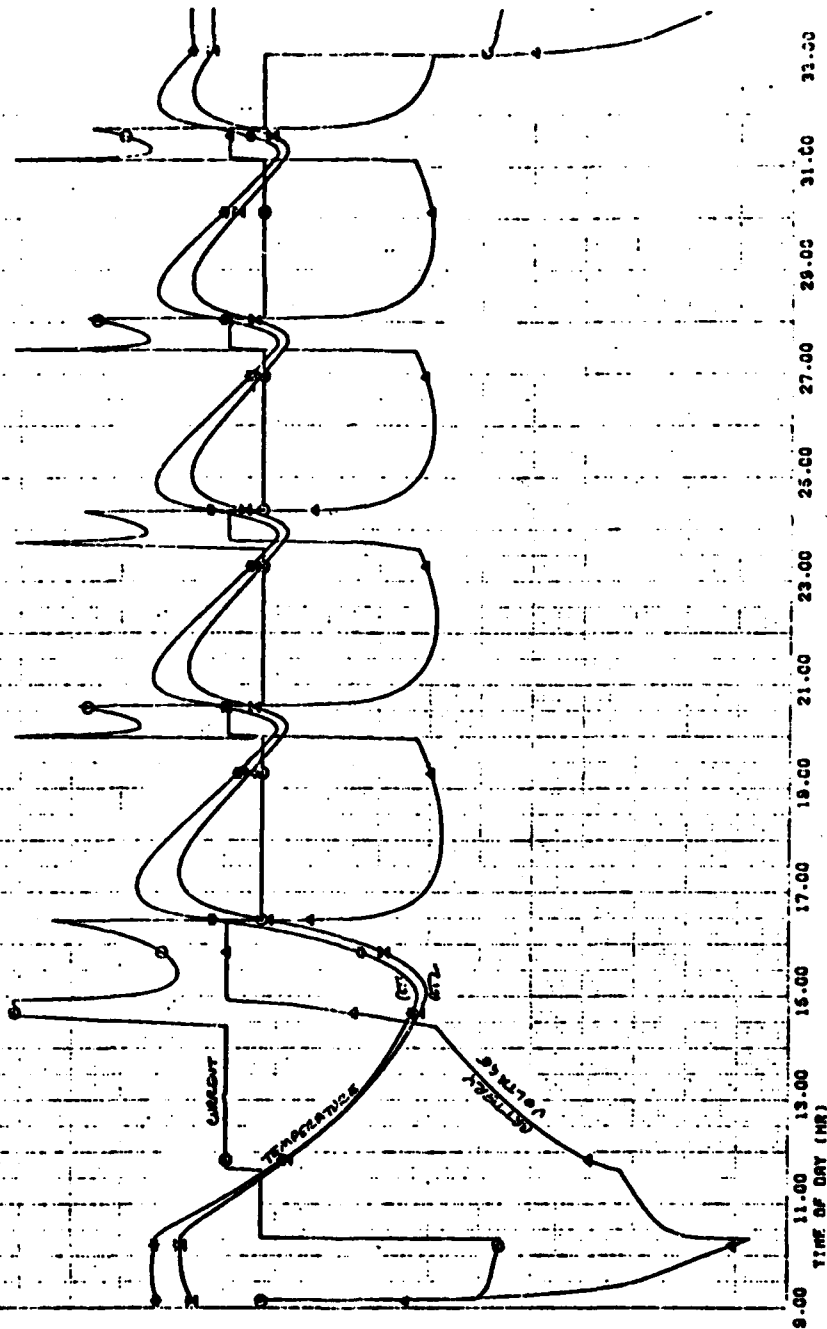
TYPICAL MIDSEASON TEMPERATURE, VOLTAGE, CURRENT PROFILE
SEASON 3 CYCLE 20
777 BATTERY S/N 3-3



DAY 91 HOUR 0000 - TEST 7736. BATTERY S/N 3-6. SEASON 3. CYCLE 20. MIDSEASON PROFILE

FIG 2

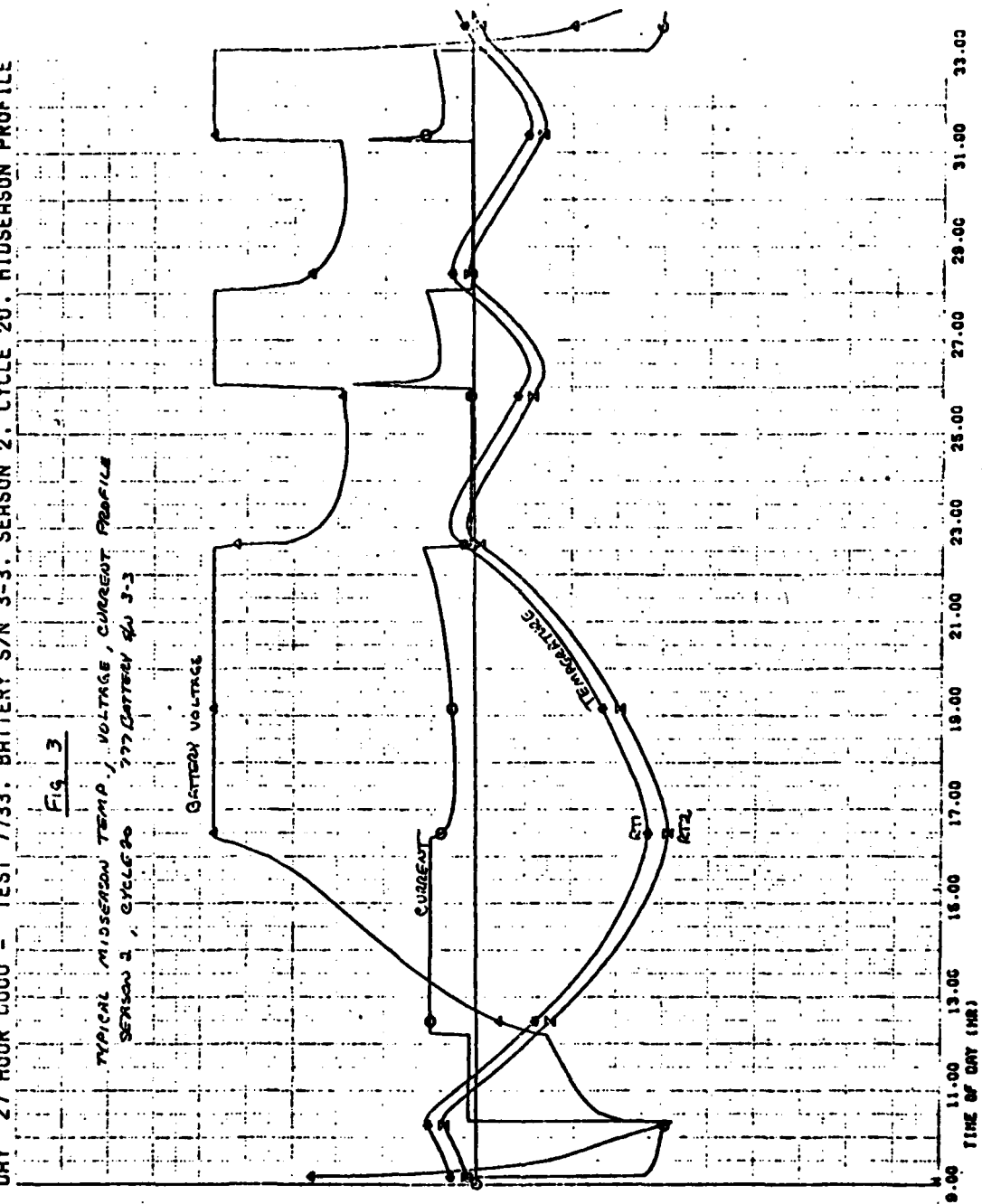
TYPICAL MIDSEASON TEMPERATURE, VOLTAGE, CURRENT PROFILE
SEASON 3 CYCLE 20
777 BATTERY S/N 3-6



DAY 27 HOUR 0000 - TEST 7733, BATTERY S/N 3-3, SEASON 2, CYCLE 20, MIDSEASON PROFILE

Fig 13

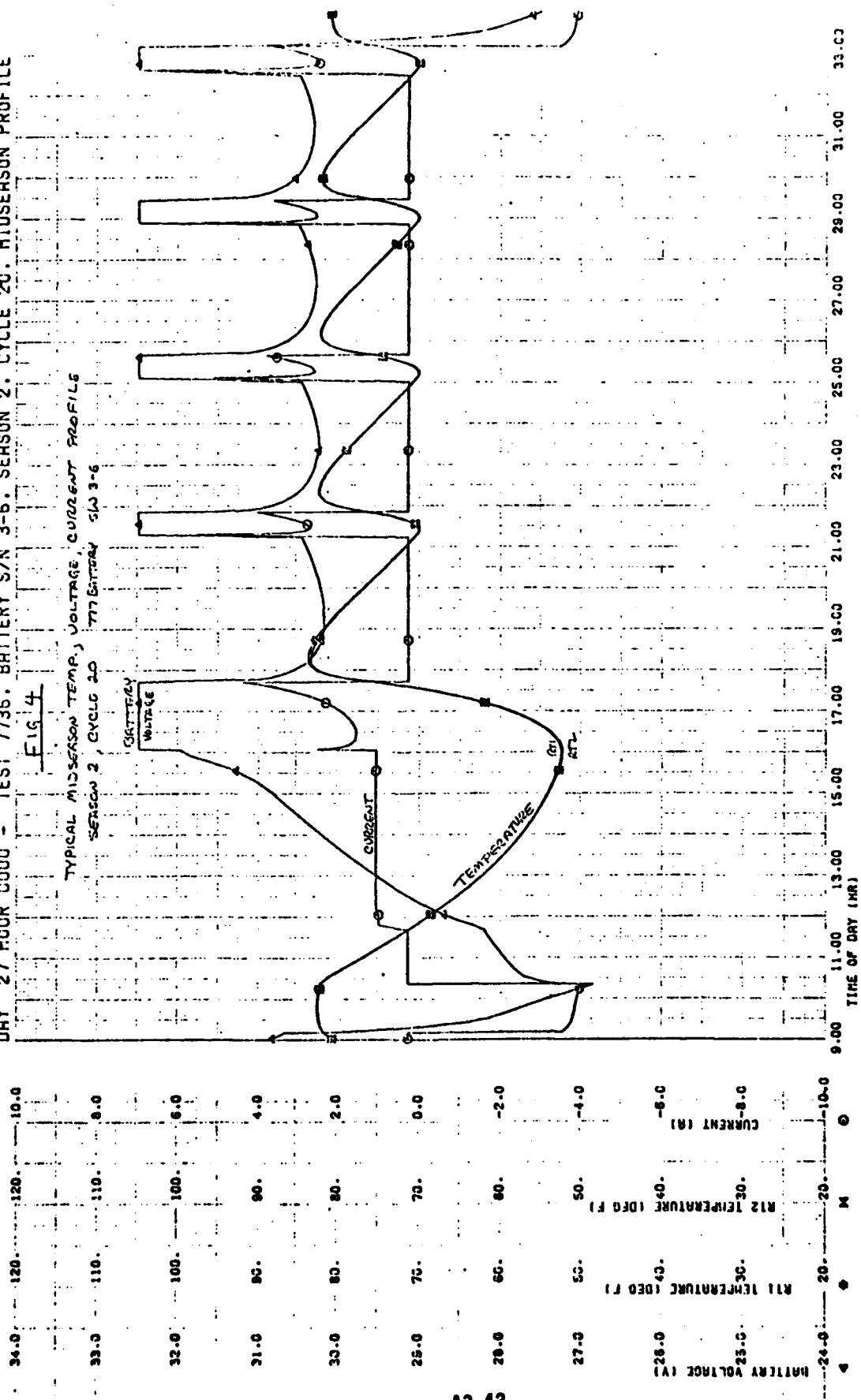
TYPICAL MIDSEASON TEMP, VOLTAGE, CURRENT PROFILE
SEASON 2, CYCLE 20, 777 BATTERY S/N 3-3



DAY 27 HOUR 0000 - TEST 7736, BATTERY S/N 3-6, SEASON 2, CYCLE 20, MIDSEASON PROFILE

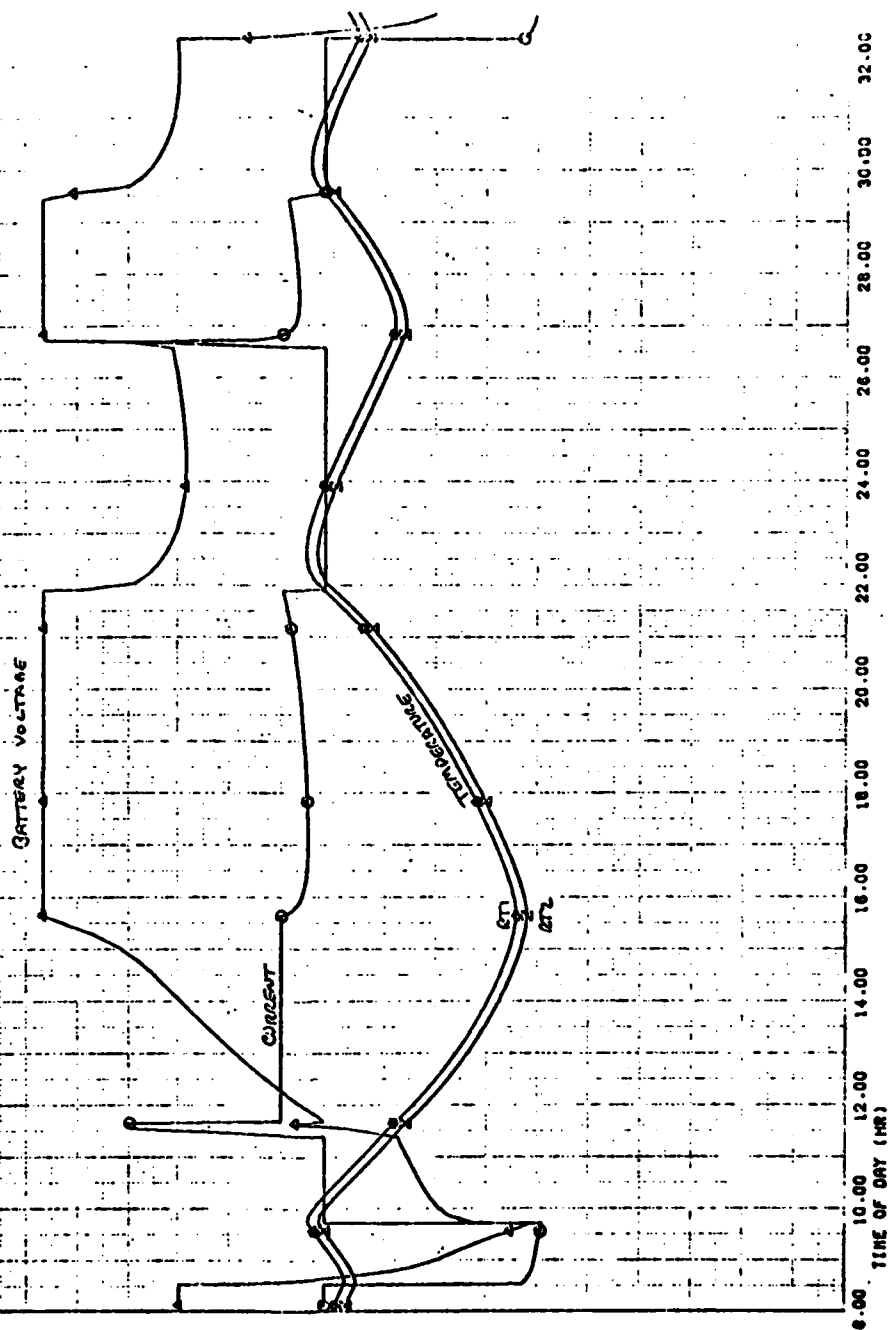
FIG 4

TYPICAL MIDSEASON TEMP., VOLTAGE, CURRENT PROFILE
SEASON 2, CYCLE 20 77 BATTERY S/N 3-6

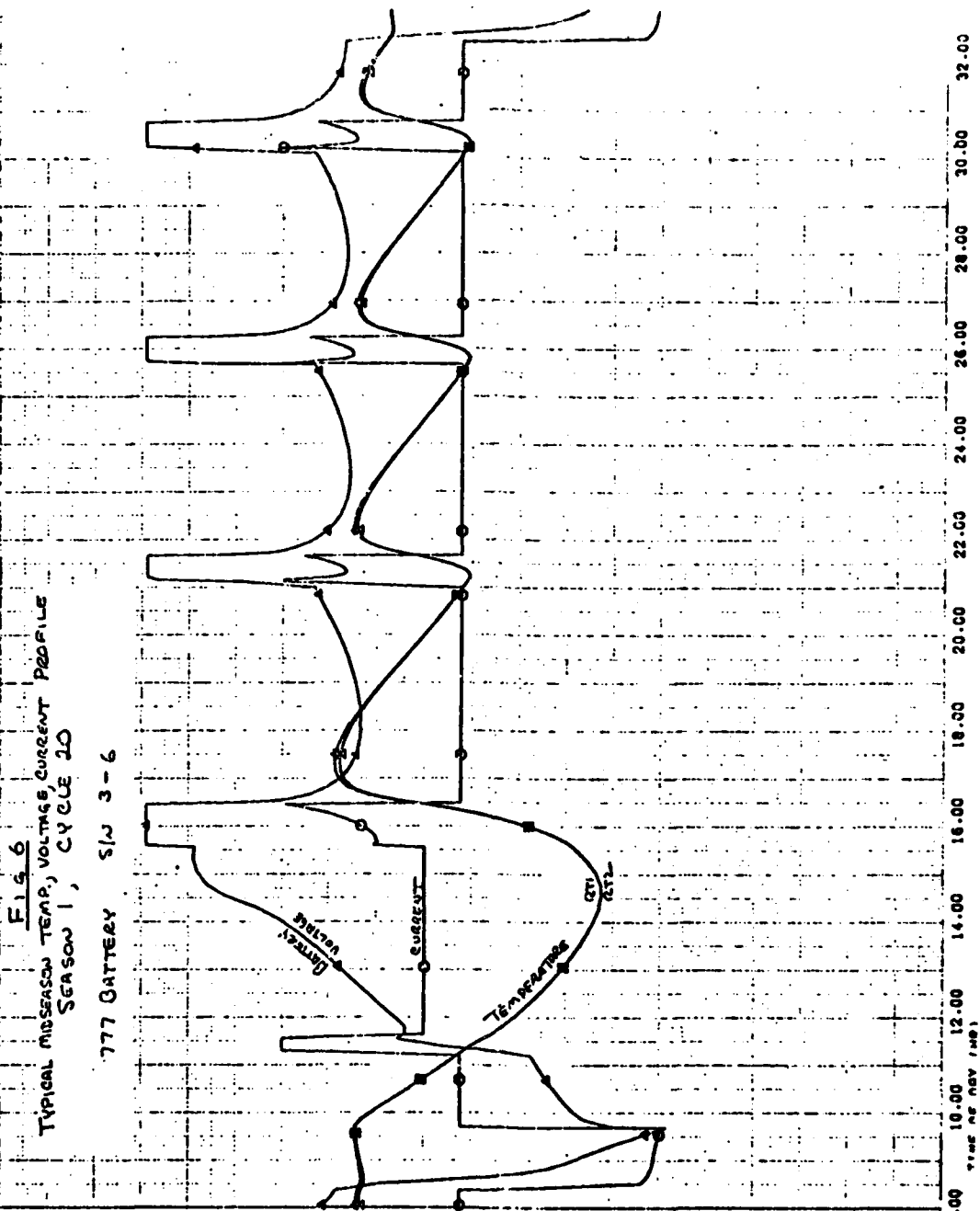


Time	Battery Voltage (V)	RT1 Temperature (deg F)	RT2 Temperature (deg F)	Current (A)
24.0	24.0	28.0	28.0	28.0
23.0	23.0	27.0	27.0	27.0
22.0	23.0	27.0	27.0	27.0
21.0	23.0	27.0	27.0	27.0
20.0	23.0	27.0	27.0	27.0
19.0	23.0	27.0	27.0	27.0
18.0	23.0	27.0	27.0	27.0
17.0	23.0	27.0	27.0	27.0
16.0	23.0	27.0	27.0	27.0
15.0	23.0	27.0	27.0	27.0
14.0	23.0	27.0	27.0	27.0
13.0	23.0	27.0	27.0	27.0
12.0	23.0	27.0	27.0	27.0
11.0	23.0	27.0	27.0	27.0
10.0	23.0	27.0	27.0	27.0

TYPICAL MIDSEASON TEMP., VOLTAGE, CURRENT PROFILE
SEASON, CYCLE 20 777 BATTERY SW 3-3



DAY 327 HOUR 0000 - TEST 7736. BATTERY S/N 3-6. SEASON 1. CYCLE 20. MIDSEASON PROFILE



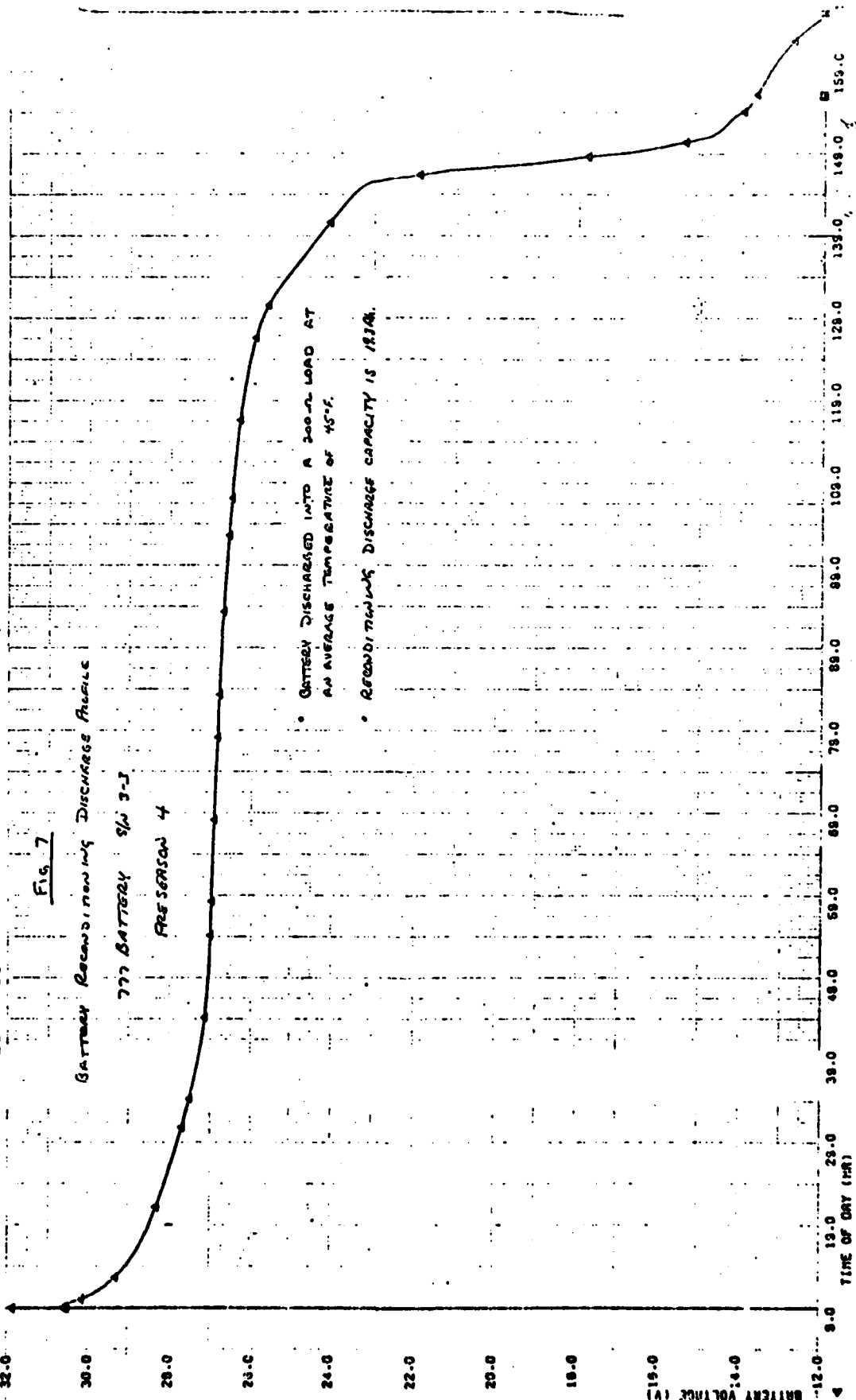
DAY 117 HOUR 0000 - TEST 7733

Fig. 7

BATTERY RECONDITIONING DISCHARGE PROFILE

773 BATTERY S/W 3-3

PRESEASON 4



DAY 117 HOUR 0000 - TEST 7736. RECOND DISCH VOLTAGE PROFILE NO. 1

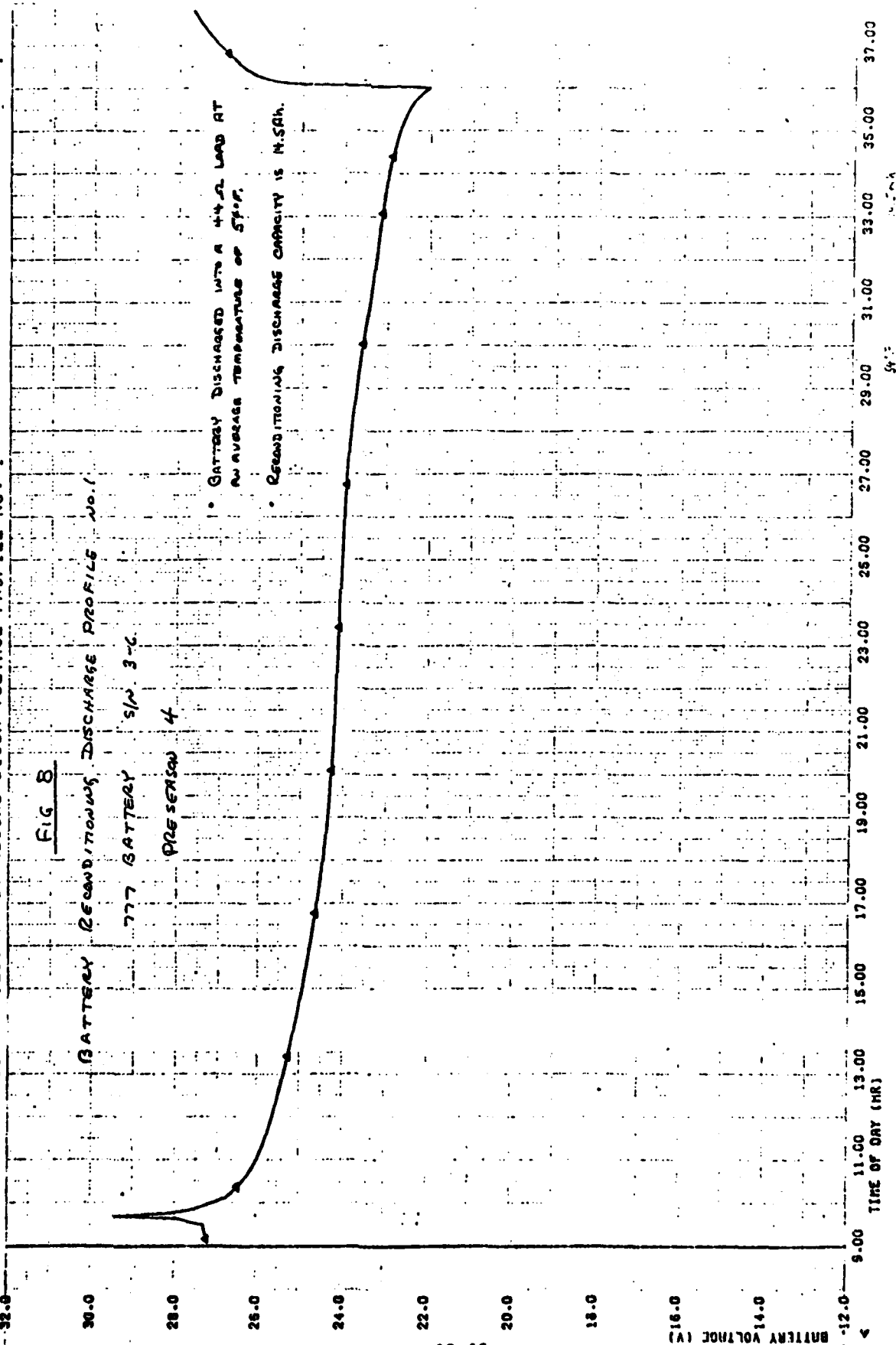
FIG 8

BATTERY RECONDITIONING DISCHARGE PROFILE NO. 1

777 BATTERY S/N 3-C

PRESENCE 4

- BATTERY DISCHARGED INTO A 44-Ω LOAD AT AN AVERAGE TEMPERATURE OF 54°F.
- RECONDITIONING DISCHARGE CAPACITY IS 14.5Ah.



DAY 121 HOUR 0000 - TEST 7736. RECOND. DISCH. VOLTAGE PROFILE NO. 2

Fig 9

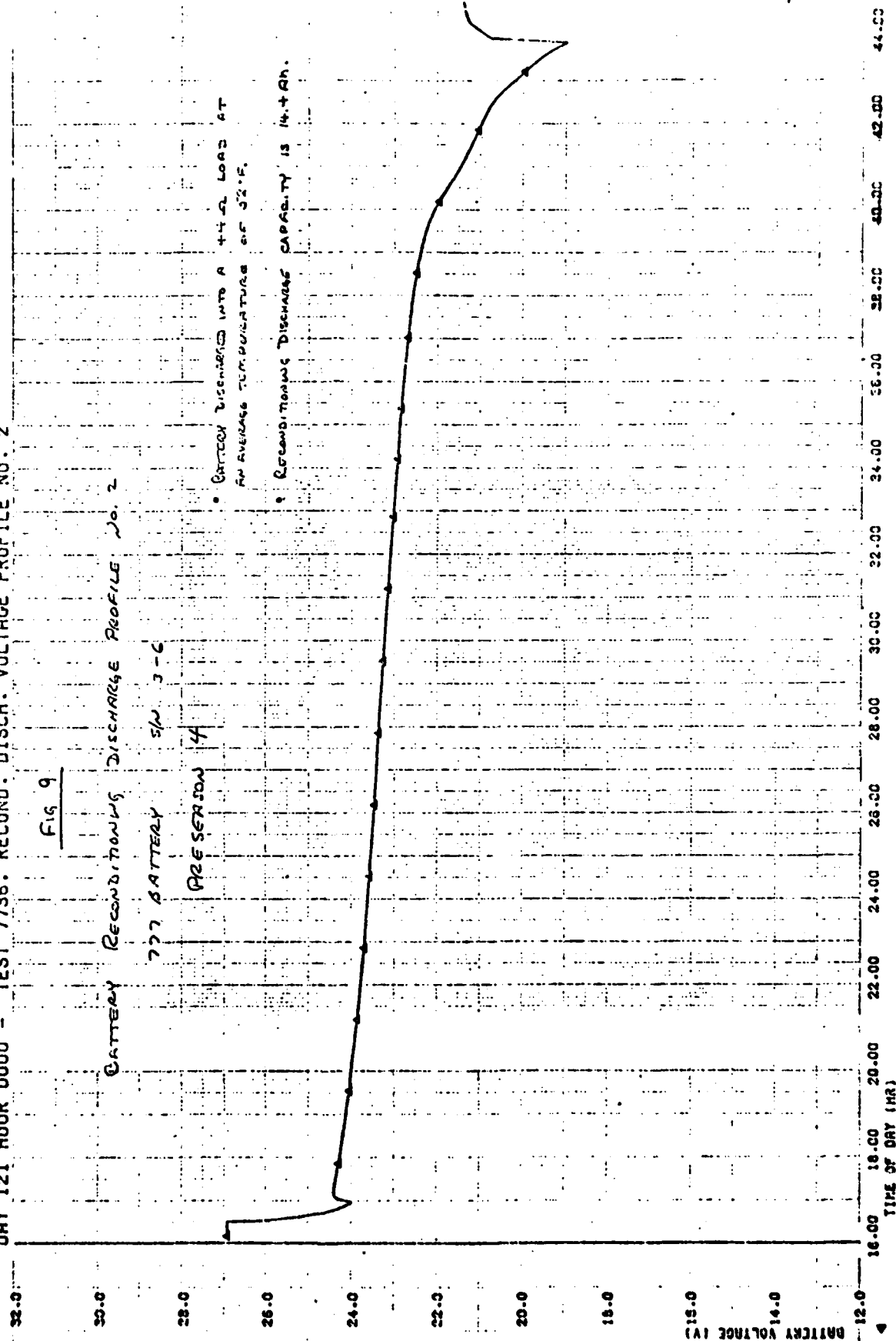
BATTERY RECONDITIONING DISCHARGE PROFILE NO. 2

777 BATTERY S/N 3-6

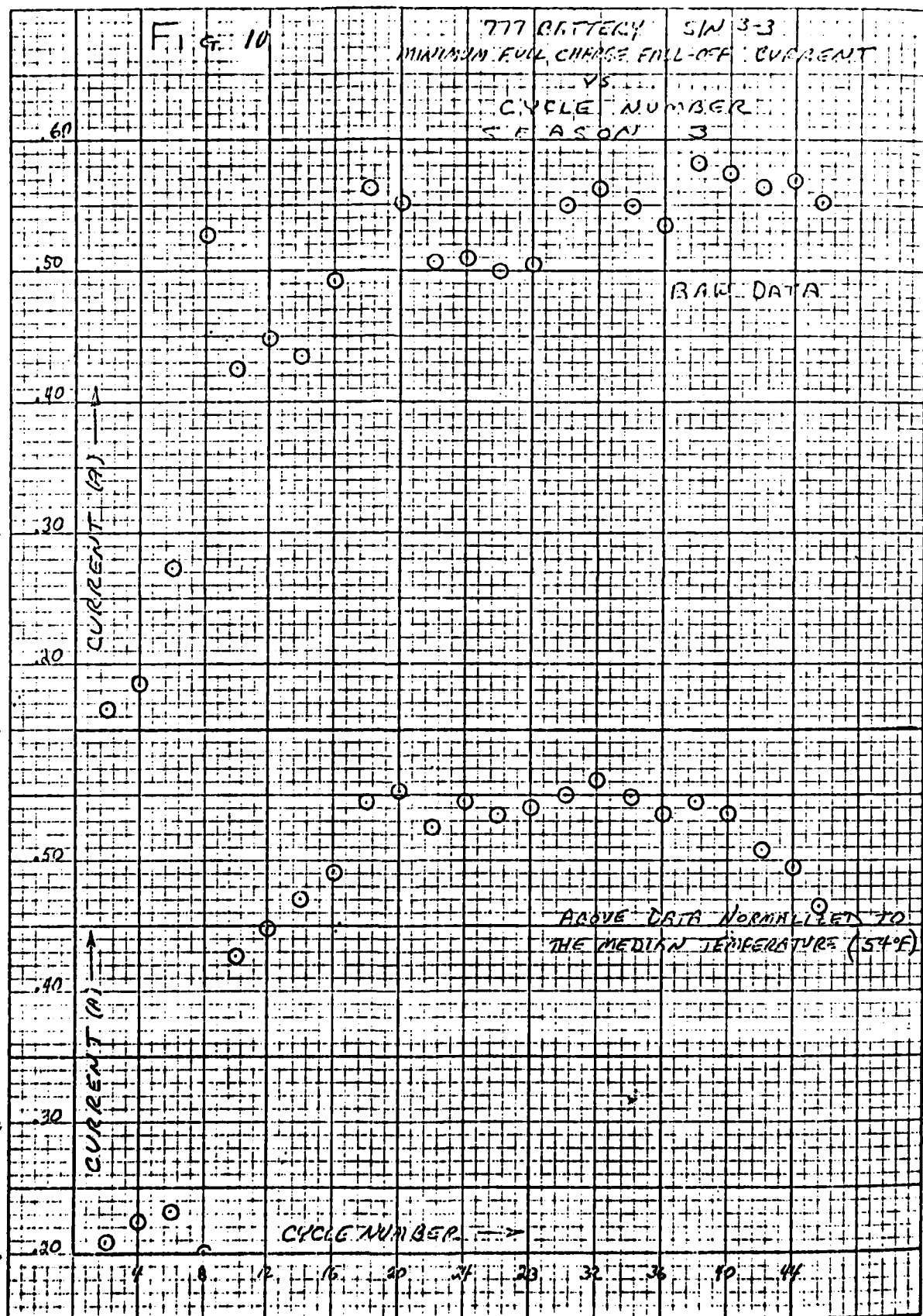
PRE-SEASON 74

BATTERY DISCHARGED INTO A 44 OHM LOAD AT AN AVERAGE TEMPERATURE OF 52°F.

RECONDITIONING DISCHARGE CAPACITY IS 14.4 AH.

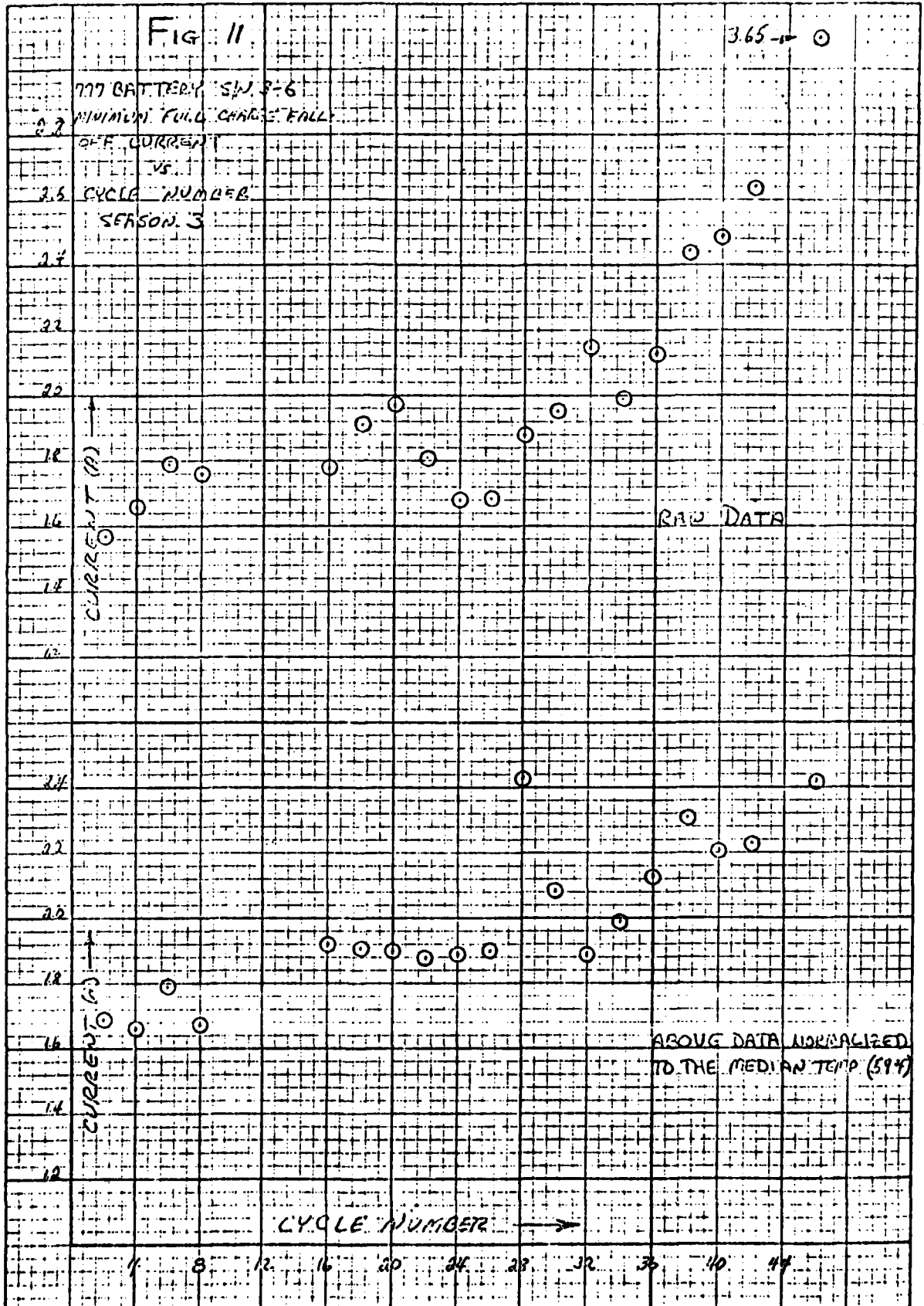


K-E 10 X 10 TO THE INCH • 7 X 10 INCHES
KUMMEL & ESSER CO. MADE IN U.S.A.

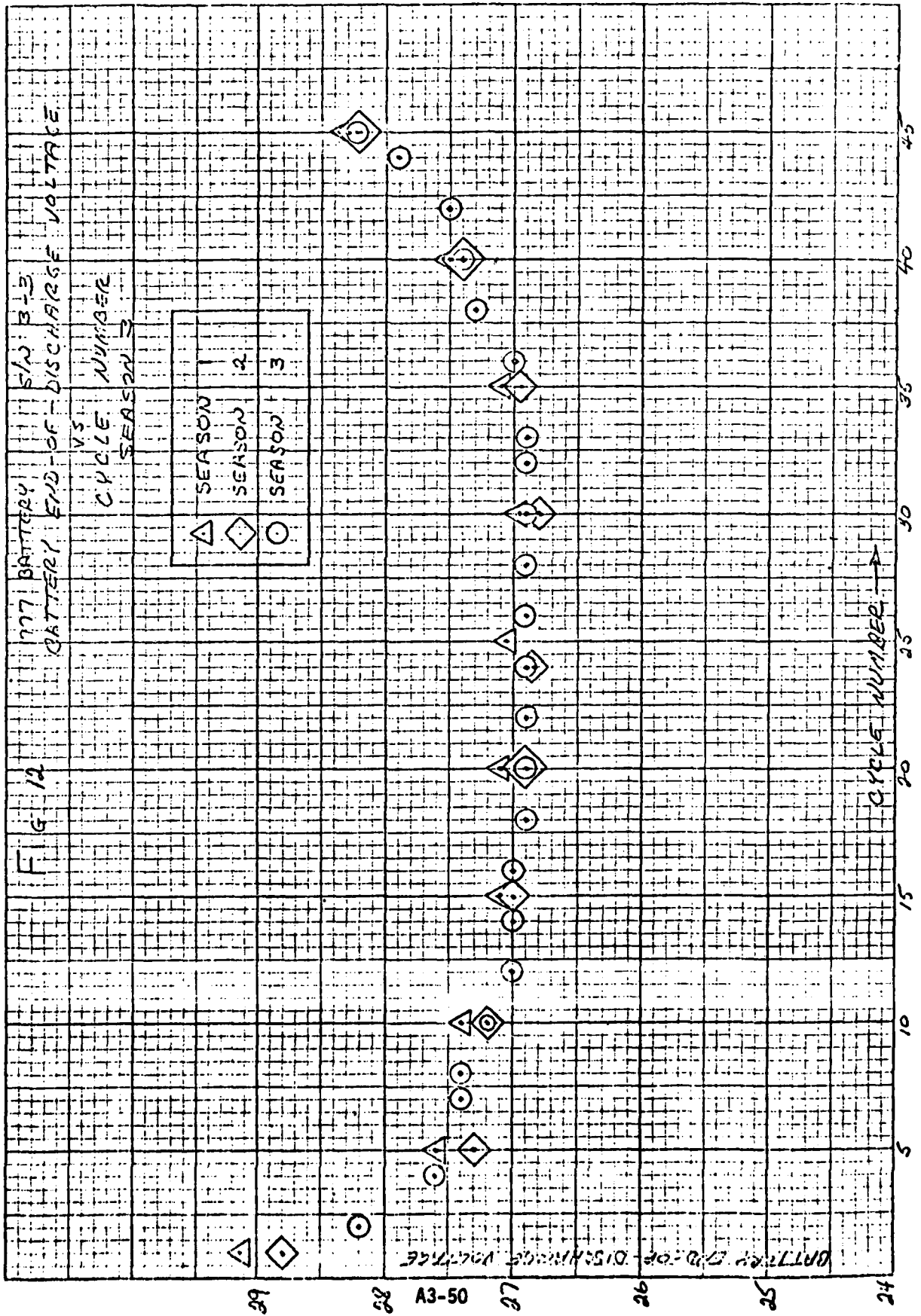


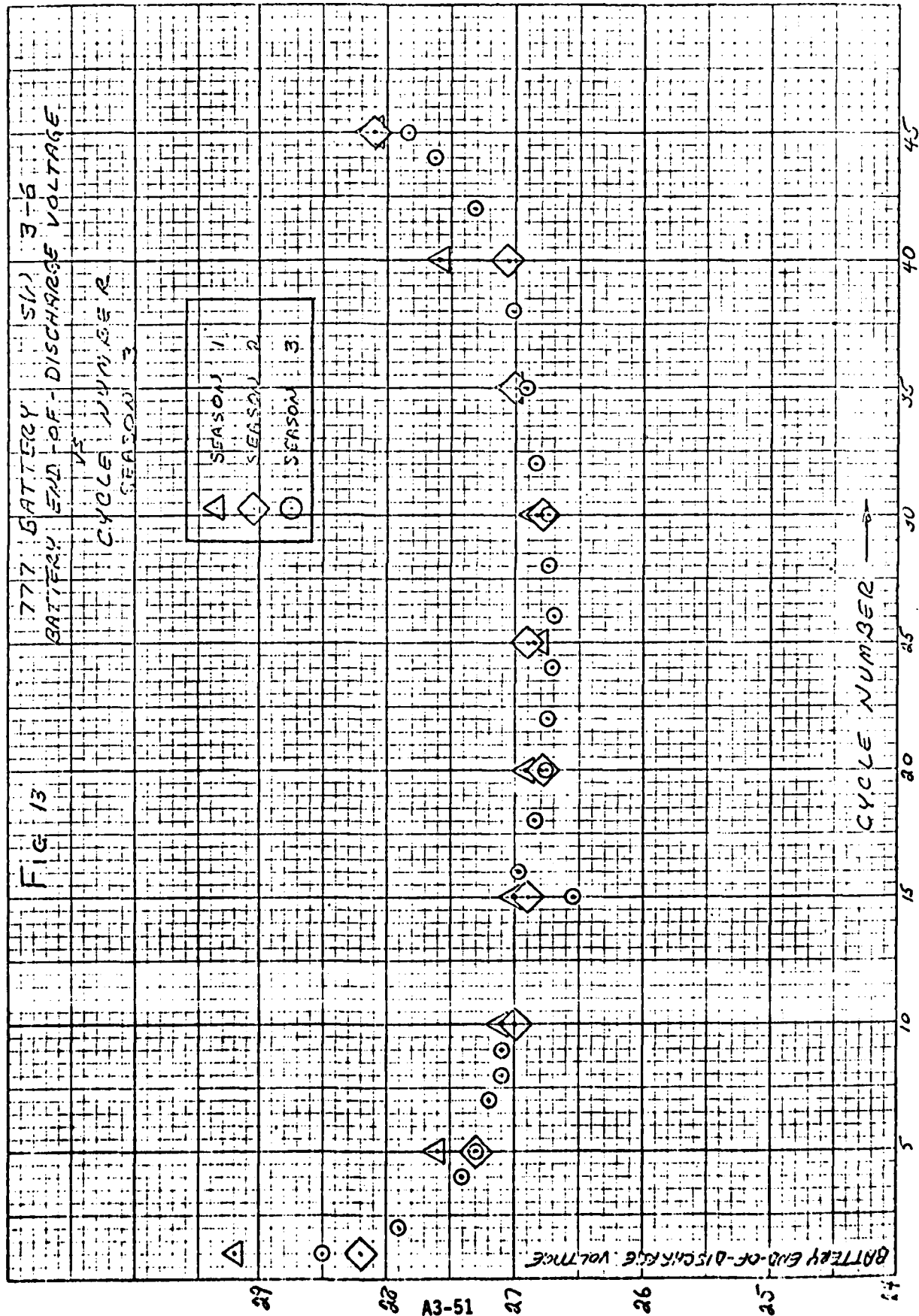
46 0780

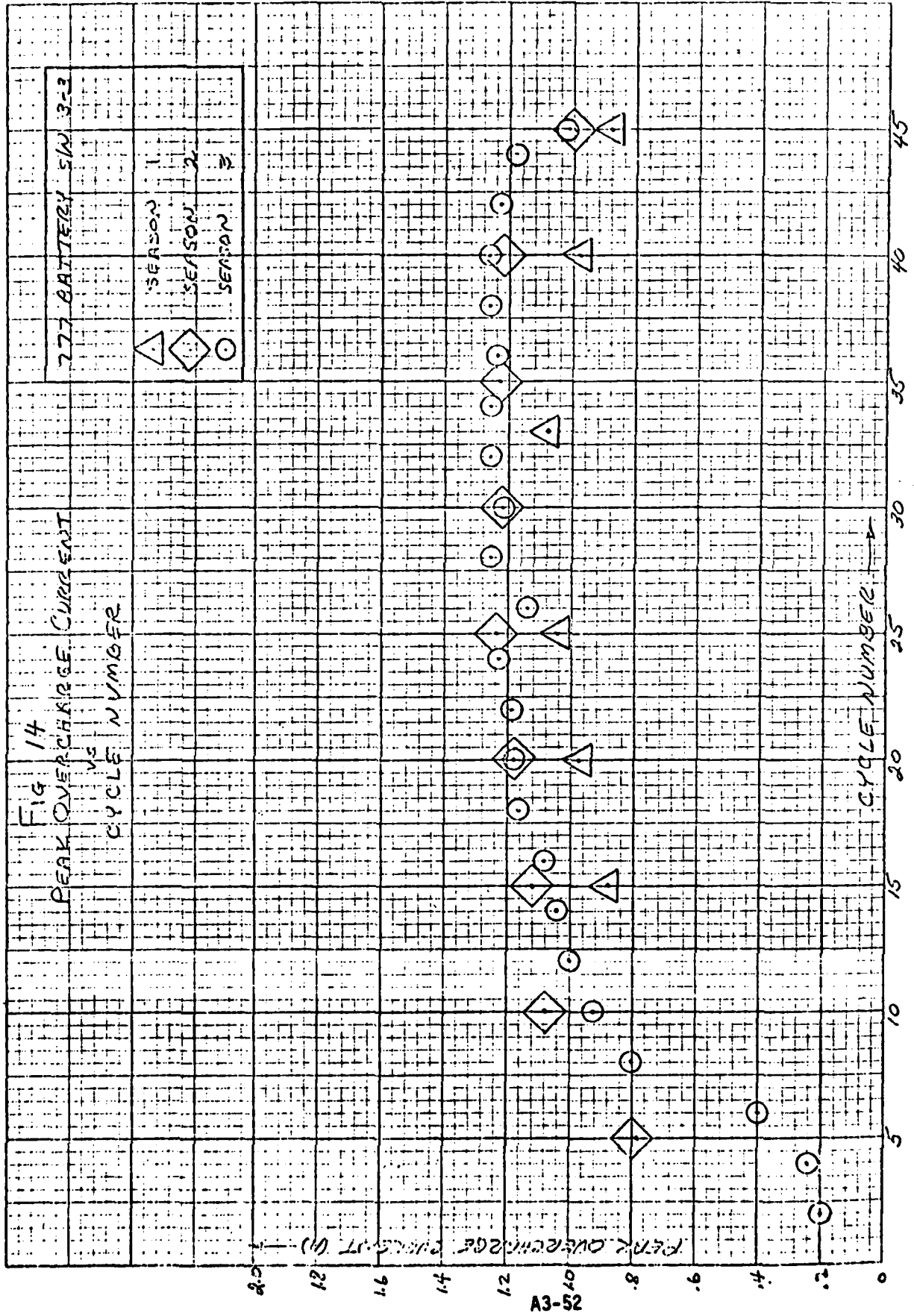
K&E 10 X 10 TO THE INCH • 7 X 10 INCHES
K&E NEUFEL & ESSER CO. MADE IN U.S.A.



10 X 10 TO THE INCHES
NEUPPEL & ESSEN CO. MADE IN U.S.A.







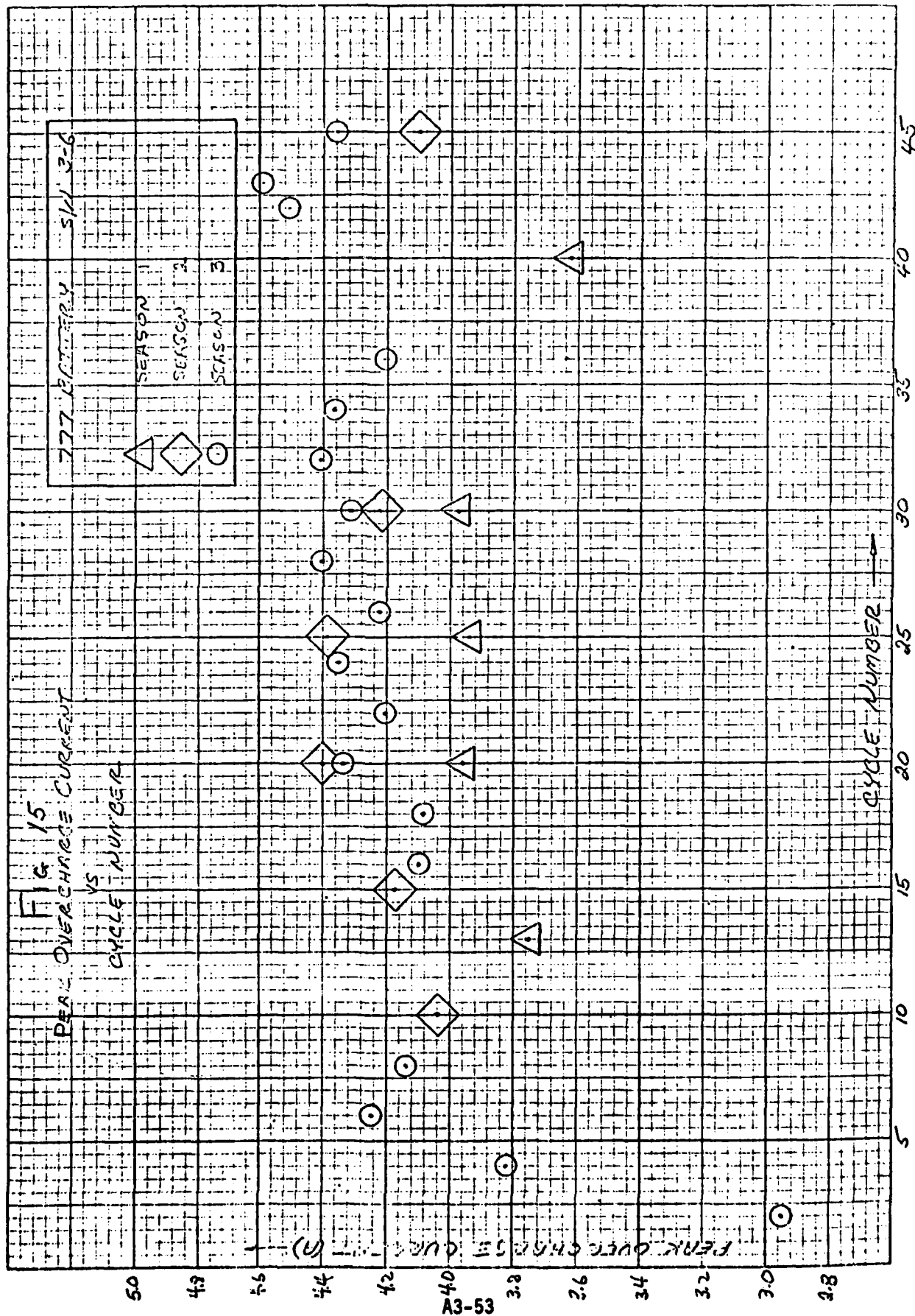


FIG 16

TEST 7736, BATTERY SW 3-6
SEASON 3, CYCLE 9

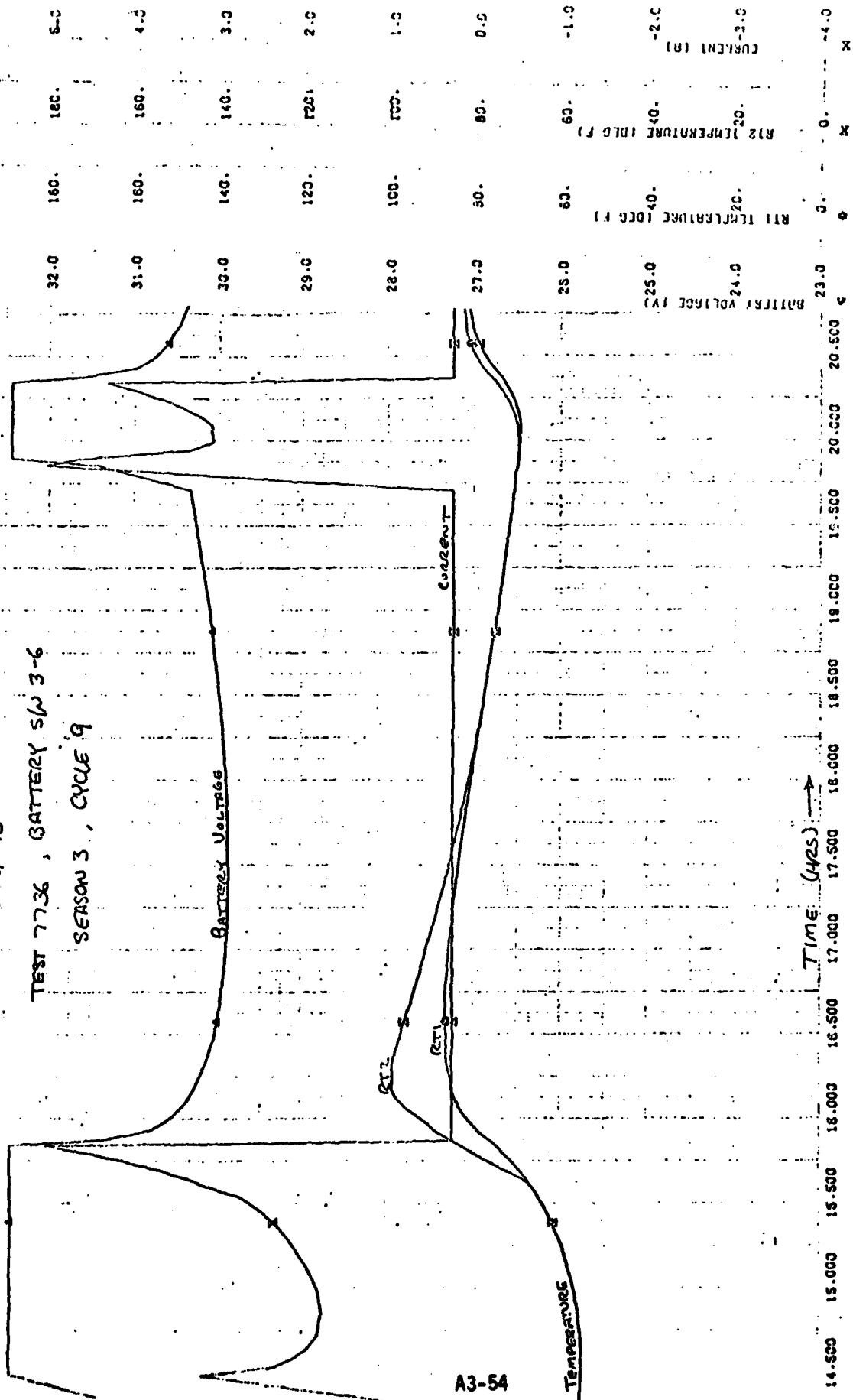


FIG 17

CELL VOLTAGE

777 PROGRAM BATTERY SW 3-6 SEASON 3 CYCLE 9 FLIGHT 7/8 SIMULATION

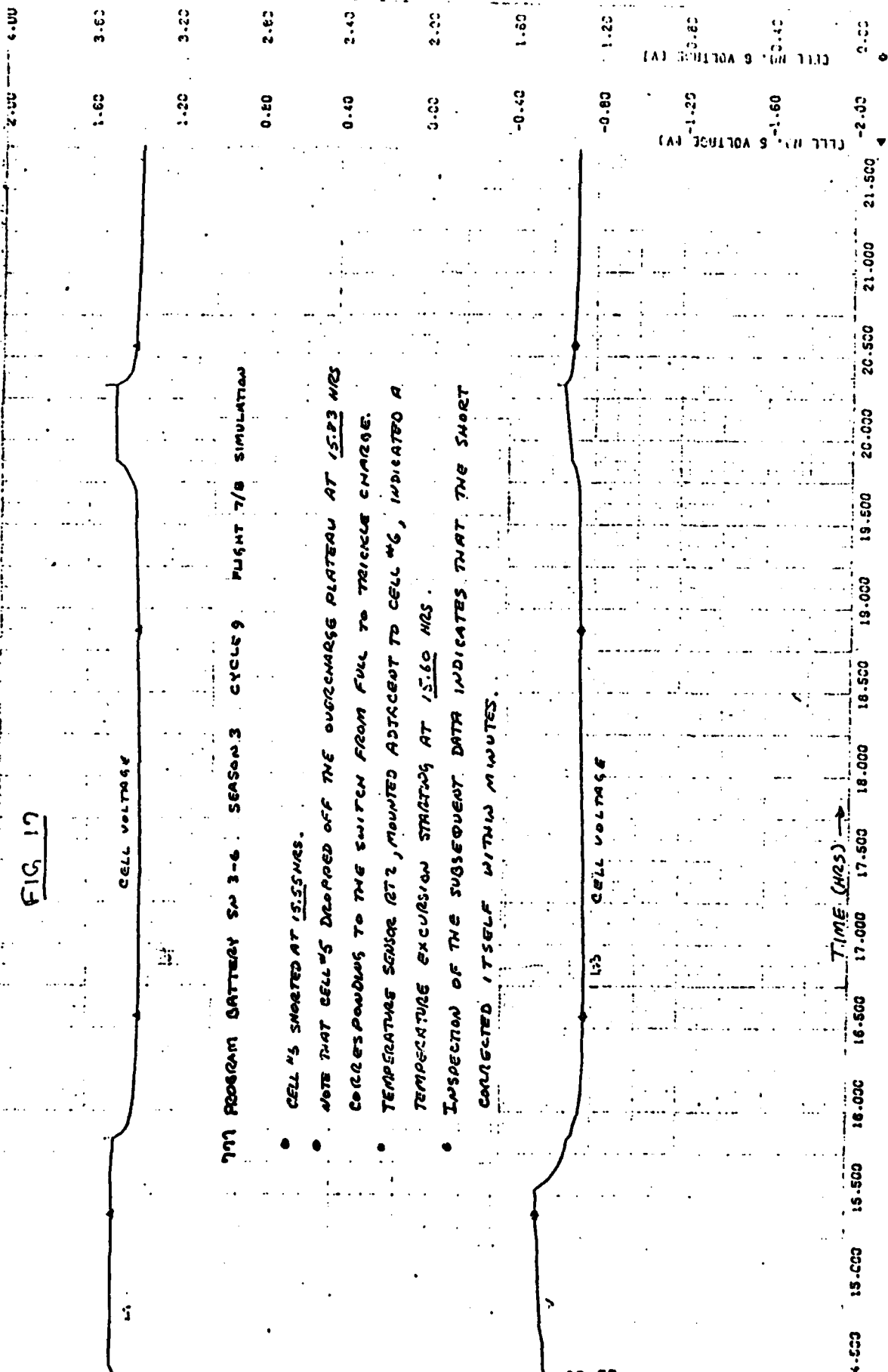
- CELL #3 SHORTED AT 15.55 HRS.
- NOTE THAT CELL #5 DROPPED OFF THE OVERCHARGE PLATFORM AT 15.23 HRS CORRESPONDING TO THE SWITCH FROM FULL TO TRICKLE CHARGE.
- TEMPERATURE SENSOR 1272, MOUNTED ADJACENT TO CELL #6, INDICATED A TEMPERATURE EXCURSION STARTING AT 15.60 HRS.
- INSPECTION OF THE SUBSEQUENT DATA INDICATES THAT THE SHORT CORRECTED ITSELF WITHIN MINUTES.

A3-55

CELL VOLTAGE

TIME (HRS)

(A) CELL #3 VOLTAGE (V) (B) CELL #5 VOLTAGE (V)



F. 9 18

EST 7736. S/N 3-6. SEASON 3. CYCLE 9

A3-56

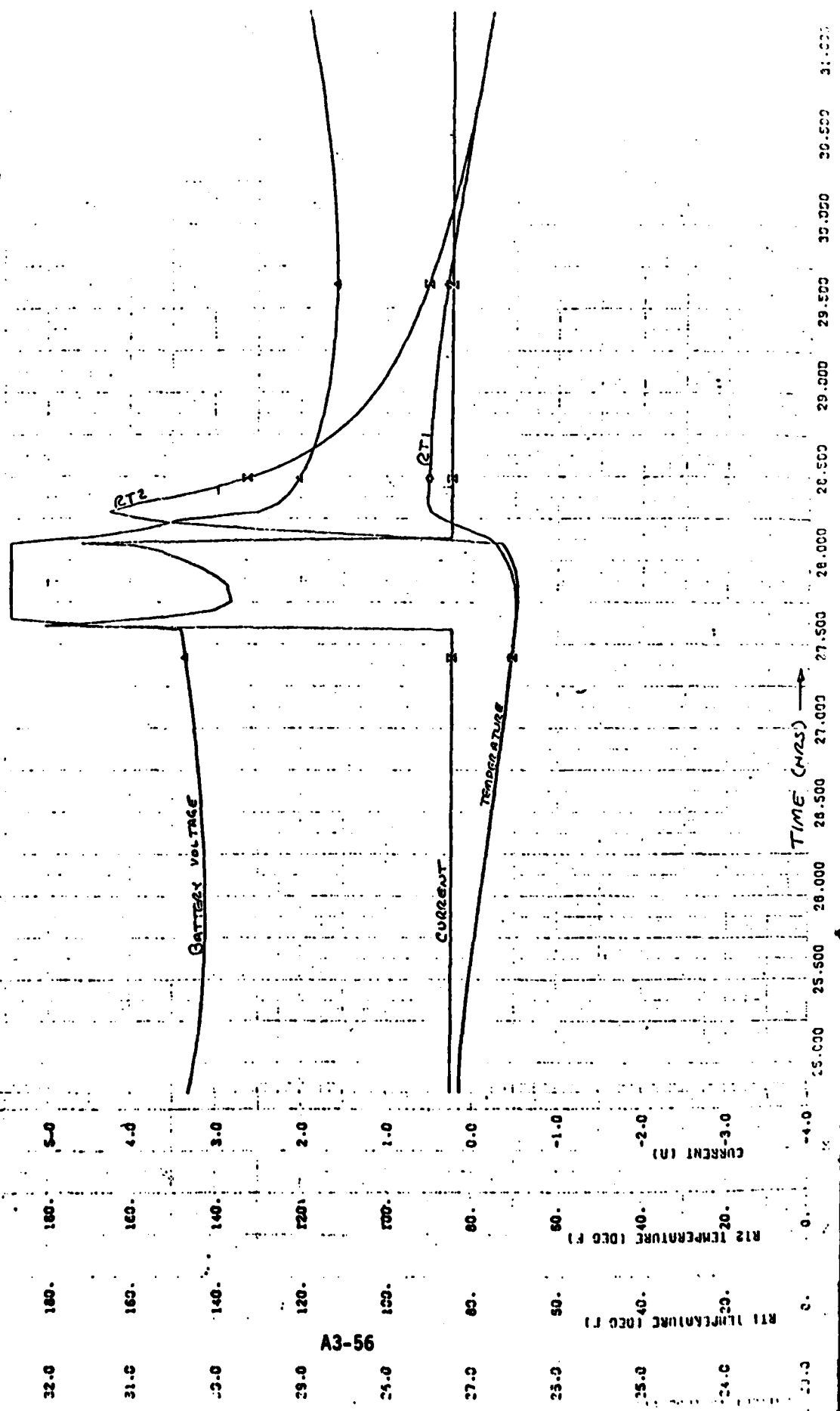
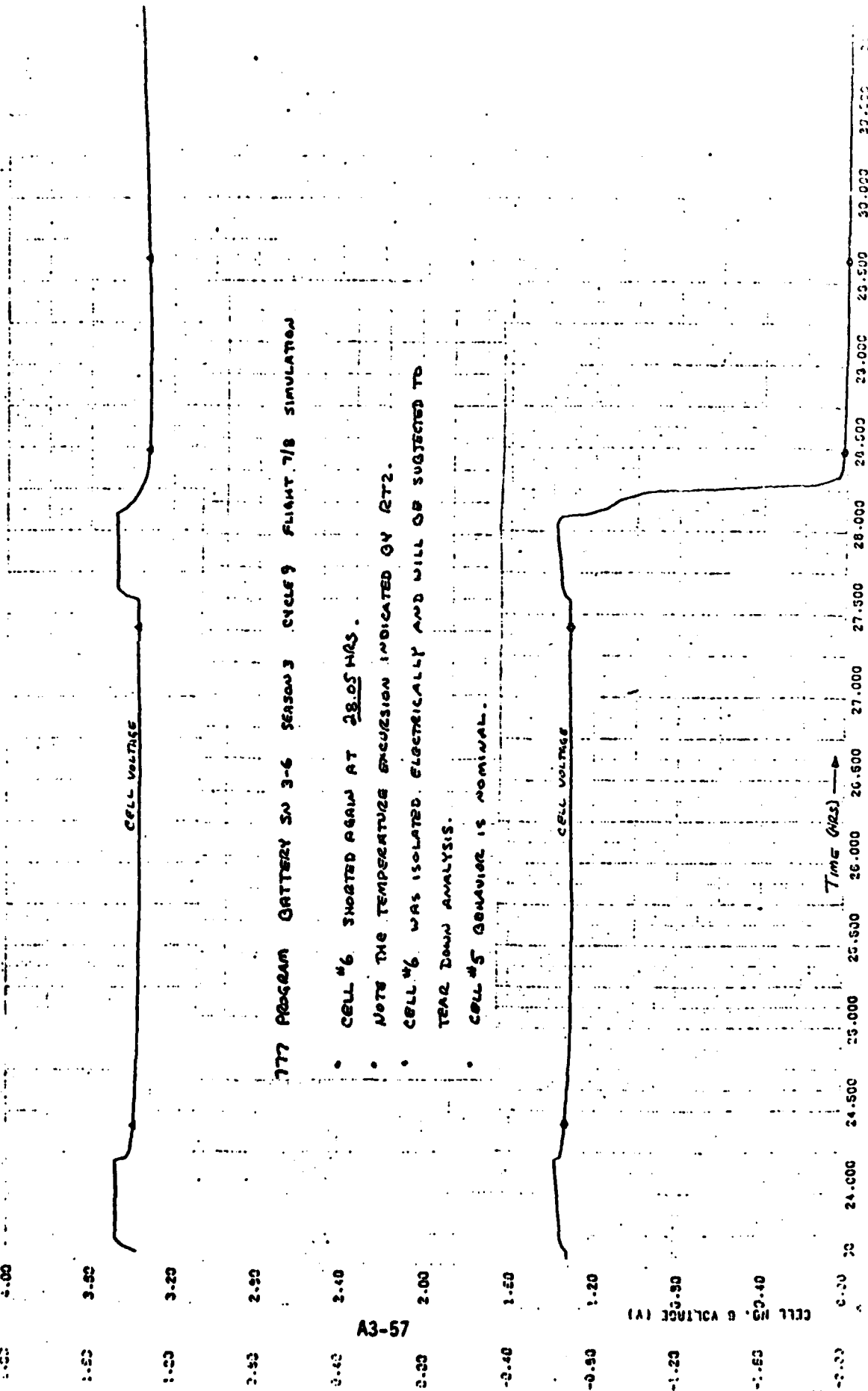


Fig 19

EST 7736. S/N 3-6. SEASON 3. CYCLE 9

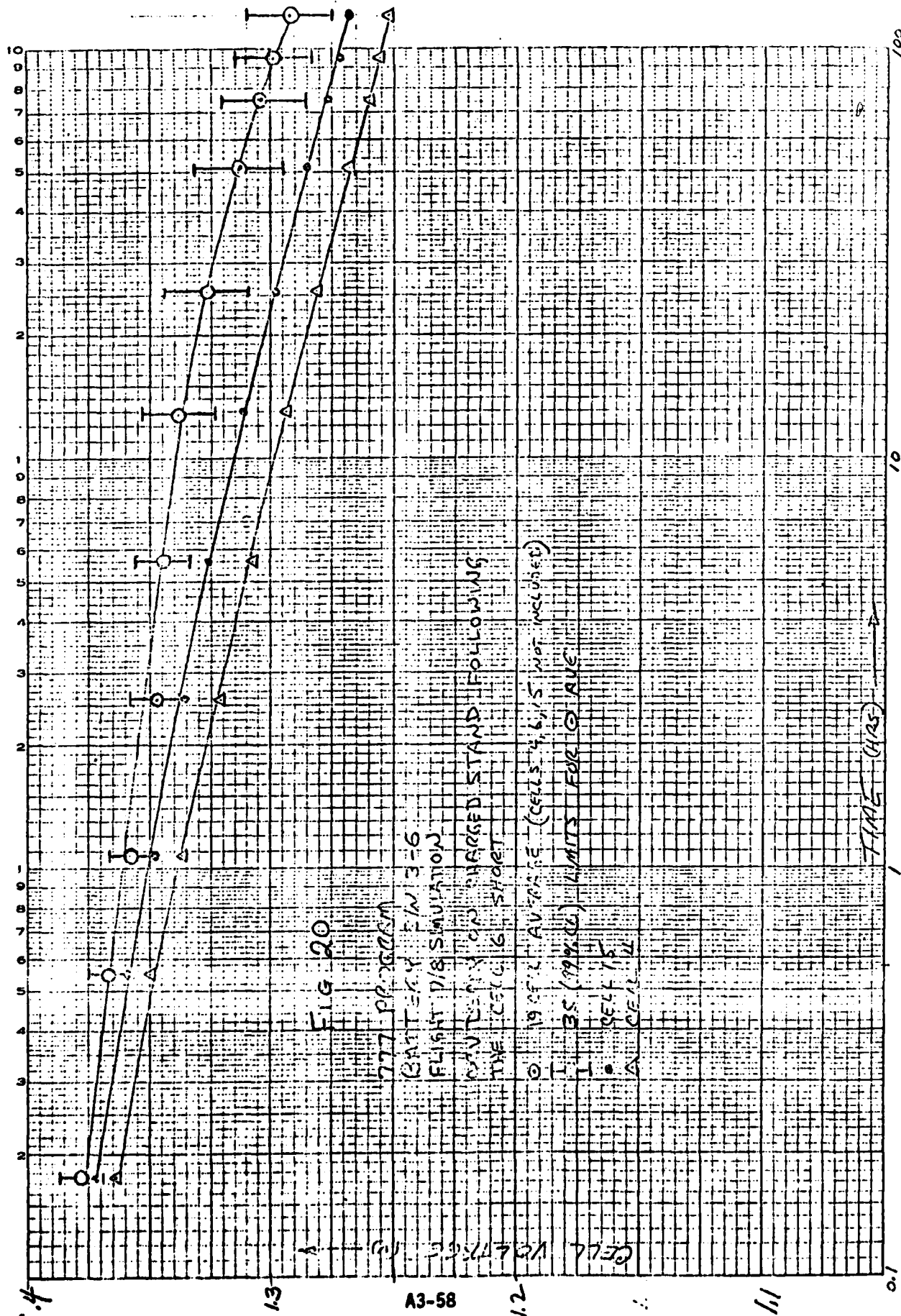


777 PROGRAM BATTERY SN 3-6 SEASON 3 CYCLE 9 FLIGHT 7/8 SIMULATION

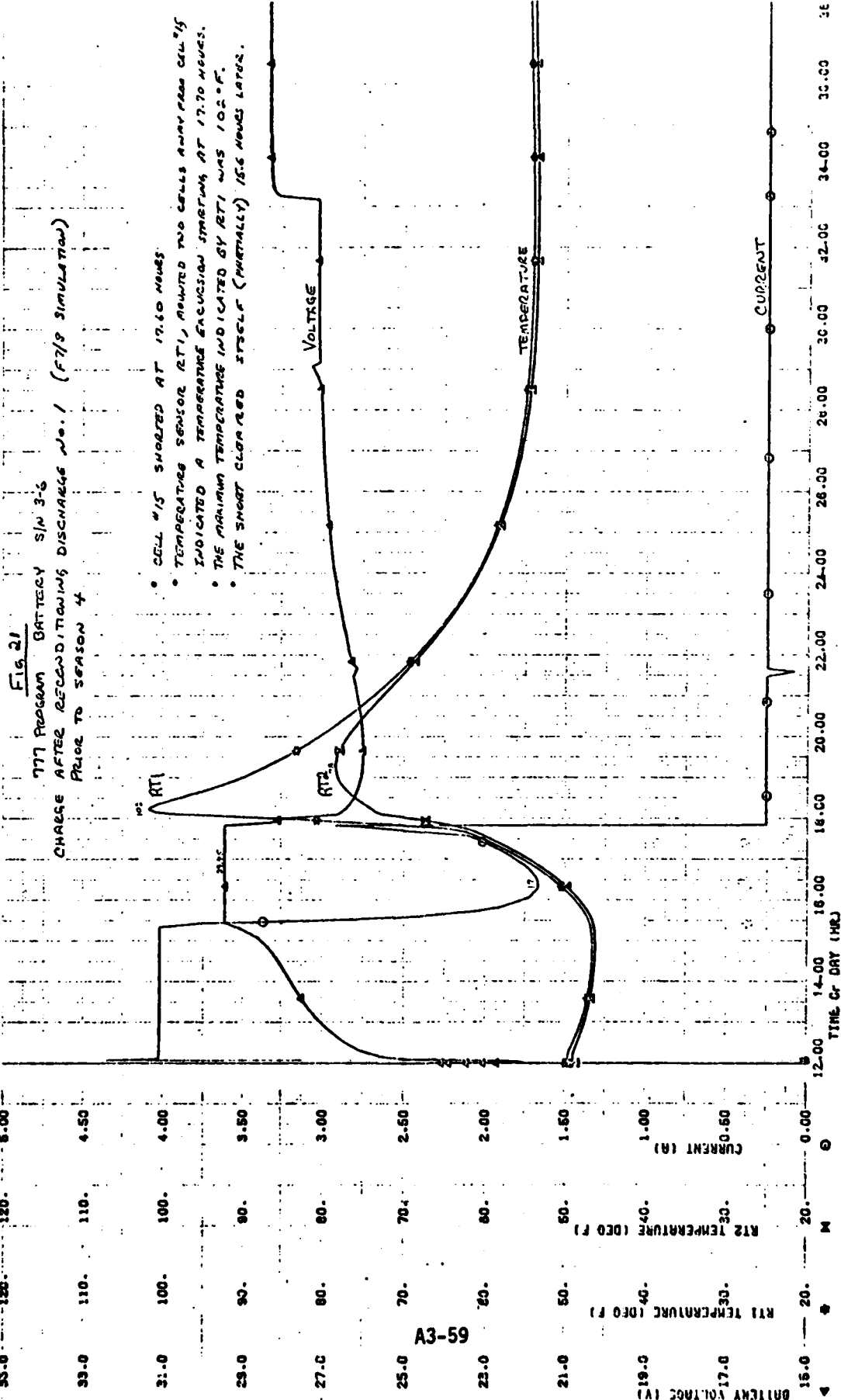
- CELL #6 SHORTED AGAIN AT 28.05 HRS.
- NOTE THE TEMPERATURE EXCURSION INDICATED BY RT2.
- CELL #6 WAS ISOLATED ELECTRICALLY AND WILL BE SUBJECTED TO TEAR DOWN ANALYSIS.
- CELL #5 BEHAVIOR IS NOMINAL.

A3-57

(A) 30017CA 9 60 7736

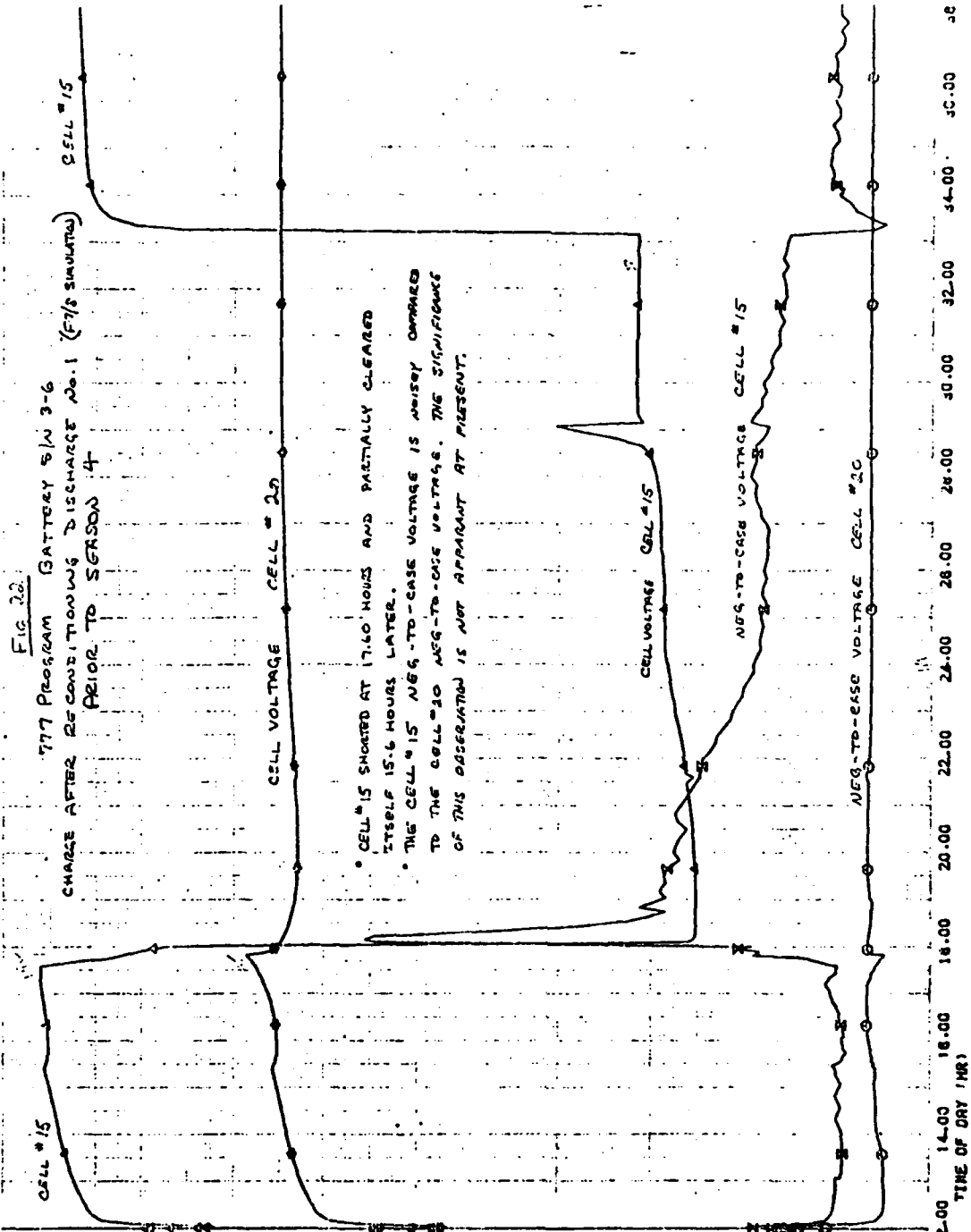


DAY 118 HOUR 0000 - TEST 7736. CHARGE AFTER RECONDITIONING DISCHARGE NO. 1



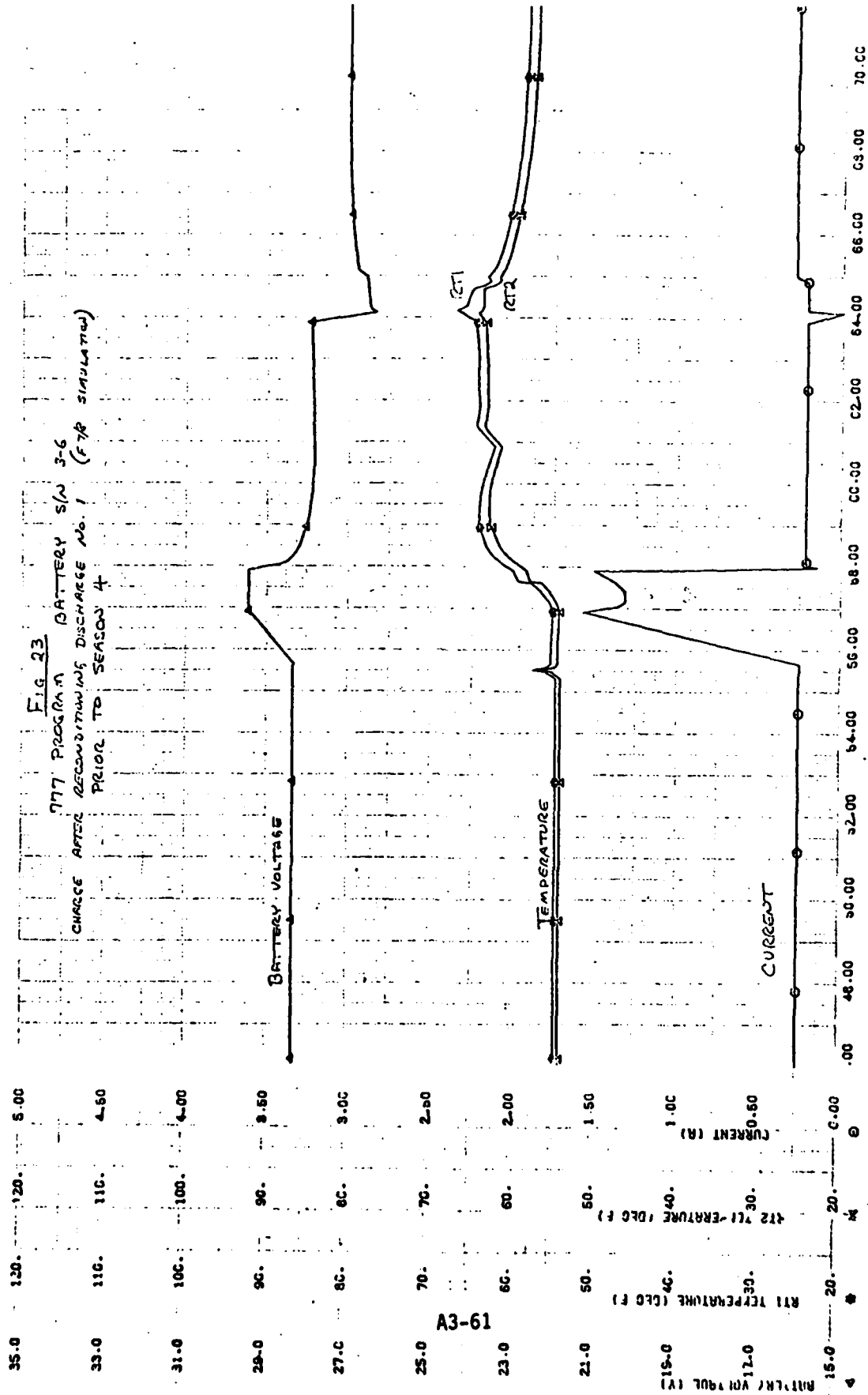
- CELL #15 SHORTED AT 17.60 HOURS
- TEMPERATURE SENSOR RT1, MONITORED TWO CELLS AWAY FROM CELL #15
- INDICATED A TEMPERATURE EXCURSION STARTING AT 17.70 HOURS.
- THE MINIMUM TEMPERATURE INDICATED BY RT1 WAS 102°F.
- THE SHORT CLEARED ITSELF (PARTIALLY) 15.6 HOURS LATER.

DRY 118 HOUR 0000 TEST 7736 - CHARGE AFTER RECONDITIONING DISCHARGE NO. 1



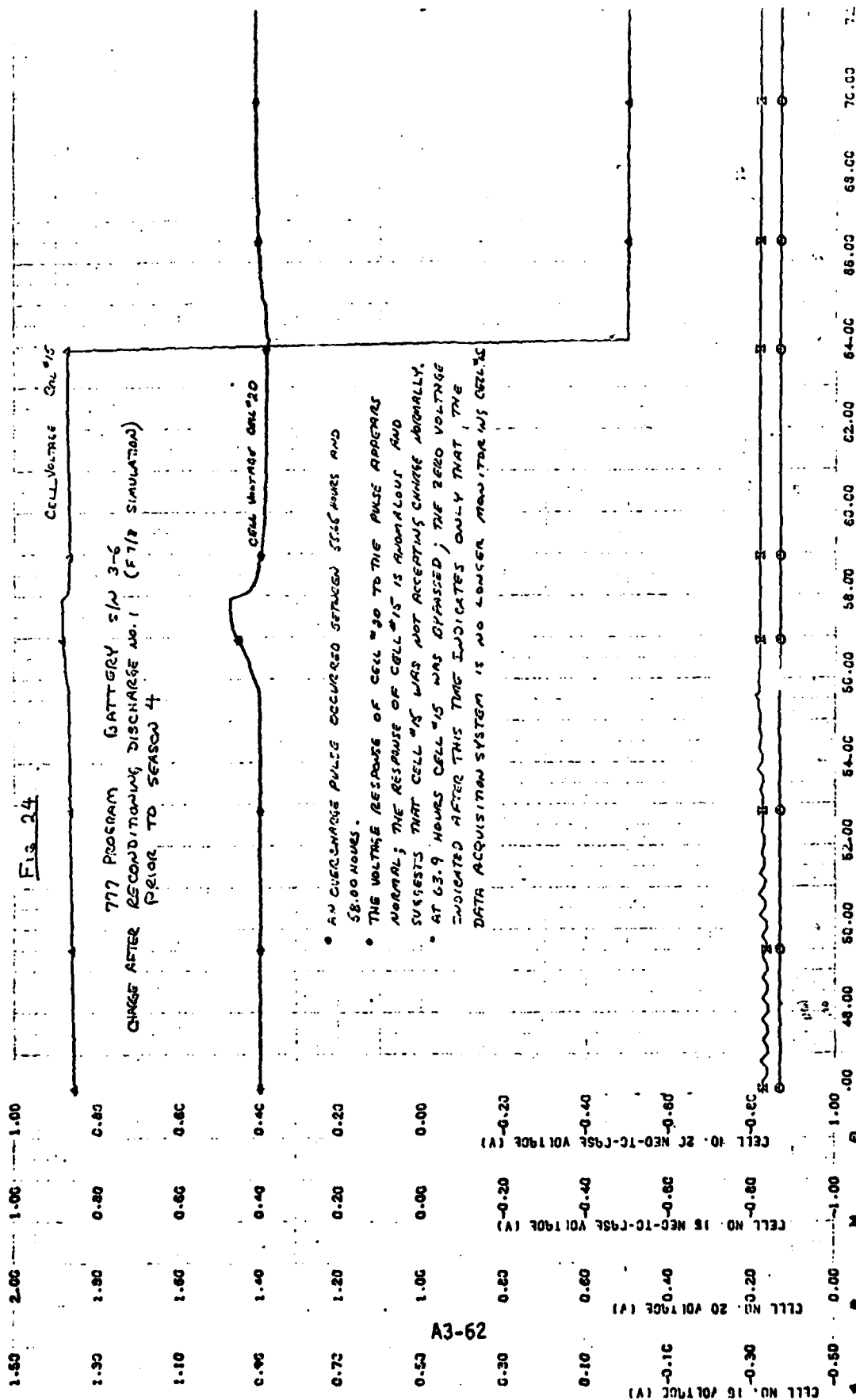
A3-60

TIME OF DRY (HR)	CELL NO. 15 NEG-TO-CASE VOLTAGE (V)	CELL NO. 20 NEG-TO-CASE VOLTAGE (V)
12.00	0.40	0.40
14.00	0.20	0.20
16.00	0.40	0.40
18.00	0.40	0.40
20.00	0.40	0.40
22.00	0.40	0.40
24.00	0.40	0.40
26.00	0.40	0.40
28.00	0.40	0.40
30.00	0.40	0.40
32.00	0.40	0.40
34.00	0.40	0.40
36.00	0.40	0.40



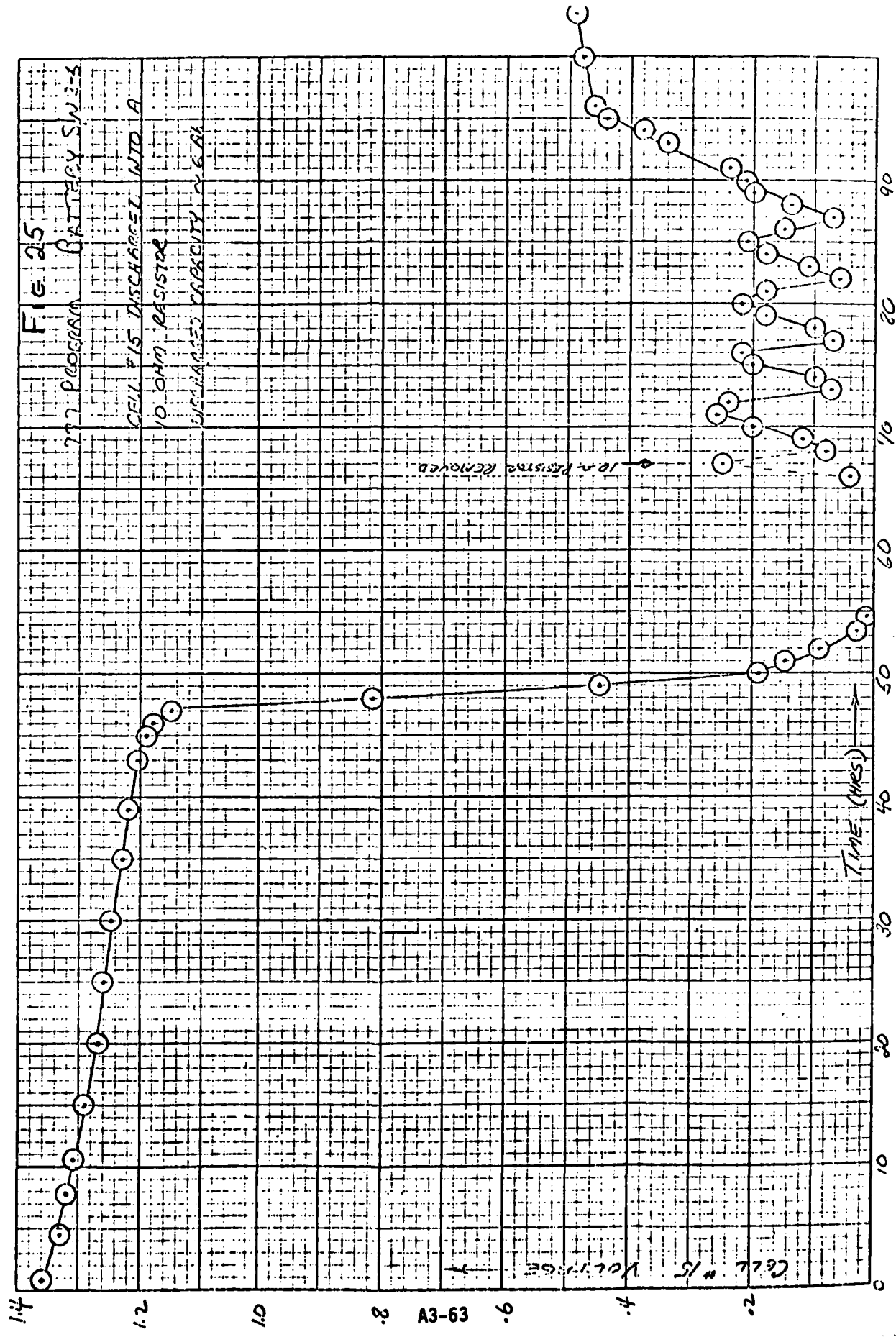
A3-61

Fig. 24



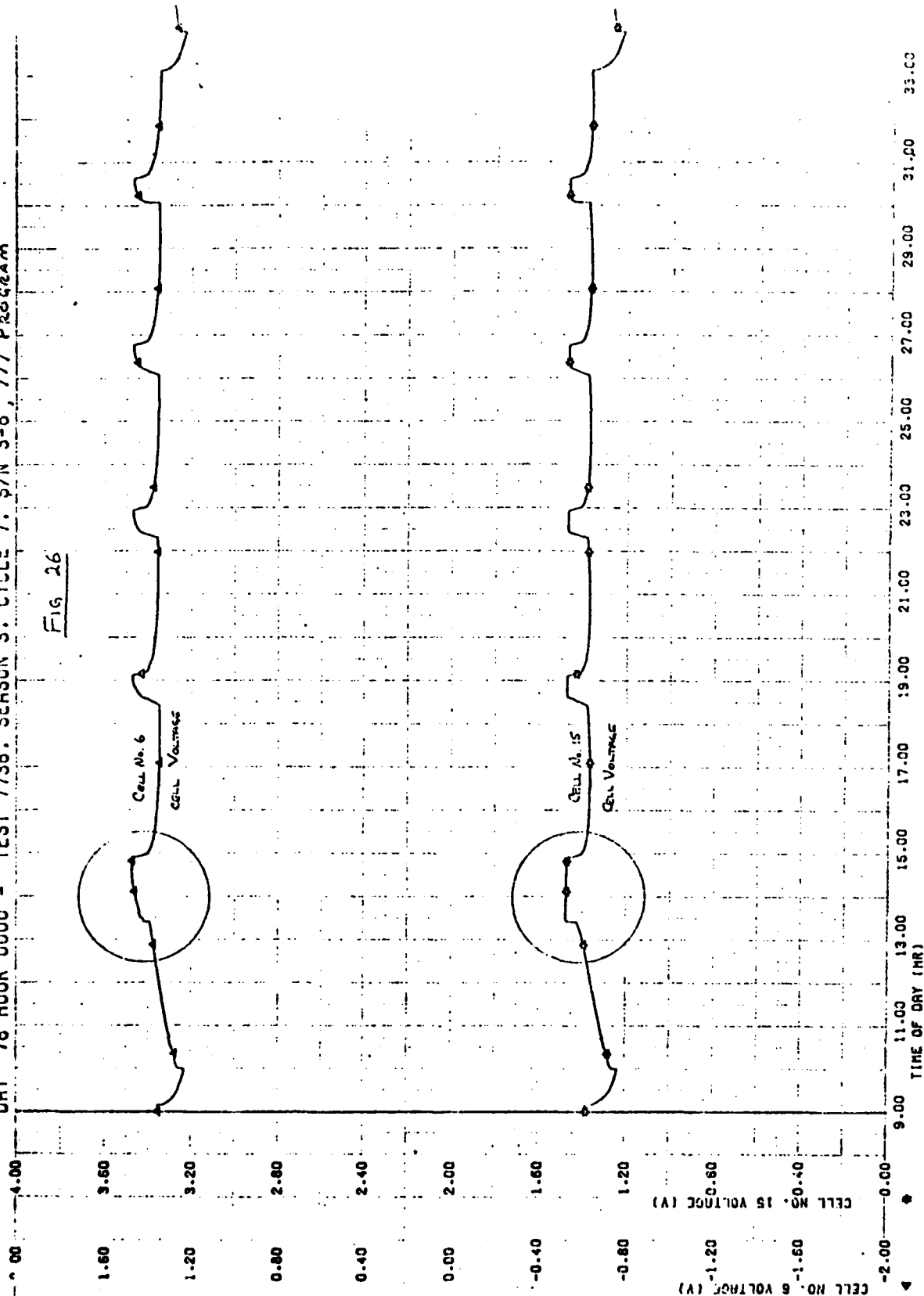
- AN OVERCHARGE PULSE OCCURRED BETWEEN 58.00 HOURS AND 58.00 HOURS.
- THE VOLTAGE RESPONSE OF CELL #20 TO THE PULSE APPEARS NORMAL; THE RESPONSE OF CELL #15 IS ABNORMAL AND SUGGESTS THAT CELL #15 WAS NOT ACCEPTING CHARGE ABNORMALLY.
- AT 63.9 HOURS CELL #15 WAS BYPASSED; THE ZERO VOLTAGE INDICATED AFTER THIS TIME INDICATES ONLY THAT THE DATA ACQUISITION SYSTEM IS NO LONGER MONITORING CELL #15.

A3-62



DRY 78 HOUR 0000 - TEST 7736, SERDON 3, CYCLE 7, S/N 3-6, 777 PROGRAM

Fig 26



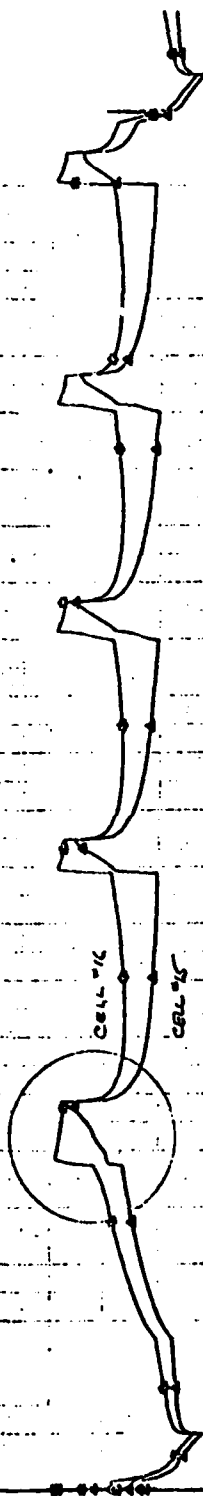
DAY 110 HOUR 0000 - TEST 7736. SEASON 3. CYCLE 39

FIG. 27

777 PROGRAM BATTERY S/N 3-6

SEASON 3 CYCLE 39

CELL VOLTAGE CELLS 15 & 16



CELL NO. 15 VOLTAGE (V)

CELL NO. 16 VOLTAGE (V)

TIME OF DAY (HR)

TRW

DEFENSE AND SPACE SYSTEMS GROUP
ONE SPACE PARK - REDONDO BEACH - CALIFORNIA 90270

Baum

INTEROFFICE CORRESPONDENCE

DSCS-C3-484
79-8725.2-068

TO: C. Sollo

CC: Distribution

DATE: 30 March 1979

SUBJECT: Test Plan - Simulation of DSCS-II F11/12 Batteries
on High Bus Trickle Charge

FROM: *cl* C. Lurie
BLDG M1 MAIL STA. 1406 EXT. 50776

The test plan designed to evaluate the performance and capability of Flight 11/12 batteries using high bus trickle charge as the primary charge mode is attached. The test started in January 1979, and is in progress.

CL:bj
Attachment

Distribution: E. Kipp
L. Mack
P. Ritterman
D. Rusta *DR-*
W. Scott
C. Stanley *CAS*
B. Alburn
E. Ames
J. Durschinger
N. North
A. Schoenfeld
DSCS-II Data Center

A3-66

Test Plan

Simulation of DSCS-II F11/12 on High Bus Trickle Charge

1.0 Scope

This plan is designed to evaluate the performance and capability of Flight 11/12 batteries using high bus trickle charge as the primary charge mode during eclipse seasons.

2.0 Test Equipment and Configuration

The battery, S/N 3-50, P/N 256107-4, shall be mounted on a thermoelectric heat exchanger as indicated in Figure 1. Baseplate temperatures shall be maintained at $40 \pm 3^{\circ}\text{F}$ throughout the test. An aluminum honeycomb panel shall be placed between the battery and heat exchanger. $1.06 \pm .03$ inches of fiberglass shims shall be placed between the honeycomb panel and baseplate to effect a simulation of the predicted orbital battery temperature profile during charge and discharge. The battery shall be covered with fiberglass insulation and a plexiglass cover to isolate it from the ambient environment.

The electrical test configuration is shown in Figure 2. All battery discharges shall be at 6 amperes constant current which simulates a two-out-of-three battery operating condition. Discharge duration shall vary in accordance with the simulated synchronous orbit eclipse charge/discharge profile shown in Table 1.

3.0 Procedure

3.1.1 Pretest Characterization

3.1.1 Visual Inspection

The battery shall be checked for physical damage.

3.1.2 Functional Bench Test

The Functional Bench Test shall be conducted in accordance with DR-14C-03, Revision E.

3.2 Eclipse Season Cycling

The test battery shall be subjected to two consecutive eclipse seasons consisting of charge/discharge cycles defined in Table 1.

All eclipse season battery discharges shall be 6 amperes constant current.

3.2 Eclipse Season Cycling cont'd.

The battery charge shall consist of trickle charging from a 32.8 volt bus through a 7-ohm resistor.

Performance degradation during the eclipse season may be evaluated as directed by the responsible test engineer by extending the duration of any one eclipse discharge (beyond eclipse cycle 26) until the battery voltage reaches 22 volts or any cell reaches 0.5 volts. The subsequent eclipse discharge shall be omitted to permit adequate recharge before resuming the test.

3.3 Solstice Season Reconditioning

The batteries shall be reconditioned after completion of each eclipse season.

The battery shall be discharged into a 200-ohm load until the battery voltage reaches 12 volts.

Following reconditioning, the battery shall be maintained on trickle charge until the start of the next eclipse season. The solstice period shall be limited to only the time required to perform one reconditioning discharge/recharge cycle.

3.4 Post-Test Characterization

A Functional Bench Test shall be conducted in accordance with DR-14C-03, Revision E.

4.0 Test Data Monitoring and Recording

Battery performance and test conditions shall be monitored continuously by the battery laboratory Digital Data Acquisition System (DDAS) at the following time intervals:

<u>Test Mode</u>	<u>Data Sampling Rate</u>
Battery Charge	Within one minute of start and completion plus every 10 minutes during charge.
Battery Discharge	Within one minute of start and completion plus every five minutes during discharge except for reconditioning discharge where the data shall be recorded every hour.

Battery test parameters are listed in Table 2. All parameters shall be monitored by the DDAS and stored on magnetic tape at the time intervals noted above.

5.0 Schedule

Figure 3 is a major task schedule in bar chart form.

Table 1

Duration of charge and discharge periods for each cycle of the eclipse season.

CYCLE NUMBER		24 Hour Cycle		
		Charge Time		Discharge Time
		Hours	Minutes	Minutes
1	45	23	40	20
2	44	23	32	28
3	43	23	25	35
4	42	23	20	40
5	41	23	17	43
6	40	23	13	47
7	39	23	10	50
8	38	23	07	53
9	37	23	04	56
10	36	23	02	58
11	35	23	00	60
12	34	22	58	62
13	33	22	56	64
14	32	22	58	66
15	31	22	53	67
16	30	22	52	68
17	29	22	51	69
18	28	22	50	70
19	27	22	50	70
20	26	22	49	71
21	25	22	49	71
22, 23	24	22	48	72

Table 2

Battery Test Parameters to be monitored and recorded during test

Parameter	Number of Parameters
Cell Voltage	22
Battery Voltage	1
Battery Current	1
Battery Temperatures RT1, RT2	2
Battery Heat Sink Temperature	2
Cycle Time	1
Battery End-of-Discharge Voltage	1

FIG 1

BATTERY / BASEPLATE CONFIGURATION

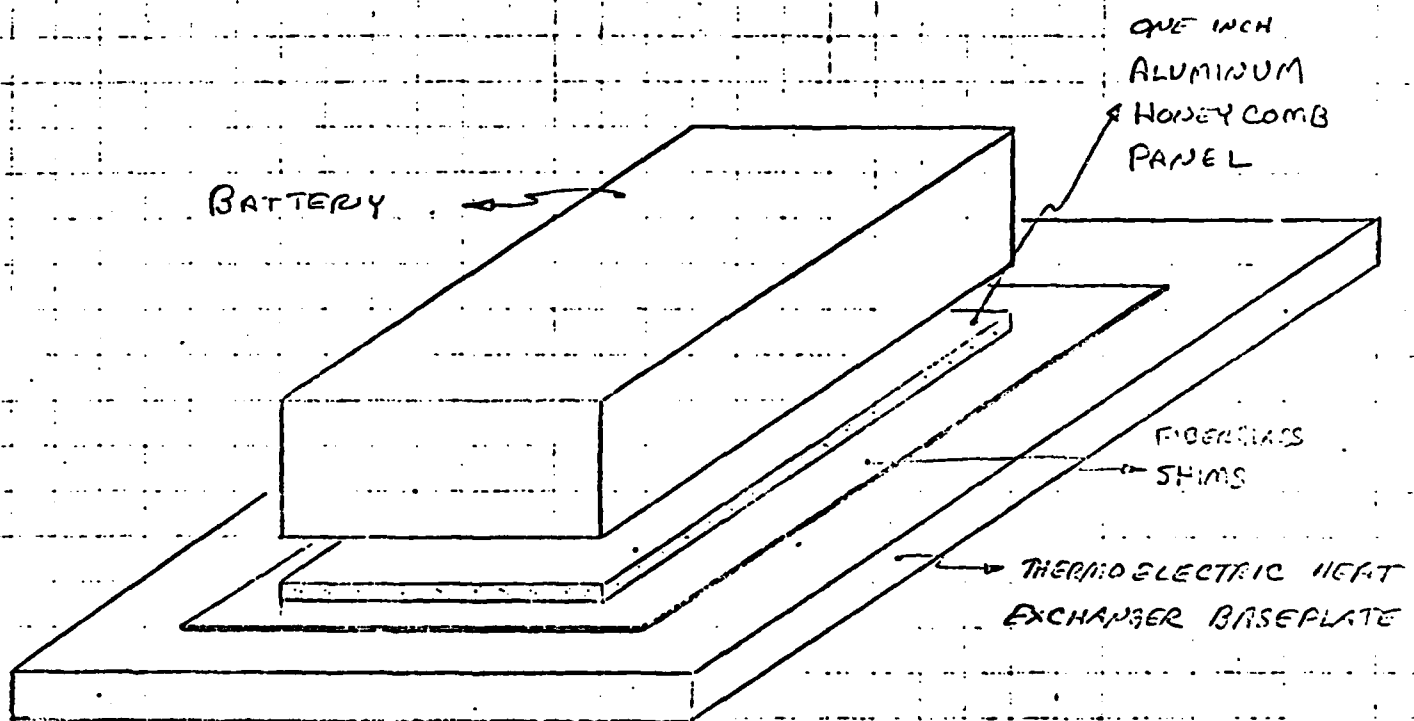
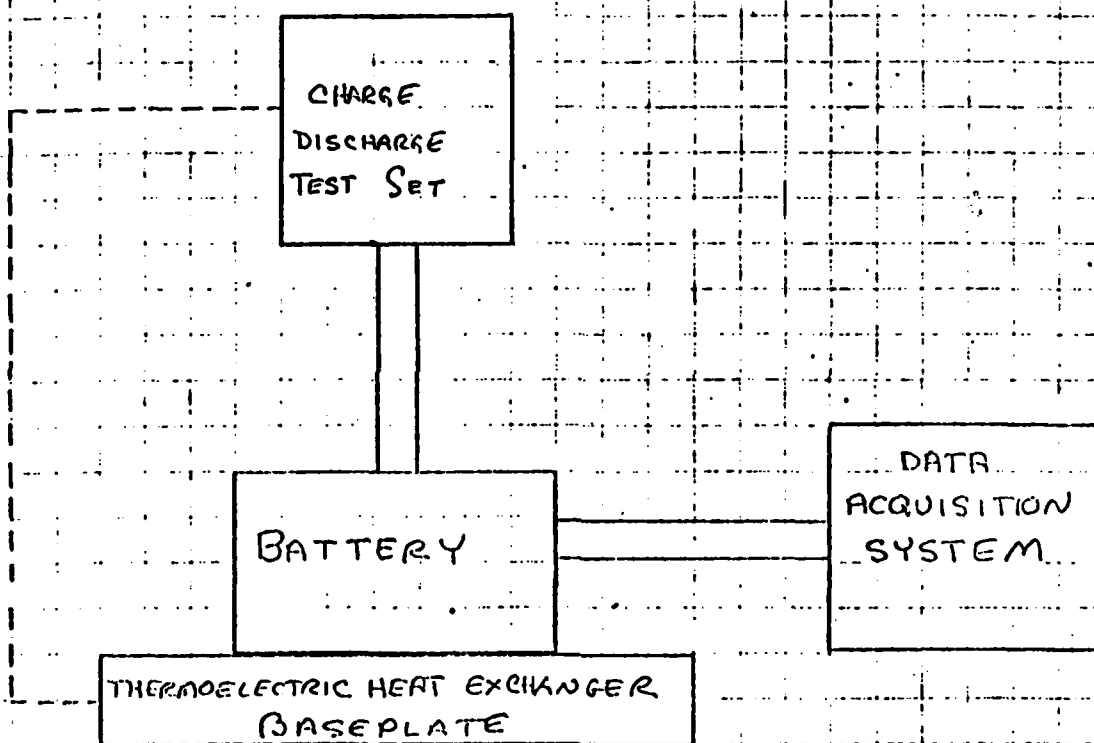
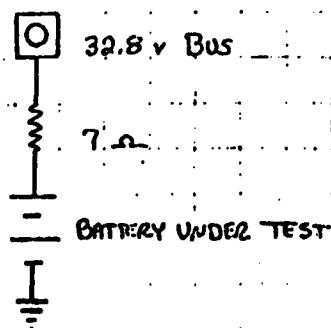


FIG 2

TEST CONFIGURATION



CHARGE CONFIGURATION



DISCHARGE CONFIGURATION

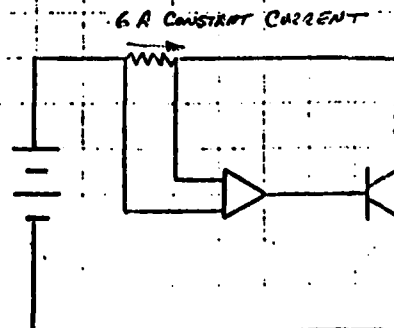

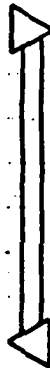
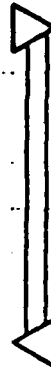



FIG 3

TEST PLAN SCHEDULE
SIMULATION OF DSCS-II F11/12 BATTERIES
ON HIGH BUS TRICKLE CHARGE

		W E E K S																											
NO	SUBTASK DESCRIPTION	1	2	3	4	5	6	7	8	9	10	11	12	13	14	15	16	17	18	19	20	21	22	23	24				
1	AREARE TEST PLAN																												
2	PERFORM DISCHARGE/RECHARGE CYCLES FOR ONE ECLIPSE SEASON; RECORD DATA; PREPARE INTERIM REPORT																												
3	PERFORM DISCHARGE/RECHARGE CYCLES FOR SECOND ECLIPSE SEASON ;RECORD DATA																												
4	PREPARE AND PUBLISH FINAL REPORT WITH TESTS, ANALYSES; DOCUMENT CONCLUSIONS AND RECOMMENDATIONS																												

TENTATIVE START DATE - JAN. 1979

DSCS-C3-486
79-8725.2-070

INTEROFFICE CORRESPONDENCE

TO: C. Sollo

CC: Distribution

DATE: 30 March 1979

SUBJECT: 777 Battery Interim Report - Flight 11/12 High Bus
Trickle Charge Simulation - Season 1

FROM: C. Lurie
BLDG M1 MAIL STA. 1406 EXT. 50776

Summary and Discussion

The subject simulation is designed to evaluate the performance and capability of Flights 11/12 batteries using high bus trickle charge as the primary charge mode.

The Season 1 results indicate that battery performance was reasonably stable and within specification. The increasing end-of-discharge voltages past mid-season suggest good response to the charge regime (Figure 2). However, the end-of-charge voltages decreased at an almost constant rate during the season (Figure 4). The decrease in voltage may be related to the low recharge ratio (1.14 for cycle 20) and low charge rate (approx. C/40) used. Accordingly, the following efforts are planned or under consideration:

- ✓ • A post-midseason capacity discharge could be run to evaluate degradation of full capacity.
- • Heat rate measurements will be made at low charge rates.
- • A parametric test will be run to determine the relationship between end-of-charge voltage and rate and end-of-discharge voltage and rate.

Figure 1 - Battery Test Parameters - Season 1, Cycle 20.

The trickle charge regime eliminates overcharge pulses and maintains an average temperature approximately 10°F lower than the auto cycling regime.

Figure 2 - End-of-Discharge Voltage versus Cycle Number

The midseason end-of-discharge voltages are approximately 0.20 volts lower than the comparable auto cycling regime (S/N 3-3 Season 1). The difference is probably related to the difference in charge rates. The increasing post-midseason end-of-discharge voltages demonstrate that battery performance was not significantly degraded. Note that data starts with Cycle 8. Cycles 1-7 were not run.

C. Sollo

-2-

DSCS-C3-486
79-8725.2-070
3 April 1979

Figure 3 - Battery Reconditioning Discharge Voltage Profile

No anomalous features were noted.

Figure 4 - End-of-Charge Voltage versus Cycle Number

The end-of-charge voltages decreased at an almost constant rate during the season. The decrease, 0.57V, is equivalent to 26 mv per cell. The consequences of the decrease in voltage are not immediately apparent.

.:bj

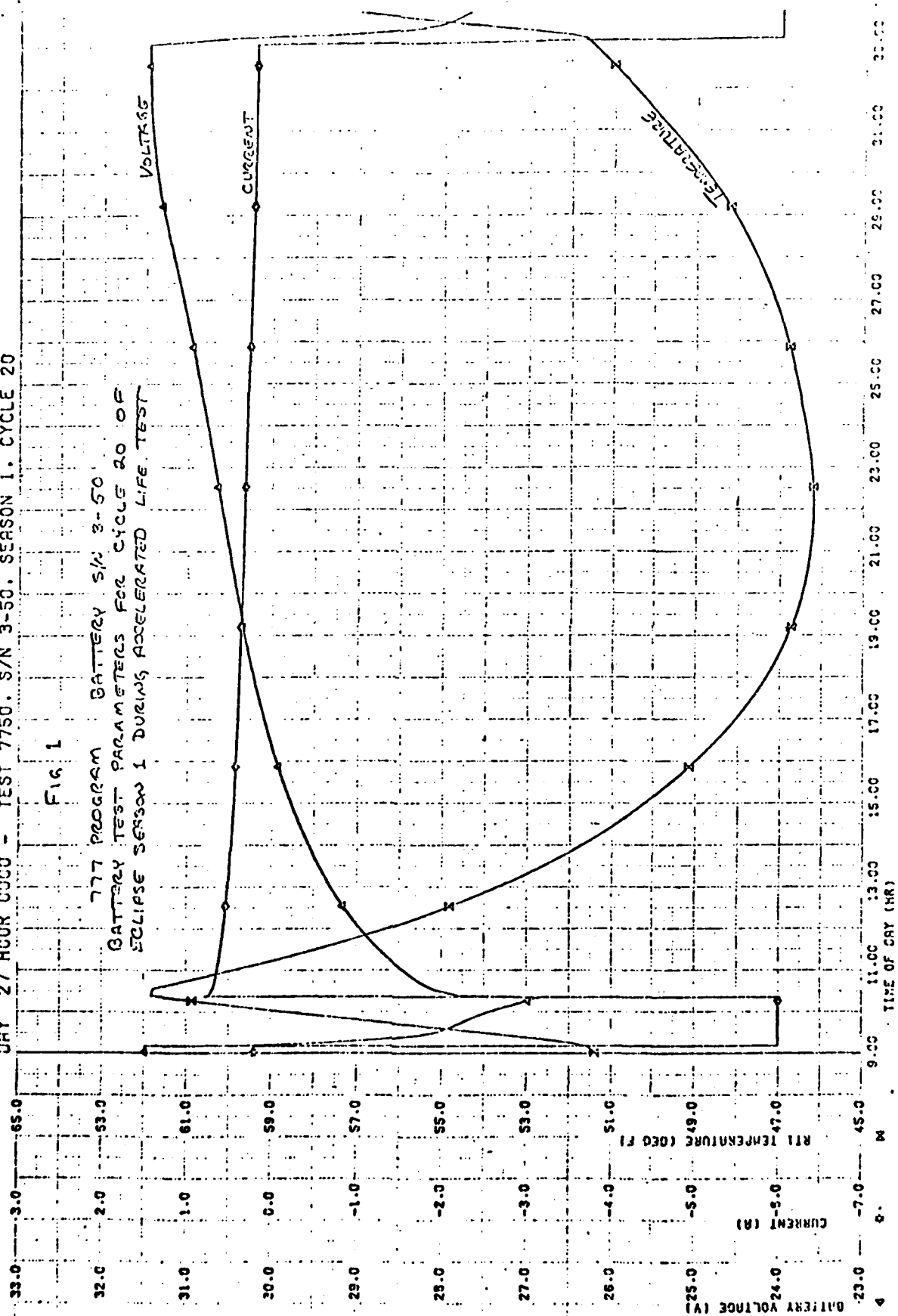
ttachment

Distribution: E. Kipp
L. Mack
P. Ritterman
W. Scott
C. Stanley
B. Alborn
E. Ames
J. Durschinger
N. North
D. Rusta *DR*
A. Schoenfeld
Data Center

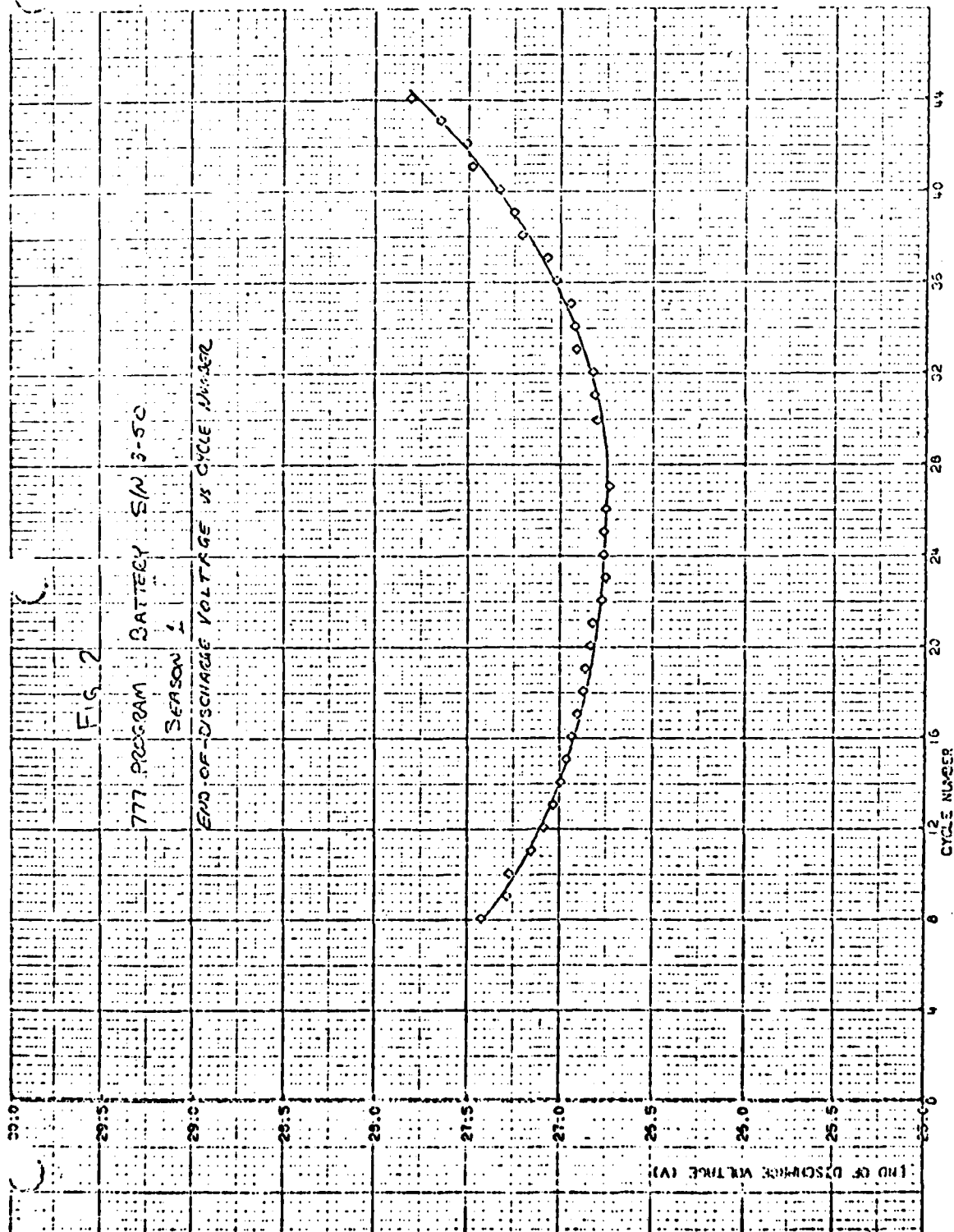
DAY 27 HOUR 0000 - TEST 7750. S/N 3-50. SEASON 1. CYCLE 20

FIG 1

777 PROGRAM BATTERY S/N 3-50
BATTERY TEST PARAMETERS FOR CYCLE 20 OF
ECLIPSE SEASON 1 DURING ACCELERATED LIFE TEST



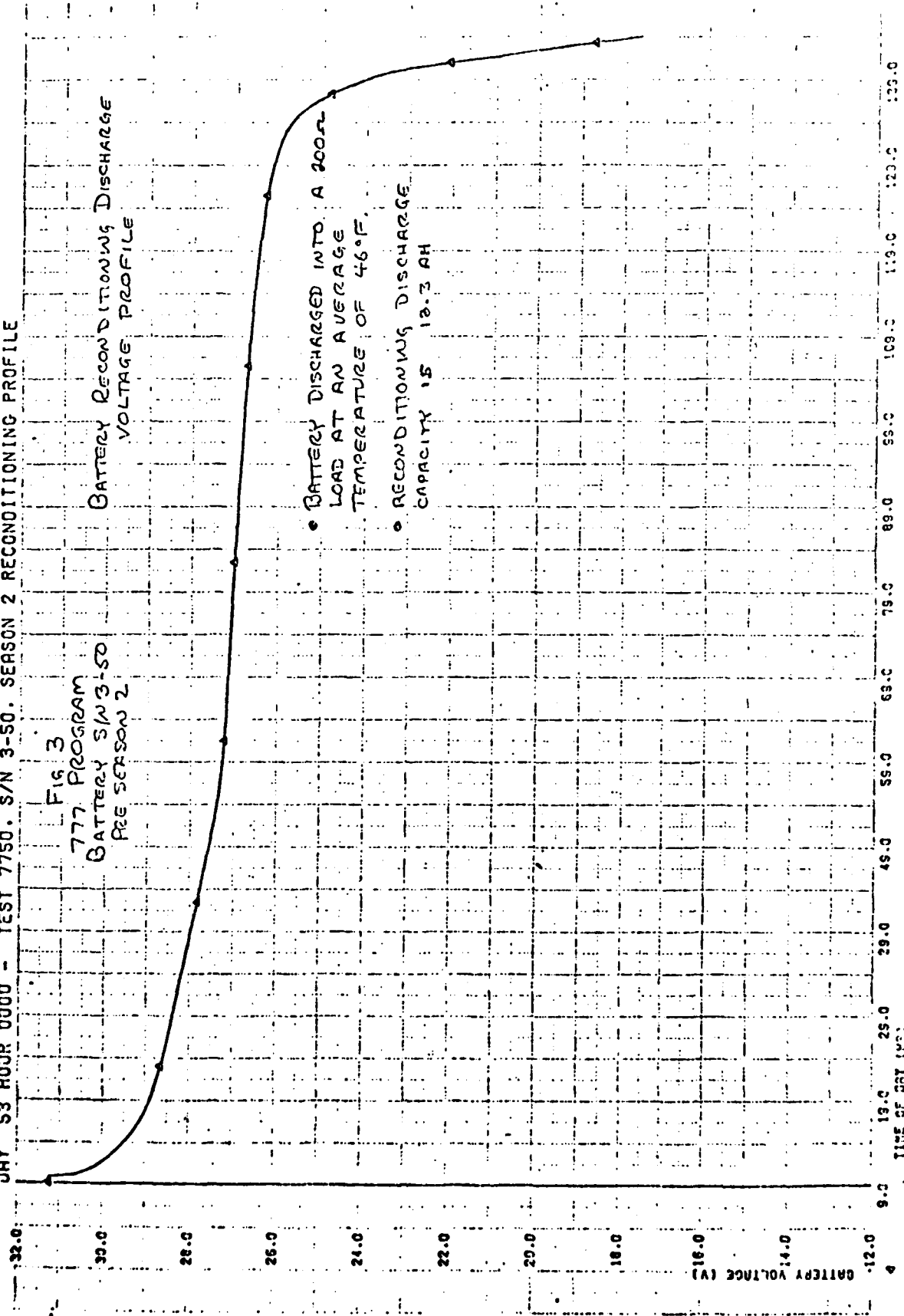
TEST 7100, S/N 3-50, SEASON 1



DAY 53 HOUR 0000 - TEST 7750. S/N 3-50. SEASON 2 RECONDITIONING PROFILE

FIG 3
777 PROGRAM
BATTERY S/N 3-50
PRE SEASON 2

BATTERY RECONDITIONING DISCHARGE
VOLTAGE PROFILE



• BATTERY DISCHARGED INTO A 200Ω
LOAD AT AN AVERAGE
TEMPERATURE OF 46°F.

• RECONDITIONING DISCHARGE
CAPACITY IS 12.3 AH

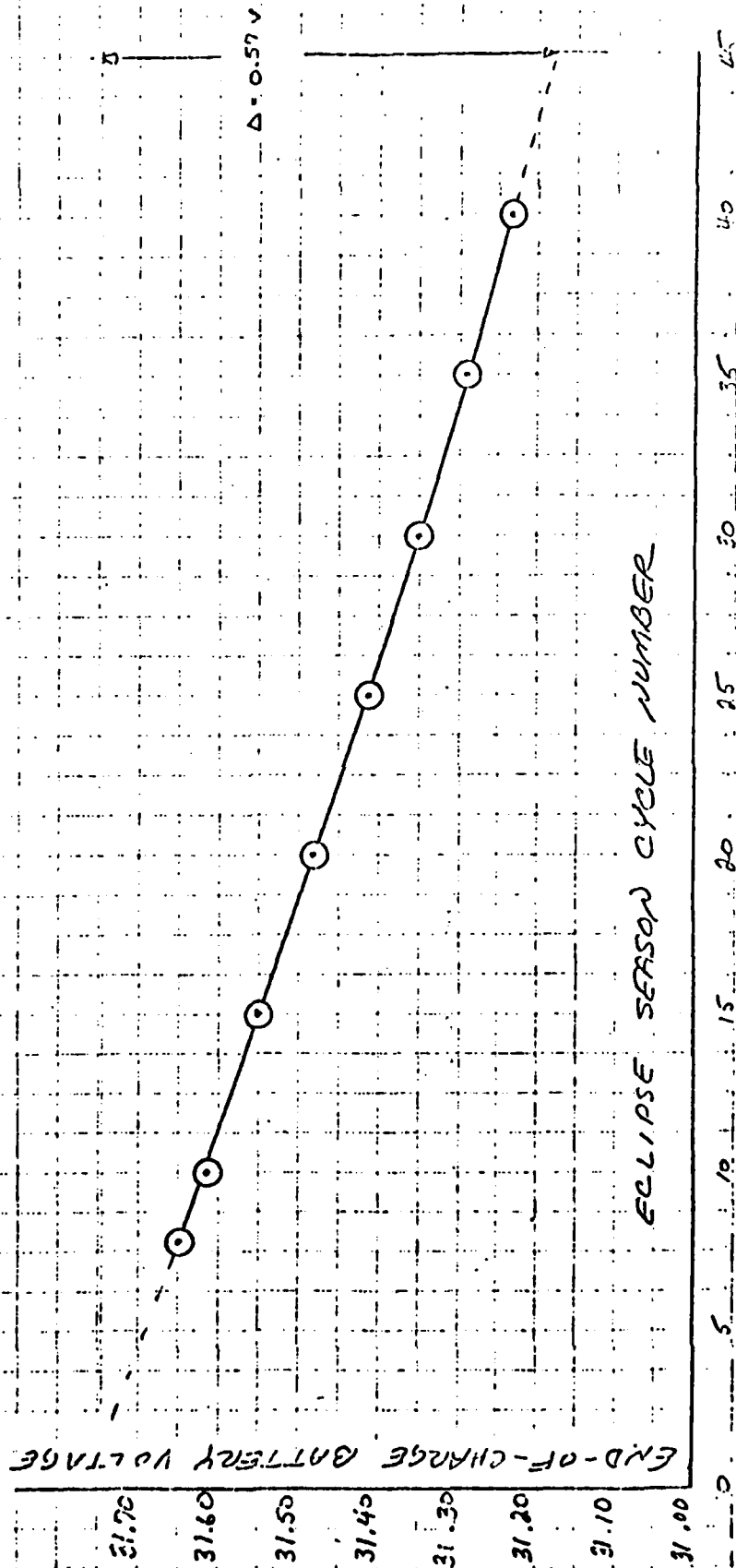
Fig 4

177 PROGRAM

BATTERY S/N 3-50

SEASON 1

END-OF-CHARGE VOLTAGE VS. CYCLE NUMBER



APPENDIX 4

TWO-BATTERY LOAD SHARING TEST SIMULATIONS



DEFENSE AND SPACE SYSTEMS GROUP
ONE SPACE PARK - REDWOOD BEACH - CALIFORNIA 90278

INTEROFFICE CORRESPONDENCE

DSCS-C3-488
79-8725.2-081

TO: C. Sollo

CC: Distribution

DATE: 30 March 1979

SUBJECT: Test Plan - Two-Battery Load Sharing Test
Simulation for 777 F7/8 Batteries

FROM: C. Murie
BLDG M1 MAIL STA. 1406 EXT. 50776

The attached Test Plan is designed to simulate a F7/8 load sharing configuration in which one battery has one shorted cell. The test started in January 1979, and is in progress. Two-seasons are scheduled.

CL:bj
Attachment

Distribution: E. Kipp B. Alborn
L. Mack E. Ames
P. Ritterman J. Durschinger
D. Rusta DR N. North
W. Scott A. Schoenfeld
C. Stanley CAS Data Center

Test Plan

777 Test Batteries S/N 3-36 and S/N 3-43

Two-Battery Load Sharing Test Simulation for 777 F7/8 Batteries

1.0 Scope

This test Plan is designed to simulate a two-eclipse season, Flight 7/8 battery configuration in which one battery has one shorted cell. The primary mode of battery charging is trickle charge from a 33.4 volt bus through a 7 ohm resistor. The two test batteries are to be discharged into a common 325 watt constant power load. Overall battery performance and degree of discharge-load-sharing will be determined with individual batteries connected either directly to the load or through one or two diodes.

2.0 Test Equipment and Configuration

The batteries shall be mounted on a common thermoelectric heat exchanger baseplate. Baseplate temperature shall be maintained at $40 \pm 3^{\circ}\text{F}$ throughout the test. An aluminum honeycomb panel shall be placed between the batteries and the heat exchanger as indicated in Figure 1. Fiberglass shims shall be placed between the honeycomb panel and baseplate to simulate the orbital battery temperature profile observed during Flights 7 and 8. The battery shall be covered with fiberglass insulation and a plexiglass cover to isolate it from the ambient environment.

The general test configuration is shown in Figure 2.

Cell 22 of Battery S/N 3-43 shall be shorted.

Batteries S/N 3-36 and S/N 3-43 shall be in parallel for both charge and discharge. The charge/discharge circuit is shown schematically in Figures 3 and 4.

3.0 Procedure

3.1 Pretest Characterization

3.1.1 Visual Inspection

3.1.2 Functional Bench Test

A Functional Bench Test shall be conducted in accordance with DR-14C-03, Revision E.

3.2 Cycling Plan

3.2.1 Season 1

The test batteries shall be subjected to the following cycling regime:

Cycle No.	Cycling Regime	Configuration (Ref. Figure 3)
1 ↓ 29	Table 1	<u>Charge</u> S/N 3-36 - 33.4 volt bus, 7 ohm resistor S/N 3-43 - same as for S/N 3-36 <u>Discharge</u> S/N 3-36 - 1 diode between battery and load S/N 3-43 - same as for S/N 3-36
30 31 32	Table 1	<u>Charge</u> Same as for cycles 1-29 <u>Discharge</u> S/N 3-36 - same as for cycles 1-29 S/N 3-43 - 0 diodes between battery and load
33 ↓ 38	<u>Fixed Cycle</u> <u>Charge</u> - 22 Hr. 48 Min. <u>Discharge</u> 72 Min.	<u>Charge</u> Same as for cycles 1-29 <u>Discharge</u> S/N 3-36 - 2 diodes between battery and load S/N 3-43 - 0 diodes between battery and load
39 ↓ 45	<u>Fixed Cycle</u> <u>Charge</u> - 22 Hr. 48 Min. 1) Charge until battery temperature is 5°F above the minimum re-charge temperature. 2) When the last battery temperature increases 5°F reconfigure as indicated. <u>Discharge</u> 72 Min.	<u>Charge</u> S/N 3-36 and S/N 3-43 1) Bus voltage = 32.4v; bus current = 5.0 amps. Short both 7 ohm resistors. 2) Increase the bus voltage to 33.4v and remove the shorting straps. <u>Discharge</u> S/N 3-36 - 2 diodes between battery and load S/N 3-43 - 0 diodes between battery and load

3.2.2 Season 2

The test batteries shall be subjected to one eclipse season consisting of charge/discharge cycles defined in Table 1. The configuration shall be as indicated in Figure 4.

3.3 Solstice Season Reconditioning

The batteries shall be reconditioned after completion of each eclipse season.

Reconditioning shall consist of discharge into a 44 ohm load until the battery voltage reaches 20v. Two reconditioning cycles shall be performed.

Following reconditioning the batteries shall be recharged at four amperes to the voltage limit and maintained on trickle charge until the start of the next eclipse season.

The total duration of the solstice season shall be limited to only the time necessary to complete battery reconditioning.

3.4 Post-Test Characterization

A Functional Bench Test shall be conducted in accordance with DR-14C-03, Rev. E.

4.0 Test Data Monitoring and Recording

Battery performance and test conditions shall be monitored continuously by the battery laboratory Digital Data Acquisition System (DDAS) at the following time intervals:

<u>Test Mode</u>	<u>Data Sampling Rate</u>
Battery Charge	Within one minute of start and completion plus every 10 minutes during charge.
Battery Discharge	Within one minute of start and completion plus every five minutes during discharge except for reconditioning discharge where the data shall be recorded every hour.

Battery test parameters are listed in Table 2. All parameters shall be monitored by the DDAS and stored on magnetic tape at the time intervals noted above.

The data shall also be printed on the line printer to facilitate real time assessment of the results by the responsible personnel.

5.0 Schedule

Figure 5 is a major task schedule in bar chart form.

Table 1

Duration of charge and discharge periods for each cycle of the eclipse season.

CYCLE NUMBER		24 Hour Cycle		
		Charge Time		Discharge Time
		Hours	Minutes	Minutes
1	45	23	40	20
2	44	23	32	28
3	43	23	25	35
4	42	23	20	40
5	41	23	17	43
6	40	23	13	47
7	39	23	10	50
8	38	23	07	53
9	37	23	04	56
10	36	23	02	58
11	35	23	00	60
12	34	22	58	62
13	33	22	56	64
14	32	22	58	66
15	31	22	53	67
16	30	22	52	68
17	29	22	51	69
18	28	22	50	70
19	27	22	50	70
20	26	22	49	71
21	25	22	49	71
22, 23	24	22	48	72

Table 2

Battery Test Parameters to be monitored and recorded during test

Parameter/Battery	Number of Parameters/Battery
Cell Voltage	22
Battery Voltage	1
Battery Current	1
Battery Temperatures RT1, RT2	2
Battery Heat Sink Temperature	2
Cycle Time	1
Battery End-of-Discharge Voltage	1

FIG 1

BATTERY / BASEPLATE CONFIGURATION

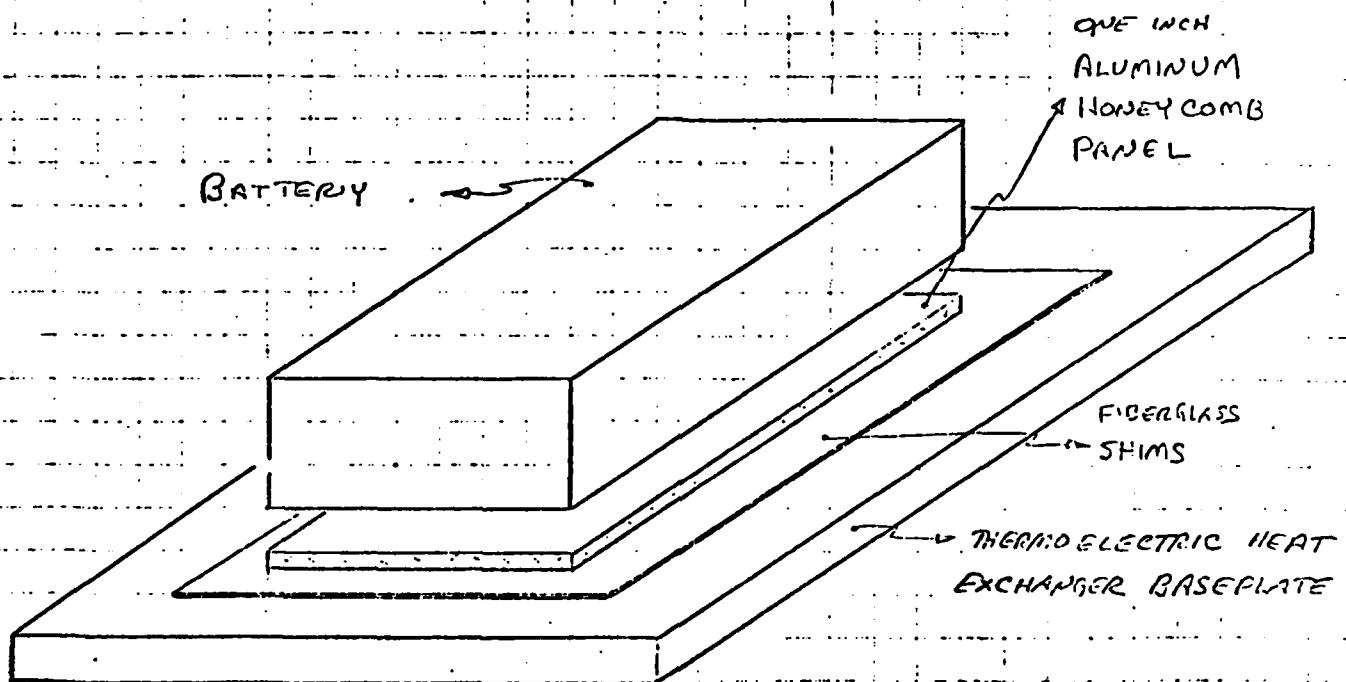


FIG 2

TEST CONFIGURATION

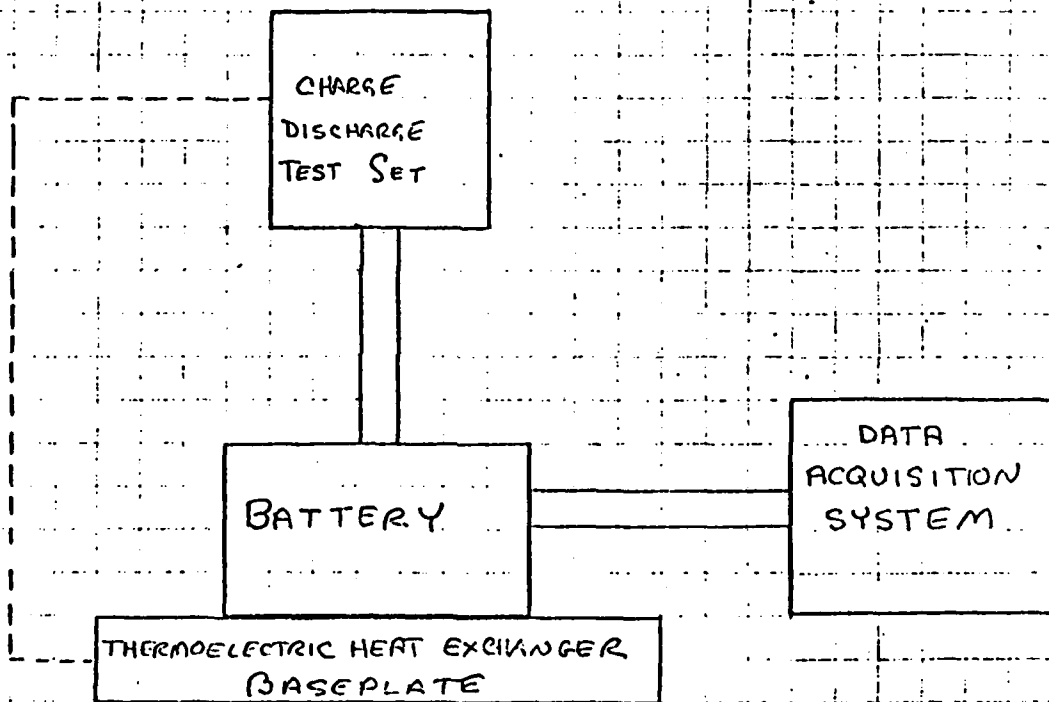


FIG 3

BATTERIES S/N 3-36 AND S/N 3-43
CHARGE / DISCHARGE CIRCUIT

SEASON 1

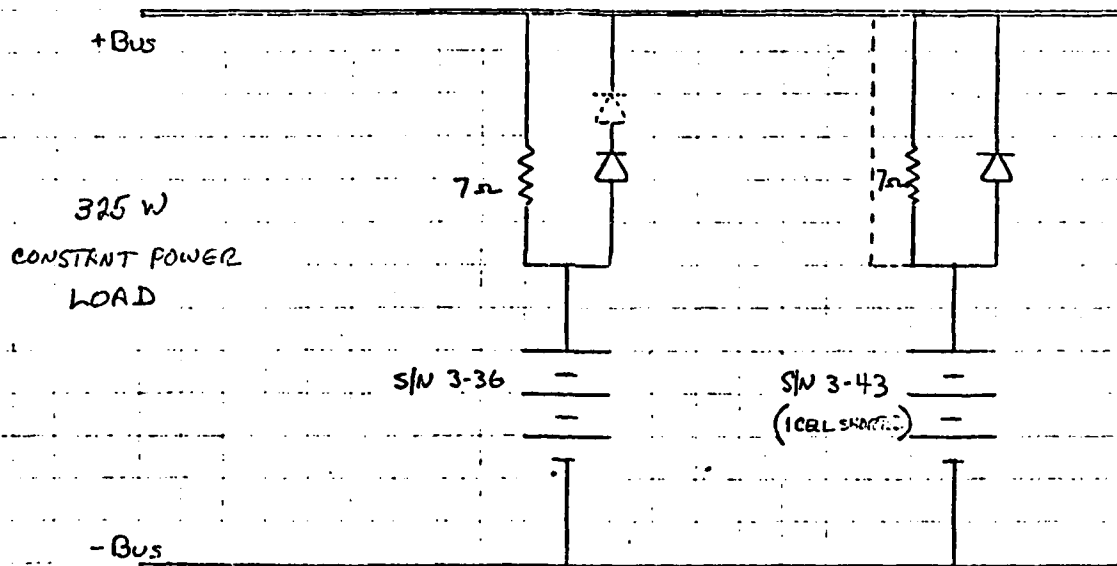


FIG 4

BATTERIES S/N 3-36 AND S/N 3-43
CHARGE / DISCHARGE CIRCUIT

SEASON 2

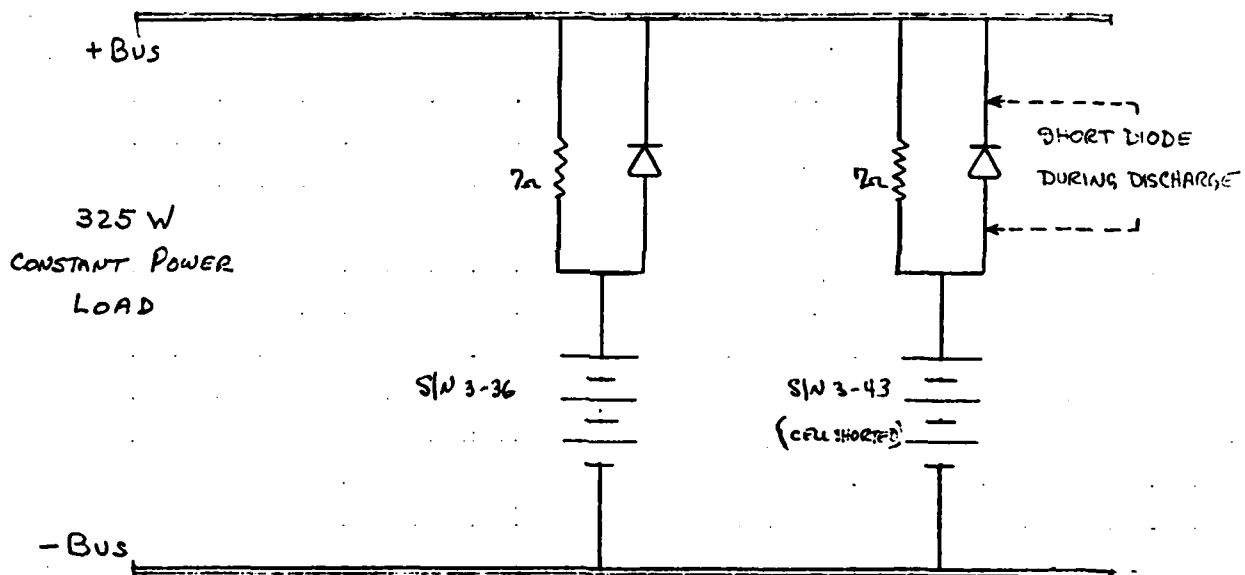


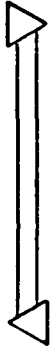



Fig 5

TEST PLAN SCHEDULE
SIMULATION OF TWO-OUT-OF-THREE BATTERY
LOAD SHARING

		W E E K S																							
No.	SUBTASK DESCRIPTION	1	2	3	4	5	6	7	8	9	10	11	12	13	14	15	16	17	18	19	20	21	22	23	
1	PREPARE TEST PLAN																								
2	PERFORM DISCHARGE/RECHARGE CYCLES FOR ONE ECLIPSE SEASON; RECORD DATA; PREPARE INTERIM REPORT																								
3	PERFORM DISCHARGE/RECHARGE CYCLES FOR SECOND ECLIPSE SEASON; RECORD DATA																								
4	PREPARE AND PUBLISH FINAL REPORT WITH TESTS, ANALYSES; DOCUMENT CONCLUSIONS AND RECOMMENDATIONS																								
5																									

TENTATIVE START DATE - JAN 1979

INTEROFFICE CORRESPONDENCE

DSCS-C3-501
79-8725.2-124

TO: C. Sollo

CC: Distribution

DATE: 5 June 1979

SUBJECT: Final Report - Two Battery Load Sharing Simulation
for 777 F7/8 Batteries

FROM: C. Lurie
BLDG M1 MAIL STA. 1406 EXT. 50776

Summary

The subject simulation is designed to evaluate 777 Battery performance using a configuration in which the load is shared by two batteries, one of which has a shorted cell. Load sharing was evaluated for configurations in which the one-cell discrepancy was compensated by 0, 1, or 2 diodes.

Two forty-five cycle real time eclipse seasons were run. The charge/discharge configurations, data, and parametric trends are summarized by the figures listed in Table 1.

Figure 10 depicts the improvement in load sharing as the voltage imbalance is progressively compensated by diodes. Average (percentage) load sharing values of 72/28, 66/34, and 51/49 were observed for the 0, 1, and 2 diode configurations run during Season 1.

Operation in the uncompensated configurations e.g., 0 diodes, resulted in the 21-cell battery (S/N 3-43) receiving a great deal of overcharge and the 22-cell battery (S/N 3-36) receiving little or none.

Season 2 was run exclusively with the one diode configuration. The average load sharing observed during Season 2 was 61/39 percent.

2.0 Conclusions

Operation with 0, 1, and 2 diode compensation modifies load sharing in a straightforward and predictable manner. The test configuration in which the load is shared by two batteries, one of which has a shorted cell, resulted in an average load sharing of 72/28 percent without compensation. Using 2 diodes (0.5-0.6V each) to compensate for the single cell difference (~1.2V) resulted in an average load sharing of 51/49 percent.

Table 1

Figure Identification

Battery S/N Season	3-36		3-43		Description
	1	2	1	2	
Figure Number	1	1	1	1	Charge/Discharge Configuration
	2	4	3	5	Typical Midseason Battery Parameter Profile
	6	8	7	9	End-of-Discharge Voltage Trend
	10	11	10	11	Load Sharing vs. Cycle Number
	12, 13	16, 17	14, 15	18, 19	Reconditioning Discharge Voltage Profile

Table 2

DSCS-C3-501
79-8725.2-124
5 June 1979
page 3

Duration of charge and discharge periods for each cycle of the eclipse season.

CYCLE NUMBER		24 Hour Cycle		
		Charge Time		Discharge Time
		Hours	Minutes	Minutes
1	45	23	40	20
2	44	23	32	28
3	43	23	25	35
4	42	23	20	40
5	41	23	17	43
6	40	23	13	47
7	39	23	10	50
8	38	23	07	53
9	37	23	04	56
10	36	23	02	58
11	35	23	00	60
12	34	22	58	62
13	33	22	56	64
14	32	22	58	66
15	31	22	53	67
16	30	22	52	68
17	29	22	51	69
18	28	22	50	70
19	27	22	50	70
20	26	22	49	71
21	25	22	49	71
22, 23	24	22	48	72

Operation in the 0 diode configuration (no compensation) suggests that load sharing imbalances more extreme than the 72/28 percent observed, would cause degradation due to insufficient charging of the 22-cell battery and excessive overcharging of the 21-cell battery. One-diode compensation resulted in stable, satisfactory operation during Season 2.

3.0 Discussion of Results

3.1 Season 1

Figure 1 describes the configurations used during the Season 1 evaluation. Note that S/N 3-43 is a 21 cell battery and S/N 3-36 is a 22 cell battery.

The charge/discharge configuration was varied during Season 1 to evaluate the following:

- "0" diode case; (no load balancing attempted) cycles 1-29.
- "1" diode case; cycles 30-32
- "2" diode case; cycles 33-45

Charge/discharge durations for Cycles 1-32 simulate eclipse season cycling as defined in Table 2. All succeeding cycles are of fixed duration (charge for 22 hours 48 minutes; discharge 72 minutes). Cycles 39-45 were charged using a special regime aimed at equalizing the state-of-charge of the batteries. The state-of-charge dispersion was a direct result of the poor load sharing during the "0" diode operation. The charge regime consisted of the following:

- Set the maximum bus current at 5.0 amperes with a bus voltage set at 32.4V.
- Charge until the battery temperatures are 5°F above the minimum re-charge temperature.
- When the last battery temperature increases 5°F increase the bus voltage to 33.4V and remove the shorting straps.

Figures 2 and 3 depict typical midseason voltage, current, temperature vs. time relationships for S/N 3-36 and S/N 3-43 respectively. The poor load sharing (approximately 70-30) occurring is reflected in the parametric responses.

- Voltage - The S/N 3-43 battery voltage peaked at about four hours and fell off to a plateau indicating that it went into overcharge early in the cycle. S/N 3-36 never did peak and was climbing sharply at the end of the cycle. S/N 3-36 was probably still accepting charge at the end of the cycle.
- Temperature - The temperature curves are consistent with the above assumption that S/N 3-43 is fully charged and S/N 3-36 may not be.
- Current - Average charging currents are not significantly different.

Figures 6 and 7 show the end-of-discharge voltage trend with respect to cycle number for Batteries S/N 3-36 and S/N 3-43.

Cycles 1-29 represent eclipse season cycling (Table 1) with a fixed configuration. Note that the midseason dispersion of S/N 3-36 values is greater than for the S/N 3-43 case. This is consistent with the previous observation that S/N 3-43 is receiving considerable overcharge and S/N 3-36 is not.

Prior to Cycle 30 the system was reconfigured to cause S/N 3-36 to have one diode in its circuit and S/N 3-43 to have none. The S/N 3-36 end-of-discharge voltage increased about 0.5 volts and the load sharing improved.

Prior to Cycle 33 a second diode was added to the S/N 3-36 circuit and the end-of-discharge voltage increased another 0.5 volt.

The increased scatter of voltages observed with S/N 3-36 may be attributed to a lower state-of-charge.

Load sharing, represented in Figure 10 as the percent of the load carried by S/N 3-36, occurred at three levels. These levels correspond to discharge configurations in which the one-cell difference between batteries is compensated by 0, 1 and 2 diodes.

With no diode compensation S/N 3-36 carried 70-75% of the load. The addition of two diodes in the S/N 3-36 circuit compensated for 1.0 volts of the approximately 1.2 volt difference and reduced the load-share to 50-52%

Figures 12, 13, 14 and 15 depict the reconditioning discharge voltage profiles observed after Season 1.

The following points are noted:

- Some evidence of second plateau voltage suppression can be seen during the last 10% of the initial discharges.
- An additional voltage suppressing feature is seen starting at about 30% depth-of-discharge. Inspection of individual cell data indicates that the shape change occurred in all cells. The cause of the shape change is not apparent at present.

3.2 Season 2

Season 2 was run exclusively with the one diode discharge configuration as indicated in Figure 1.

Figures 4 and 5 depict typical midseason voltage, current, and temperature vs. time relationships for S/N 3-36 and S/N 3-43 respectively. The parametric responses are generally similar to those observed during Season 1.

- Voltage - The S/N 3-43 battery voltage peaked at about nine hours into the charge and fell off to a plateau, indicating that it went into overcharge early in the cycle. During Season 1 an equivalent peak occurred at about four hours. The displacement of the peak is explained by the difference in discharge configuration. Cycle 20 of Season 1 was run with no diode compensation; Cycle 20 of Season 2 was run with one diode compensation.
- Temperature - The temperature curves are consistent with the discussion of the voltage parameter and are similar to the Season 1, Cycle 20 experience.
- Current - Average charging currents are not significantly different. Once again this is similar to the Season 1, Cycle 20 observation.

Figures 8 and 9 show the end-of-discharge voltage trend with respect to cycle number for Batteries S/N 3-36 and S/N 3-43. Direct comparison with Season 1 data is difficult as only Cycles 30, 31, and 32 of Season 1 were run with the one diode configuration used throughout Season 2. With the exception of the Season 1, Cycle 32 data point for S/N 3-36, which appears anomalous, the curves suggest that the Season 2 data is about 0.1 volt lower than the Season 1 data.

Load sharing is presented as a function of cycle number in Figure 11. Once again comparison with Season 1 data is difficult as only Cycles 30, 31, and 32 of Season 1 utilized the one diode discharge configuration. Two observations are made:

- Season 1 (Figure 10) load sharing during the three cycles utilizing the one-diode configuration was 66/34%. Load sharing during the same one-diode configuration of Season 2 was 60/40%. Considering the limited data available no explanation is attempted.
- The shape of the Season 1 and Season 2 curves, during the first twenty-nine cycles, is similar.

The reconditioning discharge voltage profiles, following Season 2 operations are plotted in Figures 16 through 19.

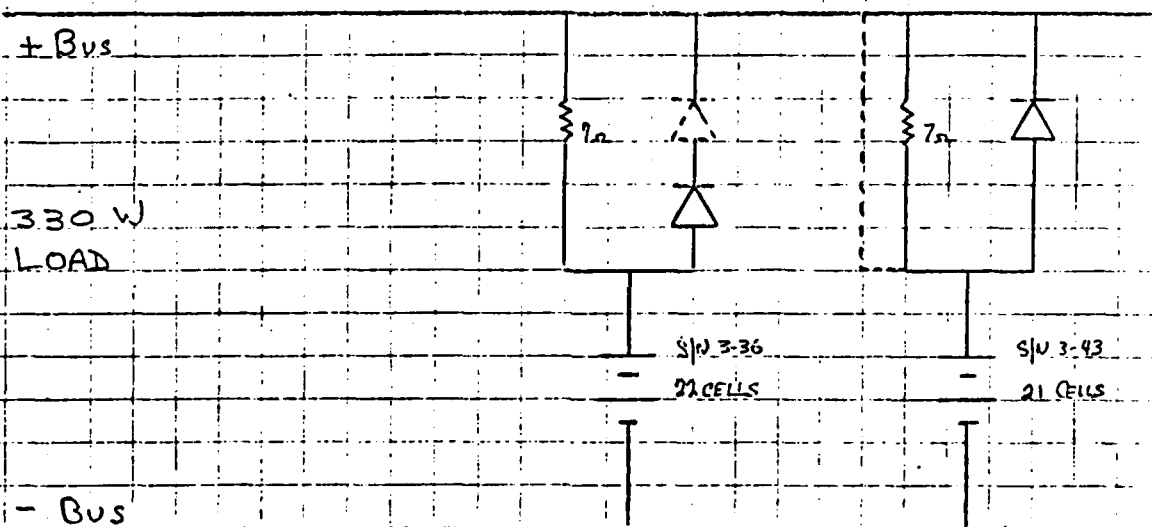
The average Preseason 3 reconditioning discharge capacity for S/N 3-36 was 0.4 Ah lower, and for S/N 3-43 0.6 Ah higher, than observed during the Preseason 2 reconditioning. This divergence may be related to the different eclipse season battery parameter profiles (Figures 4, 5) which cause S/N 3-43 to receive a great deal of overcharge and S/N 3-36 to receive very little. Large amounts of overcharge are known to increase positive capacity and insufficient overcharge can cause capacity loss. This explanation must be regarded as speculative at this point as the differences are small and only two seasons have been run.

CL:bj

Distribution:	W. Brannian	B. Alborn
	E. Kipp	E. Ames
	L. Mack	J. Durschinger
	P. Ritterman	N. North
	D. Rusta <i>DR</i>	A. Schoenfeld
	W. Scott	Data Center
	C. Stanley <i>CAS</i>	

Fig 1

CHARGE / DISCHARGE CONFIGURATION



• CHARGE CONFIGURATION

SEASON 1, CYCLE 1-29	33.4 V BUS & 7Ω RESISTOR
SEASON 1, CYCLE 30-45	START WITH 30.4V BUS AND SHORTED RESISTORS. SWITCH TO 33.4V AND REMOVE SHORTS AFTER 5°F TEMP INCREASE ACHIEVED
SEASON 2, CYCLE 1-45	33.4V BUS & 7Ω RESISTOR

• DISCHARGE CONFIGURATION

SEASON	CYCLE	BATTERY SN 3-43	BATTERY SN 3-36	DURATION
1	1-29	ONE DIODE	ONE DIODE	TABLE 2
1	30-32	SHORT DIODE / RESISTOR	ONE DIODE	TABLE 2
1	33-45	SHORT DIODE / RESISTOR	TWO DIODES	72 min
2	1-45	SHORT DIODE / RESISTOR	ONE DIODE	TABLE 2

FIG. 2
DAY 27 HOUR 0000 - TEST 77. S/N 3-36. SEASON 1. CYCLE 20

TYPICAL MIDSEASON BATTERY PARAMETER PROFILE

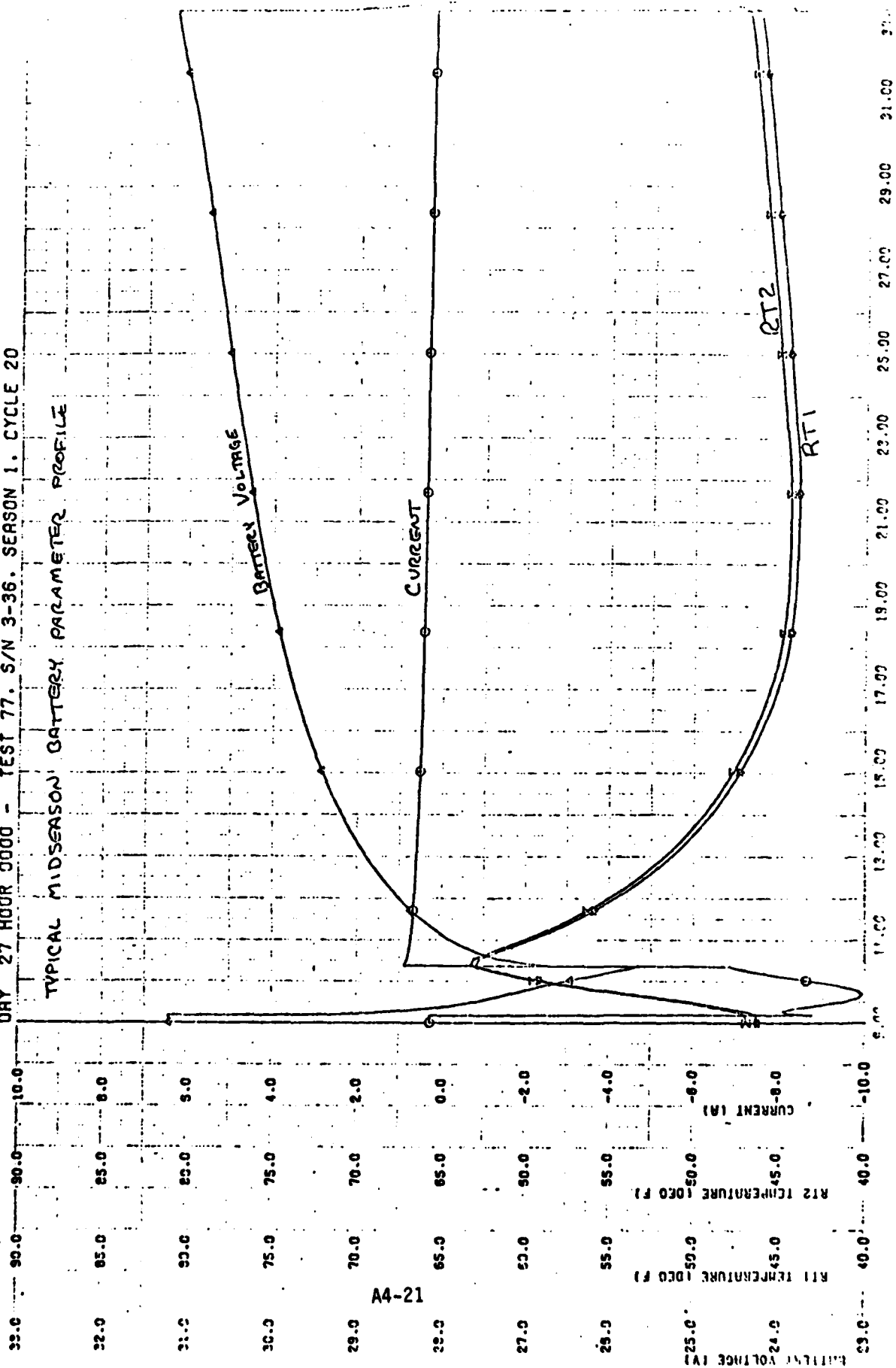
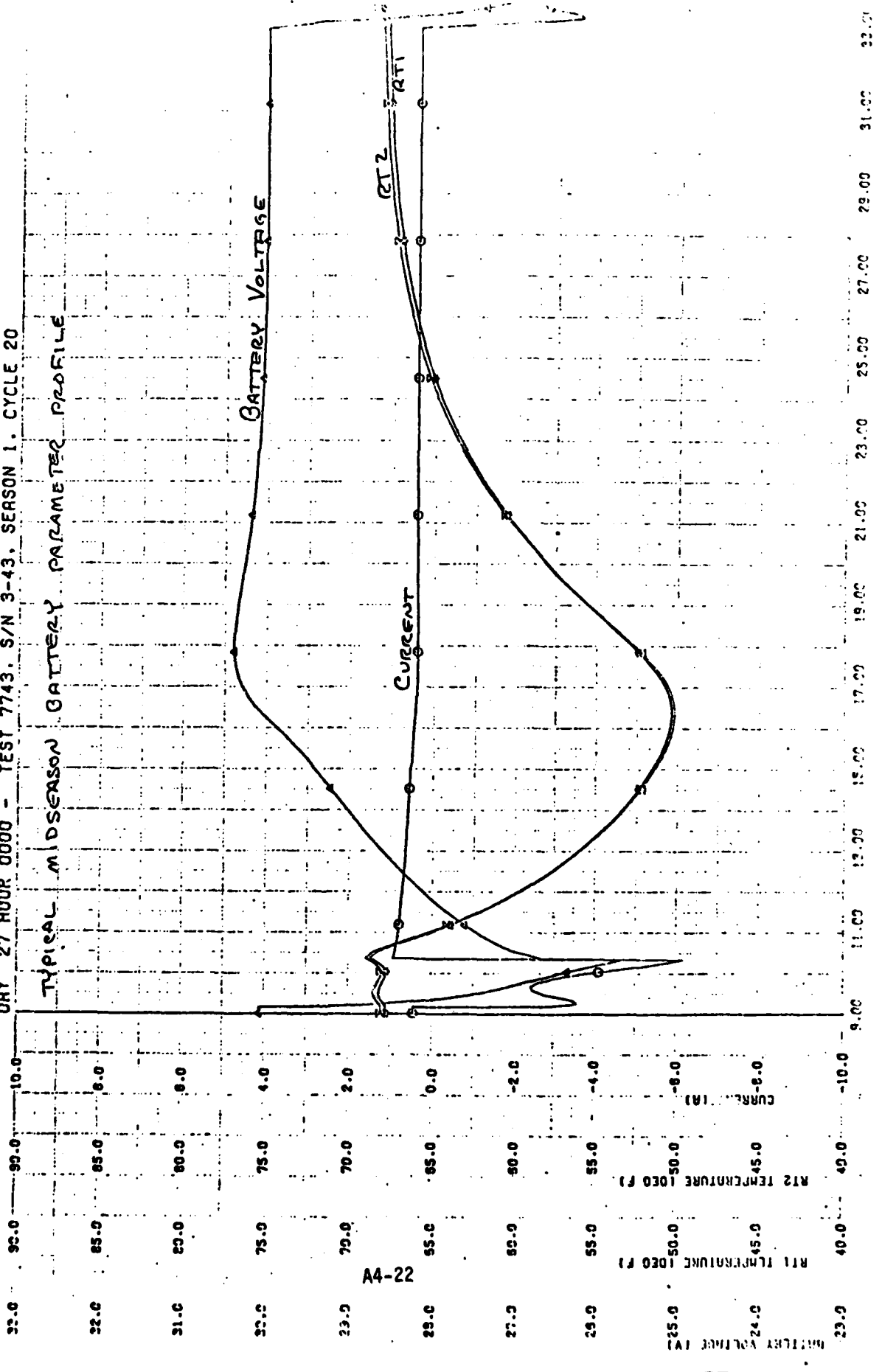


Fig 3
 DRY 27 HOUR 0000 - TEST 7743, S/N 3-43, SEASON 1, CYCLE 20

TYPICAL MIDSEASON BATTERY PARAMETER PROFILE

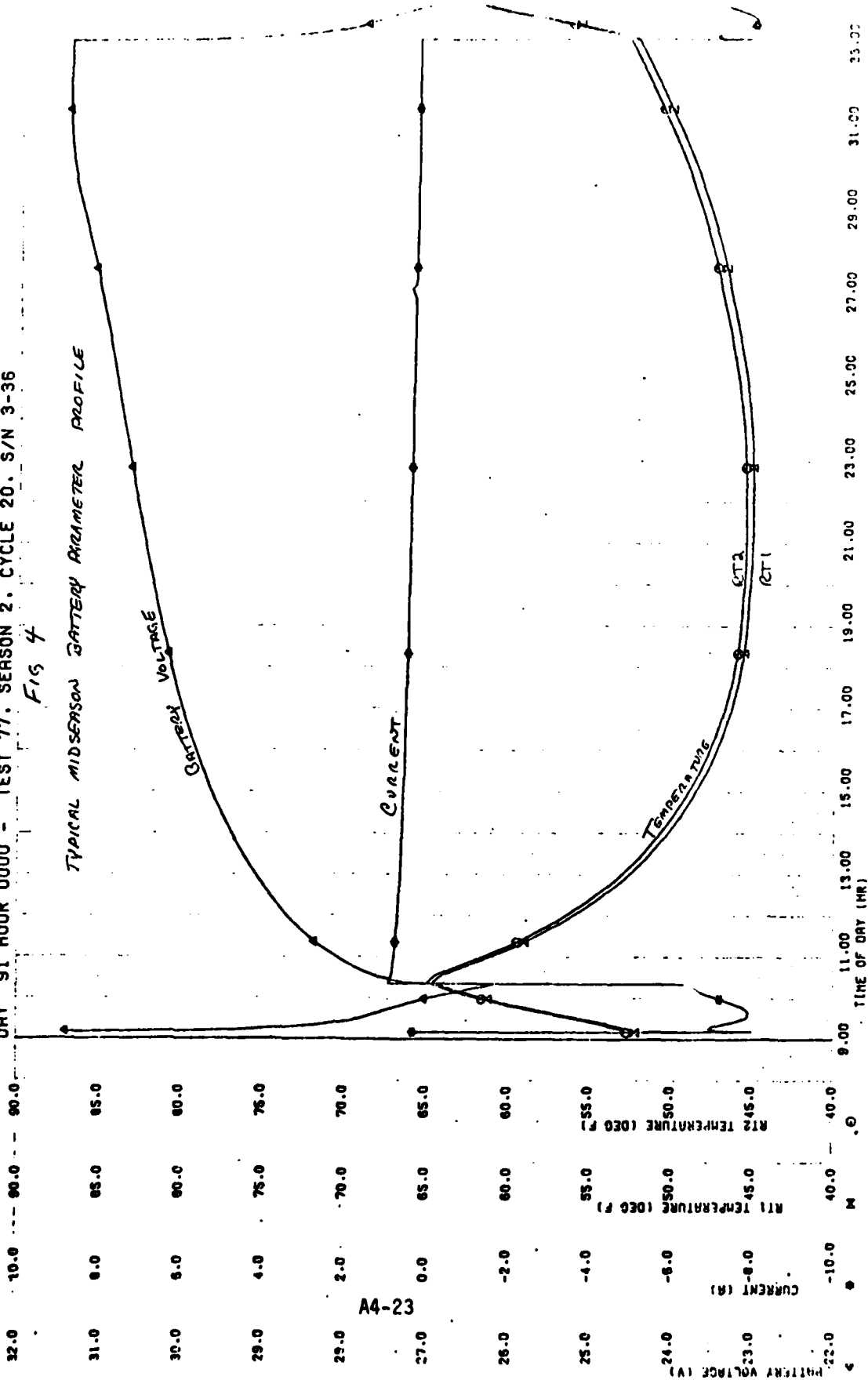


A4-22

DAY 91 HOUR 0000 - TEST 77, SEASON 2, CYCLE 20, S/N 3-36

FIG 4

TYPICAL MIDSEASON BATTERY PARAMETER PROFILE



A4-23

DRY 91 HOUR 0000 - TEST 7743, SEASON 2, CYCLE 20, S/N 3-43

Fig 5

TYPICAL MIDSEASON BATTERY PARAMETER PROFILE

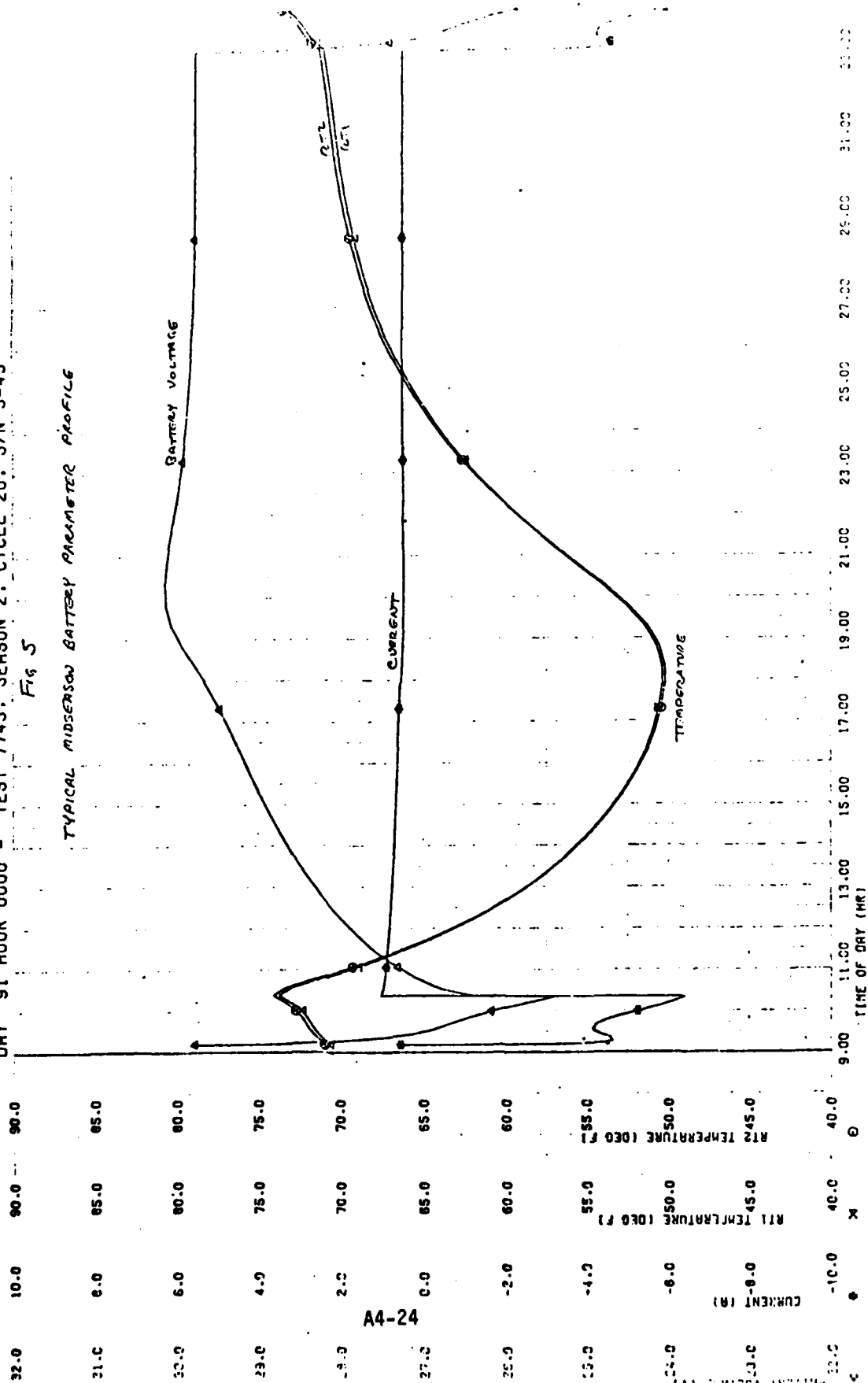


FIG 6

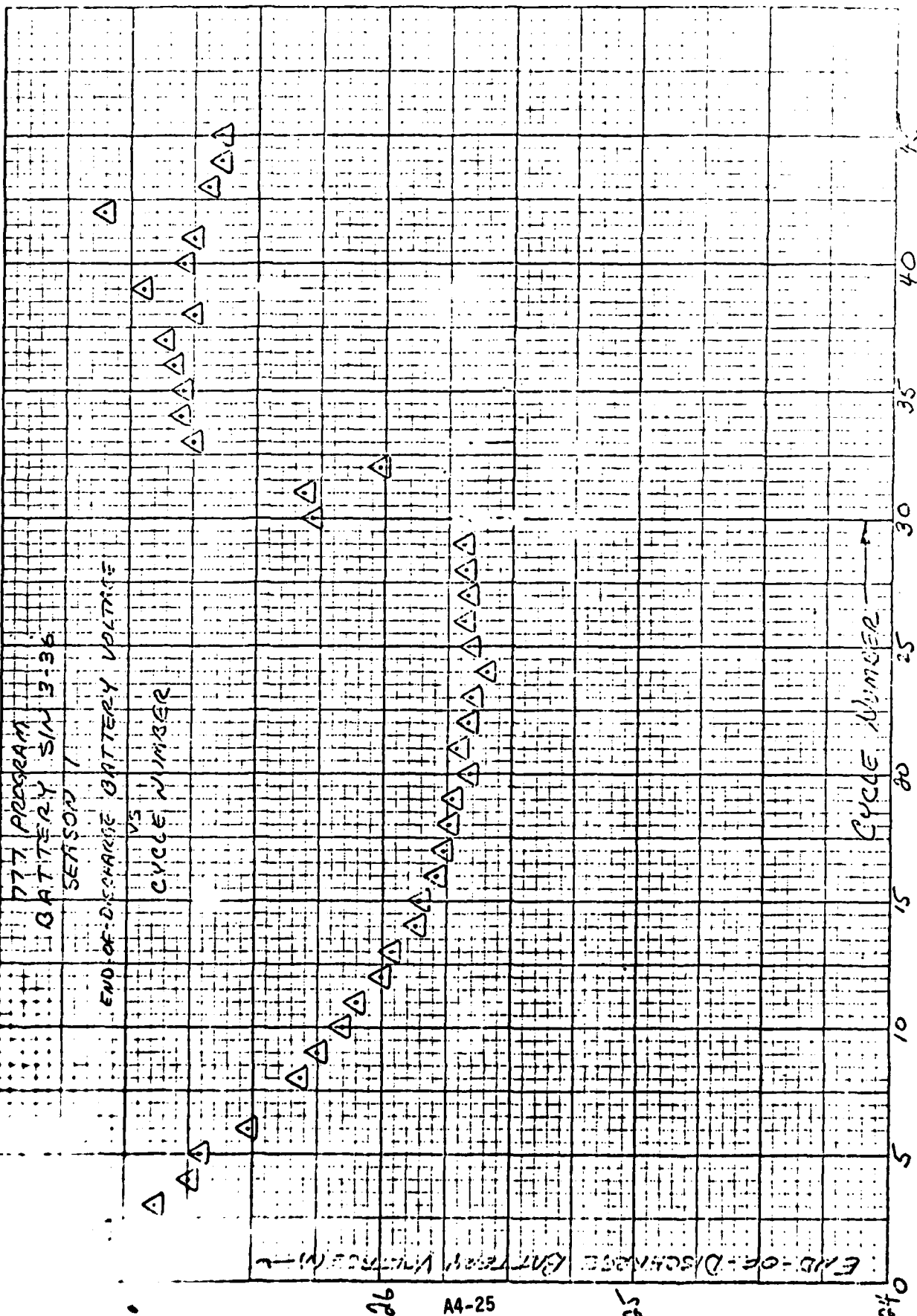
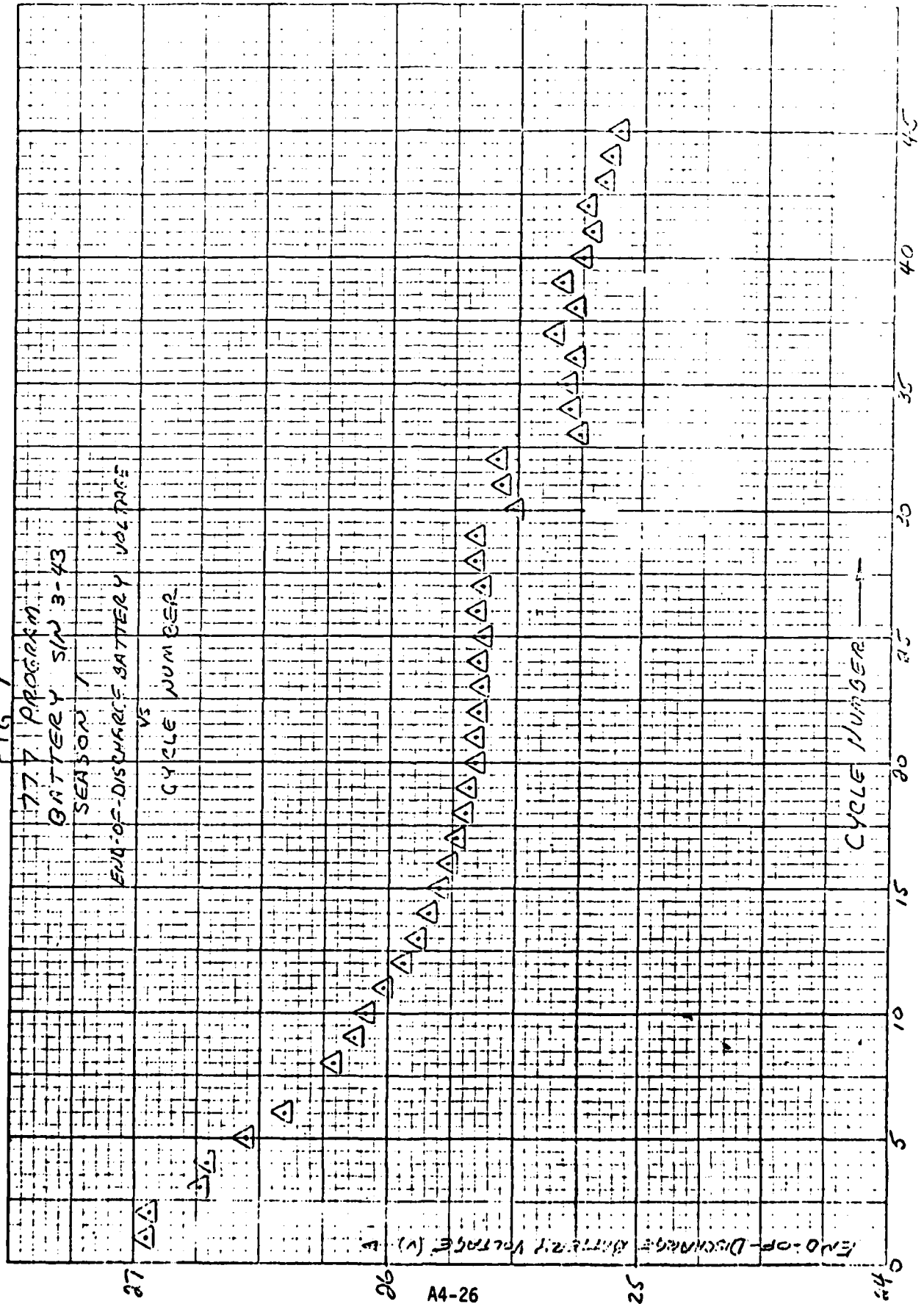
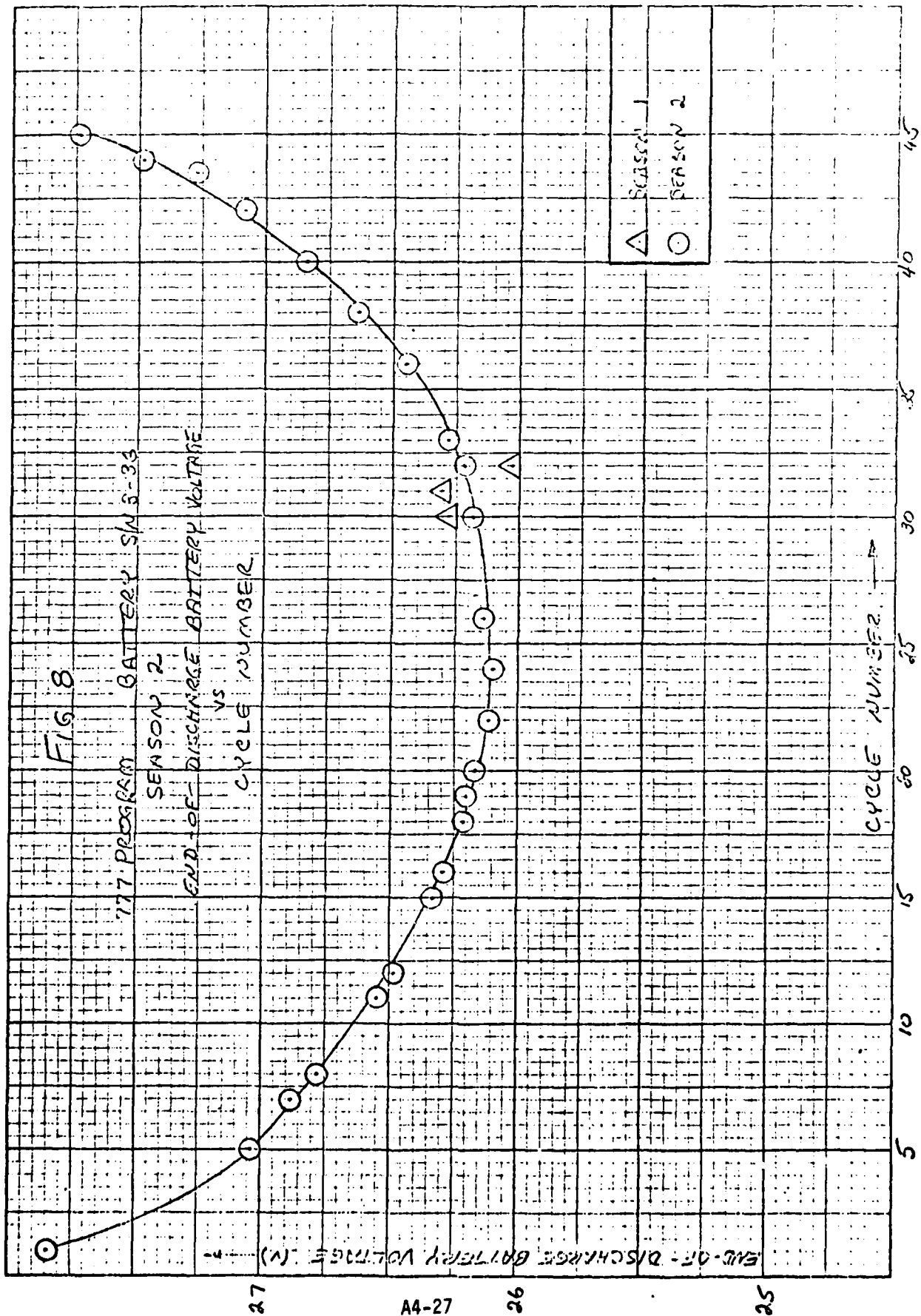
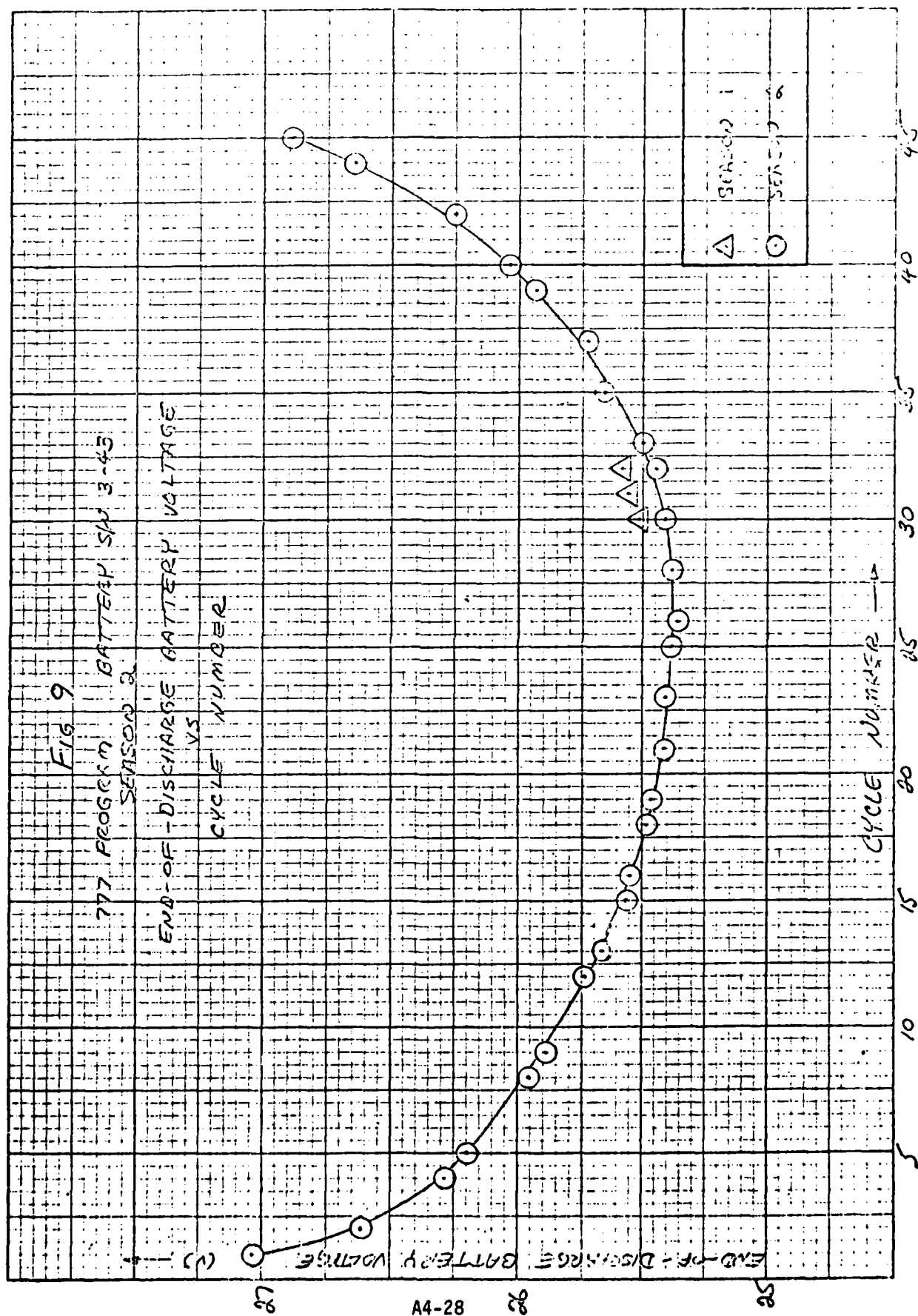
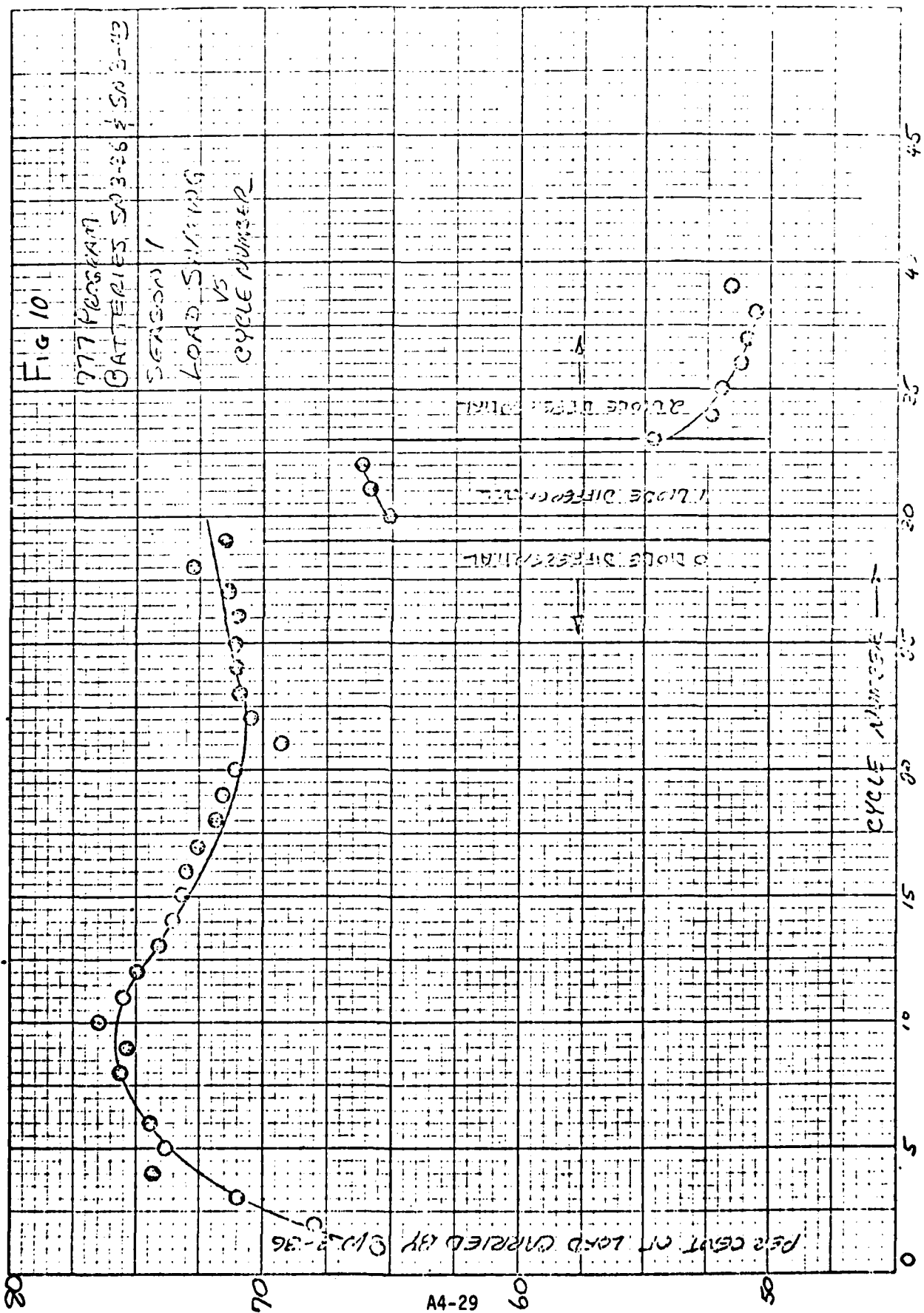


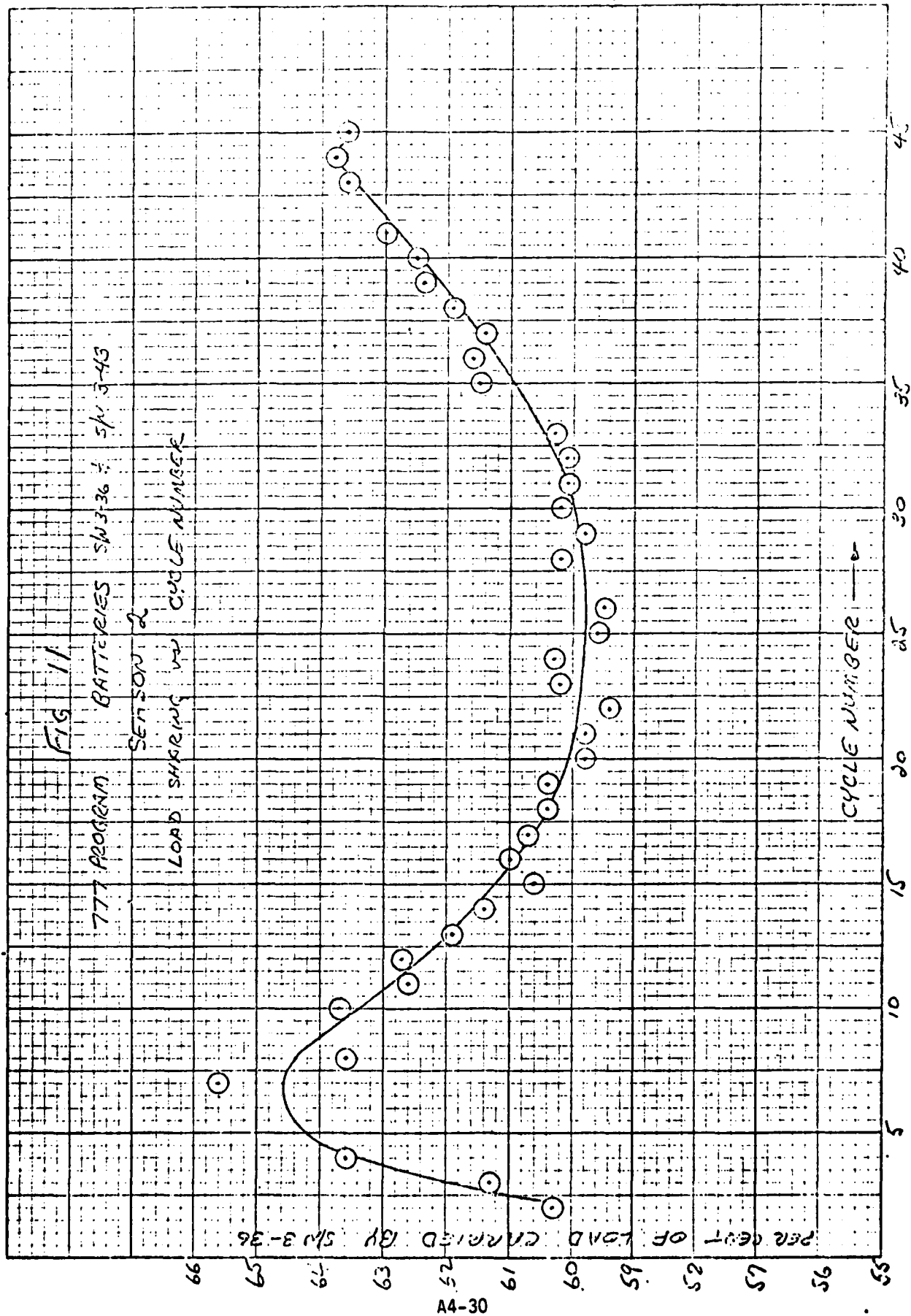
FIG 7











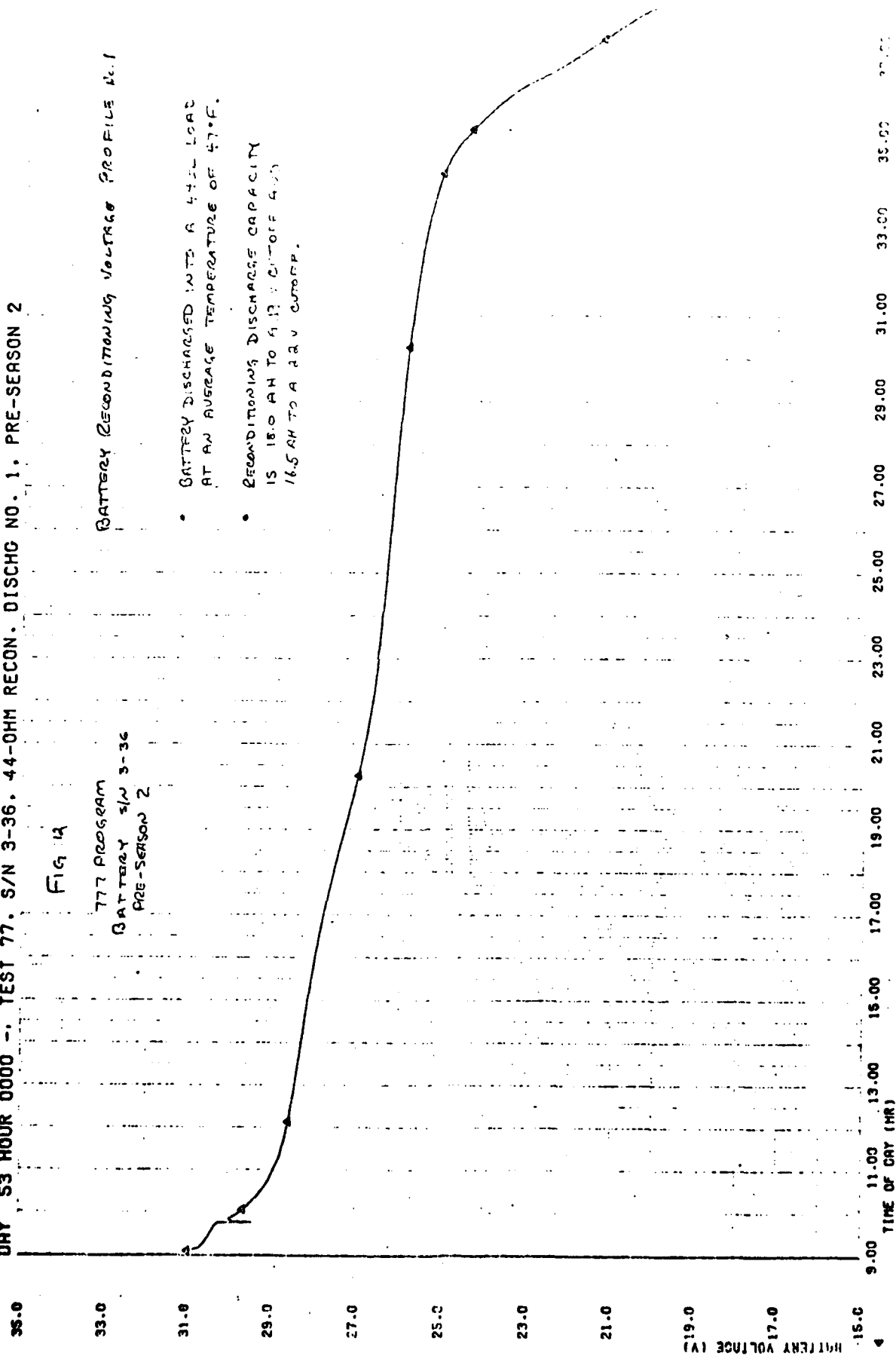
DAY 53 HOUR 0000 -- TEST 77. S/N 3-36. 44-OHM RECON. DISCHG NO. 1. PRE-SEASON 2

Fig 14

777 PROGRAM
BATTERY S/N 3-36
PRE-SEASON 2

BATTERY RECONDITIONING VOLTAGE PROFILE NO. 1

- BATTERY DISCHARGED INTO A 44Ω LOAD AT AN AVERAGE TEMPERATURE OF 47°F.
- RECONDITIONING DISCHARGE CAPACITY IS 18.0 AH TO A 12 V CUTOFF AND 16.5 AH TO A 22 V CUTOFF.



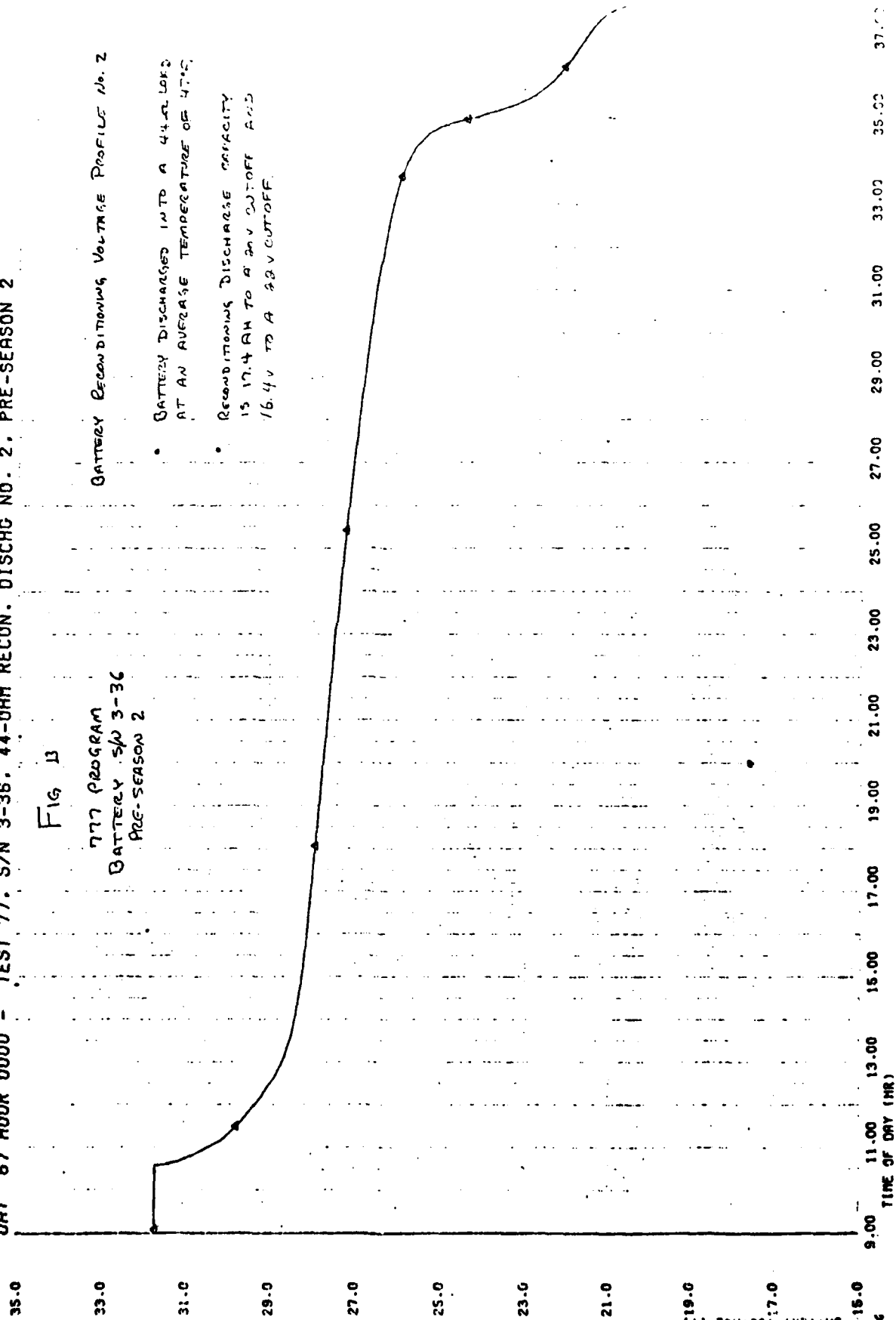
DAY 67 HOUR 0000 - TEST 77. S/N 3-36. 44-OHM RECON. DISCHG NO. 2, PRE-SEASON 2

Fig 13

777 PROGRAM
BATTERY SW 3-36
PRE-SEASON 2

BATTERY RECONDITIONING VOLTAGE PROFILE NO. 2

- BATTERY DISCHARGED INTO A 44-Ω LOAD AT AN AVERAGE TEMPERATURE OF 47°C.
- RECONDITIONING DISCHARGE CAPACITY IS 17.4 AH TO A 24V CUTOFF AND 16.4V TO A 22V CUTOFF.



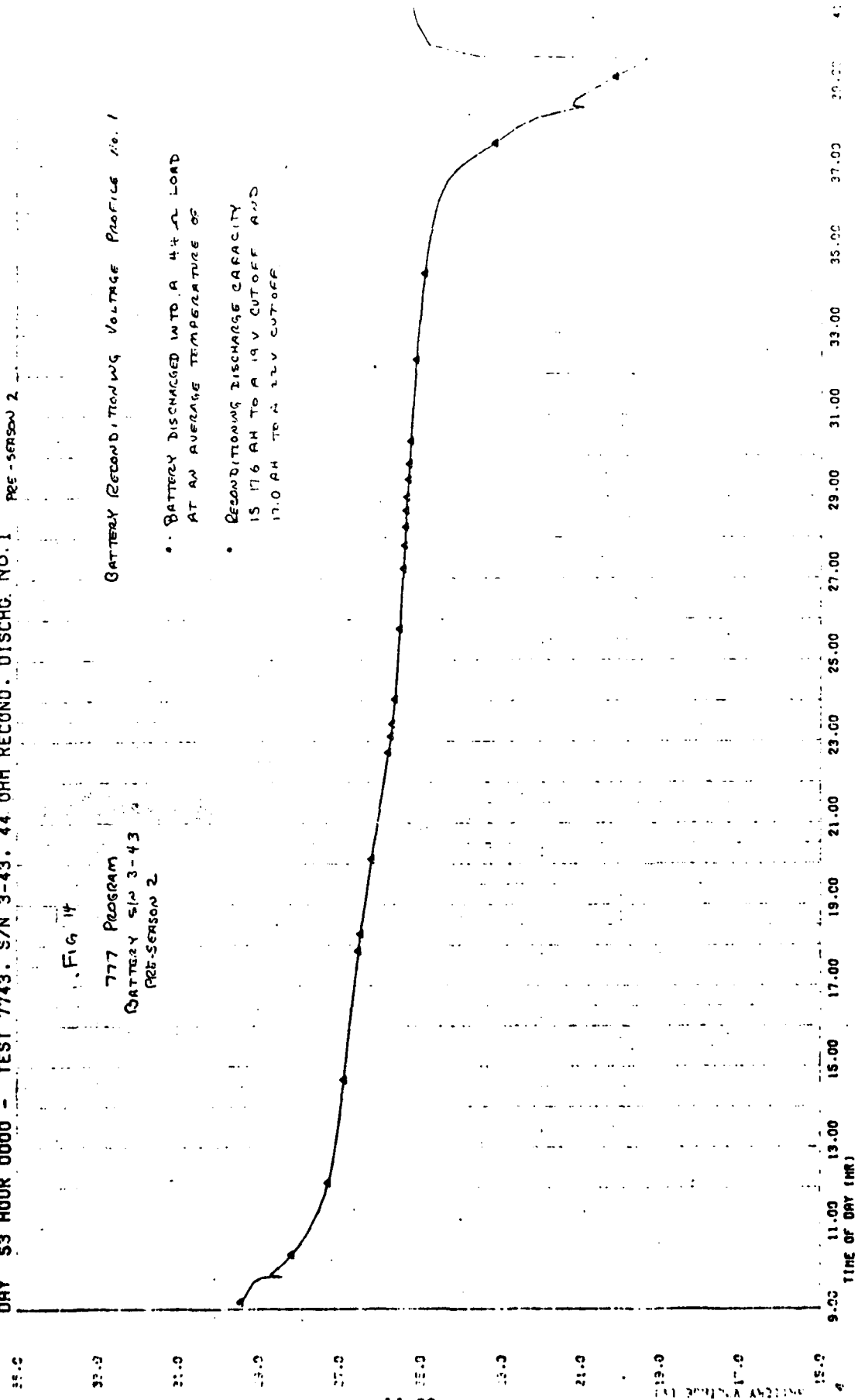
DAY 53 HOUR 0000 - TEST 7743. S/N 3-43. 44 OHM RECOND. DISCHG. NO.1 PRE-SEASON 2

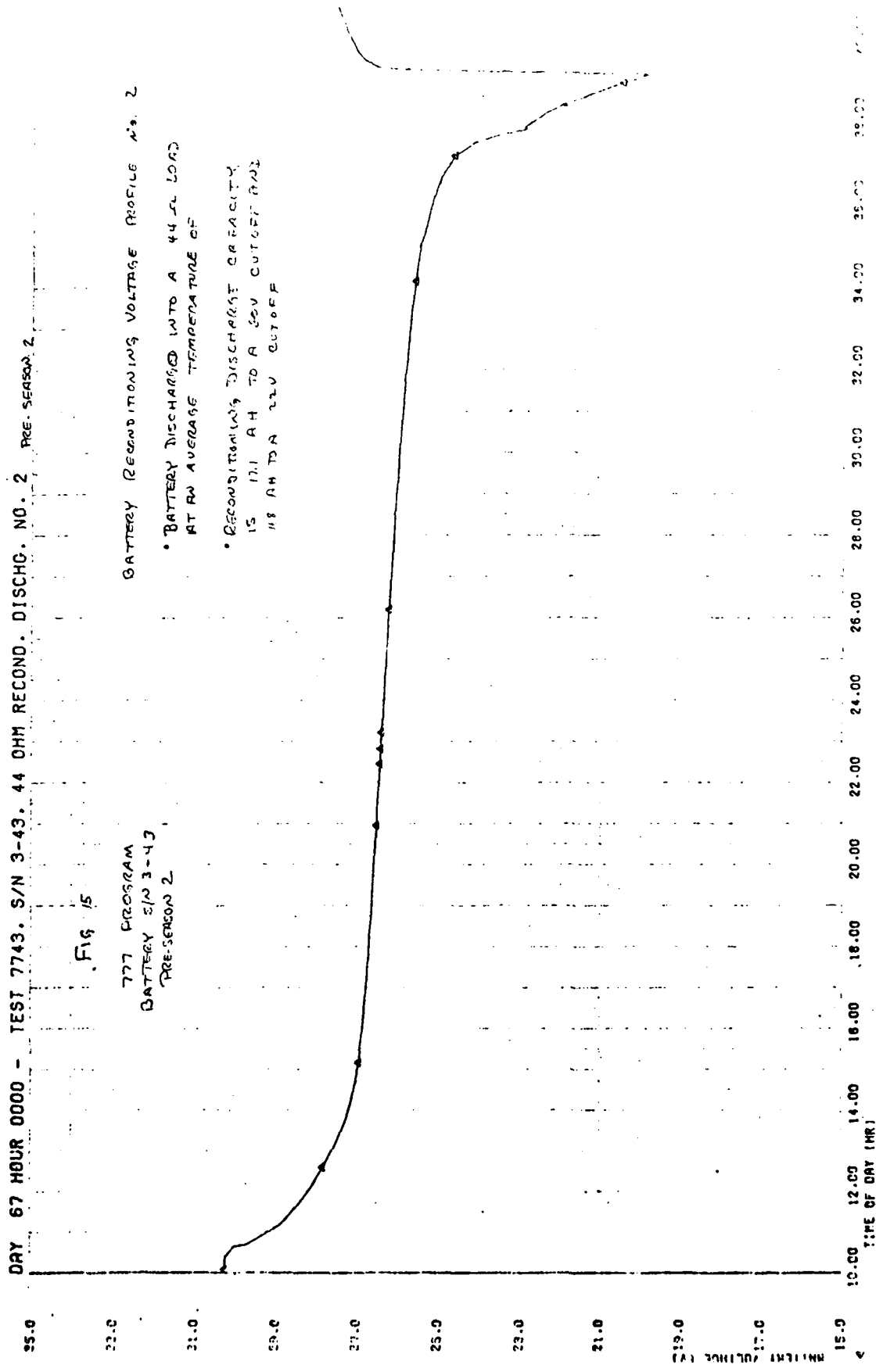
Fig 14

777 PROGRAM
BATTERY S/N 3-43
PRE-SEASON 2

BATTERY RECONDITIONING VOLTAGE PROFILE No. 1

- BATTERY DISCHARGED INTO A 44 OHM LOAD AT AN AVERAGE TEMPERATURE OF
- RECONDITIONING DISCHARGE CAPACITY IS 17.6 AH TO A 19 V CUTOFF AND 17.0 AH TO A 12 V CUTOFF





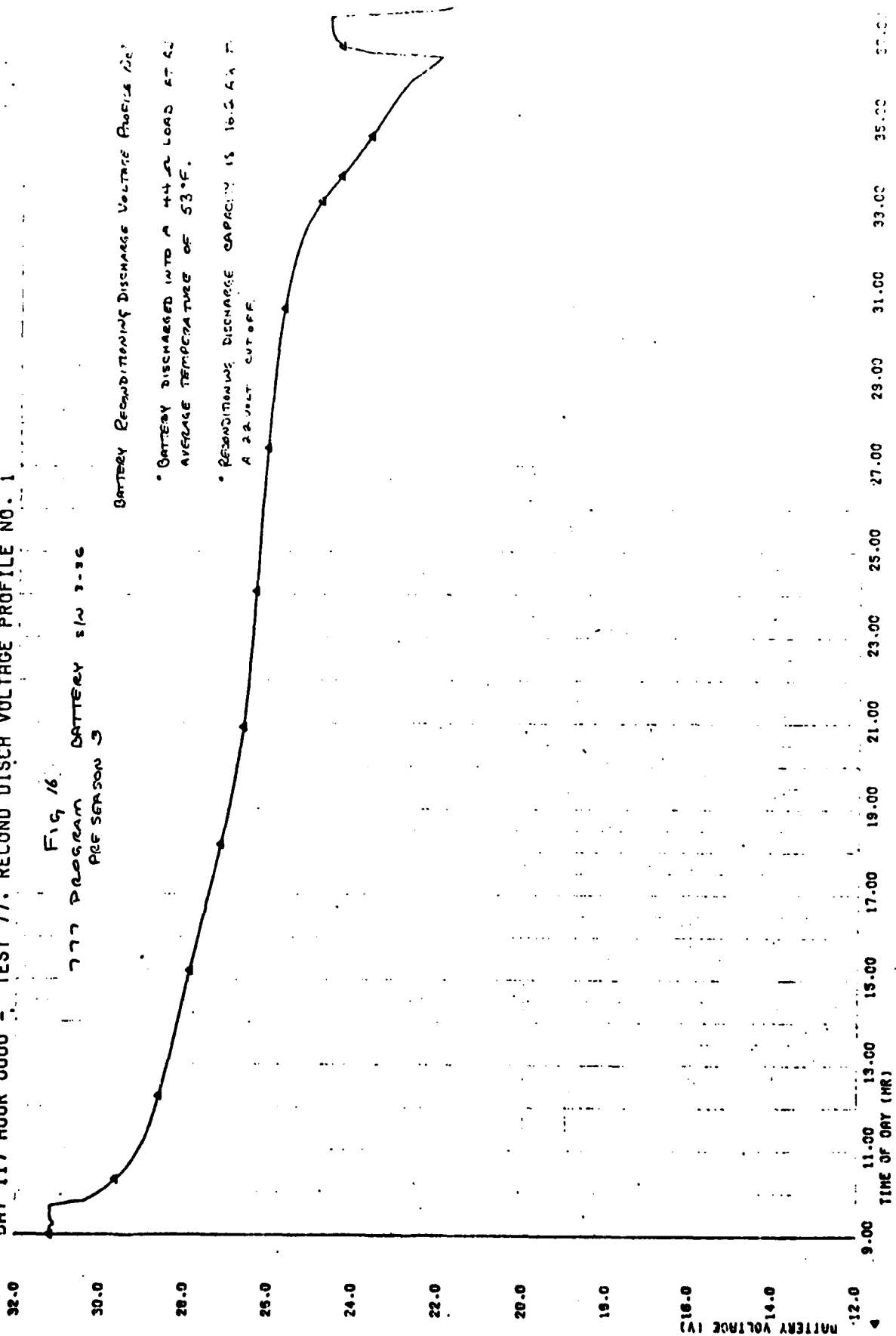
DAY 117 HOUR 0000 - TEST 77. RECOND DISCH VOLTAGE PROFILE NO. 1

Fig 16
777 PROGRAM BATTERY S/W 3-36
REF SEASON 3

BATTERY RECONDITIONING DISCHARGE VOLTAGE PROFILE NO. 1

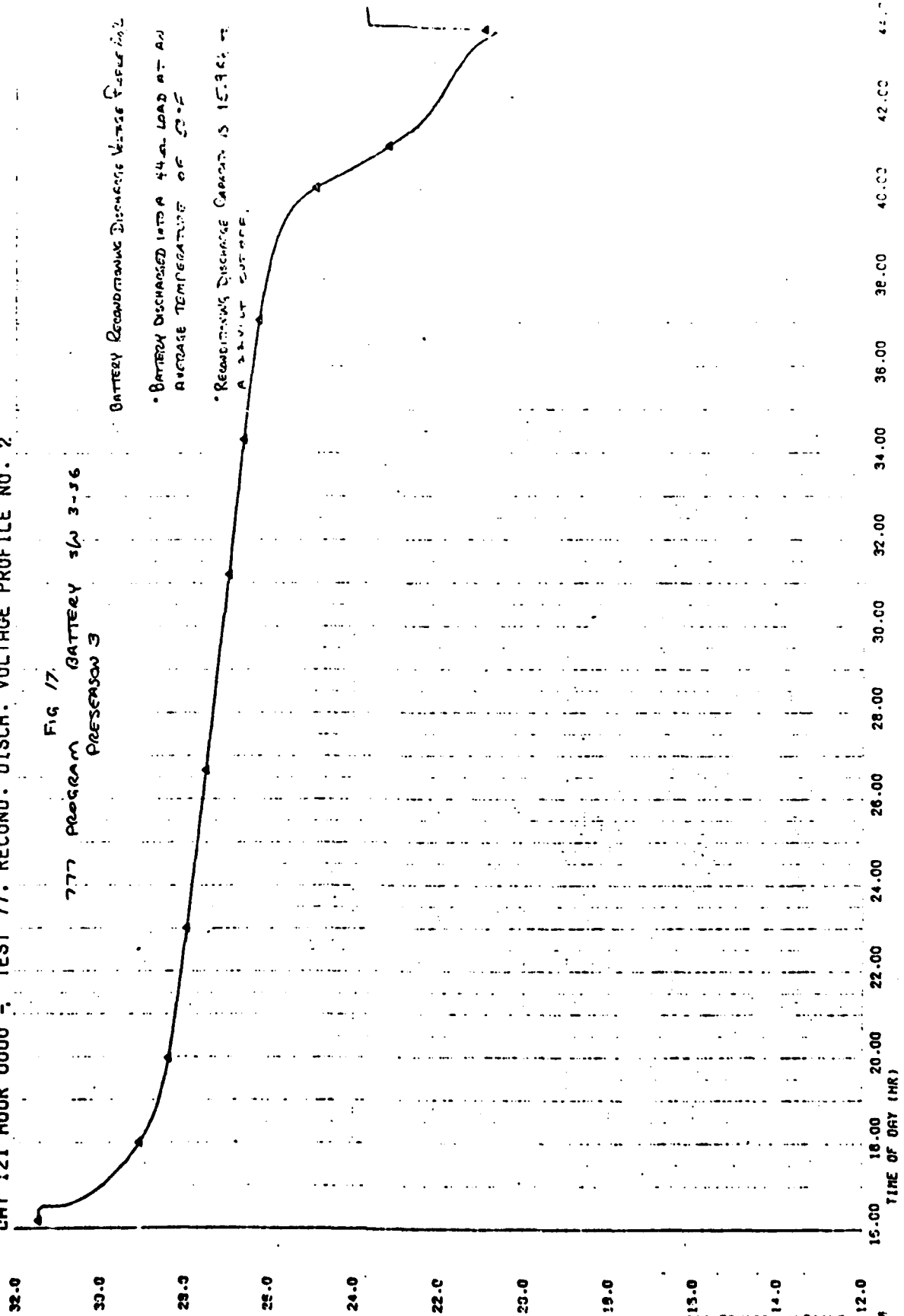
* BATTERY DISCHARGED INTO A 44 OHM LOAD AT AN AVERAGE TEMPERATURE OF 53°F.

* RECONDITIONING DISCHARGE CAPACITY IS 16.5 AH AT A 22 VOLT CUTOFF



DAY 121 HOUR 0000 - TEST 77. RECOND. DISCH. VOLTAGE PROFILE NO. 2

Fig 17.
777 PROGRAM BATTERY 36 3-36
PRESEASON 3



BATTERY RECONDITIONING DISCHARGE VOLTAGE PROFILE

BATTERY DISCHARGED INTO A 44 OHM LOAD AT AN AVERAGE TEMPERATURE OF 23°F

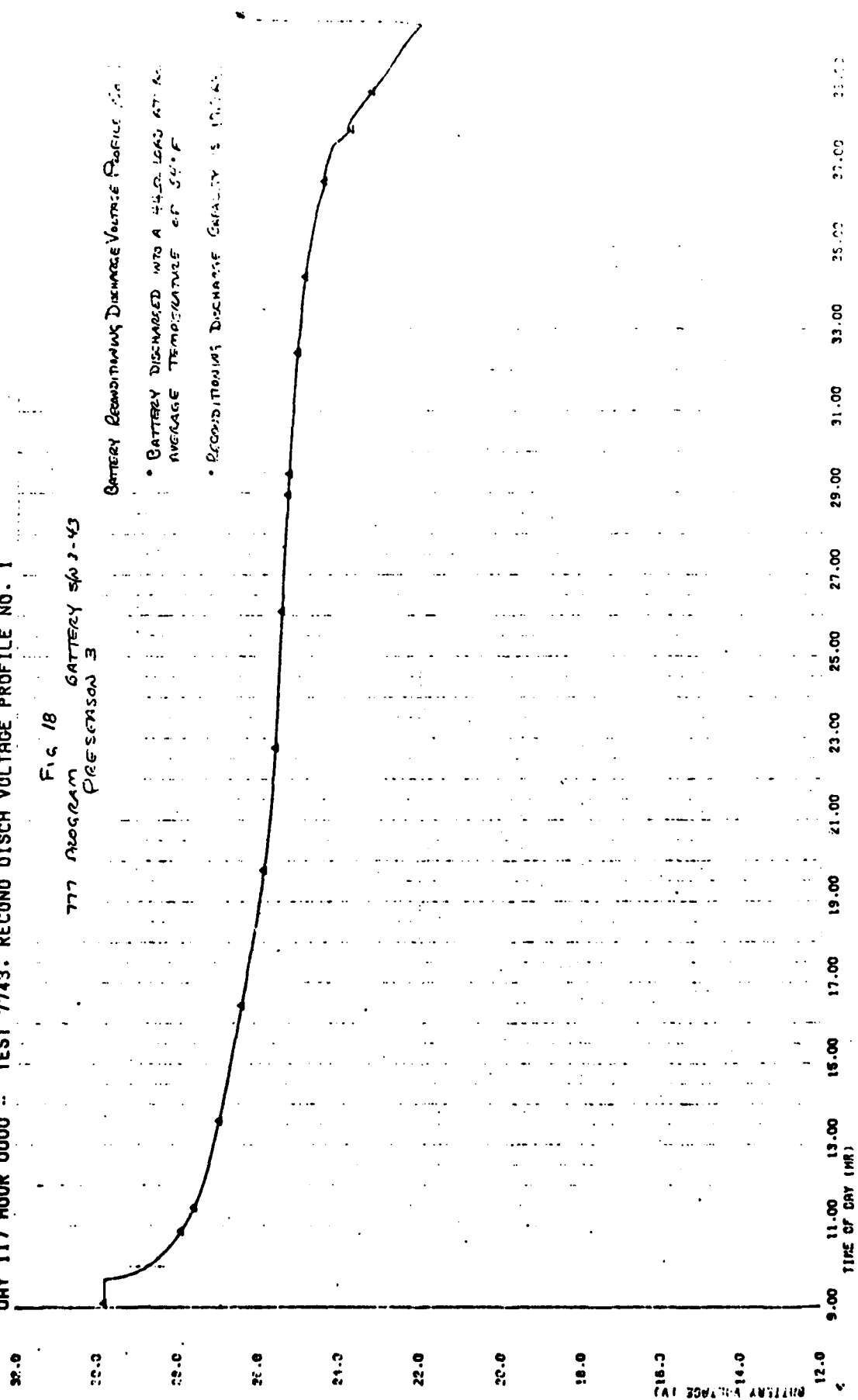
RECONDITIONING DISCHARGE CAPACITY IS 15.94 AH AT A 2.0 VOLT CUTOFF

DAY 117 HOUR 0000 -- TEST 7743. RECOND DISCH VOLTAGE PROFILE NO. 1

FIG 18
777 PROGRAM BATTERY SP-3-43
PRESERASON 3

BATTERY RECONDITIONING DISCHARGE VOLTAGE PROFILE

- BATTERY DISCHARGED INTO A 44-Ω LOAD AT AN AVERAGE TEMPERATURE OF 54°F
- RECONDITIONING DISCHARGE CAPACITY IS 17.0 AH



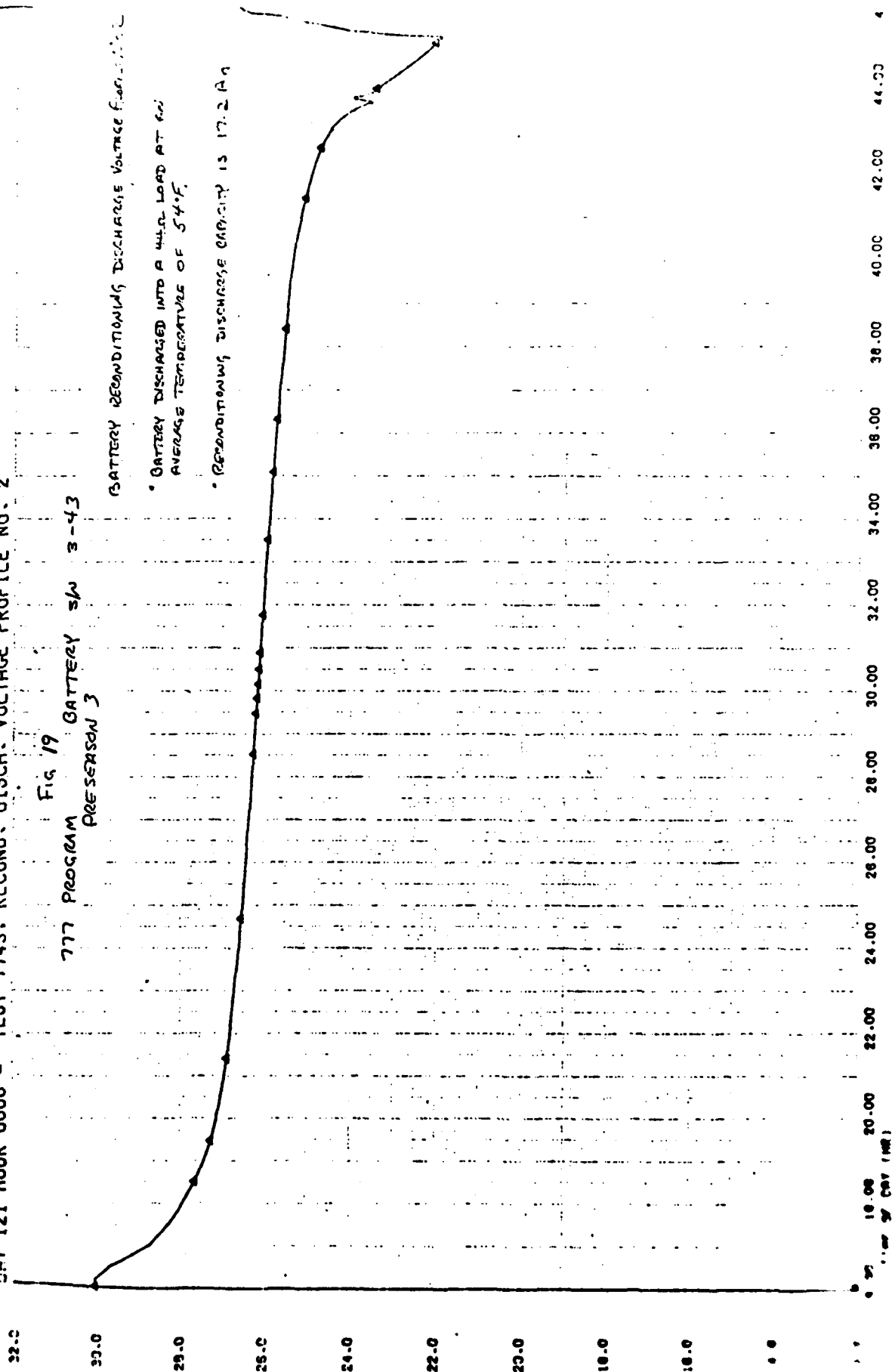
DAY 121 HOUR 0000 - TEST 7743. RECOND. DISCH. VOLTAGE PROFILE NO. 2

FIG 19
777 PROGRAM BATTERY SW 3-43
PRESEASON 3

BATTERY RECONDITIONING DISCHARGE VOLTAGE PROFILE

* BATTERY DISCHARGED INTO A 44.0 OHM LOAD AT AN AVERAGE TEMPERATURE OF 54°F.

* RECONDITIONING DISCHARGE CAPACITY IS 17.2 AH



AD-A087 390

TRW DEFENSE AND SPACE SYSTEMS GROUP REDONDO BEACH CA
DSCS II, BATTERY ANOMALY INVESTIGATION SATELLITES 9437 AND 9438--ETC
APR 80 P BAUER, C LURIE
TRW-32824-AR-019-01

F/G 10/3

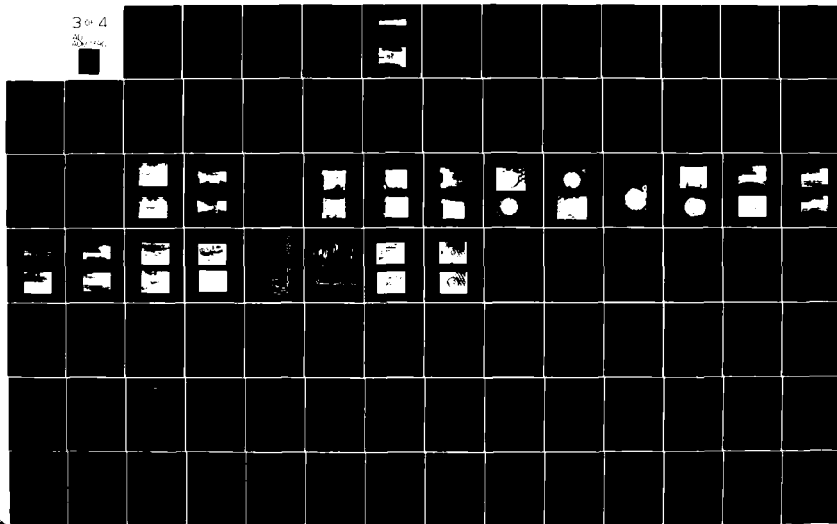
F04701-77-C-0118

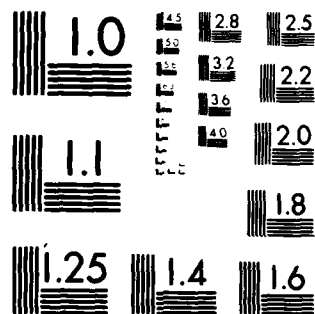
NL

UNCLASSIFIED

SD-TR-80-33

3 of 4





MICROCOPY RESOLUTION TEST CHART
NATIONAL BUREAU OF STANDARDS-1963-A

APPENDIX 5

DESTRUCTIVE PHYSICAL ANALYSIS



INTEROFFICE CORRESPONDENCE

DSCS-C3-503
79-8725.2-092

TO: C. L. Stanley

CC: Distribution

DATE: 2 May 1979

SUBJECT: Results of Destructive Physical/Chemical
Analysis of 777 Battery Cells, 12 Ah, P/N 8E005,
Lots 1, 2, 5 and 6, after Storage

FROM: W. R. Scott
BLDG MAIL STA. EXT.
M1 1406 50776

- Reference 1: "DPA of 777 15-Ah Ni-Cd Cells, S/N 127-L01 and 018-L02",
IOC #78-8725.2-152, L. P. Mack, 27 July 1978
- Reference 2: "Procedure for Analysis of Nickel-Cadmium Cell Materials",
NASA GSFC X-711-74-279, G. Halpert et al, October 1974
- Reference 3: "Results and Discussion of the DPA Procedure for FLTSATCOM
Cells, S/N 035-08 and 047-09", IOC #78-8725.2-008, L. P. Mack,
12 January 1978
- Reference 4: "Spacecraft Battery Testing - 4 Year Life", Report #16439-
93-002-601 (DSP), 9 April 1976

1. INTRODUCTION

This memo presents the results of destructive physical (and chemical) analysis of (DPA) of sample nickel-cadmium battery cells, Part No. 8E005, 12 ampere-hour nominal capacity, General Electric Catalog No. 42B012AB24, Lot Nos. 1, 2, 5 and 6. Lots 1 and 2 were those from which the batteries on board 777 flights 7 and 8 were made, whereas Lots 5 and 6 were those from which the batteries on 777 flights 11 and 12 were made. The cells analyzed had just been removed from cold storage following acceptance testing.

The analysis reported herein was performed in October 1978. DPA was not done on the 12 Ah (8E005) cells at the time of receipt of the cells at TRW (1976) because this procedure had not been instituted for the 777 program at that time.

DPA had been performed on two lots of 777 15 Ah cells, P/N 8E009, Lot Nos. 1 and 2, immediately following acceptance testing, in January 1978. This analysis was done at that time because the procedure had been established at the time these cells were received (late in 1977). The results of this analysis are described in Reference 1. Note that there are Lot Nos. 1 and 2 for both 12 Ah (P/N 8E005) and 15 Ah (P/N 8E009) cells. This is because the cell manufacturer serializes each different type of cell separately.

2. GENERAL PROCEDURE AND SAMPLING

Three cells from each of four lots of 8E005 cells on hand were opened and all plates and separators from these cells were visually inspected. Then ten positive plates, ten negative plates, and ten separators from each lot (five positives, negatives, and separators from each of two cells from each lot) were further tested and analyzed. Characteristics determined were:

- Visual appearance of plate surfaces and separators.
- Thickness of plates.
- Electrolyte analysis of plates and separators.
- Nickel active material and metallic nickel in positive plates.
- Cadmium active material and charged cadmium material in negative plates.
- Nickel and cadmium in the separators.

Details of analytical methods used are given in Reference 1 and 2.

In addition, a number of positive and negative plates were taken from these cells and subjected to electrochemical stress testing in excess electrolyte. The results of this testing is described in a separate report.

3. RESULTS OF DPA

3.1 Visual Inspection

3.1.1 General Observations

The general appearance of the cell terminals, plate tabs, and outside surfaces of the plate packs was normal for General Electric cells. The degree of "wetness" (amount of electrolyte in the pores of the plates and separators) observed during separation of the plates also appeared in the normal range, with some areas of negative plates appearing quite dry (as often seen in G.E. cells).

3.1.2 Negative Plates

The texture and general condition of the negative plate surfaces were about as usually seen in G.E. cells. A light deposit of very small crystals of $\text{Cd}(\text{OH})_2$ was seen under the stereo-microscope (20 to 60 x) on most of the negative plate surfaces. The appearance of the surfaces was not uniform, however, with respect to color, brightness, and occurrence of $\text{Cd}(\text{OH})_2$ deposits. Most plates showed variations from light, silvery appearance with little or no visible deposits (usually near the top of the plates) to a darker, dull appearance with deposits (usually near the bottom of the plates). These variations appeared to correspond with a relatively low

electrolyte content near the top and to a relatively high electrolyte content near the bottom. This effect has been seen in other G.E. cells opened in the past, but since the appearance is difficult to quantify, it cannot be said whether the degree seen in these cells was greater or less than "normal".

3.1.3 Positive Plates

The positive plates showed a greater variety of features than did the negative plates, as is usual. A majority of the positive plates from all lots showed at least one and usually many round black spots ranging up to 1/4 inch in diameter. Some plates showed irregularly-shaped small black areas, referred to as "black specks". Others showed dark brown to black parallel bands running straight across the width of the plates. Still others (less numerous) showed areas covered with a layer of black material that appeared to have been spilled or splashed onto the surface. These features occur frequently on positive plates made by G.E. and are thus considered "normal" for G.E. cells.

Several other features that were not considered normal were observed on some of the positive plates. The nature and frequency of occurrence of these is summarized in Table 1. Definitions of the names given to these features are given at the bottom of the table.

Only one of the types of special features shown in Table 1 was investigated further within the scope of the DPA. One of the plates having black spots was dried, encapsulated in epoxy resin, and sectioned through a "black spot". A photograph of the result is shown in Figure 1, wherein the section is tilted at an angle to show the spot on the original plate surface. Note the non-uniform distribution of nickel active material (black color) in the cross-section of the plate, and the relatively intense black color under the spot itself. A close-up view (75 x) of this section is shown in Figure 2. The non-uniform distribution of active material may be seen here also at the micro level.

DSCS-C3-503
79-8725.2-092
2 May 1979
page 4



FIGURE 1. SECTION THROUGH BLACK SPOT ON
A POSITIVE PLATE (12X)



FIGURE 2. METALLOGRAPH THROUGH BLACK SPOT
ON POSITIVE PLATE (75X)

Table 1 - Unusual Features on Positive Plates

Lot No.	Cell Serial No.	Raised Black Spots	Black Outcropping	Disrupted Sinter	Bumps
01	185-L01	Many plates.	Two plates, heavy.	One plate.	-----
	222-L01	Two plates.	-----	-----	One plate, heavy, both sides
	235-L02	Few, scattered.	-----	-----	-----
02	072-L02	Two plates.	Two plates.	Coincident with outcropping.	Two plates, light.
	134-L02	-----	-----	-----	-----
	158-L02	-----	One plate; heavy; covers entire plate surface.	Concident with outcropping.	One plate, heavy.
05	049-L05	Several plates.	-----	-----	None
	127-L05	-----	Two plates.	Two plates. Concident with outcropping.	-----
	132-L05	-----	One plate.	Concident with outcropping.	-----

Table 1 - cont'd.

Lot No.	Cell Serial No.	Raised Black Spots	Black Outcropping	Disrupted Sinter	Bumps
06	063-L06	-----	One plate, both sides.	-----	None
	096-L06	-----	Two plates.	Two plates; concident with outcropping.	-----
	148-L06	Several plates.	One plate, both sides.	Two plates. One concident with outcropping; one along a machine mark.	-----

- (1) **RAISED BLACK SPOT:** A protuberance on the surface, concident with a black spot, that is easily visible as a raised point, and which can be easily felt with the finger. The sinter surface may or may not be cracked. The lump is usually relatively firm, and may rise from 0.005 to 0.010 inch above the surrounding surface.
- (2) **BLACK OUTCROPPING:** A flow of relatively loosely adherent nickel active material out of the pores of the sinter onto the surface of the plate, with the sinter surface otherwise normal.
- (3) **DISRUPTED SINTER:** The normal, microporous sintered nickel surface is rough, pack-marked, covered with small craters, or appears to have been burned or subjected to an electric arc.
- (4) **BUMPS:** Roughly spherical bumps in the sinter surface, usually colored brown or grey brown, and which are larger than "RAISED BLACK SPOTS" as defined in (1). There bumps are over 0.002 inch high.

3.1.4 Separators

The separators appeared generally normal. However, dark (dark grey to black) spots were seen on at least one bag from each cell inspected. Spotting was most frequently along the top edge of the plates, just outside of the plate boundary. Other spots occurred along the long edges and along the bottom edges of the plates and in contact with black areas in the main surface of the plate. Under the microscope these spots on the separator appeared "oily" and appeared to have partially penetrated into the separator fabric. No complete penetration of the separator layer was seen. The black material has not yet been positively identified. A preliminary qualitative analysis done by Electron Microprobe indicated the presence of both cadmium and nickel.

3.2 Plate Thicknesses

Average thickness per plate for positive plates ranged from 0.027 to 0.029 inch (raised spots and bumps excepted). This thickness is normal for G.E. positive plates after acceptance testing, during which a thickening of the order of 10 percent from the original range of 0.026 to 0.028 is usually observed. Average thickness of negative plates ranged from 0.031 to 0.033 inch, indicating essentially no change during acceptance testing, as expected.

3.3 Electrolyte Content and Analysis

Electrolyte contents (as measured by the weight of water soluble material extracted) were as shown in Table 2. These values compare favorably with values seen in other G.E. cells with similar histories (References 1, 3 and 4).

Hydroxide and carbonate concentrations, obtained from electrolyte extracted from the components, are shown for each lot in Table 3. The levels shown, and the ratios of carbonate to hydroxide (carbonate concentration 8-12 percent of hydroxide) are in the normal range.

3.4 Positive Plate Chemical Analysis

3.4.1 Total Nickel Active Material Content

Values for total nickel active material (i.e., the sum of charged and discharged nickel compounds, not including metallic nickel) are shown in the first column of Table 4. Each value shown is for plates from an individual cell as shown. Those values below 12.5 g/dm^2 are below normal.

Table 2 Electrolyte Contents of (g/dm²) - Range

Lot No.	Positive Plates		Negative Plates		Separators	
	OH ⁻	LO ₃	OH ⁻	CO ₃ ⁼	OH ⁻	CO ₃ ⁼
1	13.3-17.4	1.12-2.22	17.4-19.3	1.56-2.64	5.35-7.41	0.19-1.12
2	15.0-16.1	1.12-1.56	17.1-19.9	1.32-2.44	5.82-7.32	0.56-1.12
5	13.9-15.2	1.12-2.00	15.6-19.5	1.68-2.24	5.35-7.32	0.56-0.94
6	13.9-14.6	1.12-1.50	15.6-19.5	1.32-1.88	6.80-7.61	0.60-0.99

Table 3 Hydroxide and Carbonate Contents (meq/dm²)

Lot No.	Positive Plates		Negative Plates		Separators	
	OH ⁻	LO ₃	OH ⁻	CO ₃ ⁼	OH ⁻	CO ₃ ⁼
1	13.3-17.4	1.12-2.22	17.4-19.3	1.56-2.64	5.35-7.41	0.19-1.12
2	15.0-16.1	1.12-1.56	17.1-19.9	1.32-2.44	5.82-7.32	0.56-1.12
5	13.9-15.2	1.12-2.00	15.6-19.5	1.68-2.24	5.35-7.32	0.56-0.94
6	13.9-14.6	1.12-1.50	15.6-19.5	1.32-1.88	6.80-7.61	0.60-0.99

Table 4 Positive Plate Chemical Analysis Data

Cell Lot/ Serial No.	Total Nickel Active Material (1) (g/dm ²)	Equivalent Theoretical Positive Capacity Per Cell (Ah)	Metallic Nickel (2) (g/dm ²)	Ratio of Nickel Metal to Nickel Active Material
Lot 1-185	12.45	20.21	7.81	0.629
-222	12.32	20.00	7.80	0.633
Lot 2-072	13.54	21.98	7.26	0.535
Lot 5-049	11.66	18.93	7.31	0.625
-127	13.37	21.70	7.89	0.592
Lot 6-063	11.75	19.07	7.09	0.602
-096	12.30	19.97	7.13	0.578

(1) Calculated as Ni(OH)₂ (2) Calculated as Ni

Table 5 Negative Plate Chemical Analysis Data

Cell Lot/ Serial No.	Total Cadmium Active Material (1) (g/dm ²)	Equivalent Theoretical Negative Capacity (Ah)	Residual Charged Cadmium Active Material (1) (g/dm ²)	Equivalent Residual Charged Capacity Per Cell (Ah)
Lot 1-185	16.17	37.8	2.4	5.6
-222	16.75	39.2	4.3	10.1
Lot 2-072	16.50	38.6	0.8	1.9
158	17.26	40.4	1.4	3.3
Lot 5-049	16.18	37.9	3.0	7.0
-127	16.72	39.2	1.2	2.8
Lot 6-063	17.49	40.9	2.1	4.9
-096	16.69	39.1	1.0	2.3

(1) Calculated as Cd(OH)₂

3.4.2 Metallic Nickel Content

Values for metallic nickel in the sintered matrix are shown in Table 4 for a number of individual cells. These values do not include the nickel plating on the substrate. Since the nickel content of the sinter of this plate material prior to impregnation is about 10g/dm^2 , the values in Table 4 imply 20 to 30% loss of nickel by acid attack during impregnation. Little data on this characteristic is available for comparison.

The ratio of metallic nickel to active material in the sinter is shown at the right in Table 4. The cell manufacturer has stated that the inherent strength of the sinter is a function of this ratio.

3.5 Negative Plate Chemical Analysis

3.5.1 Total Cadmium Active Material Content

Values for total cadmium active material (charged + uncharged) are shown in Table 5. These values are close to that specified by the manufacturer for this plate material.

3.5.2 Residual Charged Cadmium Content

Values for the content of charged cadmium remaining in the negative plates at the time the cells were opened is shown at the right in Table 5. Theoretically the residual charged negative capacity in these particular cells should be equal to the total pre-charge (active plus inactive), as these cells had not been discharged below zero volt before the analysis for charged cadmium was performed.* For these cells total precharge should have been 6-8 Ah. One cell (Lot 1-222) was thus quite high, and four out of eight were low. These low values were not unexpected because it is known that low results are often obtained where this analysis is performed before the cell has been electrochemically discharged down to -0.5 or -1 volt. Thus the results of the negative plate analysis on these cells show no abnormalities.

3.6 Analysis of Separators for Included Nickel and Cadmium

Several representative separator bags, some containing black stains as described in Section 3.1.4, were analyzed for nickel and cadmium content as follows: Each bag was brushed free of loosely adhering particles, then placed in a small beaker containing 50 ml of 2N hydrochloric acid and allowed to soak for 30 minutes or until all colored material had been removed from the separator.

*The analysis was purposely abbreviated relative to that normally done on newly-received cells, as a detailed analysis of the state-of-charge of the negative electrode was not required under the circumstances.

The solution was decanted away from any insoluble material. Ten ml of 1.1 of nitric acid was added to the beaker and heated to boiling to dissolve any residue. The two solutions were then combined and diluted to 100 ml. This final solution was analyzed for Ni and Cd by the Atomic Absorption method. The results are shown in Table 6.

Table 6 - Nickel and Cadmium Contents of Separators

Lot Number	Nickel Material (as g Ni(OH)_2 per bag)	Cadmium Material (as g Cd(OH)_2 per bag)
1	0.0017 - 0.0038	0.028 - 0.034
2	0.0034 - 0.005	0.034 - 0.045
5	0.0032	0.022
6	0.003	0.035

The total area of separator material (one thickness) per bag is 1.17 dm^2 . Thus the above figures are approx. the average concentrations per dm^2 of separator. No data base exists for nearly-new cells from which these values may be judged. The concentrations shown for nickel are an order of magnitude lower than those found in one cycled cell,⁽¹⁾ whereas those shown for cadmium are about half of those found for a cycled cell⁽¹⁾.

It must be noted that most of the nickel and/or cadmium material in these separators was located in less than 10 percent of the total separator area. Hence the concentration in these local areas must have been an order of magnitude greater than the average values shown in Table 6. The consequences of these deposits are not known at this time.

(1) "Low Earth Orbit Battery Development Project", AFAPL-TR-72-60,
C. E. Maiden et al, July 1972, pp. 285-297.

4. DISCUSSION

4.1 Visual Features

4.1.1 Visual Effects on Negative Plates

The only visual effect of concern on the negative plates was the uneven distribution of wetness and corresponding uneven distribution of evidence of activity on many negative plates. This phenomenon indicates that the cell current was flowing through a plate area smaller than the total apparent plate area, and thus the current density in the active areas was higher than necessary. Although no significant affect on electrical characteristics attributable to this phenomenon has been identified, there could be localized areas in these cells where current density is much greater than the average, thus overstressing the plates during overcharge even at rates that are pressured "safe" on a cell-average basis. Thus more attention should be given to assuring that the electrolyte becomes evenly distributed over all the plate area early in life of the cells.

4.1.2 Visual Effects on Positive Plates

The various black features on positive plate surfaces indicated as "normal" in Section 3.1 are the result of the cell manufacturer's interpretation and his method of compliance with his standard Manufacturing Control Document (MCD) which was used for the cells. Although we have been concerned for many years about the possible long-term deleterious effects of these black deposits, we have had no proof that they are a potential problem. Thus, in spite of our reservations we had approved G.E.'s standard MCD which allows certain black features up to certain levels of size, intensity, and frequency.

The features summarized in Table 1 are not covered by existing descriptions and criteria in G.E.'s standard MCD, either because they have not occurred frequently enough to be recognized, or they do not appear at all in plates at the point in their history when they are inspected during cell manufacturing. Because of this, a number of examples of the different features in Table 1 were shown to and reviewed with General Electric representatives.

The latter took the position that all the plates in question were of "aerospace quality" and should not result in cell failure. TRW does not necessarily agree with the assessment of G.E., and hence further testing is called for to attempt to resolve this issue.

Results of plate stress tests to date show that some black spots and deposits of surface hydrates do, under flooded and unsupported conditions, produce lumps, blisters, and plate distortion, and hence may lead to cell shorting. Such effects have not yet been observed in sealed cells (under normal compression), however.

4.1.3 Visual Effects in the Separators

The black deposits seen in the separator, if they prove to contain positive plate material could possibly result in shorting paths if they penetrate the separator. Hence the mechanism of their formation and development bears further investigation. Such an investigation was beyond the scope of this DPA, however.

4.2 Chemical Analysis of Plate Materials

4.2.1 Analysis of Positive Plate

The below-normal values of total nickel active material found in some cells are of no known concern, for, as may be seen by the theoretical positive capacities shown in Table 4, all cells have a significant excess of positive active material over the measured 15 Ah of electrochemical capacity. Also, the fact that the measured capacities of these cells were more uniform than the analysis values suggests that the chemical analysis itself may have introduced some variability in the results for some samples.

The degree of acid attack on the nickel sinter (during impregnation) indicated by the residual nickel shown in Table 4 (20-30 percent) is larger than desirable for highest reliability for long life applications. However, no quantitative relationship has been established between acid attack and plate integrity. It is of interest to note that the weight ratios shown to the far right column of Table 4 correspond to volume ratios in the range of (1 vol. Ni/3.7 vol. NiO_x) to (1 vol. Ni/3.1 vol. NiO_x) based on a bulk density of 4 g/ml for nickel active material.

4.2.2 Analysis of Negative Plate

The data for total cadmium and excess charged cadmium in Table 5 all fall within the normal, expected ranges. The relatively low values for excess charged cadmium in some cells resulted from inadvertent exposure of the negative electrodes to air during processing, whereby cadmium is chemically "discharged" by reaction with oxygen. Excess charged cadmium was not considered a key parameter at the time of these analyses, and so these values were allowed to stand. Note that no flooded electrode capacity measurements were made as part of the DPA reported herein.

4.3 Nickel and Cadmium Content of Separators

From the appearance and analysis of the dark deposits found in the separators of some of the cells inspected (See Section 3.1.4), the deposits were primarily loose negative (cadmium) plate material, but not of the type produced by the usual form of "cadmium migration" produced by cycling. Instead the material appeared to have come off the surface or out of the pores of the negative plates in the form that it exists in new plates, i.e., microcrystalline $\text{Cd}(\text{OH})_2$ mixed with nickel powder. This type of deposit has not been noticed before in other cells with this same prior history. However, in these prior inspections the separators had not been examined as carefully as in the present case. Furthermore, careful inspection of separators from some FLTSATCOM cells recently subjected to DPA has revealed similar spotting. Hence the 777 cells are not unique in this respect.

The consequences of these deposits are not known at this time. The fact that the heaviest deposits are outside the plate stack and hence not between the plates may suggest that they will have no impact on cell reliability. To date, a number of cells from these same lots have been subjected to considerable cycling in ground testing. Additional DPA of some cycled cells may shed more light on this question.

5. CONCLUSION

Although many of the cells inspected from Lots, 1, 2, 5, and 6 showed visual features that were unusual and which were considered generally undesirable, nothing was found that could be said to lead directly to rapid degradation and/or shorting under 777 orbital operating conditions. More valuable information is to be expected from DPA of cells after cycle testing.

TRW
ENGINEERING REPORT
POWER SOURCES ENGINEERING DEPARTMENT

79-8725.6-108

SUBJECT: Results of Destructive Analysis of Shorted
Cell P/N 8E005, S/N 171-L01 (DSCS Program)

PAGE **OF**
DATE: 19 July 1979

BY: W. R. Scott
BLDG. M1 MAIL STA. 1406 EXT. 50776

Abstract

A 12 ampere-hour sealed nickel-cadmium spacecraft cell that had shorted during accelerated testing was subjected to destructive analysis to determine the nature and possible cause of the short. Several unconventional procedures were used during the analysis, including measurement of impedance between individual pairs of plates, and encapsulation and metallographic sectioning of the shorted plates.

The point of the short was indicated by the damage produced by the energy of cell discharge. Sectioning showed that the short actually involved three plates: two positive and one negative plate between. The damage at the point of shorting was so severe that no evidence remained to show the original cause or mechanism of shorting.

WRS:bj

ENGINEERING REPORT

Results of Destructive Analysis of Shorted Cell P/N 8E005, S/N 171-L01 (DSCS Program)

Prepared by: W. R. Scott

Reference: IOC 79-8725.2-129 (DSCS-C3-504), "777 Program, Cell
Characterization and Overcharge Test", C. Lurie to
C. Sollo, 23 May 1979

1. INTRODUCTION

This report describes the results of a destructive analysis of a nickel-cadmium cell that failed by shorting during an electrical test being performed in connection with the 777 Spacecraft 7 and 8 battery anomaly investigation. The test leading to this failure is reported in the reference. The cell in question was a General Electric 12 Ah cell, GE Catalog Number 42B012AB24, TRW Part No. 8E005, Serial Number 171-L01 (i.e., Lot No. 1).

2. APPROACH AND PLAN

An approach different from that normally used with shorted cells was conceived for this cell.* In order to attempt to preserve the structure of the short as much as possible and to characterize the shorting path with respect to involvement of both the positive and negative plates in their original spatial relationship, the plates actually involved in the short per se were not separated from each other, but instead were encapsulated in a resin and cross-sectioned to examine the shorting path. Prior to opening the cell, however, the electrical nature of the short was carefully tested to determine whether the short was truly ohmic or not. The following outline lists the steps by which the overall analysis was carried out:

*A survey of several organizations throughout the country that had dealt with shorted cells indicated that normally all the plates within the cell were physically separated and that the thereby exposed surfaces were inspected to locate and describe the short.

- a) Test cell for I-V characteristics of short.
- b) Cut case walls.
- c) Cut plate tabs and locate individual shorted plates.
- d) Remove plate pack from case constraint and remove non-involved plates from pack.
- e) Encapsulate the plates including the short.
- f) Prepare and characterize a number of cross-sections in the vicinity of and through the location of the shorting path.

3. RESULTS

The following sections describe the methods used for and the findings of the steps listed above.

3.1 Electrical Testing of the Short

The resistance of the short was measured accurately and the nature of this resistance (i.e., ohmic or non-ohmic) was determined as follows: With the large cell faces under constraint (clamped), a precisely measured, variable current was passed through the cell (from terminal to terminal), in each direction, while the resulting terminal voltage was measured. The current was varied from zero to ± 0.4 amperes. The I-V data pairs were then plotted and the slope of the best best line through the data was taken as the resistance. This plot is shown as Figure 1. Note that all of the points fell on a straight line passing through the origin, indicating a true ohmic resistance. Other indicators of an ohmic resistance noted were that the voltage changed immediately to a stable, final value each time the current was changed, and that the voltage immediately dropped to less than 0.0000 volt each time the current source was disconnected. As may be seen from Figure 1, the measured resistance of this cell was $8.0\text{m}\Omega$.

3.2 Cutting the Case Walls

The case walls were cut in three places. Cutting was done using a 6" diamond-tipped cut-off wheel. This type of cutting tool was used because it was felt that it would produce less vibration (likely to disturb the short) than would the steel cutting wheels normally used to cut cell walls.

The three cuts were made all the way around the four sides of the cell at three places: just below the cover plate, one-half inch below the uppermost cut, and just above the cell bottom plate. The bottom was removed, as was the strip of wall material between the two upper cuts; thus revealing the plate tabs. At this point it was seen that the separator material appeared to be missing between the plate tabs for the plates in the center of the plate pack. The resistance of the cell was re-checked at this point and found to be still 8 m Ω and ohmic.

3.3 Cutting of Plate Tabs and Location of Shorted Plates

To facilitate inspection of the tab area and cutting of tabs, the plate pack (and cover) was pushed upward with respect to the remainder of the case by about one inch. Photographs of the open portion of the cell from the four sides are shown in Figures 2 through 5. Note that the separator material is not visible around two of the centermost positive plates on the positive plate tab end (Figure 4) and around four of the centermost positive plates on the negative plate tab end (Figure 5).

While continuously passing 100mA between the cell terminals and measuring the terminal voltage (to monitor the resistance characteristic), the plate tabs were cut through for one plate at a time, starting with the outside plates and working toward the center of the plate pack. Only the negative plate tabs were cut at first. No change in voltage was seen after the tabs of the first six negative plates counting from the side facing the viewer when the positive terminal is toward the left (designated plates N-1 through N-6), were cut. Also no voltage change was seen when the tabs of plate numbers N-12 through N-8 were cut (working inward from the opposite side).

At this point cutting of positive plate tabs was begun. No change was seen after cutting the tabs of the first five positive plates, designated plate numbers P-1 through P-5, and of the first four on the opposite side, designated P-11 through P-8. This was as expected from the results of cutting the negative plate tabs. However, when the P-7 tab was cut, the measured terminal voltage increased by about 50 percent. Finally, when the tab of plate P-6 (the last remaining uncut positive plate) was cut, the circuit was open, as expected. Hence the short appeared to be between plates P-6 and N-7, with some participation by plate P-7. The orientation of the group of plates of interest is shown in the diagram of Figure 6.

This was verified by connecting current and potential leads directly to the tabs of plates P-6 and N-7, whereby a resistance of 12 m Ω was measured. A similar measurement between the tabs of P-7 and N-7 gave unstable voltage readings at 100 mA, with the voltage increasing relatively rapidly but not instantaneously to about 400 mV with current on, and decreasing rapidly to 100 to 200 mV with the current off. Thus this contact was non-ohmic.

3.4 Removal of Plate Pack and Non-Involved Plates

Using a special ram made by cutting a block of bulk teflon to a size that just fit into the inside of the case at the open bottom end, the plate pack was pushed out the top end of the case. During this operation the resistance between plates P-6 and N-7 was monitored, and was found to not change appreciably from 12 m Ω during removal of the plate pack.

While continuing to monitor the resistance between plates P-6 and N-7, the outer plates were separated as follows: Using an electrically-heated knife, the side and bottom edges of all separator bags were cut open. Each successive plate was then carefully lifted, starting at one corner, until free. Separators were found all to be adhering to the adjacent negative plate surfaces. Hence the surfaces of the positive plates were immediately exposed as the negative plates were removed.

No unusual features were seen on the plates during the above process until reaching negative plate N-4, on one side of the shorted plates, and negative plate N-9 on the other side of the shorted plates. Beginning with N-4 and continuing through N-9, separator material was missing from both upper corners of each plate, with the appearance that the separator had been melted or burned away from these areas (see for example Figures 7 and 8). In addition, a round hole was seen in the separator on both faces of negative plates N-6 and N-8. One face of each of these plates is shown in Figures 7 and 8. During separation of negative from positive plates it was noted that separator material was stuck to the adjacent positive plate surface around the perimeter of these round spots. Corresponding burned-looking spots were evident on the exposed faces of positive plates P-6 (Figure 9) and P-7 (Figure 10). It was surmised that the position of these spots was the position of the shorting path.

At this point plates P-6, N-7, and P-7 had not been separated. In view of the inconclusive indication of a short between plates N-7 and P-7, the adherence between these two plates was tested and found to consist only of the sticking of separator material around the "burned" spot, as had been observed between plates P-6 and N-6, and between plates P-7 and N-8. Therefore plate P-7 was removed from plate N-7 leaving plate P-6 attached to plate N-7. The face of plate P-7 that previously had faced plate N-7 is shown in Figure 11. The negative plate (N-7) and separator layer that had faced plate P-7 are shown in Figure 12.

Enlarged views of the "burned" spots on several of these plates are shown in Figures 13 through 17. The pairs of photographs in Figures 13/14, and 15/16 show spots that faced each other in the pack. Note the wide range of morphology and color shown by the affected areas. Analysis of several points within the perimeter of the spot shown in Figure 15 using the Electron Microprobe gave results for nickel, cadmium, cobalt and iron ranging from low (i.e., 1 to 5 percent) to high (i.e., 10 or more percent) depending on just which point was being contacted with the electron beam.

3.5 Encapsulation of Plates P-6 and N-7

The shorted plates P-6 and N-7 were washed free of KOH with distilled water and then dried in a stream of N_2 gas at $50^{\circ}C$. The plate pair was then encapsulated as follows: The plates were placed oriented vertically in a section of lucite tubing 3 inches in inside diameter and 3 inches high. Most of the void space inside the tubing was filled with sections of 1 inch plastic tubing pre-filled and cured with casting resin. A thermocouple was located close to the plate specimen and the remaining void volume was filled with epoxy casting resin (room temperature setting type). The highest temperature recorded by the thermocouple during curing was $130^{\circ}F$.* A photograph of the fixture after curing is shown in Figure 18. After encapsulation in this manner the resistance between the two plates had increased to 30 $m\Omega$. The large cylinder was then cut perpendicular to its axis at two points, one on each side of the "burned" spot. A photograph of the resulting section of the cylinder, looking perpendicular to the

*The details of the above procedure were worked out in advance in a rehearsal run with some non-critical plate samples.

encapsulated plates, and showing the "spot" as seen through the transparent resin, is shown in Figure 19.

3.6 Sectioning of the Shorted Plate Specimen

The encapsulated mounting of plates P-6 and N-7 was ground in a plane normal to the plane of the plates, and this plane was moved in the direction of the center of the "burned" spot. At certain points (described below) the ground surface was polished and the result viewed under the microscope.

The first set of such views was taken at what is designated as Section I. This section was just inside the tangent to the round "burned" spot, and was studied because it intersected a relatively large particle between the plates. Figure 20 is a view looking obliquely at the polished surface, and shows the remainder of the "spot" behind the polished edge of the (upper) negative plate. No separator was visible between these plates at the location of the spot. The particle may be seen toward the right in the dark band between the plates. A metallograph image of the "particle" is shown in Figure 21. This particle and the adjacent positive and negative plate cross-sections were analyzed for nickel, cadmium, and cobalt and certain other elements by the Electron Microprobe. The level of cadmium in the particle was very low, but was also very low in the negative (cadmium) plate adjacent to the particle. Furthermore, the particle contained no cobalt, the negative plate contained no cobalt, and the positive plate contained cobalt as expected (as cobalt is added to the positive plate during impregnation). Thus the particle was judged to have come from the negative plate. Up to this point no gaps had been seen in the negative plate from which such a particle may have come, although such may have been missed due to limited visibility while grinding.

The electrical resistance from point to point within the particle and that between the particle and each of the plates was measured using a low-resistance ohmmeter and microprobe contacts. The resistance within the particle was in the range from 0.2 to 1.5 ohms, while that from the particle to either plate was greater than 1000 ohms, which was the upper limit of the instrument used. Thus this particle was not the cause of the short between the plates.

Continuation of grinding toward the center of the "spot" revealed several other smaller particles between the plates. One of these, located at a point

about 1/4 inch from the center (designated as Section II) is shown in Figure 22. This particle was colored orange-red, and clearly did not contact both plates. No analysis was made at this point.

At the approximate center of the "burned" spot, designated as Section III, considerable damage to the plates was evident, and considerable debris was seen between the plates, but no obvious shorting path was apparent. See Figure 23. Note that the microstructure of the sinter of the negative plate toward the right in this photograph is considerably different from that of normal negative plate sinter seen at the left, and that the sinter of both plates is cracked and pulling away from the substrate (grid) in this area.

Another particle of significant size, but not large enough to contact both plates, was found at a section just past the center of the spot (designated as Section IV). This particle is shown toward the left in Figure 24. A photograph of this section under the metallograph (with a much shallower depth of focus than in Figure 24) is shown in Figure 25. The image in Figure 25 is transposed left to right relative to that in Figure 24. Here the degree of decomposition of the negative plate sinter at this point is more obvious. From these photographs it was concluded that the particle came from the negative plate; however no material analysis was performed.

As grinding continued beyond the center of the "burned" spot, a relatively large particle was encountered which appeared to bridge the gap between the plates (designated Section V). Figures 26 and 27 show two views of this section taken with an ordinary camera, while Figures 28 and 29 were taken with the metallograph (images transposed left to right relative to Figures 26 and 27). The particle does not appear to be as large, compared to the space between the plates, as it does in Figures 26 and 27. This is because only the material in the plane of the section shows in the metallograph, whereas in Figures 26 and 27 one is able to see through the polished surface of the resin and hence to see the bulk of the particle located behind the section plane. Note in Figure 28 the missing piece of the negative plate sinter (center photo).

A set of point-to-point resistance measurements was made on the surface of Section V, as follows:

<u>Point A</u>	<u>Point B</u>	<u>Resistance (ohms)</u>
Positive Plate Sinter	Positive Plate Sinter	0.5-2.5 (range)
Negative Plate Sinter	Negative Plate Sinter	0.1-0.3 (range)
P-6 Sinter	N-7 Sinter	1.1
P-6 Sinter	Particle	1.0
N-7 Sinter	Particle	1.0

Note that the plate to plate resistance measured was 1.1 ohms compared to the 0.03 ohms measured from tab-to-tab before sectioning was begun. This apparent increase is probably due to the relatively high resistance of the microcontacts involved in the measurements.*

The data above show that the resistance between the particle and either plate is the same as that from plate-to-plate. Hence the particle must be in electrical contact with one or both plates. It could not be said at this point that this particle was contacting both plates, because the combination of (1) this particle's contacting one plate only, and (2) the presence of another (as yet undetected) low-resistance short would produce the results in the table above.

Section V was further characterized by Electron Microprobe analysis. Figures 30 and 31 are scanning EMP intensity images for nickel and cadmium of the particle and its immediate surroundings. The shape and topography of the particle in Figure 30 are seen to correspond to those in Figure 31. The strong response for nickel is from the nickel sinter. The dark spots are voids or inclusions of non-nickel material. The bright band at the bottom of Figure 30 is the positive (nickel) plate.

The cadmium intensity image in Figure 31 shows that cadmium existed in the particle area only in a few spots. Comparison of these spots with Figure 29 shows

*The instrument used was equipped with separate current and potential leads out to near the tips of the probes. Current and potential paths were then merged into a single probe for each polarity. Hence test current flowed through the contacts across which the voltage was measured.

these spots were inclusions of material (black-appearing in Figure 29) that are not the same as the material of the particle as a whole. This "black" material (Figure 29) is cadmium hydroxide that had crystallized on the surface of the negative plate during electrical cycling of the cell before failure. Thus no significant indigenous cadmium was found in this particle. Similarly, the cobalt intensity image (not shown) revealed no significant cobalt concentration in the particle. The low level of cobalt detected in the positive plate was unexpected. It was subsequently discovered that the EMP instrument was not functioning properly during the preparation of the cobalt image, and hence these cobalt data are questionable.

Analysis by EMP line scan proved to be more productive. Simultaneous scans for (a) cadmium and cobalt and (b) nickel and cadmium were made in a direction, normal to the plane of the plates and through the particle cross-section. As shown in Figures 32 and 33, nickel content was high in all sintered material scanned; cadmium content was very low in all sintered material (including that portion of the negative plate scanned); and cobalt content was relatively high in positive plate sinter but negligible in the particle. The peaks of cadmium intensity seen correspond to the location of pre-formed cadmium hydroxide crystals and not to high concentrations of cadmium in the sinter matrix. This information indicates that the particle came from the negative (cadmium) plate.

After the above-described characterization of Section V, grinding and polishing was continued to examine the bridging particle further. This process culminated in the final section, designated Section VI, at which point the two plates were no longer shorted. The specimen was then ground at 90° to the previous section until particle was intersected by the new section. Metallographs at the corner of intersection are shown in Figures 34 and 35. The physical analysis was concluded at this point.

4. DISCUSSION

The evidence presented above clearly shows that the particle found between the two plates of the specimen at metallographic Section V (and VI) was producing a short between plates P-6 and N-7, and that this shorting path was the main source of the shorted condition of the cell at the time it was opened for analysis. However, there was also some degree of shorting initially present between plates N-7 and P-7.

A review of all the microphotographs taken during the sectioning of encapsulated plates P-6 and N-7 shows no evidence that a large current (such as must have flowed when the cell first discharged after shorting) had flowed from negative plate N-7 to positive plate P-6, as no damage to the surface of P-6 closest to N-7 was seen such as might be caused by the shorting current. It is particularly noted that none of the particles seen between plates P-6 and N-7 appear to have been the path of a large current, inasmuch as the points of contact between these particles and the plates show none of the effects to be expected (e.g., structural damage, fusion, etc.) from the high temperature generated by I^2R heat dissipation.

On the other hand the larger particles appear to have broken off of the sintered surface of negative plate N-7 and became wedged between the two plates sectioned together. It is postulated that the particles broke off because of stresses produced by high temperature in the negative plate. The cause of this high temperature was the initial discharge current of the charged cell, but the discharge path was not to plate P-6.

Note in Figures 20, 22, 23, and 24 that there is a lump of material near the center of "burned" spot and on the face of plate N-7 opposite from plate P-6. The thickness of this buildup is about equal to the separation distance between plates in the original cell. Note further from the photographs in Figures 15 and 16 that considerable structural damage has occurred to positive plate P-7 in the "burned" spot, especially near the center. From these observations it is deduced that the original short occurred between plates N-7 and P-7, and not between plates N-7 and P-6. The high local temperatures produced by the rapid discharge through this original short then produced the variety of secondary effects observed during this analysis, including the ejection of negative plate sinter particles from the face of negative plate N-7 opposite from that involved in the original shorting path.

The intense heat of the rapid discharge left the original discharge path structurally weak and with a high resistance compared to the resistance of a piece of relatively undamaged negative plate sinter such as was found wedged between plates N-7 and P-6. Thus the investigation became diverted to uncover the source of the latter, low-resistance path. The energy involved in the original discharge also obliterated any evidence that might have indicated what the underlying cause was for the short and its development mechanism.

After the sectioning of the encapsulated plates (described above) had been completed and the above conclusions drawn, the burned spots on the two faces of plate P-7 was re-photographed at higher magnification than before. The results are shown in Figures 36 and 37. It may be seen that some of the sinter was missing from the center of the spot at the time these photographs were taken. The missing material was very fragile and disintegrated during storage. The surface of the grid thereby revealed on Face 1 of this plate shows many tiny pits. This condition suggests that the affected area had been subjected to a high current density, and explains why iron was found throughout the "burned" areas on the plates close to the short. These observations are consistent with the postulation that the primary short occurred between plates P-7 and N-7.

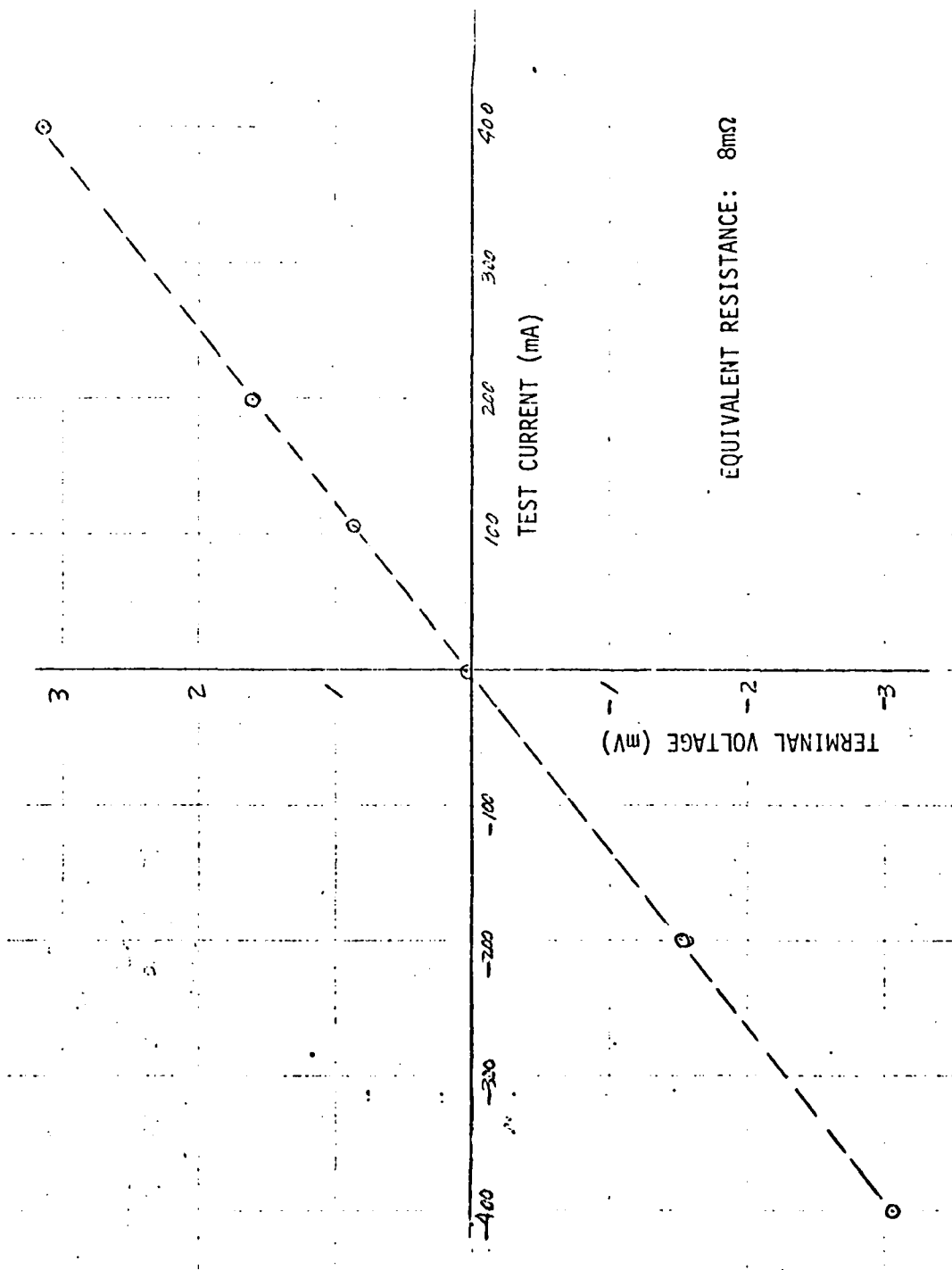


Figure 1. Current voltage plot for cell resistance of shorted cell, 8E005, S/N 171-L01.



Figure 2. Front view of cell with plates partially withdrawn
(TRW 153392-79)



Figure 3. Rear view of cell with plates partially withdrawn
(TRW 153391-79)



Figure 4. Positive terminal end view of cell
(TRW 153394-79)

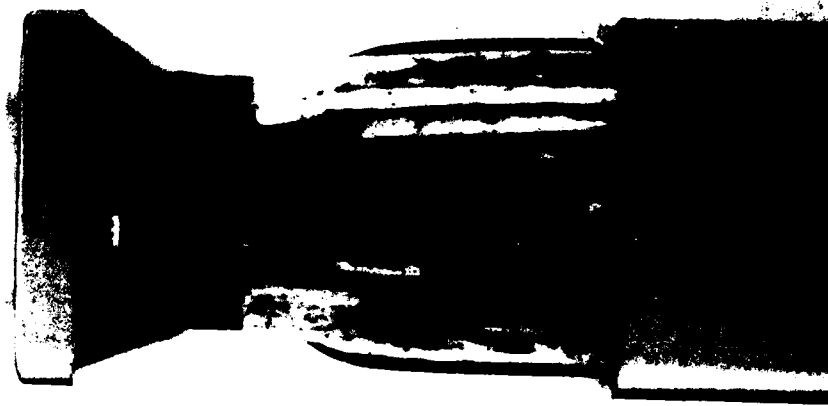


Figure 5. Negative terminal end view of cell
(TRW 153393-79).

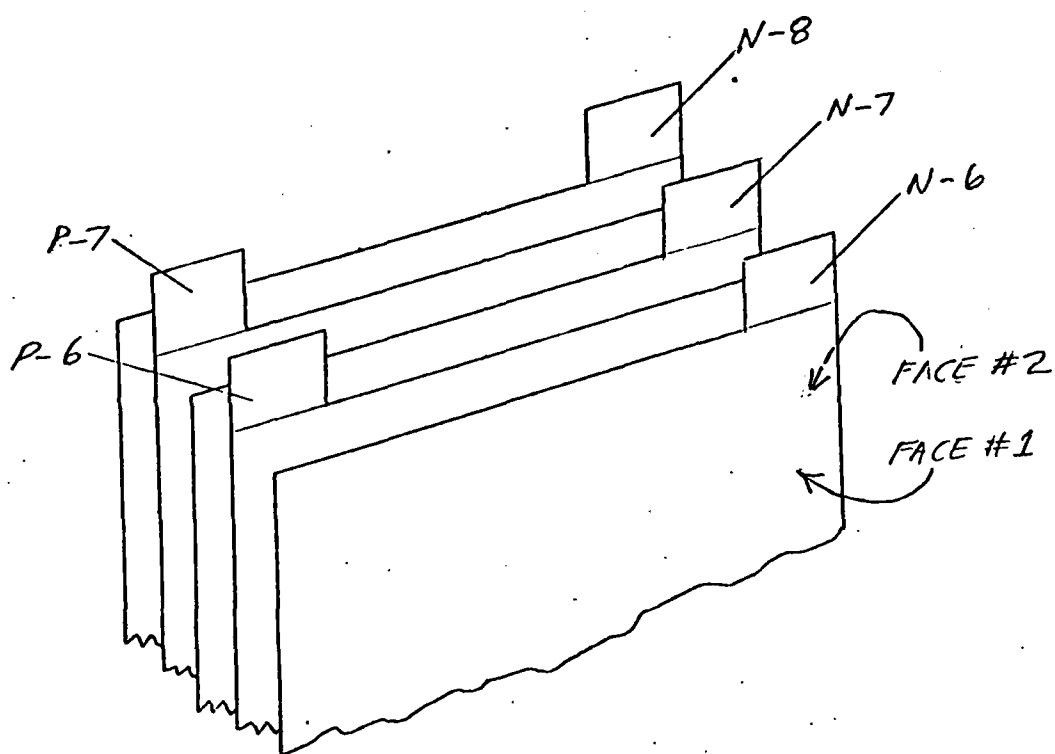


Figure 6. Designation and orientation of plates near center of pack.

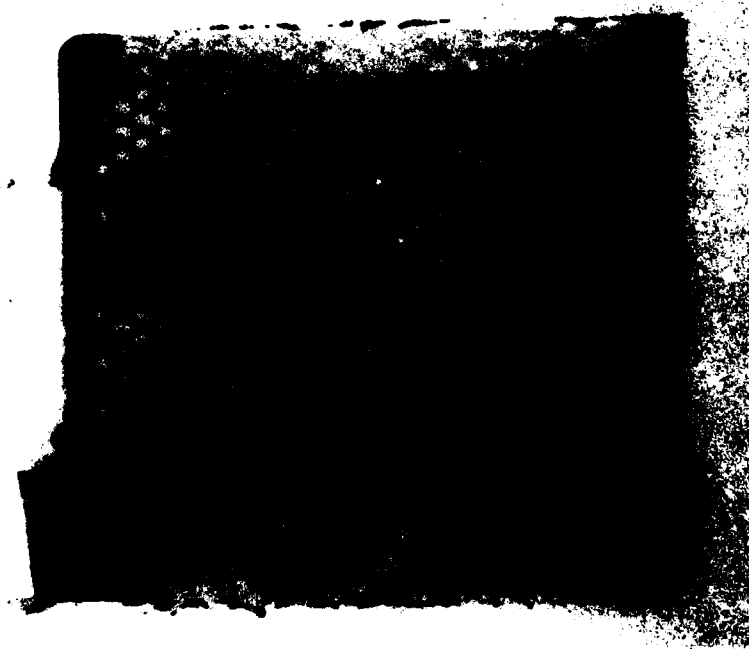


Figure 7. Negative plate No. N-6, face No. 2,
with separator. (TRW 153484-79)

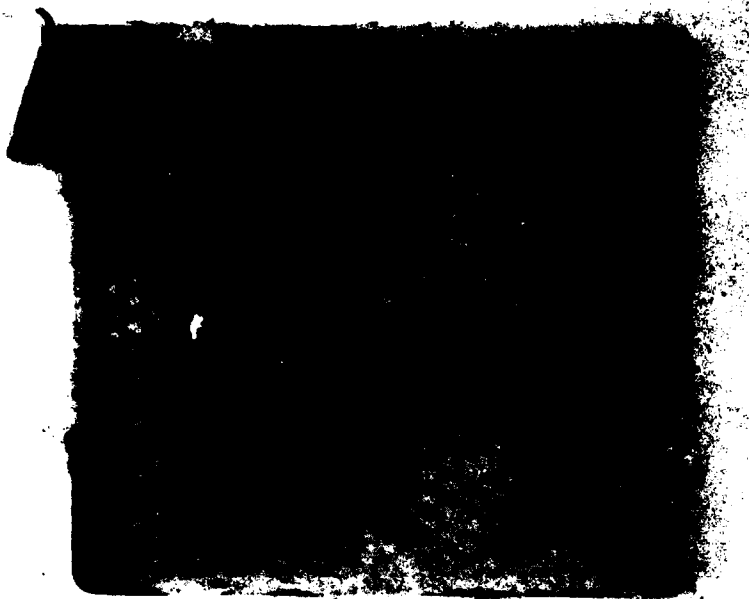


Figure 8. Negative plate No. N-8, face No. 1,
with separator. (TRW 153478-79)

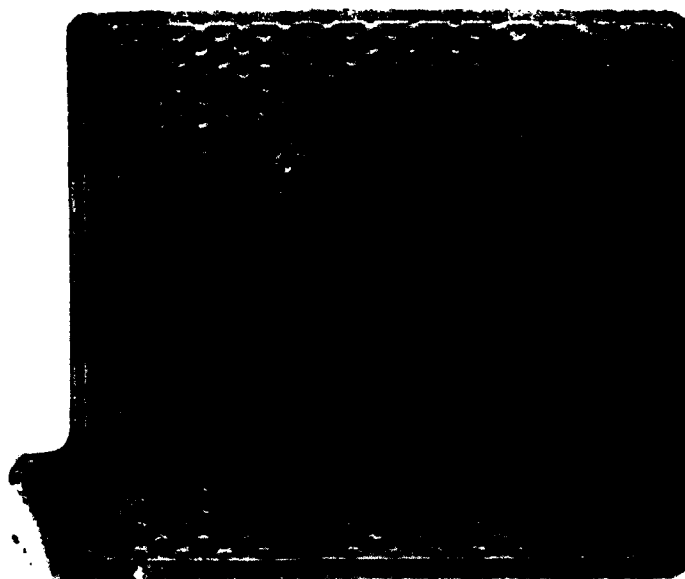


Figure 10. Positive plate No. P-7, face No. 1
(TRW 153481-79).

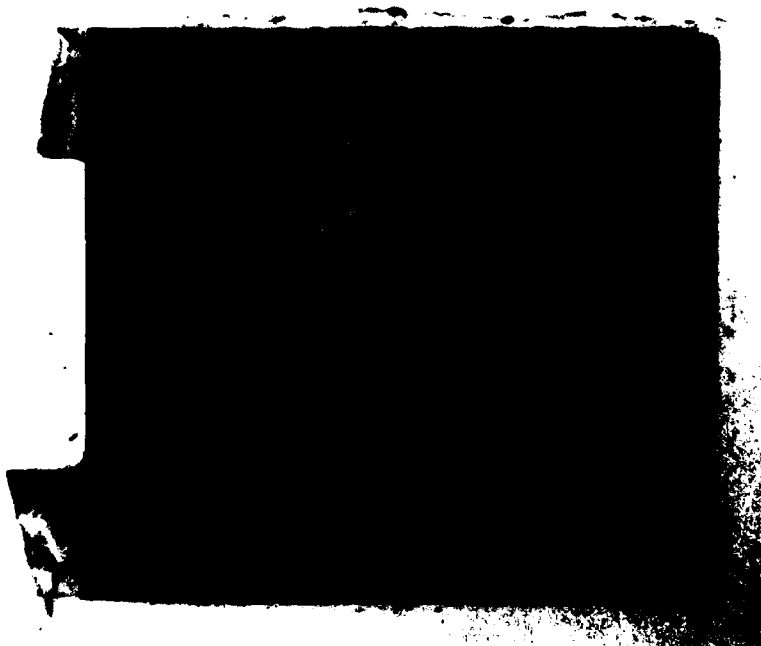


Figure 9. Positive plate No. P-6, face No. 1
(TRW 153480-79).

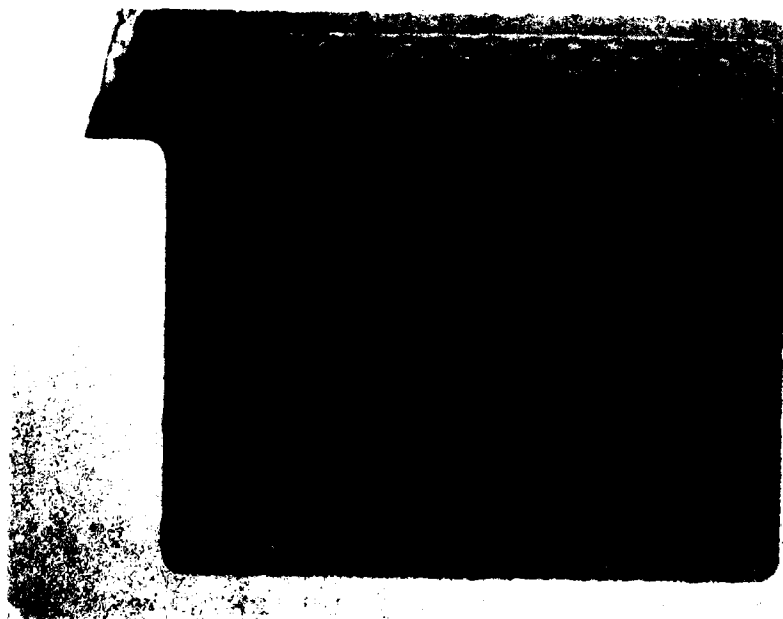


Figure 11. Positive Plate No. P-7, Face No. 2
(TRW 153479-79).

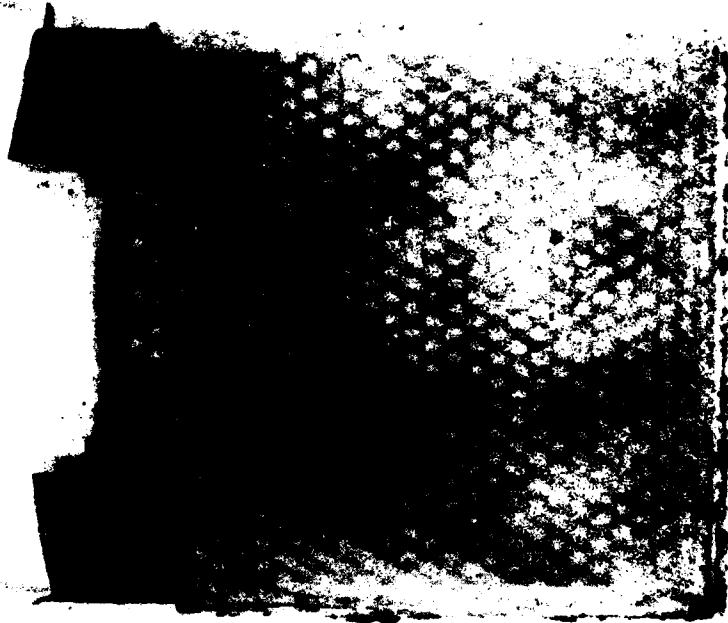


Figure 12. Negative Plate No. N-7, Face No. 2,
with separator (TRW 153483-79).

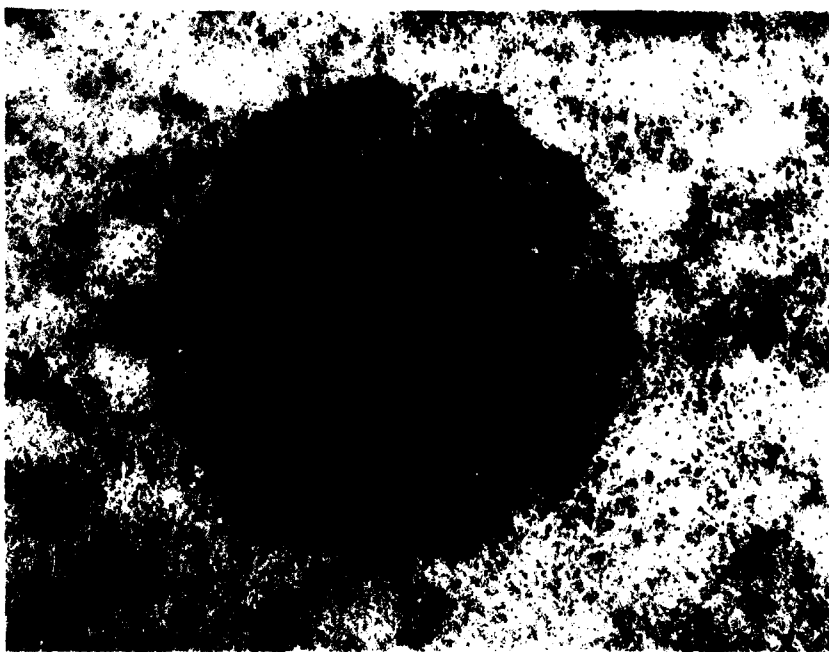


Figure 13. Close-up of spot on negative plate,
No. N-6, face No. 2 (TRW 153476-79)

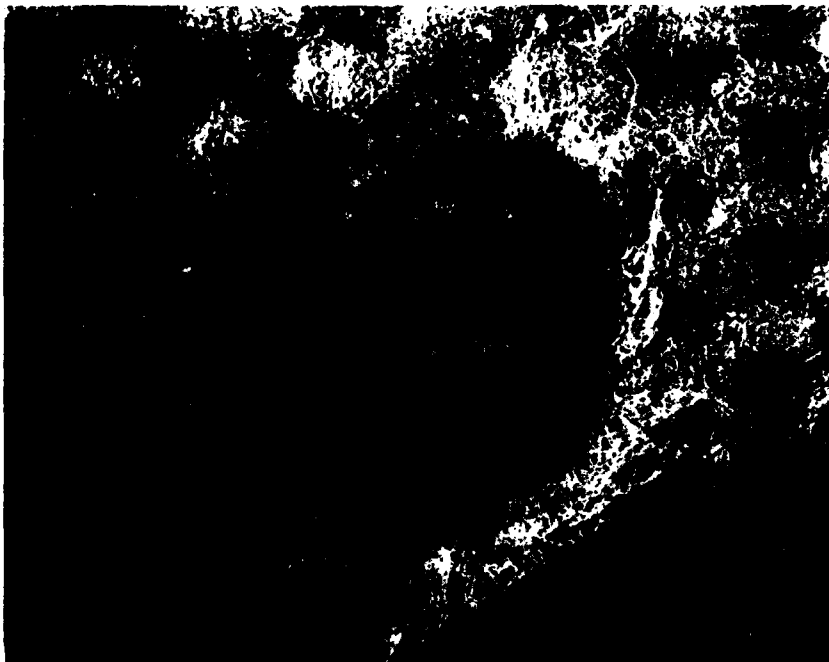


Figure 14. Close-up of spot on positive plate
No. P-6, face No. 1 (TRW 153474-79).



Figure 15. Close-up of spot on positive plate
No. P-7, face No. 2 (TRW 153473-79)

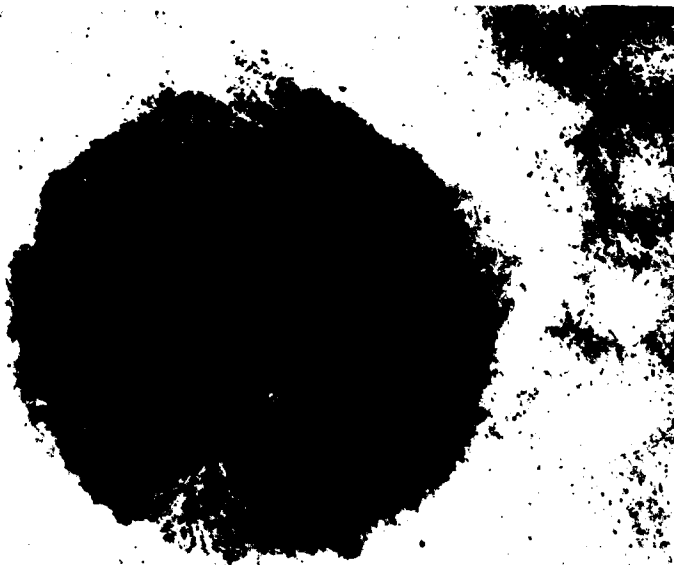


Figure 16. Close-up of spot on negative plate
No. H-8, face No. 1 (TRW 153472-79)

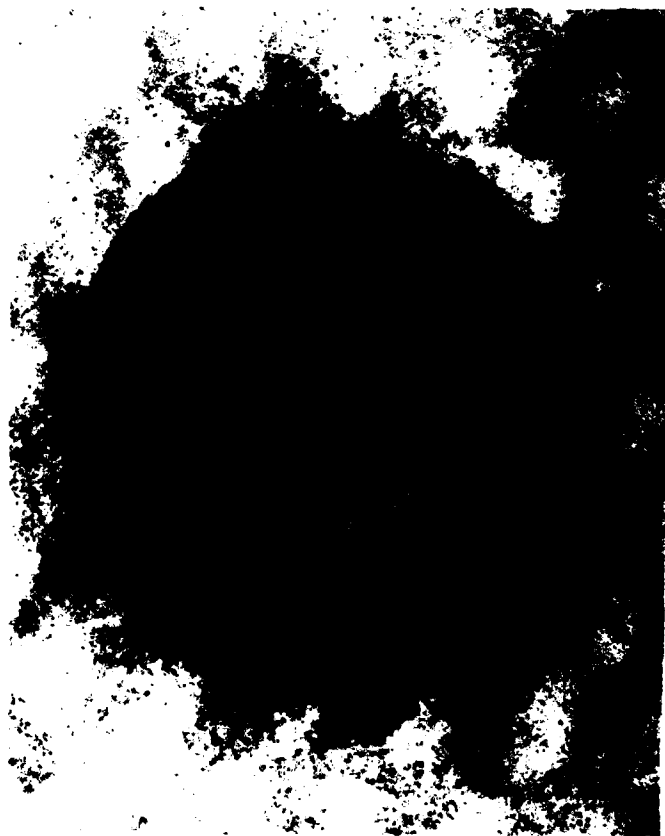


Figure 17, Close-up of spot on negative plate No. N-7, face No. 2 (TRW 153475-79).

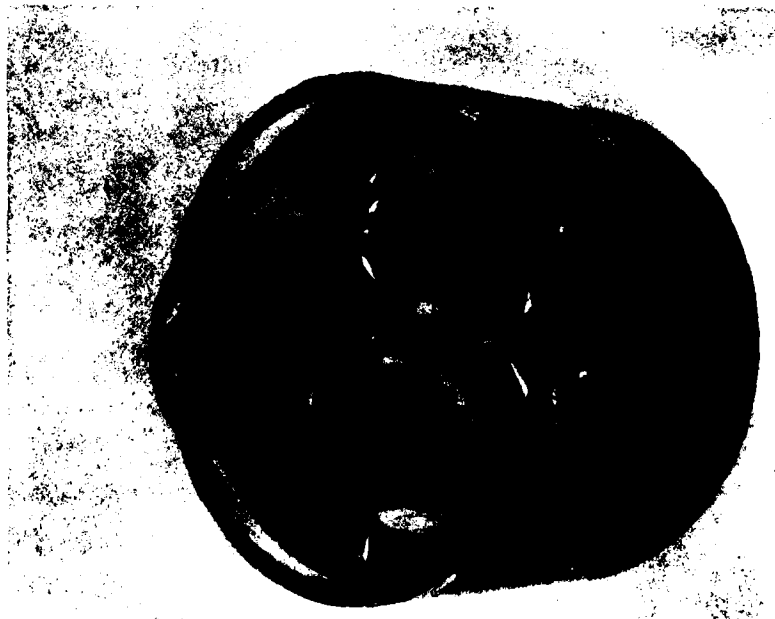


Figure 18. Plates P-6 and N-7 encapsulated in epoxy resin.

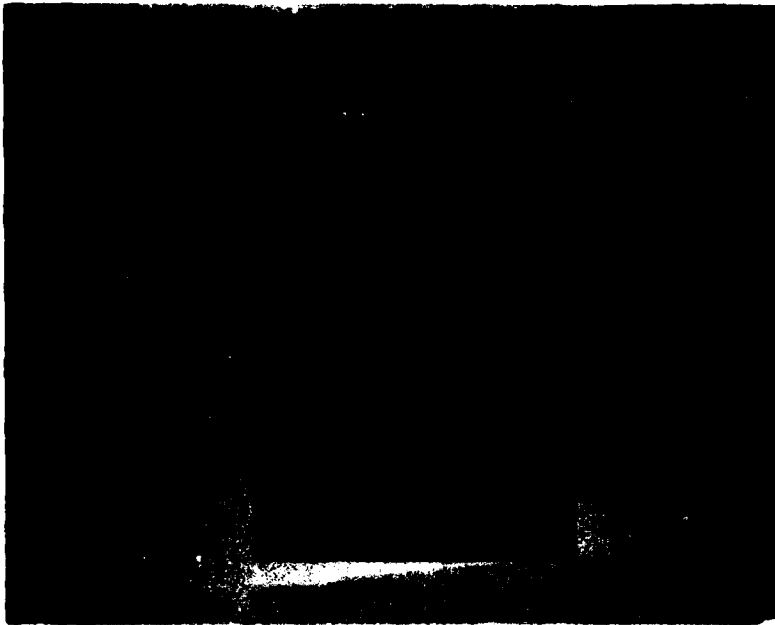


Figure 19. Encapsulated plates after rough cutting.

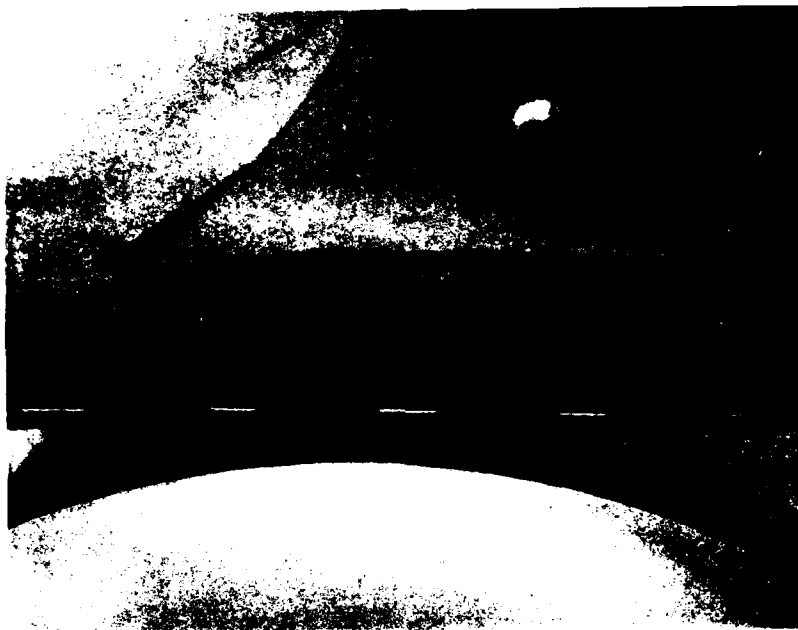


Figure 20. Oblique view of Section I, 8x



Figure 21. Metallograph of particle between plates at Section I, 80x



Figure 22. View of Section II, 20x



Figure 23. View of Section III, 20x

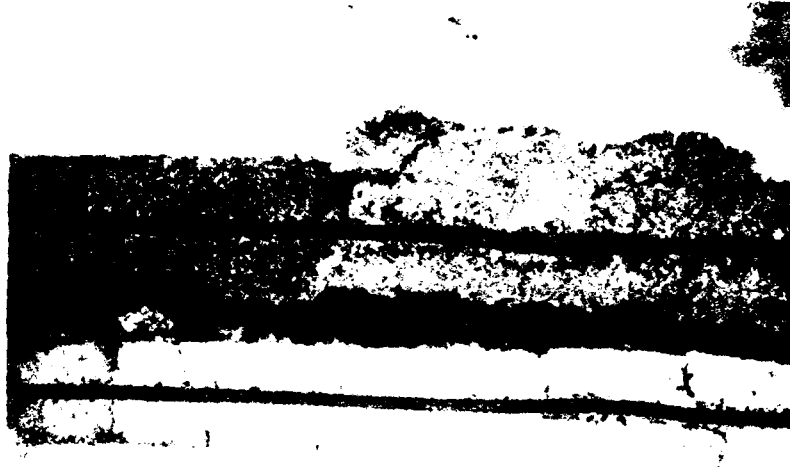


Figure 24. View of Section IV, 20x

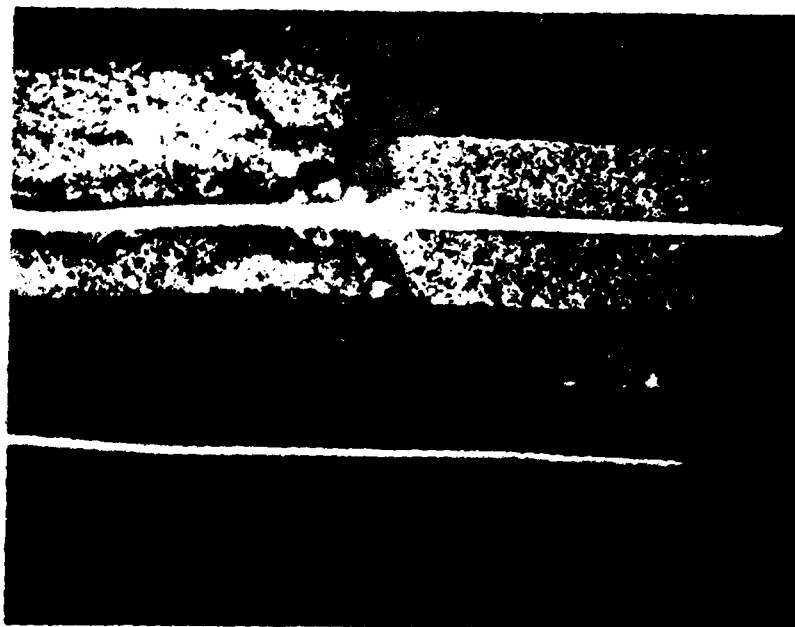


Figure 25. Metallograph of Section IV, 30x



= Figure 26. View of Section V, 12x

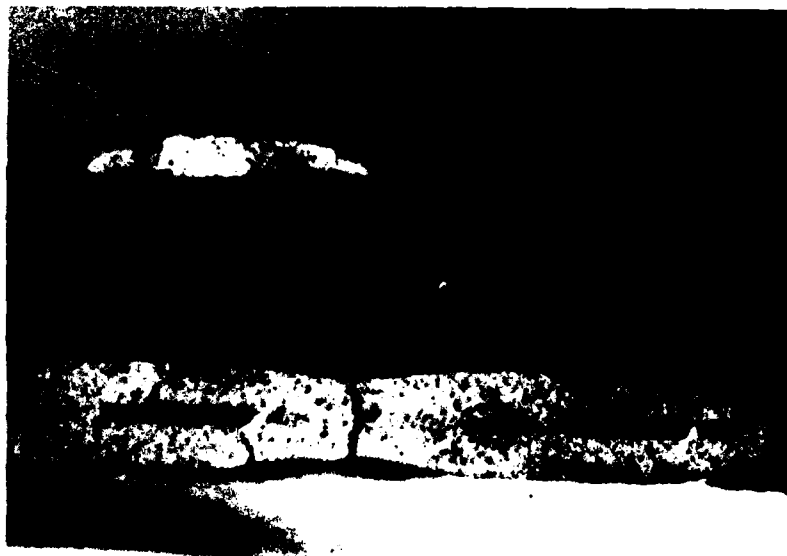


Figure 27. View of Section V, 20x

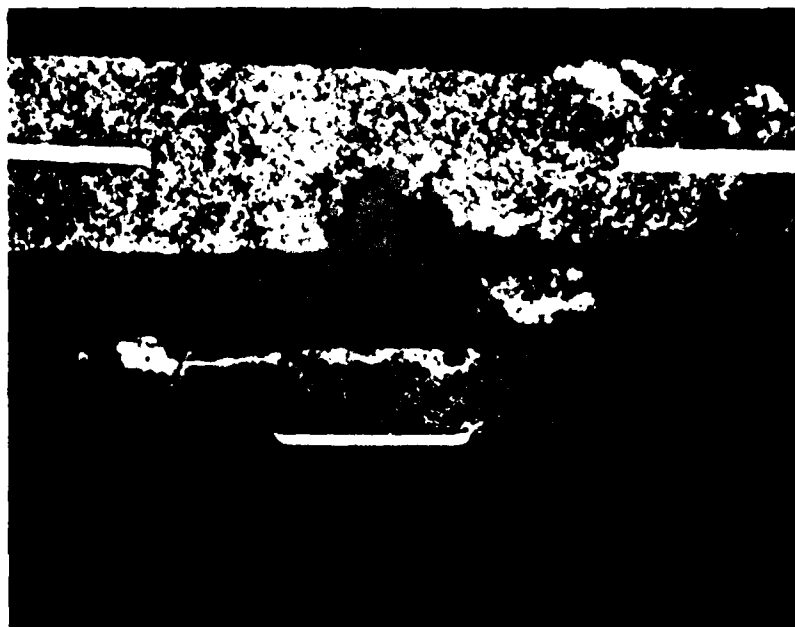


Figure 28. Metallograph of Section V, 35x



Figure 29. Metallograph of Section V, 100x

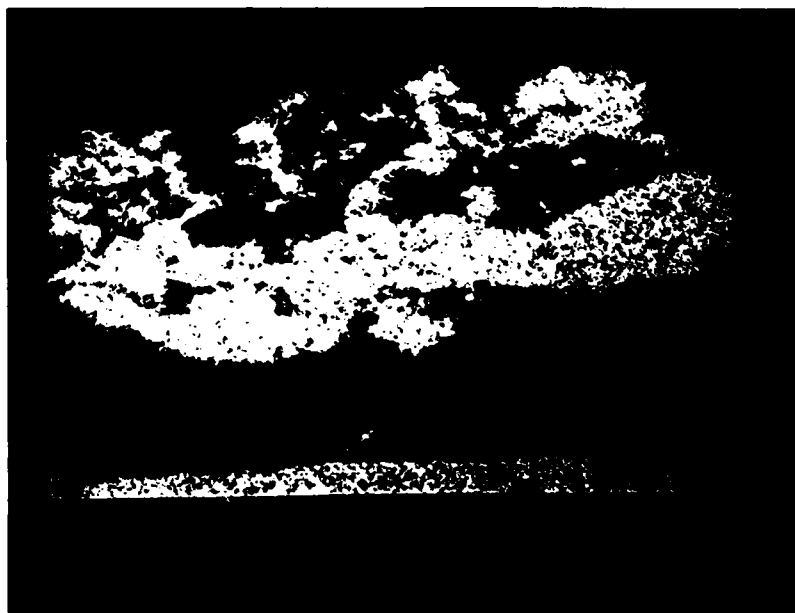


Figure 30. Scanning EMP Intensity Image for nickel: particle at Section V.

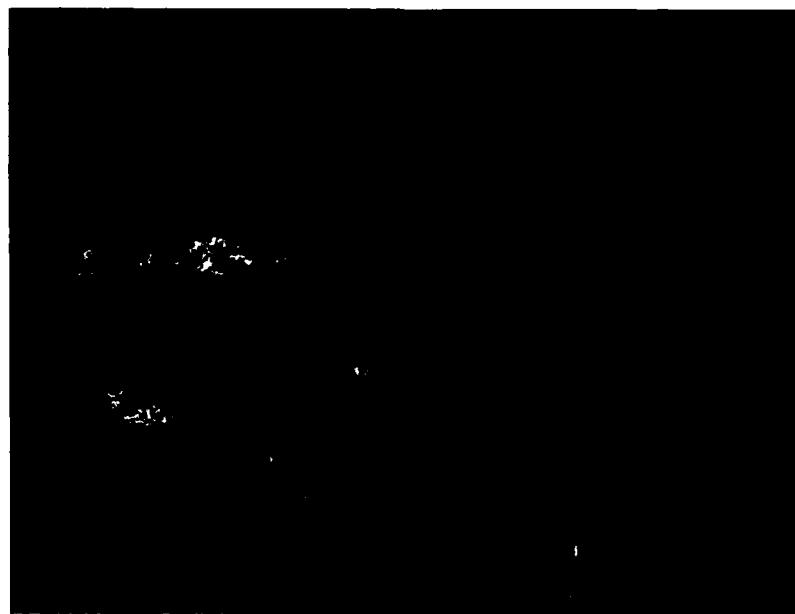


Figure 31. Scanning EMP Intensity Image for cadmium: particle at Section V.

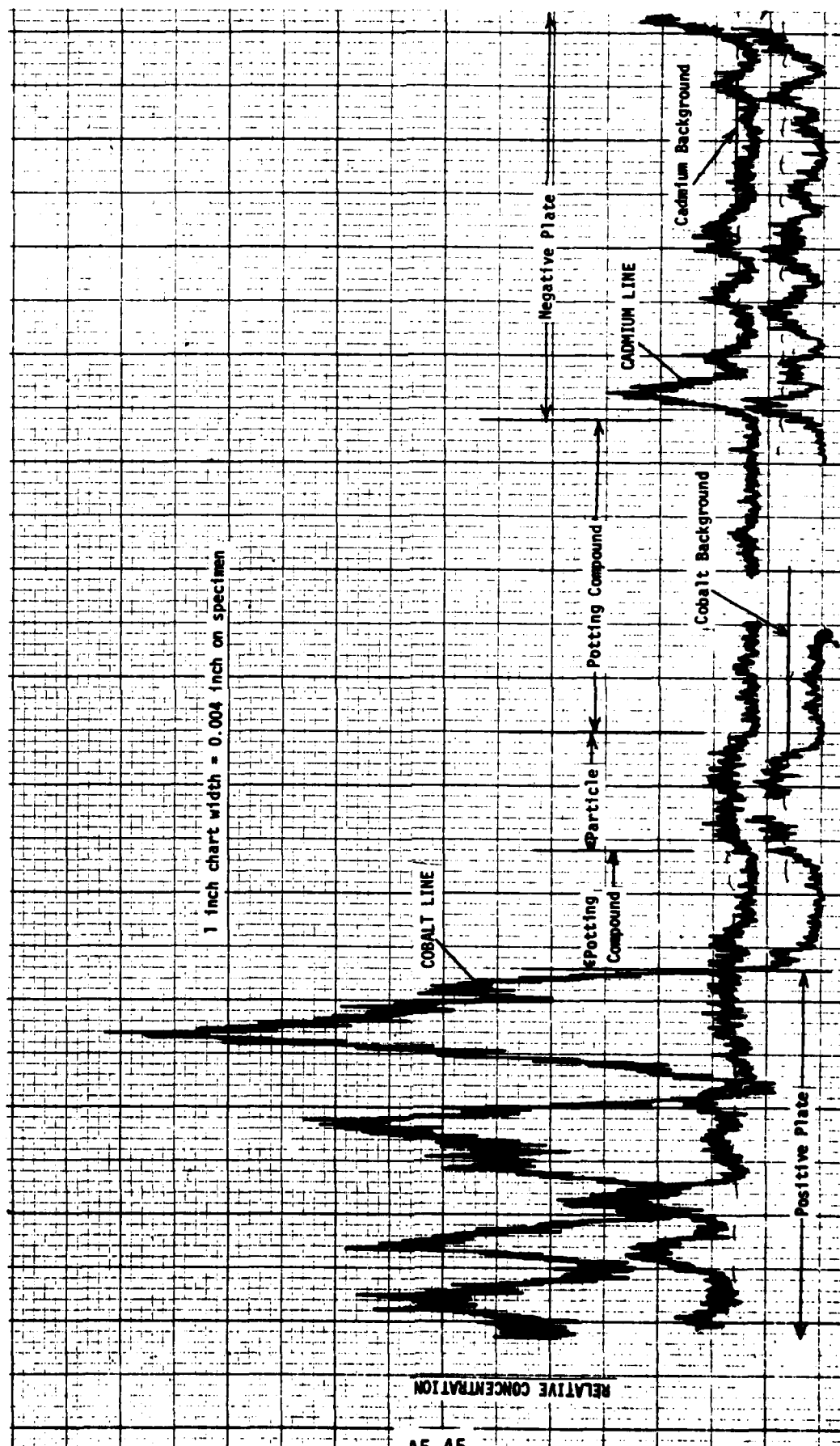


Figure 32. EMP line scan analysis for cadmium and cobalt. Section V, across the particle

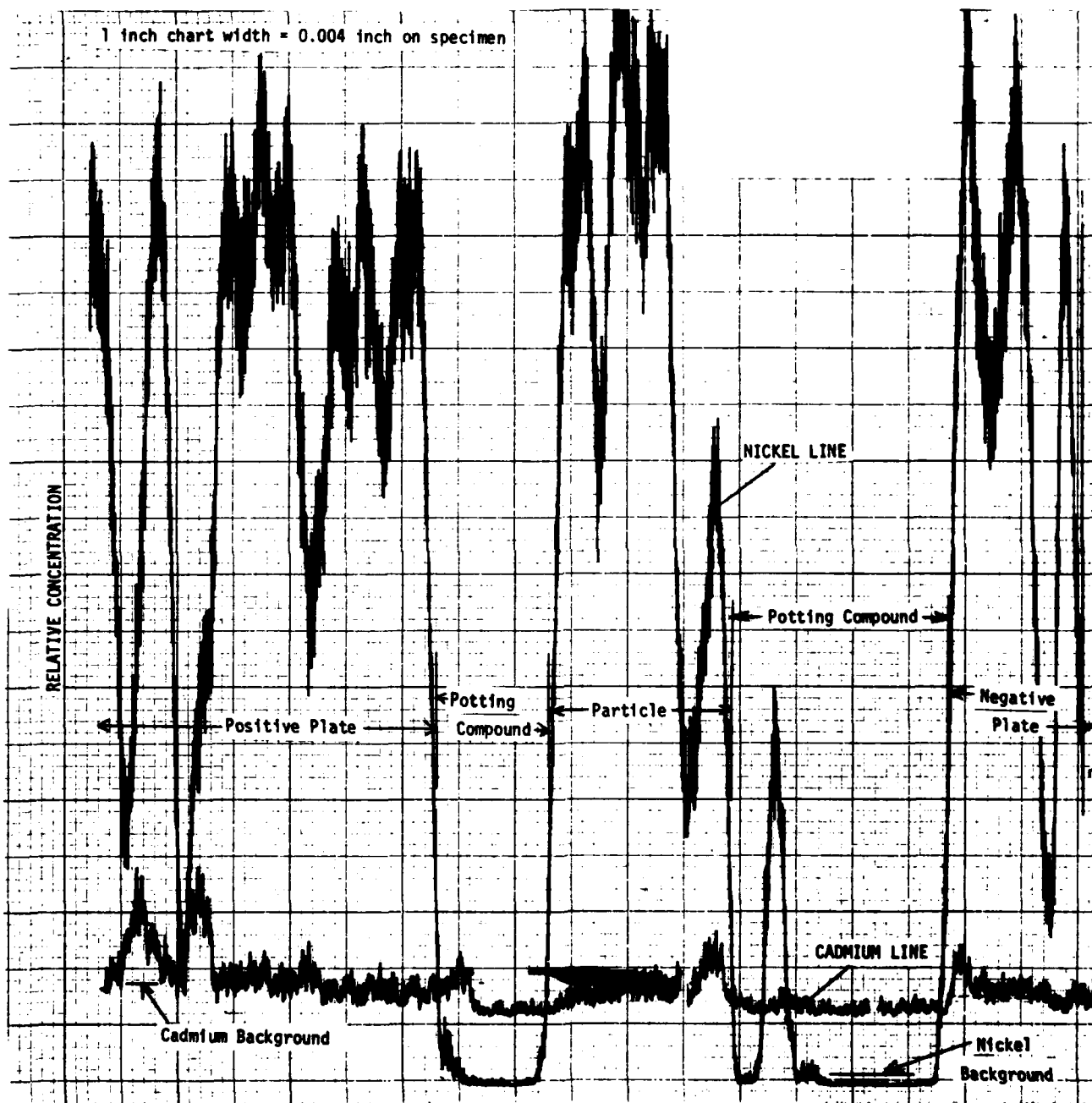


Figure 33 EMP line scan analysis for cadmium and nickel, Section V, across the particle

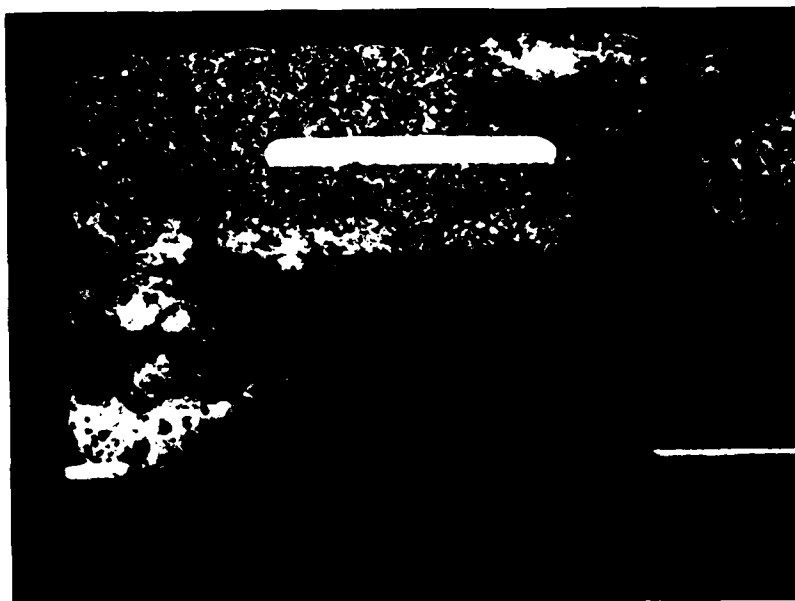


Figure 34. Metallograph at location of particle in Section VI. (40x)

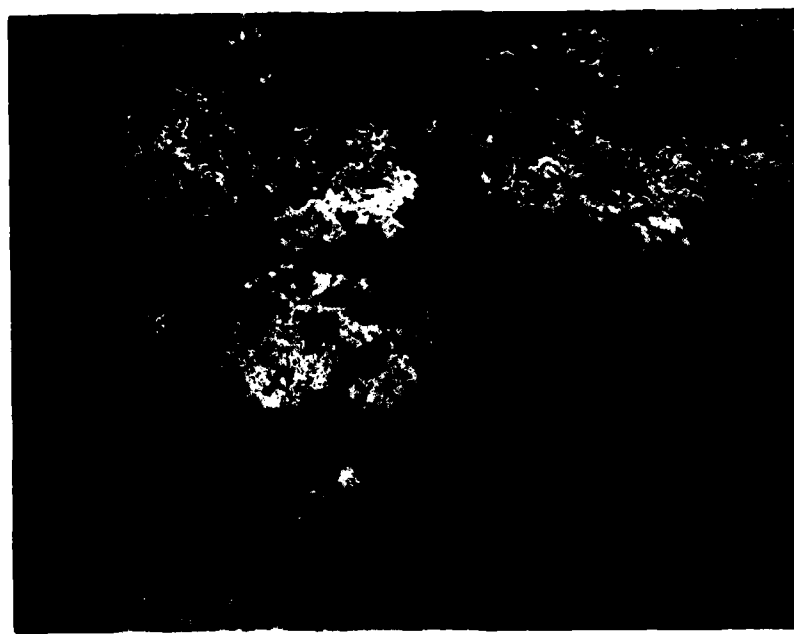


Figure 35. Metallograph at location of particle, Section VI, 100x.

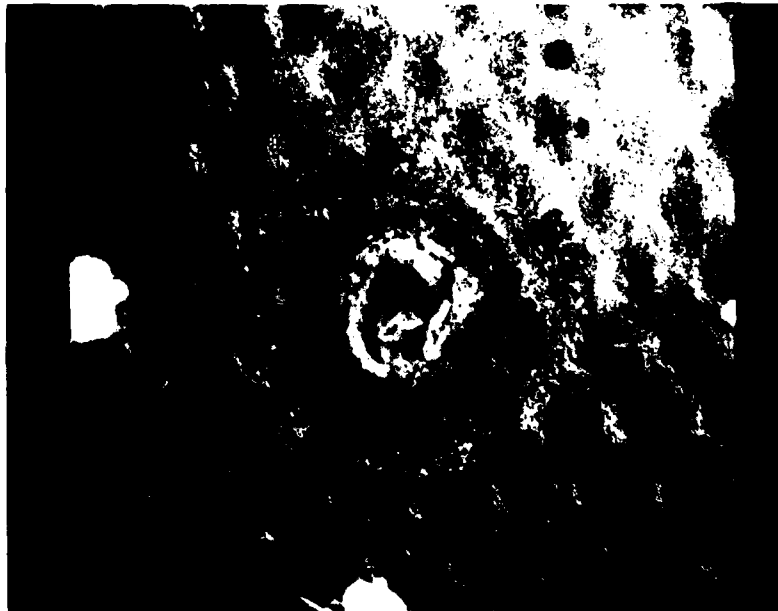


Figure 36. Burned spot on positive plate P-7, face 1, after storage.



Figure 37. Burned spot on positive plate P-7, face 2, after storage.

APPENDIX 6

SSTS FAILURE MODES AND EFFECTS ANALYSIS



INTEROFFICE CORRESPONDENCE

TO: R. Sparks

CC: Distribution

78-8723.0-054
DATE: 13 October 1978

SUBJECT: Failure Modes and Effects Analysis
on 777 SSTS

FROM: D. W. Zerbel
BLOG M2 MAIL STA. 2145 EXT 50606

Reference: 1, IOC 78-8725.0.217, "Failure Modes and Effects Analysis of Program 777 Solid State Temperature Switch (SSTS) Circuit, dated 21 September 1978 by J. E. Brooks to R. W. Sparks.

Background

On September 4, 1978, Battery 3 of S/C 9438 was observed to be in mini-trickle charge. A possible cause of this high temperature excursion may have been a failure of the SSTS to switch at or near its nominal set point of 77°F. Again on September 21 during a recharge after reconditioning, this battery was observed to reach 98°F even though the over-temperature switch did not switch the battery to mini-trickle. On September 22 battery 2 on S/C 9437 was observed to be in mini-trickle charge. In none of the above cases was data available during the transition to the high temperature, so the exact switch point of the SSTS is unknown. In the two cases where the 95° switch actuated, it cannot even be determined if the SSTS operated at all since the 95° switch also switches K1 to trickle charge.

Data gathered during the 48 hour continuous pass on 9438 and the 24 hour pass on 9437 is summarized in Table I. Also plotted in Figure 1 is the switch point data for battery 3 on 9438 versus the rate of change at the time of switching of battery temperature as measured by the telemetry thermistor. This plot suggests some possible correlation of switch point with rate of change of temperature which in turn suggests that the thermistor might not be tracking shim temperature. On cool down the suspect switches all switch within tolerance of their 70°F reset point. The possibility of the two thermistors (RT1 for telemetry and RT2 for the SSTS) not tracking each other has also been checked and what little temperature differential there is, as predicted by analysis, is in the wrong direction to explain the observed behavior.

In summary, then, what we are looking for in this analysis is an electronic part failure or drift in the SSTS that could cause the set point to drift approximately 8°F high (corresponding to a ΔR in the thermistor value of 313 ohms) and also allow the reset point to remain at its nominal value.

Analysis

This analysis is an expansion upon Ref. 1 with emphasis on those components that showed some promise of explaining the anomaly. In addition, breadboard testing was used to verify the analysis.

As seen from Reference 1 and Figure 3, the best candidates are:

- o VR3 - operates at wrong point
- o VR2 - short
- o C1 - open

The second and third candidates can be disposed of quickly:

- o By analysis and by test a shorted VR2 moves the set point up to 1643 ohms (86°F) however, there is no hysteresis and the switch would continuously toggle about this point.
- o By analysis and by test, with C1 open, the output tends to switch at a lower temperature if noise is also present. Without noise, the circuit operation is unaffected.

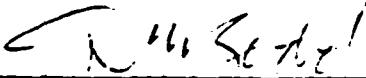
Operation of VR3 (Reference Figure 2) with various modes of degradation and the resulting effect on set point is tabulated in Table II. As can be seen, none of these modes can result in the observed orbital operation.

Conclusion

Reference 1 ruled out most catastrophic failures of parts as being the cause and this analysis has ruled out the rest as well as ruling out more subtle variations of VR3.

Another postulated failure mode that fits the observed data is that RT2 is lagging the shim temperature as a function of the rate of change of temperature. The mechanical mounting of RT2 to the shim has been investigated and it seems to be adequate and not suspect. The thermal characteristics of RT2 have been investigated by components with no evidence of a problem.

Further investigation is recommended on the relative temperature distributions on the battery under various cell failure modes (i.e., is there any way that RT1 and S6 could actually be 7-10° higher on charge than RT2). More orbital data would also be helpful.



D. W. Zerbel, Manager
Power Control & Distribution Dept.

DWZ:ch

Attachments

TABLE I

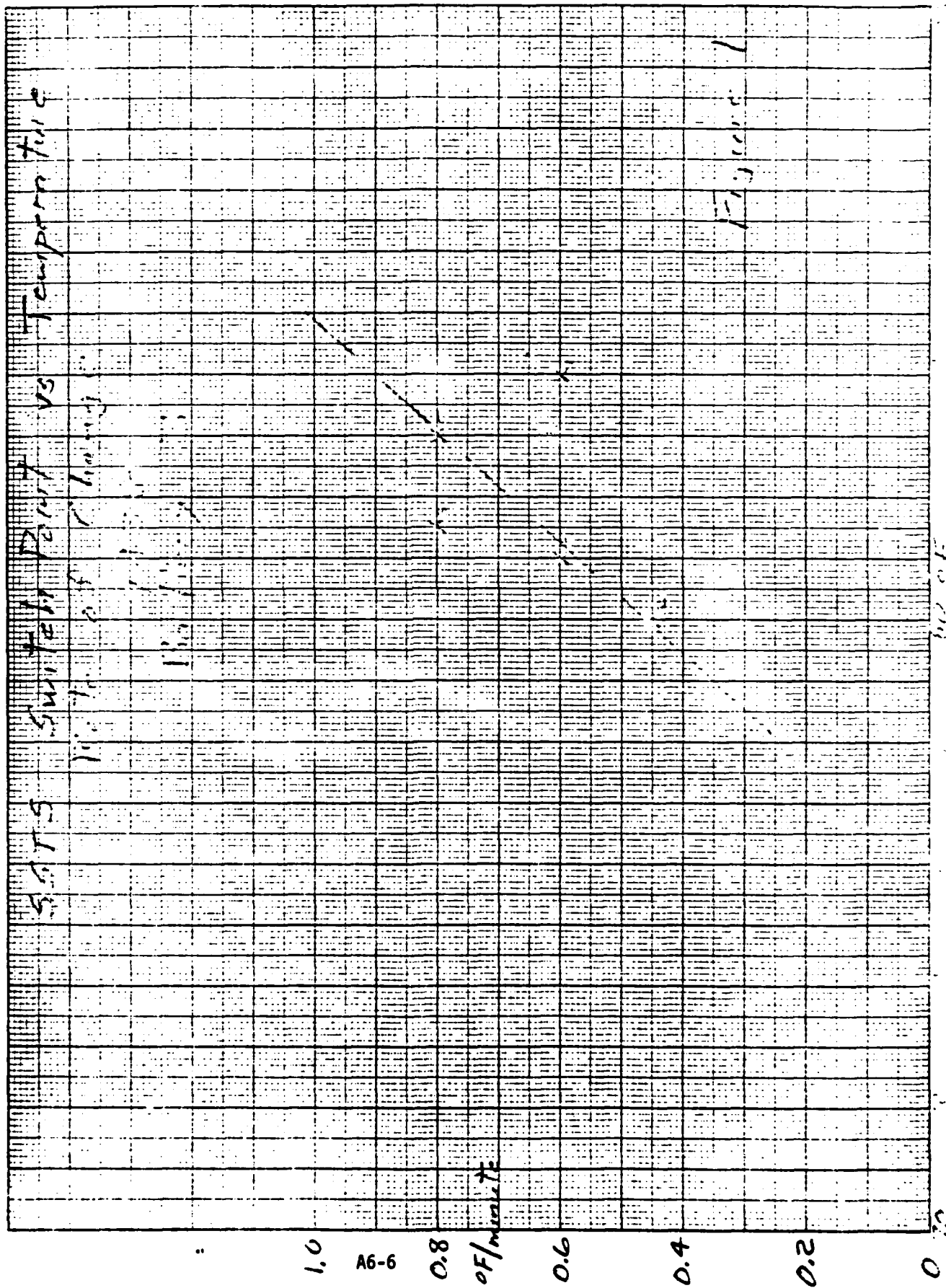
Battery \ Cycle	1	2	3	4	5
9437					
1	80°F	80°F	80°F	78°F	--
2	77	79	79	78	--
3	81	80	80	--	--
9438					
1	78	78	78	78.5	78
2	79	80	79	79	78
3	84	80	81.5	81	83

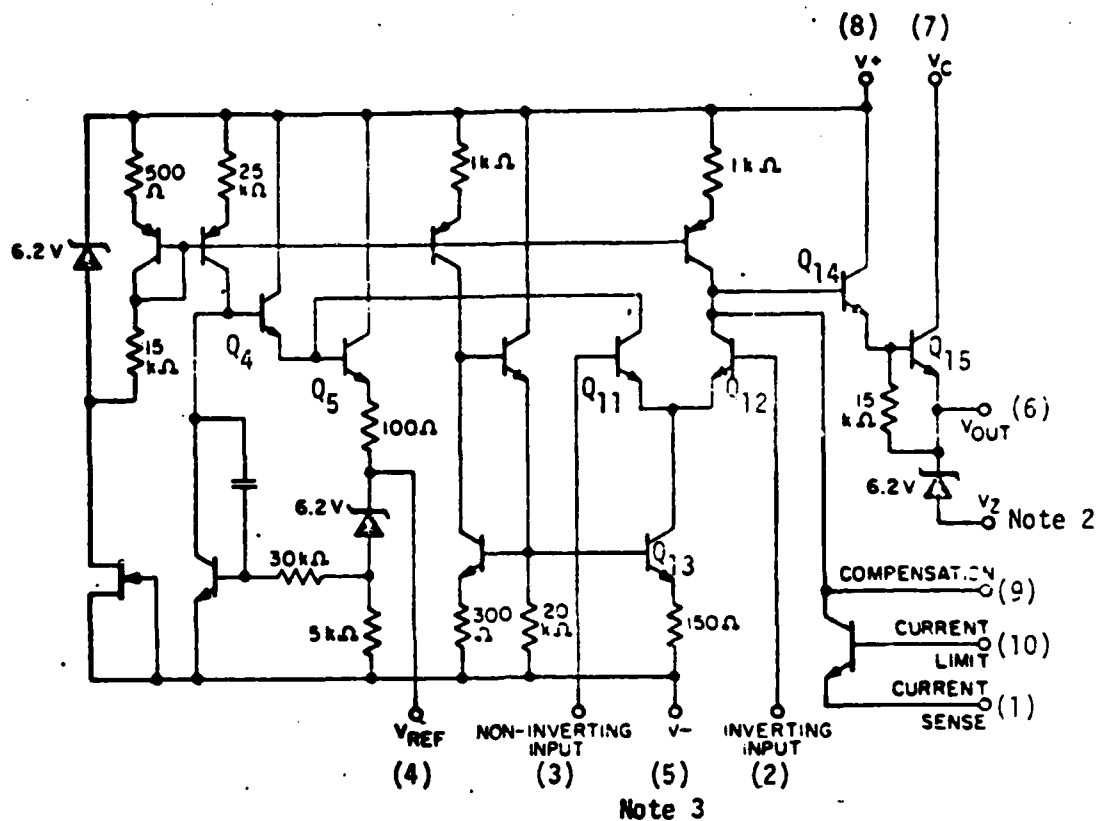
SSTS Switch Points Observed during Continuous Passes

TABLE II
Circuit Operation with Degraded VR3

<u>Degradation</u>	<u>Effect on SSTS Operation</u>
Lowered gain, both Q11 & Q12	Raised set point; lowered reset point
Increased leakage, Q11 & Q12	Raised set point; lowered reset point
Lowered gain Q11 or increased leakage Q12	Raised set point and reset point
Lowered gain Q12 or increased leakage of Q11	Lowered set point and reset point

K-E 10 X 10 TO 1/4 INCH 46 1473
 7/16 X 10 INCHES
 MADE IN U.S.A.
 NEUFEL & ESSER CO.





- NOTES:
1. All resistance and capacitance values are nominal.
 2. V_Z is not connected in the 10-lead round can.
 3. Pin 5 is connected to case.
 4. Numbers in parentheses are lead numbers.
 5. This schematic is for reference only.

FIGURE 2. SCHEMATIC DIAGRAM

SIZE	CODE IDENT NO.		REV.
A	11932	1H021	H
SCALE		SHEET 20	



Figure 3

Reference 1
78-8723.0-054

INTEROFFICE CORRESPONDENCE

78-8725.0.217

TO R. W. Sparks

CC: T.F. Castle
C.L. Stanley
C.E. Tock
B.W. Zerbel

DATE: 21 September 1978

SUBJECT: Failure Modes and Effects Analysis
of Program 777 Solid State Temperature
Switch (SSTS) Circuit

FROM: J. E. Brooks

BLDG. M2 MAIL STA. 2170 EXT. 64590

An anomaly in the telemetered battery 3 temperature indication has been detected on two satellites as well as an overtemperature trip related to battery 3 on one of these satellites. Telemetry data suggests the possibility that the thermistor in the SSTS circuit is lagging the telemetry sensing thermistor. This problem is being investigated in several areas including test simulations. The FMEA presented in this memo is part of the overall investigation of this anomaly. Sensitivity analysis was performed on critical parts of this circuit which could affect the high temperature set point as follows.

R4 - Approximately 300 Ω shift is required to change the set point by 1 $^{\circ}$ F. The resolution of this wirewound part is 22 Ω /turn. Absolute worse case end-of-life drift of this part is 400 Ω . Resistance changes which could offset the set point as much as 1.5 $^{\circ}$ F are not considered to be credible failure modes.

R2 - The sensitivity of the set point to drift of this resistor is approximately 50 Ω / $^{\circ}$ F. Absolute worse case end of life drift for this part is less than .05% year (1.5 Ω). Resistance changes which would significantly affect the set point voltages are not considered to be credible failure modes.

R1 and R3 - Worse case resistance changes for these resistors would have negligible impact on set point voltage.

The Failure Mode and Affects Analysis is summarized in the following table.


J. E. Brooks

JEB:kd

SSTS FMEA

Page	Failure Mode	Failure Effect
Q1	CE Open	Battery remains at full charge.
	CE short or excessive leakage	Battery remains at trickle charge.
R9	Open	Leakage current may turn Q1 on and hold battery in trickle charge condition.
	Short	Battery remains at full charge.
R8	Open	Same as R9 short.
	Short	Possible damage to R5, Q1, VR1 and VR3 when battery is hot.
VR1	Open	Same as R8 open.
	Short	If VR3 was leaking Q1 could possibly be held on maintaining trickle charge condition.
VR3	Output remains high	Battery remains in trickle charge.
	Output remains low	Battery remains at full charge.
	Output toggles at wrong point.	Battery charging circuit switches at wrong temperature.
VR2	Short	Moves both set points up in temperature.
	Open	Moves lower set point down in temperature. Possible damage to VR3-3.
R6	Open	Moves lower set point up in temperature.
	Short	Damage to VR2, VR3 and R5.
R7	Open	Moves lower set point up in temperature.
	Short	Battery remains in trickle charge condition.
R3	Open	Battery remains in trickle charge condition.
	Short	Battery remains in full charge condition.
R1	Short	Battery remains in trickle charge condition.
	Open	Battery remains in full charge condition.

SSTS FMEA

Page	Failure Mode	Failure Effect
R2 or R4	Open	Battery remains in trickle charge condition.
	Short	Battery remains in full charge condition.
RT2	Open	Battery remains in full charge condition.
	Short	Battery remains in trickle charge condition.
R5	Open	Battery remains in full charge condition.
	Short	No effect.
C1	Open	Erratic toggling of VR3 output.
	Short	Battery remains in full charging condition.

SUMMARY OF SSTS TESTING

1) Normal

- o HI, 77°F = 2002Ω Q1 on (T.C.)
- o LO, = 70°F = 2325Ω Q1 off (F.C.)
- o Δ = 323Ω

2) VR2 Shorted

- o Switches to T.C. @ 1643Ω = 86°F
- o Δ = 359Ω
- o No hysteresis

3) R6 Open or R7 Open

- o No change in trip point
- o No hysteresis

4) Simulate increased leakage of Q12 in VR3 by placing an external resistor across pins 9 to 2.

R9-2Action

30K

- o Both set and reset points go higher in temp.
- o Hysteresis decreases

28K

- o Set and reset points go higher
- o Hysteresis goes to zero

<25K

- o Output does not come on (system would stay in full charge)

5) Simulate increased leakage of Q11 in VR3 by placing an external resistor across pins 3 to 8.

R3-8Action

900K

- o Set and reset points decrease 2°F

100K

- o Set and reset points decrease 14°F

6) Open C1

- o No change

Page 2

- 7) Simulate decreased gain of Q11 by inserting resistance in series with Q11 base.

R_{B11}

Action

200K

o Set and reset points increase by 10°F

Attachment 3

9438

Time from when RT1 reaches 77°F until SST5 switches (based on 48 hour run data).

Batteries

Cycle	1	2	3
1	3 min	5 min	10 min
2	3 min	5 min	10 min
3	3 min	7 min	6 min
4	5 min	7 min	7 min
5	3 min	3 min	8 min

INTEROFFICE CORRESPONDENCE

DSCS-D3-2136

TO: R. E. Doyle
R6/2188

CC: M. Kendziorak
J. A. Nisenbaum
L. O. Stuck
D. Zerbel
Data Center

DATE: 29 September 1978

SUBJECT: 777 Battery Anomaly Investigation
C255151-021 (1H021-004V-xxx) LDC 7414
(Upgraded from 1H021-001V-xxx)PO 171/PM3

FROM: C. B. Irwin

BLOG: R4 MAIL STA: 1174 EXT: 61881

Reference: 1H021 PIN Specification Document

To establish confidence in subject parts already installed in 777 F7-F12 systems, the following stability test is to be performed.

1. Remove all available 1H021 devices from Group B part inventory and residual stock.
2. Perform Group A, Subgroup 1 tests as per Table III of the referenced 1H021 PIN specification. Read and record parameter values.
3. Perform burn-in tests as defined in Para. 4.6.5 of the specification except the duration of this burn-in shall be for a period of 500 hours. Readings are to be taken and recorded at 168, 330 and 500 hour points.
4. The electrical end points to be measured are as shown in Table II of the specification with the delta limits as defined in Para. 4.6.6.

At the conclusion of the above testing, review all data. In the event that any delta limits are exceeded prior to the 500 hour point, i.e., at the 168 or 330 hour points, perform an immediate data examination.

Charge to J/N 3473-95 to complete this task.

CBI:h

C. B. Irwin

C. B. IRWIN

777 - BATTERIES P/N 256107-3

Attachment 10

BATTERY	SSTS			VR3			
S/N	P/N	MSO #	S/N	P/N	P.O.	D.C.	PCWO
(FLT #7)							
3-30	276944-2	DRBHYEE670	008	C255151-021	171PM3	7414	40462
3-31	276944-2	DRBHYEE630	004	C255151-021	171PM3	7414	40462
3-32	276944-2	DRBHYEE640	005	C255151-021	171PM3	7414	40462
(FLT #8)							
3-33	276944-2	DRBHYED290	003	C255151-021	171PM3	7414	40462
3-34	276944-2	DRBHYED280	002	C255151-021	171PM3	7414	40462
3-35	276944-2	DRBHYEE650	006	C255151-021	171PM3	7414	40462
(FLT #11)							
3-44	276944-2	DRBHLET930	016	C255151-021	171PM3	7414	40462
3-45	276944-2	DRBHLET900	013	C255151-021	171PM3	7414	40462
3-46	276944-2	DRBHLET870	018	C255151-021	171PM3	7414	40462
(FLT #12)							
3-47	276944-2	DRBHLET920	021	C255151-021	171PM3	7414	40462
3-48	276944-2	DRBHLET950	021	C255151-021	171PM3	7414	40462
3-49	276944-2	DRBHLET970	023	C255151-021	171PM3	7414	40462
(SPARE)							
(7 & 8) S/N 3-36	276944-2	DRBHYEE660	007	C255151-021	171PM3	7414	40462

NOTE: EO, BI DWG. 276944 (SSTS)
Replaced (VR3) C255151-001
with (VR3) C255151-021.

MSO's for SSTS located in
Ron Zher's Data Center
M3/1641 X63311.

MSO's for batteries located
in R. Yasui's Data Center
M1/1308 X52846.

C/29/78

Tony M.

APPENDIX 7

SPACECRAFT THERMAL CONTROL

SPACECRAFT THERMAL CONTROL

Thermal control for the 777 spacecraft is achieved through the use of passive elements (i.e., multilayered insulations, surface finishes, second surface mirrors, and low thermal conductivity isolators) augmented by thermostat controlled heaters. The baseline thermal design is presented schematically in Figure A7-1. The components within the despun platform are thermally isolated from the spinning platform by reflective radiation shields. Heat dissipated within the despun platform is rejected to the space heat sink through the forward closure and the aft radiator. Heat dissipated within the spinning platform is rejected to the space heat sink through the solar array and the battery radiators. On-orbit, the solar array is irradiated by the sun continuously except for short periods during the equinox eclipses. Between equinox, winter solstice, and equinox, the aft radiator and the battery radiators are irradiated by the sun by diffuse reflection from the inside of the solar array in the aft-cavity region, and by direct incidence around winter solstice. The forward closure is irradiated by the sun between equinox, summer solstice, and equinox. For the spinning platform, the hot condition occurs during winter solstice and cold condition occurs during equinox eclipse. For the despun platform, hot condition occurs during summer solstice, and cold condition occurs during equinox eclipse.

A review of orbital temperature data showed no failure or degradation in the thermal control subsystem. Other than batteries, all subsystem components were working in the expected manner. Table A7-1 presents some selected spinning platform temperature sensor data for the period immediately preceding the dates when the batteries were commanded into automatic mode. A comparison of these sensor temperatures for this eclipse season and the two preceding eclipse seasons show nearly identical temperatures.

Table A7.1. Spinning Platform Temperatures
Before Eclipse Season Entry

Temperature Measurement	Minitrickle	Minitrickle	Manual Trickle
<u>Spacecraft 9437</u>			
	(9/5→Auto) 9/4/77	(3/2→Auto) 3/1/78	(9/1→Auto) 8/31/78
SOLR1T	55°F	55°F	55°F
SOLR2T	60	59	61
TANK1T	56	55	57
TANK2T	57	56	58
EIAT	96	95	96
BA1T	55	55	59
BA2T	47	49	52
BA3T	51	51	56
<u>Spacecraft 9438</u>			
	(9/4→Auto) 9/2/77	(3/2→Auto) 3/1/78	(9/3→Auto) 8/31/78
SOLR1T	55°F	55°F	56°F
SOLR2T	59	59	59
TANK1T	55	55	56
TANK2T	57	55	57
EIAT	95	93	95
BA1T	52	53	57
BA2T	47	48	53
BA3T	50	49	53

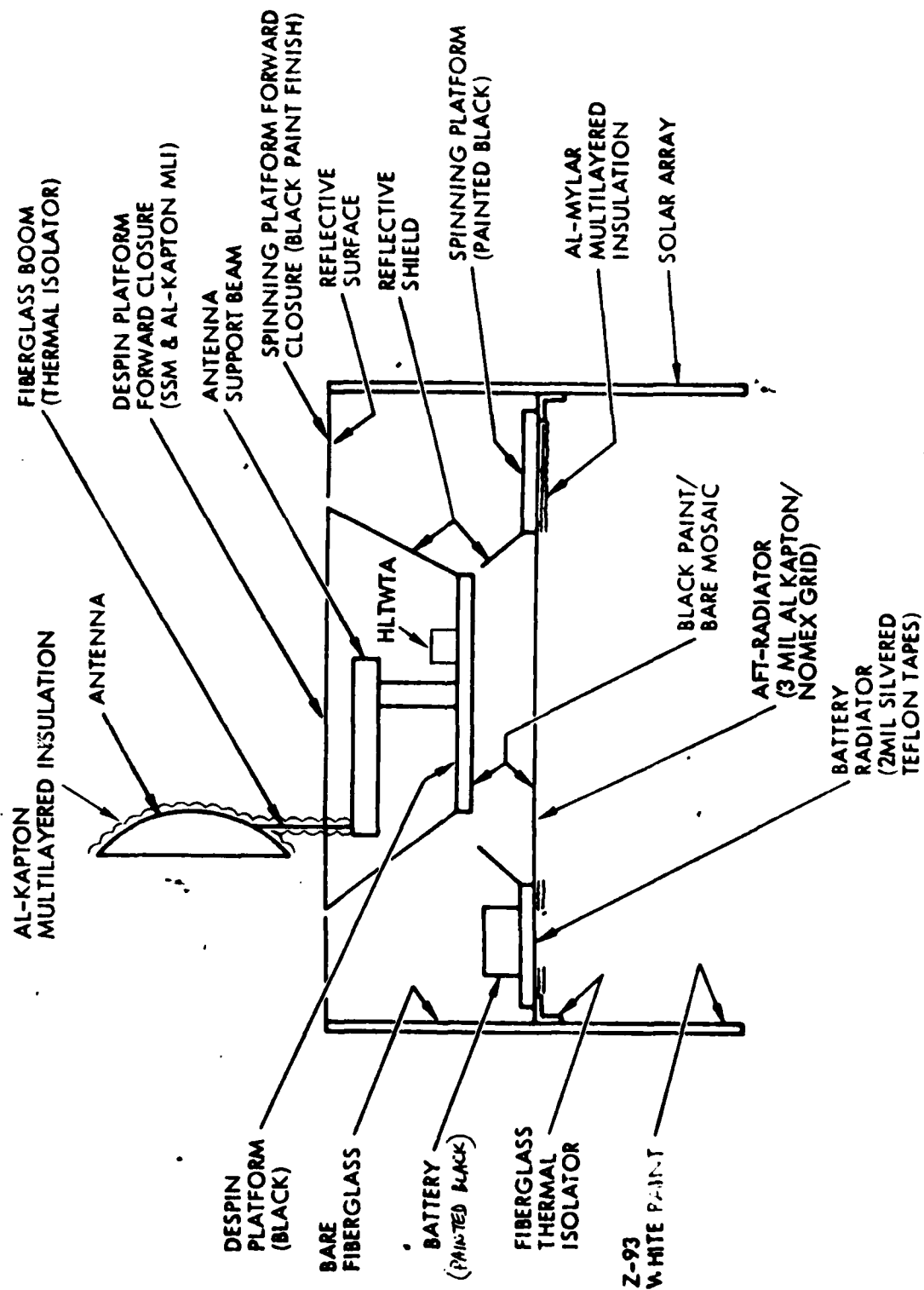


Figure A7-1. 777 Thermal Design

INTEROFFICE CORRESPONDENCE

8715.1.3-78-8

TO: R. H. Sparks / CC: See Distribution DATE: 28 September 1978

SUBJECT: 777, 9437/9438 Battery Anomaly Investigation,
 Thermal Effects of Increasing Battery C
 Radiator Area to 108 Square Inches

FROM: H. M. Pan *hmp.*
 BLDG MAIL STA. EXT.
 M3 2542 61050

SUMMARY

The effect of increasing Battery C radiator opening from the present area of 90 square inches to 108 square inches was analyzed, and the results showed minimal effect on the Thermal Control Subsystem. Results of the analysis are summarized below.

1. Effects on Battery C and surrounding component temperature.
 Battery C: -3°F (during trickle charge)
 PCM Encoder: -1°F
 PCU: -1 °F
2. Increases orbital averaged battery heater power consumption during Summer Solstice by about 2 watts.
3. Effects on Battery C heat rejection capability during Equinox sunlight based on partially degraded solar array (Batteries A and B capabilities are also presented for comparison).

Battery No.→	Battery C		Battery A	Battery B
Temp. °F ↓	(90 in ²)	(108 in ²)	(108 in ²)	(108 in ²)
50	4.5w	5.6w	4.5w	5.2w
65	10.6w	11.8w	10.6w	10.9w
80	17.0w	18.4w	17.0w	16.9w
95	23.8w	25.3w	23.7w	23.2w

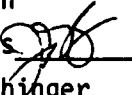
DISCUSSION

The analysis showed, in the temperature range of 50°F to 80°F, Battery B has the most heat rejection capability, while Batteries A and C have about the same heat rejection capability. Battery C has smaller radiator area than both

Batteries A and B, because it is located in a cooler part of the Spinning Platform. A review of on-orbit data for the period prior to the Fall 1978 eclipse season showed Battery A had the least heat rejection capability, and Battery B had the most heat rejection capability. Battery C heat rejection capability lay somewhere between Batteries A and B. During manual trickle charge condition, Battery A was warmer than Batteries B and C by between 3°F to 7°F. During the first charge-overcharge cycle following the long eclipse, Battery A switched earlier over to trickle charge from the full charge condition. The proposed change in Battery C radiator area would cause its heat rejection capability to be approximately equal to that of Battery B or even slightly greater. This would increase the heat rejection "unbalance" between Batteries A and C.

HMP:am

DISTRIBUTION:

R. H. Alborn	R4/1098
J. T. Bevens 	M3/2542
J. A. Durschinger	R4/1182
A. P. Fay	R4/1182
W. M. Kendziorek	R4/1198
W. B. J. Shakespeare	82/1034
C. L. Stanley	M1/1406
M. White	82/1042
D. W. Zerbel	M2/2145

RECEIVED

NOV 6 1978
9:15am

R. H. SPARKS

TRW

DEFENSE AND SPACE SYSTEMS GROUP
ONE SPACE PARK • REDONDO BEACH • CALIFORNIA 90278

INTEROFFICE CORRESPONDENCE

H. N. Luhrs
H. N. Luhrs

DSCS-D4-062

7335.1-250

TO: R. Sparks *M1/1208* cc: Distribution

DATE: 26 October 1978

SUBJECT: Temperature Distributions and Differentials for
Batteries Operating in a Normal Mode for
Orbital Conditions - Project 777

FROM: J. N. Woo *J. N. Woo*
BLOG: MAIL STA. EXT. 52202
R5 B231

- References: (1) 78-8725.0-233, "Plan for F11/F12 Final Readiness Review-Battery System Changes", from R. Sparks to Distribution, dated 23 October 1978.
- (2) 7415.1-669 (777-E3-1462), "Final Thermal Analysis of Project 777 Battery", from J. N. Woo to J. D. Armantrout, dated 30 July 1970.

INTRODUCTION

In partial response to your request of Reference (1), the final thermal analysis of Project 777 Battery (Reference 2) was reviewed. The primary purpose of the review was to obtain the temperature distributions and differentials for batteries operating in a normal mode for orbital conditions - Project 777. The temperature data are included herein.

RESULTS

Based on the results of the analysis (Reference 2), the temperature distributions and differentials are shown in Table I. The heat dissipations assumed for analysis are shown in Table II. The detailed temperature-time histories can be obtained from Reference (2).

DISCUSSION

The temperature data for batteries operating in a normal mode for orbital conditions, as shown in Table I, indicated a maximum temperature differential of 8°F between the center cell and the end cell. The two center cells (cells No. 6 and 17) are the hottest among the 22 cells of the battery pack, the four cells adjacent to the two center cells (cells No. 5, 7, 16, and 18) are slightly colder, and the four end cells (cells No. 1, 11, 12, and 22) are the coldest. The reason for this condition to exist is that the end cells are thermally coupled to the end plates, which radiate heat away to the surrounding.

TABLE I. Temperature Distributions and Differentials for Batteries Operating in a Normal Mode for Orbital Conditions - Project 777.

Condition	Equinox		Winter Solstice (Steady State Only)
	(Steady State and Cold Case	Transient) Hot Case	
Temperature Range of Cells (°F) Top Surface Bottom Surface Electrode Plates	42 - 70	63 - 83	76 - 79
	37 - 57	61 - 73	74 - 75
	43 - 73	63 - 91	78 - 82
Temperature Range of Baseplate (°F)	34 - 64	60 - 68	73
Maximum Temperature Differentials (°F) Among the Electrode Plates from Cell to Cell Between the Electrode Plates and the Bottom Surface of the Cell Between Charge Control Thermal Switch and the Electrode Plates Between Heater Control Thermal Switch and the Top Surface of the Cell	8	4	3
	22	18	7
	3	12	1
	0.4	0.8	0.1

TABLE II. Heat Dissipations as a Function of Time for Each of the Three Batteries.

Condition	Time (hrs.)	Battery Operating Mode	Heat (Watts)
Equinox - Cold Case	0 - 1.2	Discharge	22 Constant
	1.2 - 7.8	Charge	0
	7.8 - 11.0	Full Charge	0 - 23 Linearly Increasing
	11.0 - 24.0	Trickle Charge	5 Constant
Equinox - Hot Case	0 - 0.3	Discharge	32 Constant
	0.3 - 2.4	Charge	0
	2.4 - 3.2	Full Charge	0 - 110 Linearly Increasing
	3.2 - 24.0	Trickle Charge	8.5 Constant
Winter Solstice	Steady-state	Trickle Charge	10.0 Approximately



INTEROFFICE CORRESPONDENCE

TO: R. H. Sparks

cc: Distribution

DATE: 78-8715.1.3-9
2 October 1978

SUBJECT: 777, 9437/9438 Battery Anomaly Investigation,
Effects of Changing Battery Temperature Set
Points and Main Bus Voltage on the Thermal Control
Subsystem

FROM: H. M. Par

BLDG
M3

MAIL STA.
2542

EXT.
61050

SUMMARY

A thermal analysis has been performed to determine the feasibility of lowering the Trickle-to-Full temperature set point of 70°F, and its overall thermal effect on the thermal control subsystem. The following summarizes the results of the analysis.

1. The Trickle-to-Full temperature set point can be lowered to 63°F from the present 70°F.
2. The lower temperature set point has no effect on the minimum predicted temperatures for the other Spinning Platform components.
3. Changing the main bus voltage from 32.4 volt to 31.8 volt has negligible effect on the thermal control system.

DISCUSSION

The Trickle-to-Full temperature set point can be lowered from the present value of 70°F because the battery trickle charge dissipation dropped by almost 50% due to the lowering of the main bus limit from 32.4 volts to 31.8 volts. At 70°F, the maximum trickle charge dissipation for the 32.4 volt bus limit is about 8 watts and is about 4.6 watts (from C. L. Stanley) for the 31.8 volt bus limit. Predicted steady-state battery trickle charge temperature for the Equinox EOL condition is about 61°F at 8 watts and about 54°F at 4.6 watts. The present set point of 70°F provides a margin of 9°F for the predicted steady-state trickle charge temperature of 61°F, thus lowering the bus limit to 31.8 volts (consequently lowering the trickle charge dissipation) allows the lowering of the set point to 63°F and still provides the same margin of about 9°F between the set point and the lower predicted steady-state trickle charge temperature of 54°F.

The lower temperature set point has no effect on the minimum predicted temperatures for other components. The minimum predicted component temperatures were predicted based on the condition with all three batteries operating in manual trickle charge prior to entering eclipse. This mode of operation results in lower predicted temperatures for other components. Spacecraft T/V acceptance test was conducted with the batteries in manual trickle charge condition prior to entering eclipse during the Phase II Equinox thermal equilibrium test condition.

HMP:ms

Distribution:	R. H. Alborn	R4/1098
	J. T. Bevans <i>JTB</i>	M3/2542
	J. A. Durschinger	R4/1182
	A. P. Fay	R4/1182
	W. M. Kendziorek	R4/1198
	W. B. J. Shakespeare	82/1034
	C. L. Stanley	M1/1406
	M. White	82/1042
	D. W. Zerbel	M2/2145

Thermal Effects of Recommended Changes

- I. Increasing Battery C radiator from 90 in² to 108 in².
 - A. Temperature effect: Battery C -3°F (during trickle charge)
PCM Encoder -1°F
PCU -1°F
 - B. Increases orbital averaged battery heater power consumption during Summer Solstice by about 2 watt.
 - C. Increases battery C heat rejection capability during Equinox Sunlight by about 1.5 watt.
- II. Changing battery trickle-to-full set point from 70°F to 65°F and full-to-trickle set point from 77°F to 72°F.
 - A. Reduces battery temperature during Auto-Mode by at least 5°F.
 - B. Battery may not cycle during late life Equinox condition (battery remains in trickle charge after the first full charge cycle).
 - C. Have no effect on minimum temperature condition for other spinning platform components. Minimum temperature condition analyzed was with the battery in manual trickle charge prior to entering eclipse (T/V acceptance test was with the battery in manual trickle charge prior to entering eclipse during phase 2 thermal equilibrium condition).

DATE 3/8/78

TIME	SC TIME	RII	BI	TEMP	RII	BI	TEMP	RII	BI	TEMP	RII	BI	TEMP	RII	BI	TEMP	REMARKS
		by	off	by	off	by	off	by	off	by	off	by	off	by	off	by	
10:30	3775	.23	.23	80	80	.29	3.00	72	72	.51	.47	88	87	T	T	T	
11:18	40674	.30	.30	80	80	2.25	.21	79	80	.51	.51	85	85	T	F	T	
12:23	44614	-5.47	-3.94	73	72	-5.17	-3.68	77	77	-2.04	-4.95	73	73	T	T	T	
12:32	45138	-4.49	-5.79	70	70	-4.19	-2.46	75	74	-4.05	-1.97	70	70	T	T	T	
13:04	47096	1.64	.54	68	68	.01	2.09	72	72	1.69	.82	66	66	F	T	F	
15:55	57328	.19	1.34	56	56	.29	2.01	58	58	2.99	.43	83	85	F	F	F	
17:20	62422	1.64	1.80	68	69	2.64	1.21	78	79	.51	.55	87	86	F	F	T	
17:48	64070	2.50	.19	78	79	.33	.33	84	84	.55	.51	85	85	F	T	T	

SSTS OPERATING POINT

9/7 To 9/8 Data

	<u>Close</u>	<u>Open</u>
Batt 1	78	70
	77-78	70
	<u>77-79</u>	70
Range	77-79	
Batt 2	79-80	72
	79	72
	79-80	72
Range	<u>78-79</u>	72
Batt 3	81-83	73
	81-82	73
	<u>83-85</u>	73
Range	81-85	

APPENDIX 8

BATTERY CONTROL NETWORK DESIGN FOR DSCS II FLIGHTS 13-16



INTEROFFICE CORRESPONDENCE 79.8723.3-014

TO: C. Sollo

CC:

DATE April 25, 1979

SUBJECT: Redesign of Battery Control
Network for DSCS-II
Spacecraft 13 through 16 - ECP 124

W. B. North
FROM: N. B. North
BLDG M1 MAIL STA. 1406 EXT. 51402

Resistance values have been calculated for the 6B Battery charge control option as modified for optional direct connection. This effort was accomplished in partial support of ECP 124 for DSCS-II spacecraft 13 through 16.

Report Number 79.8723.18-001 (attached) gives details of the analysis.

NBN:11h

Attachment

DISTRIBUTIONL G. V. Anderson
F. Barany
W. R. Brannian
R. H. Hazen
H. M. Pan
G. M. Reppucci *MR*
A. D. Schoenfeld
W. R. Scott
E. Kipp
C. Lurie
L. D. Smith
C. Sollo (2)
R. H. Sparks
C. L. Stanley *CS*
D. W. Zerbel
E. I. Reeves
B. Pinkston
H. Riess
D. W. Rusta
J. Durschinger (10)
M. Schwartzburg
R. D. Stevenson
P. Bauer
DSCS DATA CENTER R4/1195
A. D. Schoenfeld

TRW

DEFENSE AND SPACE SYSTEMS GROUP
ONE SPACE PARK
REDONDO BEACH, CALIFORNIA 90278

POWER CONTROL AND DISTRIBUTION DEPARTMENT

TECHNICAL REPORT

BATTERY CONTROL NETWORK DESIGN

FOR DSCS-II FLIGHTS 13-16

ECP-124

79.8723.18-001
DSCS-C3-490

25 April 1979

N. B. North

PREPARED BY: N. B. North

CONCURRENCE:

G. M. Reppucci
G. M. Reppucci

C. L. Stanley
C. L. Stanley

TABLE OF CONTENTS

	<u>PAGE</u>
1. SUMMARY	1
2. BATTERY CHARGE CONTROL REQUIREMENTS	1
2.1 Bus Voltage	2
2.2 Electromagnetic Compatibility	2
2.2.1 Array Voltage Limiting Mode	2
2.2.2 Battery Discharge Mode	3
2.2.3 Transition Between Voltage Limiting Mode and Battery Discharge Mode	3
2.3 Minimum Low-Rate Trickle Charge Current	3
2.3.1 Beginning of Mission	3
2.3.2 End of Mission	3
2.4 Maximum Battery Temperature During Low-Rate Trickle Charging	3
2.4.1 Battery with 22 Unshorted Cells	3
2.4.2 Battery with 21 Unshorted Cells	4
2.5 Minimum Current During High-Rate Charging	4
2.5.1 Battery Heater Turn-On Temperature	4
2.5.2 Expected Temperature Range	4
2.6 Maximum Current During High-Rate Charging	4
2.7 Maximum Temperature of 22-Cell Battery During Isolation Mode	4
2.8 Maximum Temperature of 21 Cell Battery During Battery Isolation Mode	5
2.9 Minimum Current During Battery Isolation Mode	5
2.10 Minimum Temperature During Battery Isolation Mode	5
2.11 Temperature Turn-Around of Battery in Direct Connection to Bus	5
3. CHARGE CONTROL NETWORK	6
4. SYNTHESIS OF RESISTANCE VALUES IN NETWORK	6
4.1 High-Rate Limiting Resistance	9
4.1.1 Bus Resistance	9
4.1.2 Maximum Overcharge Current	9
4.1.3 Minimum Recharge Current	9
4.1.3.1 Battery Heater Turn-On Temperature	10
4.1.3.2 Expected Temperature Range	11

4.1.4	Bus Voltage	11
4.1.5	Combined Requirements for High-Rate Recharging	11
4.1.6	Allowable Combinations of Bus Voltage and High-Rate Limiting Resistance	12
4.2	Low-Rate Limiting Resistance	14
4.2.1	Minimum Trickle Charge Current During Normal Operation	14
4.2.1.1	Beginning of Mission	14
4.2.1.2	End of Mission	14
4.2.2	Maximum Battery Temperature During Low-Rate Trickle Charging	15
4.2.2.1	Battery with 22 Unshorted Cells	15
4.2.2.2	Battery with 21 Unshorted Cells	17
4.2.3	Combined Requirements for Low-Rate Trickle Charging	18
4.2.4	Allowable Low-Rate Limiting Resistance	18
4.3	Choice of Values of Limiting Resistance For Low and High-Rate Charging	18
4.4	Direct Connection Between Battery and Bus	20
4.4.1	Constraints on Selection of Lower Bus Voltage Limit	20
4.4.1.1	Battery Self-Heating	21
4.4.1.2	Maximum Overcharge Current in Direct Connection	23
4.4.1.3	Selection of Lower Bus Voltage Limit	27
4.5	Battery Isolation	27
4.5.1	Maximum Temperature of Battery With 22 Unshorted Cells During Isolation Mode	28
4.5.2	Maximum Temperature of Battery With 21 Unshorted Cells	28
4.5.3	Minimum Temperature of Battery With 22 Unshorted Cells During Isolation Mode	30
4.5.4	Minimum Current During Battery Isolation	30
4.5.5	Bus Voltage Limit	32
4.5.6	Combined Requirements for Battery Isolation Mode	32
4.5.7	Back To The Drawing Board For Battery Isolation	33

4.5.7.1	Fifty-Five Ohm Battery Isolation Resistance	33
4.5.7.2	Open-Circuited Battery	42
4.5.8	Evaluation of Alternate Battery Isolation Mode Approaches	42
4.6	EMC Considerations	44
5.	CONTINGENCY MODE OPERATION	45
6.	CONCLUSIONS	45
7.	ACKNOWLEDGEMENT	45
	REFERENCES	47

FIGURE 3-1	BATTERY CONTROL NETWORK (Typical of 3)	7
FIGURE 4-1	OVERCHARGE CHARACTERISTICS FOR GENERAL ELECTRIC NICKEL-CADMIUM CELL	8
FIGURE 4-2	HIGH RATE RECHARGE MODE CONSTRAINTS	13
FIGURE 4-3	777 FLIGHTS 13-16 HEAT REJECTION-EQUINOX	16
FIGURE 4-4	LOW-RATE TRICKLE MODE CONSTRAINTS	19
FIGURE 4-5	777 FLIGHTS 13-16 HEAT REJECTION-EQUINOX	22
FIGURE 4-6	OVERCHARGE CURRENT - BATTERY CONNECTED DIRECTLY TO BUS (CELL VOLTAGE UNCERTAINTY 0.000 V/CELL RE TAFEL CURVES)	24
FIGURE 4-7	OVERCHARGE CURRENT - BATTERY CONNECTED DIRECTLY TO BUS (CELL VOLTAGE UNCERTAINTY +0.015 V/CELL RE TAFEL CURVES)	25
FIGURE 4-8	SENSITIVITY OF OVERCHARGE CURRENT TO BUS VOLTAGE	26
FIGURE 4-9	777 FLIGHTS 13-16 HEAT REJECTION-WINTER	29
FIGURE 4-10	777 FLIGHTS 13-16 HEAT REJECTION-SUMMER	31
FIGURE 4-11	CONSTRAINTS ON BATTERY ISOLATION RESISTANCE	34
FIGURE 4-12	777 FLIGHTS 13-16 HEAT REJECTION-EQUINOX	35

FIGURE 4-13	777 FLIGHTS 13-16 HEAT REJECTION-WINTER	36
FIGURE 4-14	777 FLIGHTS 13-16 HEAT REJECTION-SUMMER	37
FIGURE 4-15	777 FLIGHTS 13-16 HEAT REJECTION-EQUINOX	38
FIGURE 4-16	777 FLIGHTS 13-16 HEAT REJECTION-WINTER	39
FIGURE 4-17	777 FLIGHTS 13-16 HEAT REJECTION-SUMMER	40
FIGURE 6-1	SELECTED COMPONENT VALUES FOR BATTERY CONTROL NETWORK (Typical of 3)	46

TABLE 4-1	CONSEQUENCES OF SELECTING 55 OHM VALUE FOR LIMITING RESISTANCE, BATTERY ISOLATION MODE	41
TABLE 4-2	CONSEQUENCES OF SELECTING INFINITE RESISTANCE, BATTERY ISOLATION MODE	43

BATTERY CONTROL NETWORK DESIGN
FOR DSCS-II FLIGHTS 13-16

ECP 124

N. B. NORTH

1. SUMMARY

Battery charging must be controlled for DSCS-II flights 13 through 16 so that high-rate overcharge current does not exceed C/10 (1.62 amperes), so that recharge current prior to overcharge will be at least C/30 (0.54 amperes), at 50°F, and so that battery temperature will remain within desired limits for long-lived operation.

This report documents detailed design requirements for battery control and presents synthesis and analysis of the "6B" configuration as modified to provide direct connection of batteries to the bus for special-situation charging at a low bus voltage. Conclusions of the analysis are, assuming that battery temperature sensor switch points are at 64 and 71°F:

- The bus voltage limits should be set at nominal values of 31.6 and 33.8 volts.
- The resistance in the low rate path of the charge control network should be 20 ohms.
- The resistance in the high-rate path of the charge control network should be 3.095 ohms (operating in parallel with a low-rate path).

2. BATTERY CHARGE CONTROL REQUIREMENTS

Each battery is to be controlled in one of three selectable charge modes, namely:

- High-rate recharge mode
- Low-rate trickle mode
- Battery isolation mode

The bus is to be operated at one of two available voltage limit settings in automatic "hands-off" mode whenever possible.

High-rate recharge mode consists of connection of the battery to the bus either by direct connection or through a low-value limiting resistance (this replaces the former "full charge" mode). Low-rate trickle mode consists of connection of the battery to the bus through a higher-value limiting resistance (this corresponds to earlier terminology of "trickle charge" mode). The isolation mode is provided for isolation of a battery from the bus to preclude excessive overcharge in case of inadvertent degradation beyond the stage at which the battery can safely be operated in high or low-rate mode. This isolation mode is represented in the earlier replenishment series by the minitrickle mode; the high-value finite limiting resistance for minitrickle charging is not required -- it could conceivably be infinite (open circuit).

The discharge path for the batteries in the three modes is either direct connection or a single series diode for the high-rate recharge mode, a single series diode for the low-rate trickle mode, or two diodes in series for the battery isolation mode.

The battery control requirements and goals given herein are an expansion of requirements set forth in Reference 1. In case some possible combination of requirements or goals cannot simultaneously be satisfied under certain conditions, then these conditions are identified and alternate design requirements are developed where appropriate.

2.1 Bus Voltage

The bus voltage shall not exceed 34.0 volt, including allowance of ± 0.2 volt for lifetime drift of the shunt limiter.

2.2 Electromagnetic Compatibility

2.2.1 Array Voltage Limiting Mode

The primary bus output impedance shall be less than 1 ohm for dc to 100 kHz when the bus is in the voltage limiting

mode and shunt current is greater than 1.2 amperes.

2.2.2 Battery Discharge Mode

The primary bus output impedance shall be less than 1 ohm from dc to 100 kHz when the bus is being supplied by the batteries.

2.2.3 Transition Between Voltage Limiting Mode and Battery Discharge Mode

The combined resistance from the batteries to the bus shall not exceed 1 ohm when all three battery control networks are in high-rate recharge configuration.

2.3 Minimum Low-Rate Trickle Charge Current

2.3.1 Beginning of Mission

Current during low-rate trickle charging mode shall be at least C/150 (0.108A) at a temperature of 42°F, at beginning of mission, with cell voltage uncertainty relative to nominal Tafel overcharge data of 0.000V.

2.3.2 End of Mission

Current during low-rate trickle charging mode shall be at least C/150 (0.108A) at a temperature of 59°F, at end of mission, with cell voltage uncertainty relative to nominal Tafel overcharge data of +0.015V.

2.4 Maximum Battery Temperature During Low-Rate Trickle Charging

2.4.1 Battery with 22 Unshorted Cells

Sustained low-rate trickle charge current to a 22-cell battery shall not exceed a value which would preclude battery temperature from cooling to a temperature of 64°F, with an added margin of -5°F, in eclipse season sunlight periods, at the high bus voltage level with worst case uncertainty in cell voltage of -0.015V from nominal Tafel overcharge data at BOM and 0.000V at EOM.

2.4.2 Battery with 21 Unshorted Cells

Sustained low-rate charge current to a 21-cell battery shall not exceed a value which would cause battery temperature to be in excess of 75°F in eclipse season sunlight periods, at the high bus voltage level, with worst case uncertainty in cell voltage of -0.015V from nominal Tafel overcharge data at BOM and 0.000V at EOM.

2.5. Minimum Current During High-Rate Charging**2.5.1 Battery Heater Turn-On Temperature**

Charging current shall be at least C/35 (0.463A) during high-rate charging if the battery temperature decreases to the battery heater turn-on temperature of 42°F, when accounting for worst-case cell voltage uncertainty (+0.015V/cell from nominal Tafel overcharge characteristics at EOM, 0.000V/cell at BOM).

2.5.2 Expected Temperature Range

Charging current shall be at least C/35 (0.463A) during high-rate charging within the expected battery temperature range of 50 to 71°F, when accounting for worst-case cell voltage uncertainty (+0.015V/cell from nominal Tafel overcharge characteristics at EOM, 0.000V/cell at BOM).

2.6 Maximum Current During High-Rate Charging

Charging current to a battery with 21 unshorted cells shall not exceed C/10 (1.62 A) following the initial inrush transient when the battery temperature is within the range of 42 to 71°F, accounting for worst case cell voltage uncertainty (-0.015V/cell from nominal Tafel overcharge characteristics at BOM, 0.000V/cell at EOM).

2.7 Maximum Temperature of 22-Cell Battery During Isolation Mode

The current in a battery containing 22 unshorted cells shall not exceed a value during battery isolation mode which would prevent the battery from cooling to a temperature below 64°F with a

margin of 9°F, at all times, accounting for worst case cell voltage uncertainty (-0.015V/cell from nominal Tafel overcharge characteristics at BOM, 0.000V/cell at EOM). (This goal cannot be met under all conditions; see Sections 4.5.1 and 4.5.6 through 4.5.8).

2.8 Maximum Temperature of 21-Cell Battery During Battery Isolation Mode

The current during battery isolation mode shall not exceed a value which would prevent a 21-cell battery from cooling to a temperature below 75°F at all times, accounting for worst-case cell voltage uncertainty (-0.015V/cell from nominal Tafel overcharge characteristics at BOM, 0.000V/cell at EOM).

2.9 Minimum Current During Battery Isolation Mode

As a goal, the current during battery isolation mode shall not be less than C/200 (0.081 A) accounting for worst-case cell voltage uncertainty (+0.015V/cell from nominal Tafel overcharge characteristics at EOM, 0.000V/cell at BOM). (This goal cannot be met; see Sections 4.5.6 through 4.5.8).

2.10 Minimum Temperature During Battery Isolation Mode

The current during battery isolation mode shall be sufficient to maintain a battery with 22 unshorted cells at a temperature above 42°F, accounting for worst-case cell voltage uncertainty (+0.015V/cell from nominal Tafel overcharge characteristics at EOM, 0.000V/Cell at BOM).

2.11 Temperature Turn-Around of Battery in Direct Connection to Bus

The low bus voltage limit must be sufficiently great that, during direct connection of a battery to the bus during eclipse season, internal dissipation in the battery will be sufficient to heat the battery to at least the upper SSTS switch point of 71°F.

3. CHARGE CONTROL NETWORK

The charge control circuitry for each battery shall be as shown in Figure 3-1. Automode charging is controlled via opening and closing of contacts of the K1 relay, using the SSTS thermistor for the control sensor.

Resistor R_{LR} is used for low-rate charging, with K1 contacts open. Resistor R_{HR} is used in parallel with R_{LR} for normal high rate charging with K1 contacts closed. The battery will normally discharge through the diode upon demand from the loads in absence of sufficient solar array current. The "K5" contacts are closed for special situations to provide direct connection between the battery and the bus.

4. SYNTHESIS OF RESISTANCE VALUES IN NETWORK

The restrictions on battery current are for overcharging only. Cell overcharge voltage-current density (Tafel) characteristics for General Electric nickel-cadmium cells are graphed for a range of temperatures in Figure 4-1. This graphical data has been fitted for cell voltage (V_{cell}) as a function of cell current (I , amperes) and cell temperature (T , °F) for the 777 F13-16 case where positive plate area is 7.91 dm², to yield

$$V_{cell} \approx \frac{\log_{10} I - B_0 - B_2 T}{B_1 + B_3 T} \quad (4-1)$$

where

$$\begin{aligned} B_0 &= -34.77167 \\ B_1 &= 22.78185 \\ B_2 &= 0.0440618 \\ B_3 &= -0.0086788 \end{aligned}$$

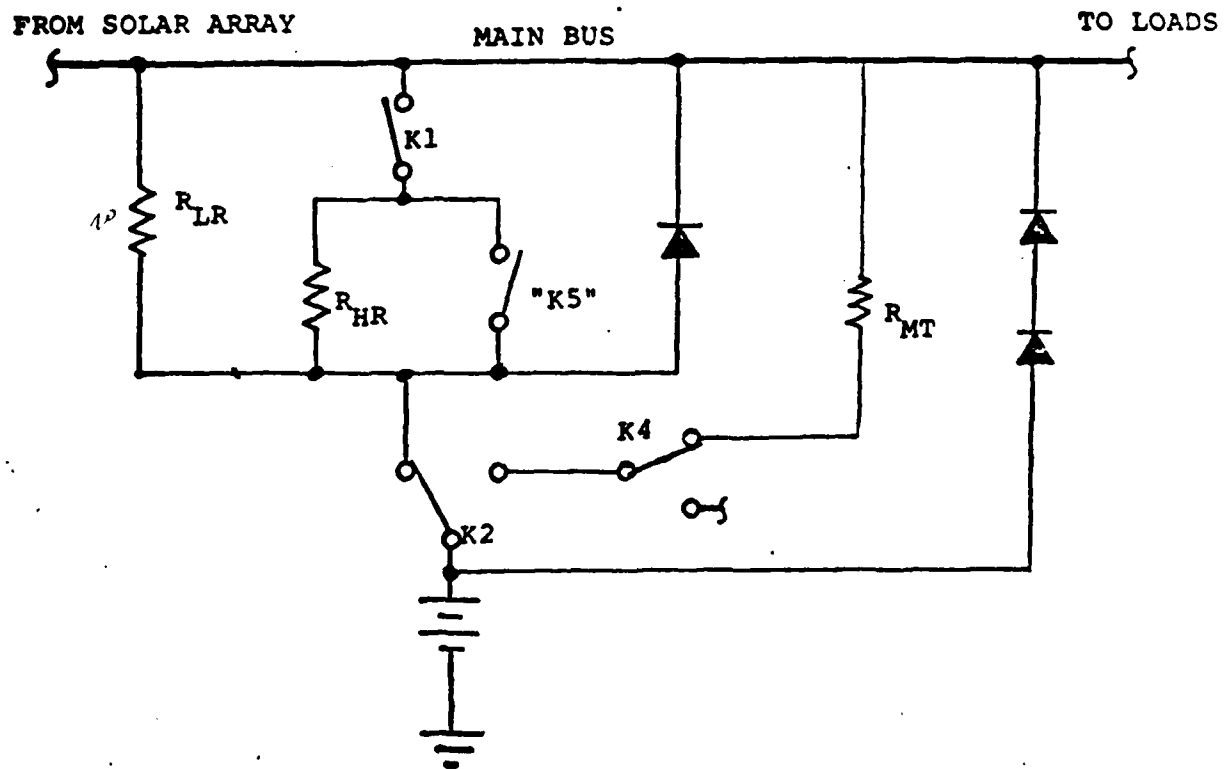


FIGURE 3-1. BATTERY CONTROL NETWORK
(Typical of 3)

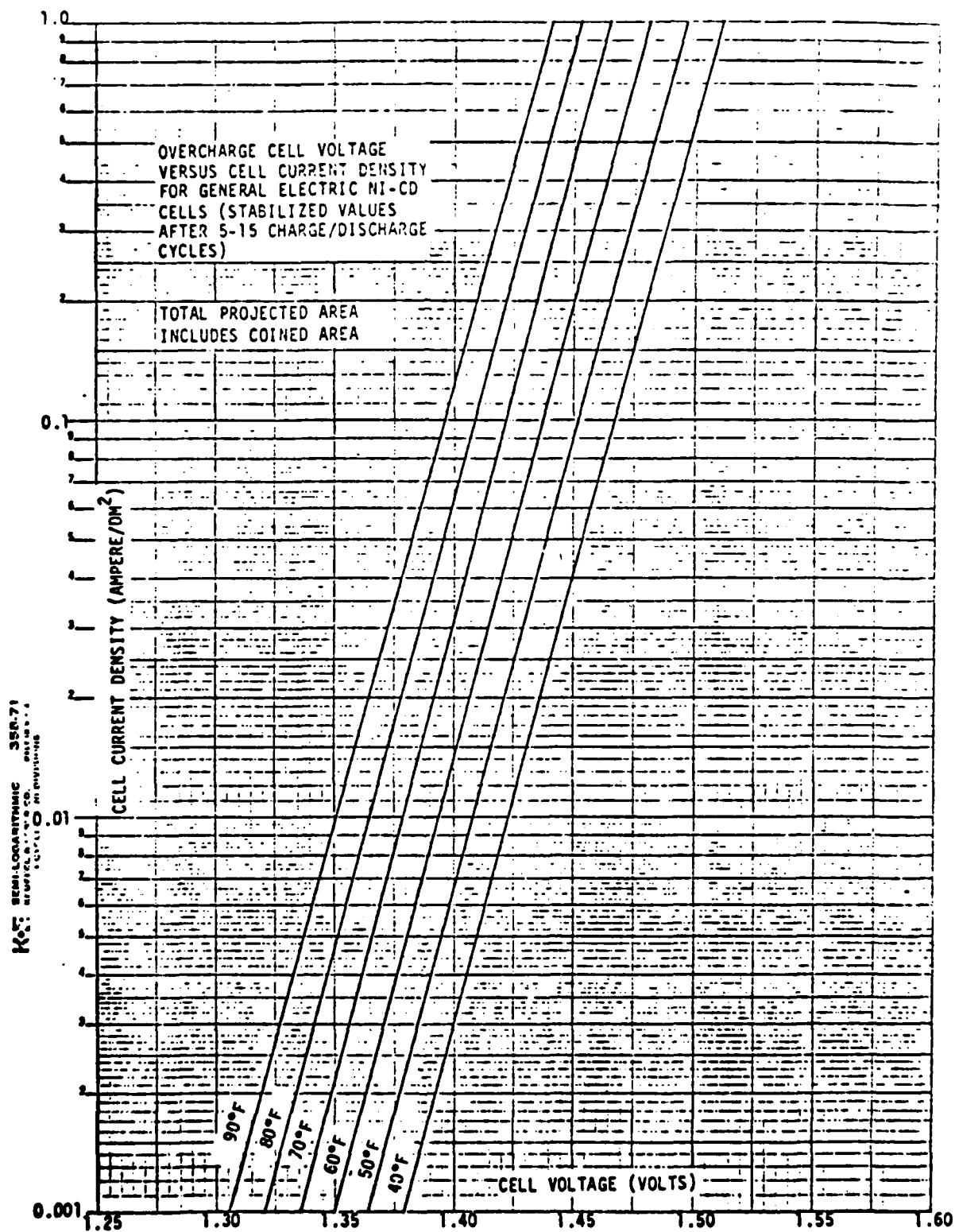


FIGURE 4-1. OVERCHARGE CHARACTERISTICS FOR GENERAL ELECTRIC NICKEL-CADMIUM CELL

In each case where it turns out to be appropriate and tractable, the allowable combinations of limiting resistance and bus voltage are examined. This bounds the design problem and helps avoid the situation of analytically experimenting with a large number of potential solutions and finding out that many of them fail to meet one or more of the requirements. More specifically, the requirements are formulated in terms of inequalities to represent allowable limiting resistance in terms of bus voltage.

Segments of the battery controls are analyzed in the sequence:

- High-rate limiting resistance
- Low-rate limiting resistance
- Direct connection
- Battery isolation mode

4.1 High-Rate Limiting Resistance

The requirements governing high-rate charging through the parallel combination of R_{HR} and R_{LR} are dealt with individually. The symbol R_{PL} is used for the resistance of the parallel combination:

$$R_{PL} = \frac{R_{HR} \cdot R_{LR}}{R_{HR} + R_{LR}} \quad (4.1-1)$$

4.1.1 Bus Resistance

The combined resistance from the three batteries to the bus must not exceed 1 ohm when the control network for each battery is in high-rate recharge configuration (Section 2.2.3). Resistance R_{PL} for each battery circuit must then be limited to 3 ohms.

$$R_{PL} \leq 3.0 \quad (4.1-2)$$

in order that the parallel combination for three batteries not exceed 1 ohm.

4.1.2 Maximum Overcharge Current

Overcharge current must not exceed 1.62A when the battery control network is in high-rate mode, with the battery being

charged through R_{PL} , except during initial turn-on of current through R_{PL} (Section 2.6)

$$I \leq 1.62A$$

In order to accomplish this, R_{PL} is limited by

$$R \geq \frac{V_{BUS} - V_{BAT}}{1.62A}$$

V_{BAT} is a function of worst-case cell temperature T , cell current, the minimum specified quantity of unshorted cells (21), cell voltage, and worst-case uncertainty of cell voltage (-0.015 V/cell at BOM). Current will be greatest when cell temperature is greatest. This will occur in high-rate overcharge as the battery reaches the temperature at which the SSTS causes relay K1 contacts to open to reconfigure the charge control network to low-rate mode. This temperature is nominally 71°F. From either Figure 4-1 or equation 4-1, nominal cell voltage at a current of 1.62A and temperature of 71°F is 1.437V. The worst-case uncertainty in cell voltage for the maximum overcharge current requirement is -0.015V, to give a modified cell voltage of 1.422V. The voltage of a 21 cell battery is then 29.863V.

The maximum overcharge current constraint thus becomes

$$R_{PL} \geq \frac{V_{BUS} - 29.863}{1.62} \quad (4.1-3)$$

4.1.3 Minimum Recharge Current

4.1.3.1 Battery Heater Turn-On Temperature

The minimum recharge current must be C/35, or 0.463 A at the battery heater turn-on temperature of 42°F (Section 2.5.1). The parallel resistance to accomplish this is

$$R_{PL} \leq \frac{V_{BUS} - V_{BAT}}{0.463}$$

V_{BAT} in this case is a function of temperature, cell current of 0.463 A, the maximum quantity of unshorted cells, cell voltage, and worst-case uncertainty of cell voltage (+0.015 V/cell at EOM). The overcharge data of Figure 4-1 or equation 4-1 yields nominal cell voltage of 1.454 V. Application of worst-case uncertainty of +0.015 V/cell gives a modified cell voltage of 1.469 V. The voltage of a 22-cell battery is thus 32.310V. The minimum recharge current constraint for 42°F then becomes

$$R_{PL} \leq \frac{V_{BUS} - 32.310}{0.463} \quad (4.1-4A)$$

4.1.3.2 Expected Temperature Range

The minimum recharge current to a battery within the temperature range of 50 to 71°F must be C/30, or 0.54 A (Section 2.5.2). Using analysis similar to that for Section 4.1.3.1 above, the minimum recharge current constraint for this temperature range is

$$R_{PL} \leq \frac{V_{BUS} - 32.128}{0.54} \quad (4.1-4B)$$

4.1.4 Bus Voltage

The bus voltage is required to not exceed 34.0 V (Section 2.1). This is represented simply by:

$$V_{BUS} \leq 34.0 \text{ V} \quad (4.1-5)$$

4.1.5 Combined Requirements for High-Rate Recharging

The combined constraints of expressions 4.1-2 through 4.1-5 are graphed in Figure 4-2. In addition, constraints representing other combinations of cell parameters are shown for information, even though they are dominated by constraint expressions 4.1-2 through 4.1-5.

AD-A087 390

TRW DEFENSE AND SPACE SYSTEMS GROUP REDONDO BEACH CA

F/G 10/3

USCS II. BATTERY ANOMALY INVESTIGATION SATELLITES 9437 AND 9438--ETC

APR 80 P BAUER, C LURIE

F04791-77-C-011A

UNCLASSIFIED

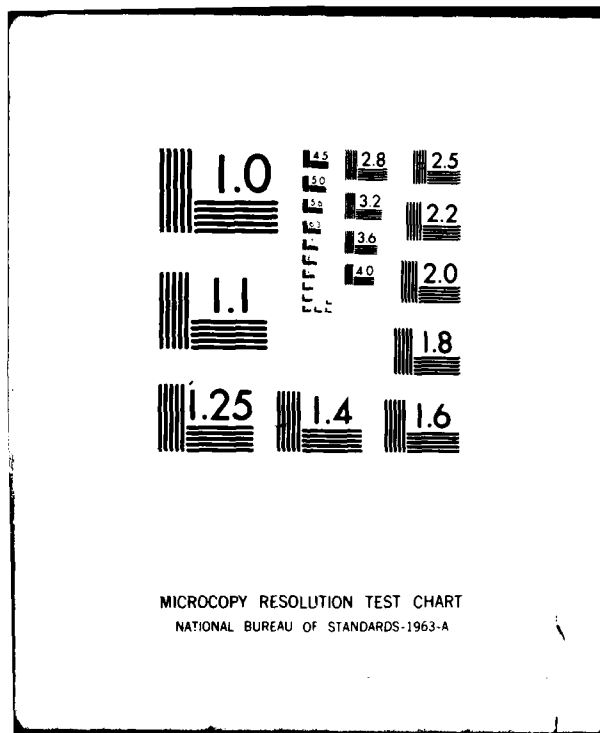
SD-TR-80-33

NL

 $\Delta \in \mathcal{L}$

Δ₁ = 2.0 m.

END
DATE
FILMED
9-80
DTIC



4.1.6 Allowable Combinations of Bus Voltage and High-Rate Limiting Resistance

An allowable combination of bus voltage and high-rate limiting resistance would be any point which simultaneously resides on the unshaded side of each and every defined constraint line. However, the bus voltage can be controlled with existing spacecraft circuitry only to a band not exceeding ± 0.2 volt above and below the nominal setting. Thus the allowable combination of nominal bus voltage and high-rate limiting resistance is defined by the space on the graph in which a vertical line of 0.4 volt dimension will fit within the constraining boundaries. This region is shown in Figure 4-2 as the triangle with dotted interior, bounded by the three points:

V_{BUS} (V)	R_{PL} (Ω)
33.66	2.468
33.80	2.554
33.80	2.726

A portion of the allowable combination of R_{PL} and V_{BUS} was accepted jointly by 777 Systems Engineering, Power and Distribution Subproject, and Battery Engineering, as that space in the graph which fits directly against the 34.0 volt upper limit on bus voltage, including +0.2 V allowance for long-term drift. This yields the range of design points as a point setting of 33.8 V for the nominal bus limiter setting and a range of 2.554 to 2.726 ohms for the parallel resistance R_{PL} .

The determination of actual high-rate limiting resistance R_{HR} is deferred until selection of low-rate limiting resistance R_{LR} .

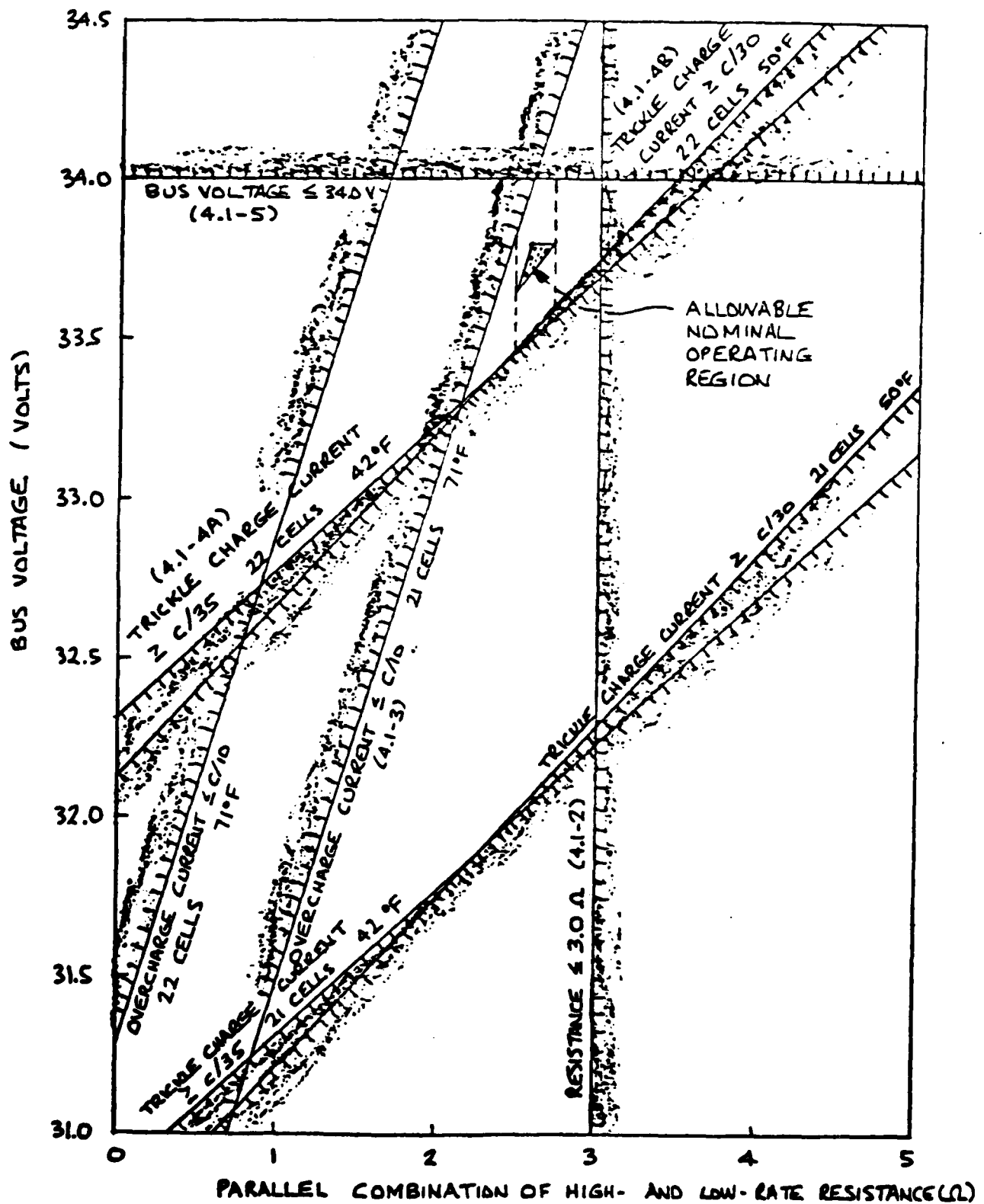


FIGURE 4-2. HIGH-RATE RECHARGE MODE CONSTRAINTS

4.2 Low-Rate Limiting Resistance

Each individual requirement relating to low-rate trickle charging is transformed into a mathematical constraint similarly to the methods of Section 4.1.

4.2.1 Minimum Trickle Charge Current During Normal Operation

4.2.1.1 Beginning of Mission

Minimum trickle current will be supplied to a battery with 22 unshorted cells when it is at its coldest allowable temperature of 42°F at beginning of mission, with the worst-case uncertainty in cell voltage of 0.000 V/cell. This minimum current must be at least 0.108 A (Section 2.3.1). The bus-voltage-resistance constraint to accomplish this is

$$R_{LR} \leq \frac{V_{BUS} - V_{BAT}}{0.108}$$

The cell voltage under the stated conditions will be 1.425V and the resultant battery voltage will be 31.360 V. The constraint is thus

$$R_{LR} \leq \frac{V_{BUS} - 31.360}{0.108} \quad (4.2-1A)$$

4.2.1.2 End of Mission

Minimum trickle current will be supplied to a battery with 22 unshorted cells when it is at its coldest expected temperature of 59°F at end of mission, with the worst-case uncertainty in cell voltage of +0.015 V/cell. This minimum current must be at least 0.108 A (Section 2.3.2). The bus-voltage-resistance constraint to accomplish this is

$$R_{LR} \leq \frac{V_{BUS} - V_{BAT}}{0.108}$$

The nominal cell voltage under the stated conditions will be 1.401 V. Application of +0.015 V uncertainty allowance to this value gives worst-case cell voltage of 1.416 V and battery voltage of 31.157 V. The constraint is thus

$$R_{LR} \leq \frac{V_{BUS} - 31.157}{0.108} \quad (4.2-1B)$$

4.2.2 Maximum Battery Temperature During Low-Rate Trickle Charging

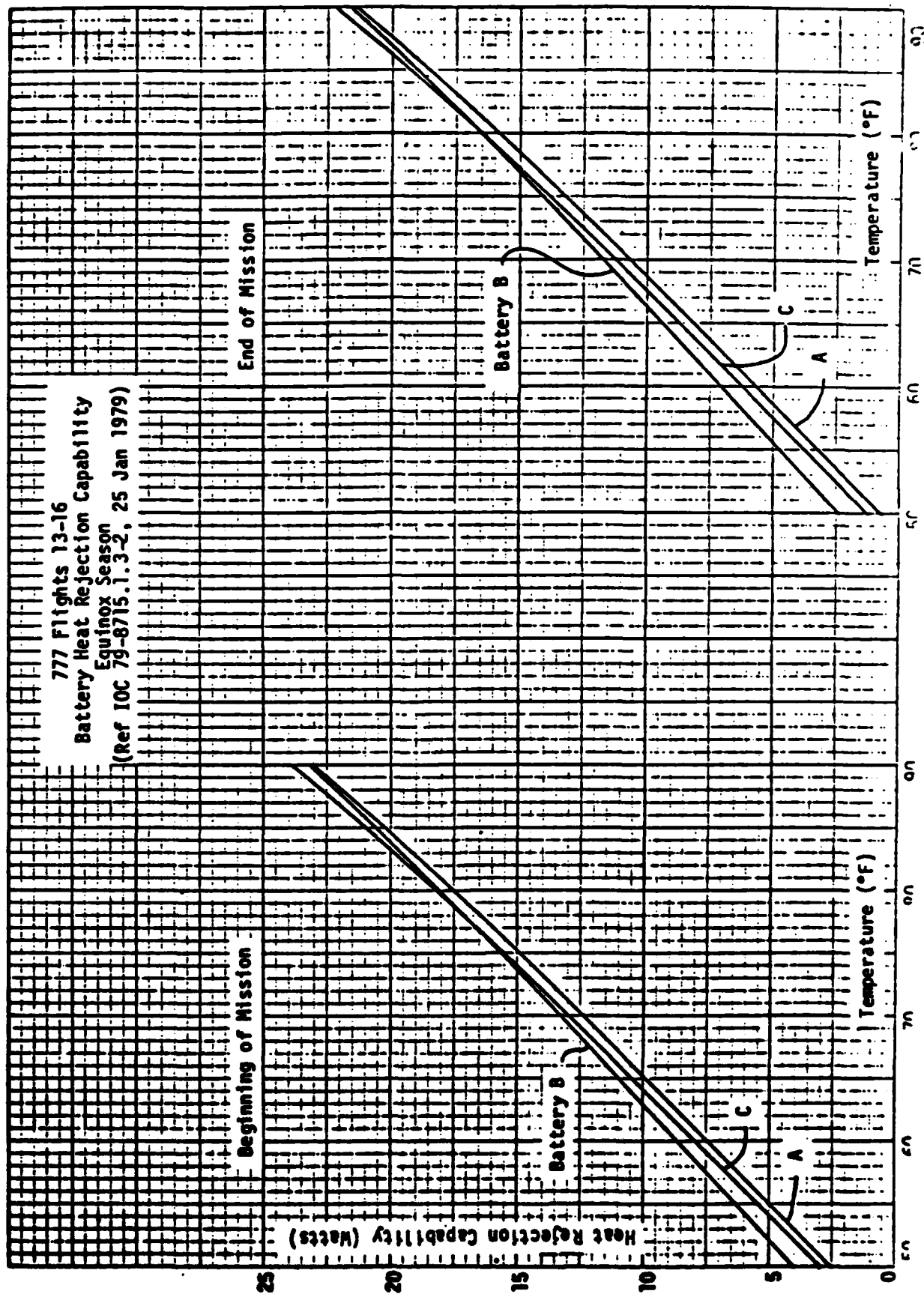
Low-rate charging must be controlled so that minimum current will be supplied to each battery and so that battery temperature does not exceed the stated maximum temperature. Heat rejection capability is given for each battery at beginning and end of mission in equinox in Reference 3. This data is graphed in Figure 4-3.

4.2.2.1 Battery With 22 Unshorted Cells

The low-rate trickle resistance must not be less than a value which will limit dissipation of a 22-cell battery to less than the heat rejection capability for the battery at a temperature of 59°F during eclipse season, with worst-case uncertainty in cell voltage of 0.000 V/cell at EOM (the worst case occurs at end of mission when heat rejection capability of a satellite battery is decreased).

Examination of the end-of-mission portion of Figure 4-3 reveals that battery dissipation of 5.2 watts will result in steady-state battery temperature of 59°F or less (59°F for battery A, 57°F for battery B, and 58°F for battery C).

FIGURE 4-3



The overcharge current at which battery dissipation equals 5.2 watts, using cell voltage uncertainty of zero, is determined by trial and error with equation 4-1 to be 0.16766 ampere. At this operating point, cell voltage is 1.410 volt and battery voltage is 31.016 volt. The limiting resistance required to limit maximum temperature is determined in general by

$$R_{TL} \geq \frac{V_{BUS} - V_{BAT}}{0.16766}$$

and specifically by

$$R_{TL} \geq \frac{V_{BUS} - 31.016}{0.16766} \quad (4.2-2)$$

4.2.2.2 Battery With 21 Unshorted Cells

The low-rate trickle resistance must exceed a value which will cause overcharge dissipation in a 21-cell battery to limit battery temperature to a maximum of 75°F during eclipse season and end-of-mission, with worst-case cell voltage uncertainty of 0.000 V/cell relative to nominal overcharge characteristics. From Figure 4-3, it is determined that battery dissipation of no more than 13.1 watts will result in steady-state temperatures of 75°F. The battery operating point at which this dissipation occurs at this temperature is determined from equation 4-1 to be 0.44371 amperes at 29.524 volts. The limiting resistance required to limit maximum temperature for this case is specified by

$$R_{TL} \geq \frac{V_{BUS} - 29.524}{0.44371} \quad (4.2-3)$$

4.2.3. Combined Requirements for Low-Rate Trickle Charging

The combined constraints of expressions 4.1-5 and 4.2-1 through 4.2-3 are graphed in Figure 4-4. Also, constraints representing other combinations of cell quantity and time in mission are shown for information.

4.2.4 Allowable Low-Rate Limiting Resistance

The feasible region for combinations of low-rate limiting resistance and bus voltage limit is bounded by the polygon containing the unshaded side of each of the constraint lines for expressions 4.1-5 and 4.2-1 through 4.2-3. This region is further limited by the decision to use a bus limit of 33.8 ± 0.2 volts (see Section 4.1.6). The remaining feasible space is represented by the space in which a vertical line of dimension 0.4 volt (the peak-to-peak band of allowable bus limiter drift) can fit against the bus voltage constraint expression (4.1-5) and within the 42°F temperature and C/150 constraints (expressions 4.2-1 and 4.2-2). This space is indicated as the hatched rectangle in Figure 4-4. The low-rate trickle resistance value is thus constrained to be within the range (in ohms):

$$17.80 \leq R_{LR} \leq 20.74 \quad (4.2-4)$$

4.3 Choice of Values of Limiting Resistance For Low and High-Rate Charging

The actual value of low-rate limiting resistance has been chosen to be 20.0 ohms (implemented as two $10.0 \text{ ohm} \pm 1\%$ resistors in series) based on standard resistor values chosen to have the shortest procurement time (Reference 4)

The allowable values for high rate resistance are those which allow the parallel combination of high and low-rate resistances (in ohms) to be in the range (Section 4.1.6):

$$2.554 \leq R_{PL} \leq 2.726 \quad (4.3-1)$$

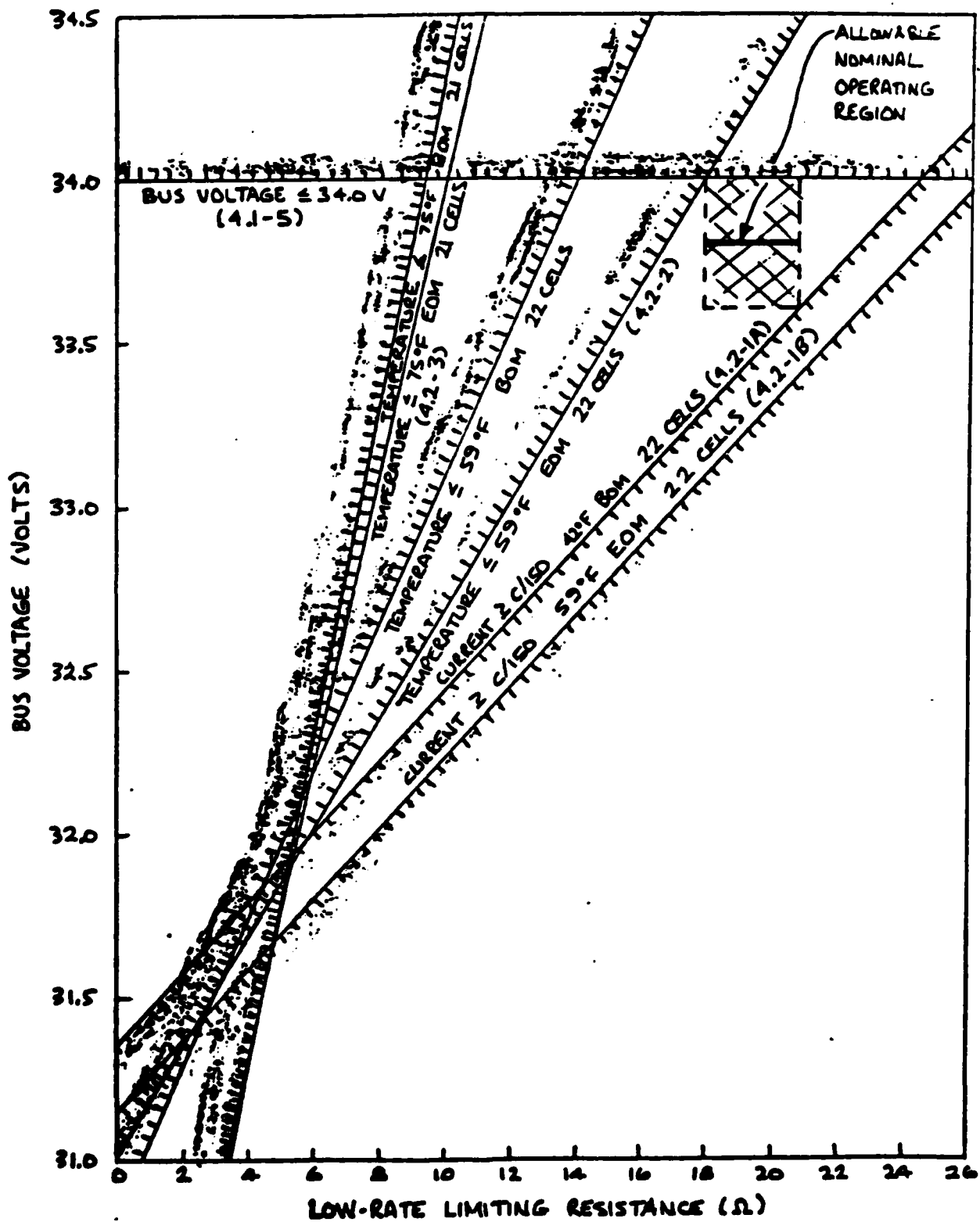


FIGURE 4-4. LOW-RATE TRICKLE MODE CONSTRAINTS

Combining expressions 4.3-1 and 4.1-1 yields

$$2.93 \leq R_{HR} \leq 3.16 \quad (4.3-2)$$

The actual value which has been chosen for R_{HR} is 3.095 ohms, formed by a parallel pair of two 6.19 ohm $\pm 1\%$ resistors (Reference 4).

4.4 Direct Connection Between Battery and Bus

It is desirable to allow direct connection between any one or more batteries and the bus to provide added flexibility for accommodation of possible partially failed batteries. Direct connection offers two advantages:

- added flexibility to control load sharing during discharge; i.e., zero diodes in series with a battery, as well as one or two diodes, and
- a backup, contingent method for giving a manually controlled high-rate boost charge in case present dependance on lower rate charging turns out to be less than adequate for maintaining energy balance through all conceivable phases of the spacecraft mission (including accommodation for potential failures outside the power subsystem).

It is apparent from Figure 4-2 that high-rate parallel resistance of zero ohms between a battery and the bus does not meet all identified constraints together with all worst-case allowances for uncertainty in cell and bus voltage, for unattended operation of the power subsystem. It is therefore important that any use of direct battery connection be accompanied by adequate surveillance so that charging a battery through direct bus connection can be manually terminated before any potentially hazardous high-rate overcharging can occur.

The bus voltage limit must be as low as possible in order to limit the potential for high-rate overcharging, but must be high enough that the battery has sufficient dissipation to preclude too low a battery temperature.

4.4.1 Constraints on Selection of Lower Bus Voltage Limit

The lower bus voltage limit is determined using two constraints, both

applicable for eclipse season (equinox);

- The battery must heat during direct connection to at least 71°F (Section 2.11), and
- Overcharge current at a temperature of 71°F must not exceed C/10 (1.62A) (Section 2.6).

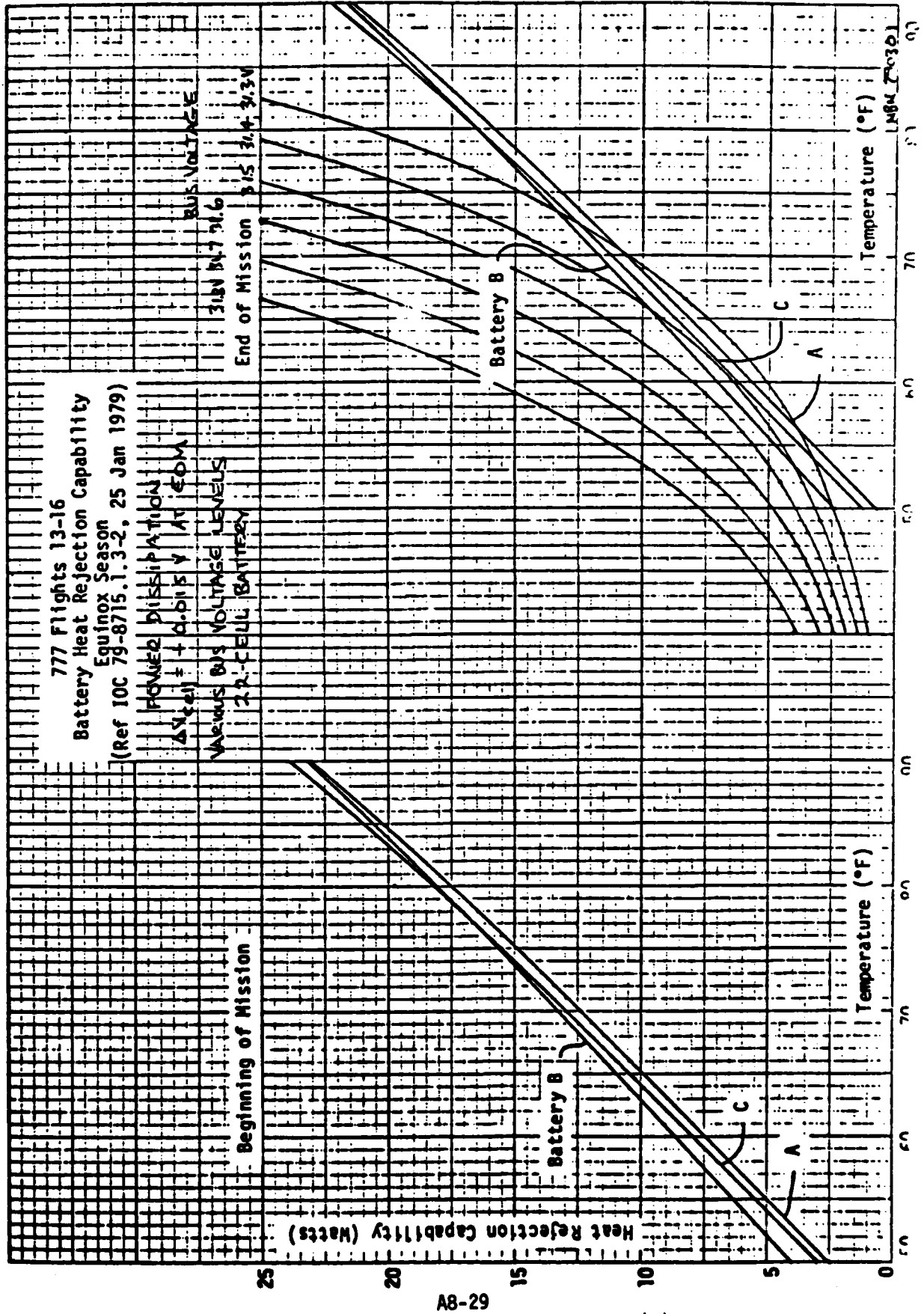
4.4.1.1 Battery Self-Heating

Battery dissipation is calculated as a function of temperature for a range of bus voltage limits; this is graphed simultaneously with heat rejection capability of each battery during equinox in Figure 4-5. In this figure, worst-case cell voltage of +0.015 V/Cell is incorporated for end-of-mission conditions, to represent the minimum-dissipation case for the battery.

The curves on Figure 4-5 reveal that, for example, use of bus voltage of 31.3 V allows battery dissipation during direct, full charge connection to be less than the heat rejection capability of one or more of three spacecraft batteries within the temperature range of approximately 50 to 73°F. This means that if the bus voltage is this low, the battery will not be able to reach the upper SSTS switch point of 71°F and be reset back into low-rate trickle charge.

The heat rejection capability characteristics are estimated to have uncertainty in temperature of approximately $\pm 5^\circ\text{F}$ (Reference 5). An allowable bus voltage which will assure

FIGURE 4-5



self-heating of each battery is determined by selecting a dissipation curve on Figure 4-5 which is displaced horizontally from the lowest heat rejection curve (namely battery B) by at least 5°F. The dissipation curve for bus voltage of 31.6 volts just barely meets this criterion. Higher bus voltages meet this criterion by greater margins.

4.4.1.2 Maximum Overcharge Current In Direct Connection

A battery that is connected directly to the bus will have overcharge current that increases with increasing temperature, as shown in Figures 4-6 and 4-7. These figures show sensitivity to cell voltage uncertainty at end-of-mission of 0.000 and +0.015 V/cell, respectively.

This data is reformatted in Figure 4-8 to show overcharge current at battery temperature of 71°F as a function of bus voltage. Cell voltage uncertainty is shown as a parameter in the range from +0.015 to -0.015 volt per cell.

The greatest interest for use of direct connection of a battery to the bus occurs when cell voltage increases during continued recharging, to the point where charging at the high bus voltage of 33.8 volts would conceivably be inadequate. This would be a contingency in which direct bus connection would be used at a lowered bus voltage. Thus the positive variation of cell voltage in overcharge is of no apparent significance for examination of direct bus connection.

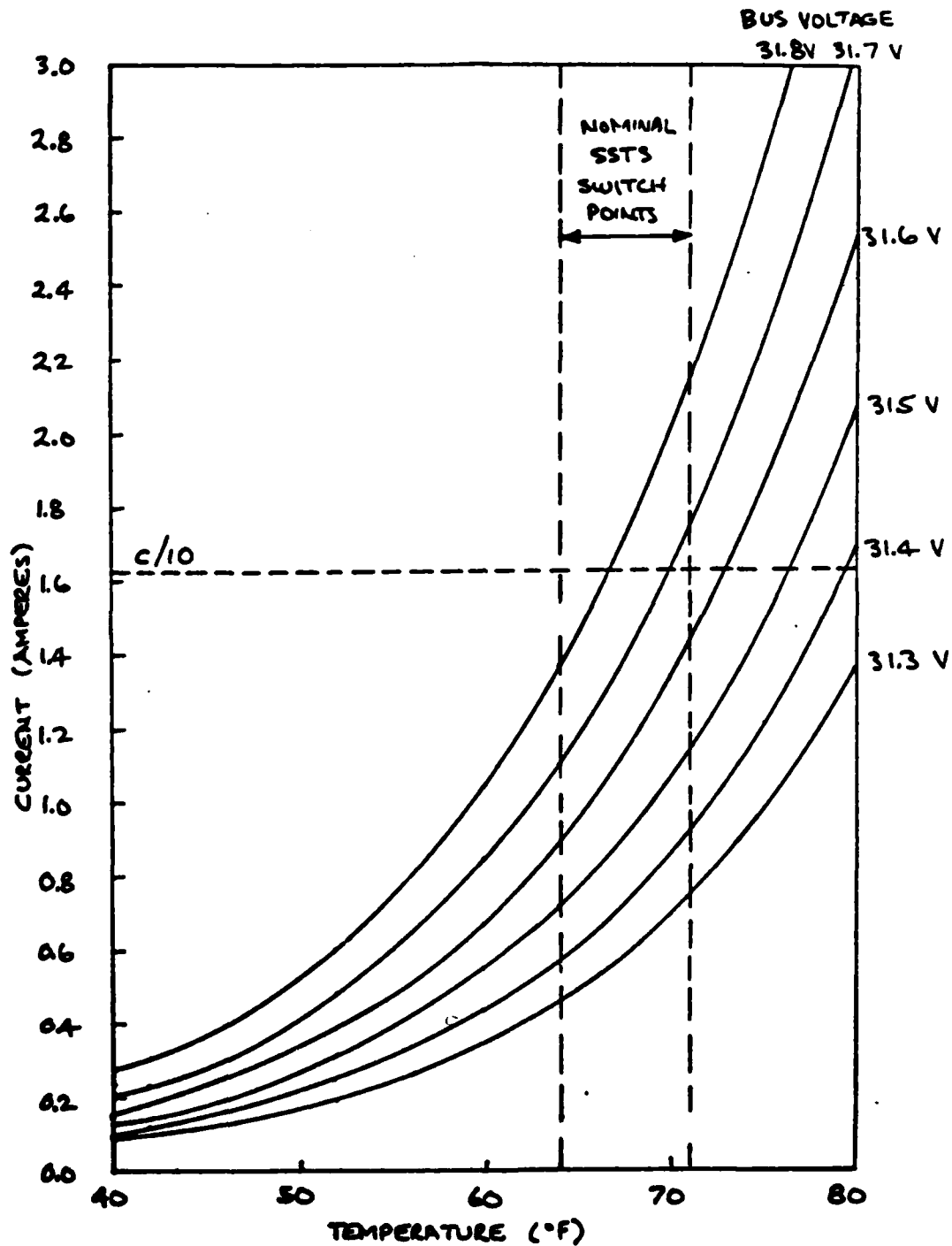


FIGURE 4.6. OVERCHARGE CURRENT —
BATTERY CONNECTED DIRECTLY TO BUS (CELL
VOLTAGE UNCERTAINTY 0.005 V/CELL RE TAPEL CURVES)

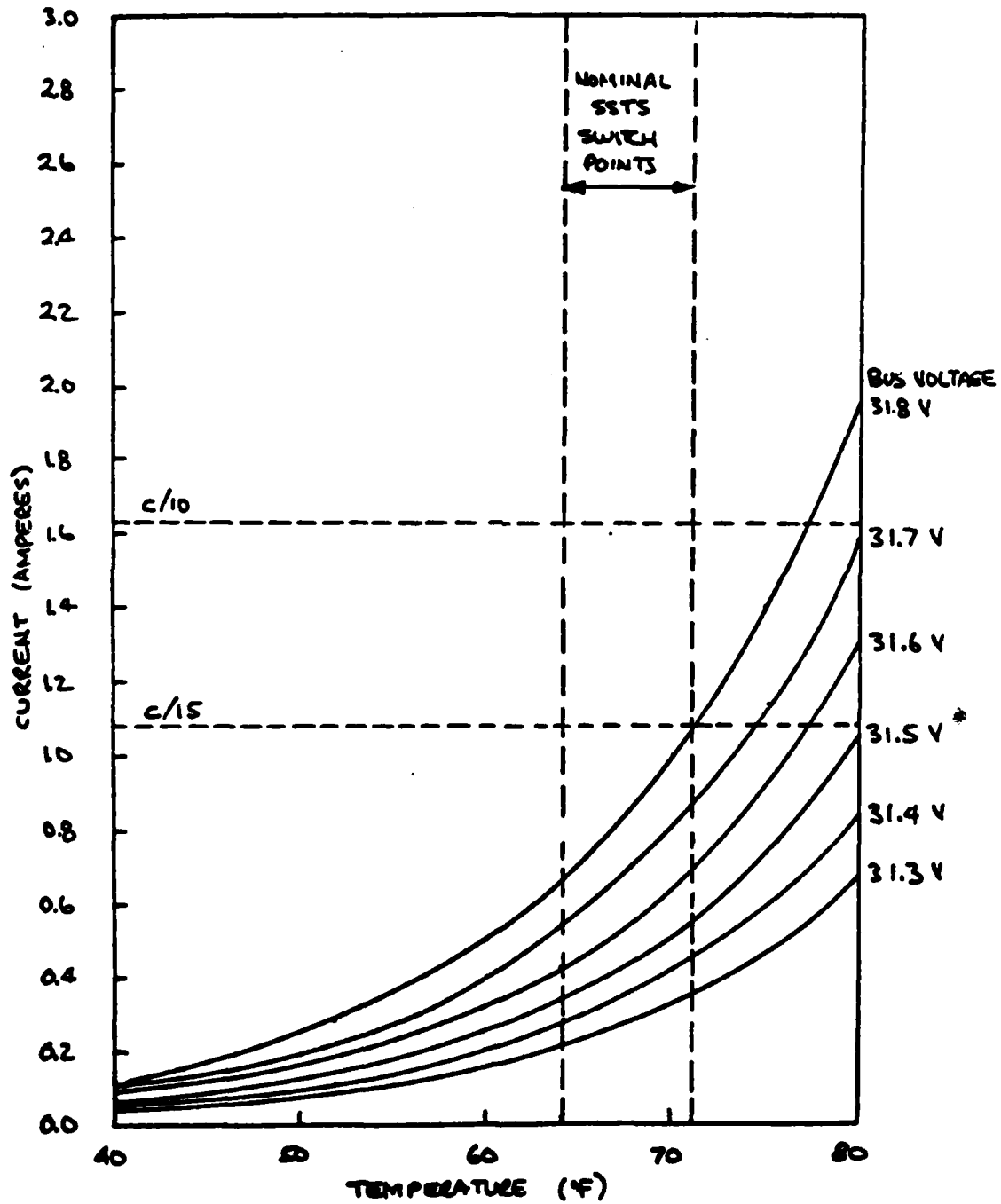


FIGURE 4.7. OVERCHARGE CURRENT —
 BATTERY CONNECTED DIRECTLY TO BUS (CELL
 VOLTAGE UNCERTAINTY ± 0.015 V/CELL SEE TAFEL CURVES)

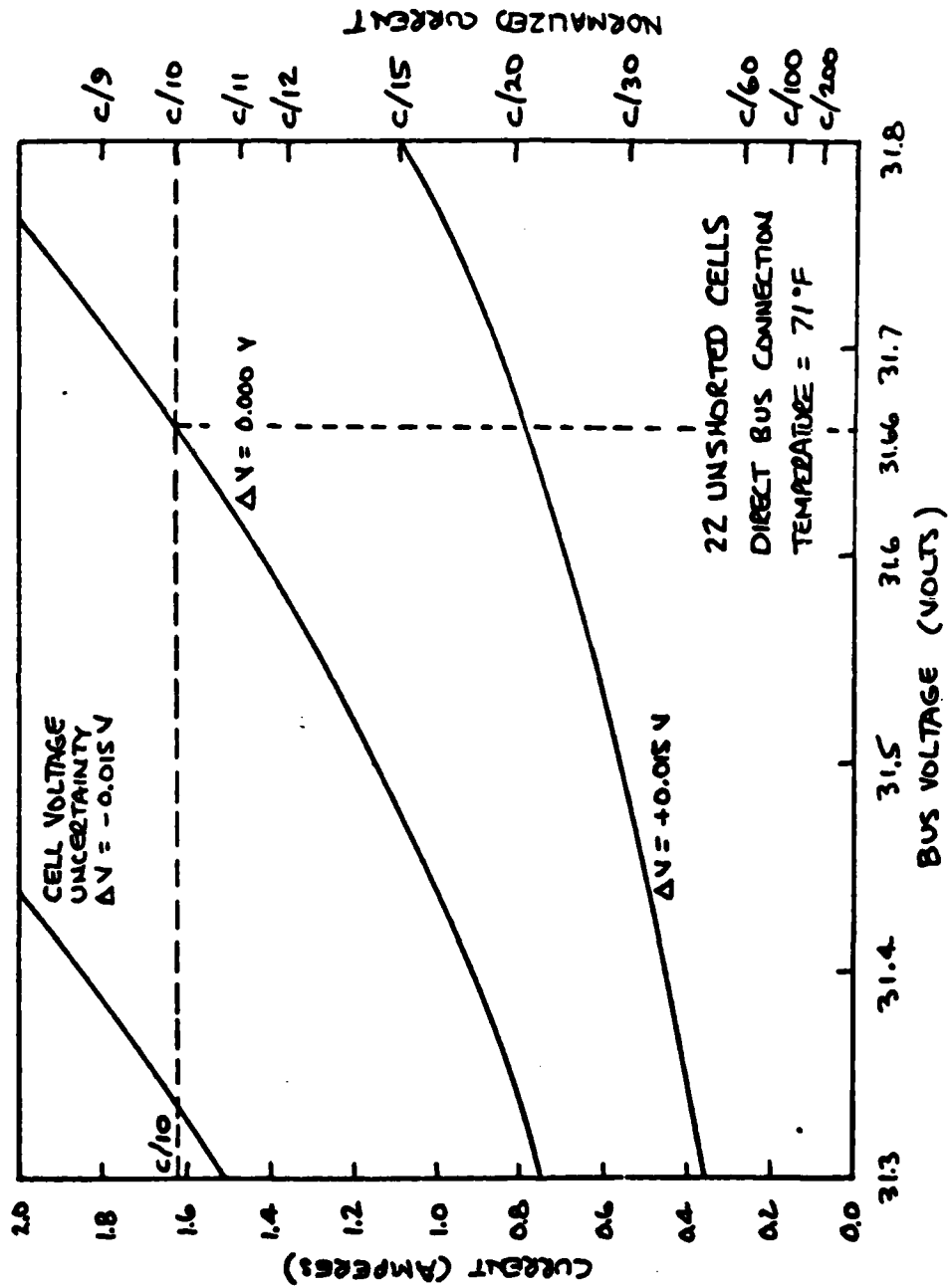


FIGURE 4.8. SENSITIVITY OF OVERCHARGE CURRENT TO BUS VOLTAGE

If we accept nominal cell voltage ($\Delta V = 0.000 \text{ V/Cell}$) in overcharge as the worst case in which direct bus connection might be considered, then the highest bus voltage at which cell current will remain below the maximum overcharge current criterion of C/10 (1.62A) at 71°F is 31.66 volts.

4.4.1.3 Selection of Lower Bus Voltage Limit

The nominal bus voltage for use during direct connection of the batteries to the bus must be at least 31.6 volts (Section 4.4.1.1). The actual bus voltage must be less than 31.66 volts in order to limit overcharge current to less than C/10 (4.4.1.3), at least early in the mission. If actual bus voltage exceeds 31.66 volts because of shunt limiter drift from its original setting, then manual control may be necessary to ensure battery switching to manual trickle before overcharge current becomes excessive. The value of 31.6 volts is chosen as the best available compromise.

The very narrow range of an acceptable level of nominal bus voltage, in concert with the assigned long-term tolerance for bus voltage drive of ± 0.2 volt, emphasizes the need for careful monitoring of battery and power subsystem performance whenever the spacecraft may be in direct bus-battery connection mode. It should be used only for the contingency in which high-bus voltage operation for some reason does not meet expectations.

4.5 Battery Isolation

The aggregate of desired requirements for isolation of a battery during charging turn out not to be achievable simultaneously. These requirements are examined in this section, and alternate requirements are determined and implemented.

4.5.1 Maximum Temperature of Battery With 22 Unshorted Cells During Isolation Mode

The battery is not supposed to exceed a temperature of 55°F (64°F less margin of 9°F) at any time, according to Section 2.7. This condition cannot be met with any value of current at winter solstice. Heat rejection capability of the batteries during winter solstice is plotted in Figure 4-9 (Reference 5). Battery C cannot cool below 59°F at BOM or 69°F at EOM even with zero dissipation from recharging or overcharging current. Batteries A and B cannot cool below 57°F at BOM or 68°F at EOM with zero dissipation.

4.5.2 Maximum Temperature of Battery with 21 Unshorted Cells

Current during battery isolation mode must be low enough that temperature of a 21 cell battery will cool down to no greater than 75°F. The limiting case for this requirement is winter solstice at EOM. From Figure 4-9, it is determined that maximum dissipation from the batteries to meet this temperature is:

3.6 watts for Battery A,
3.6 watts for Battery B, and
3.1 watts for Battery C

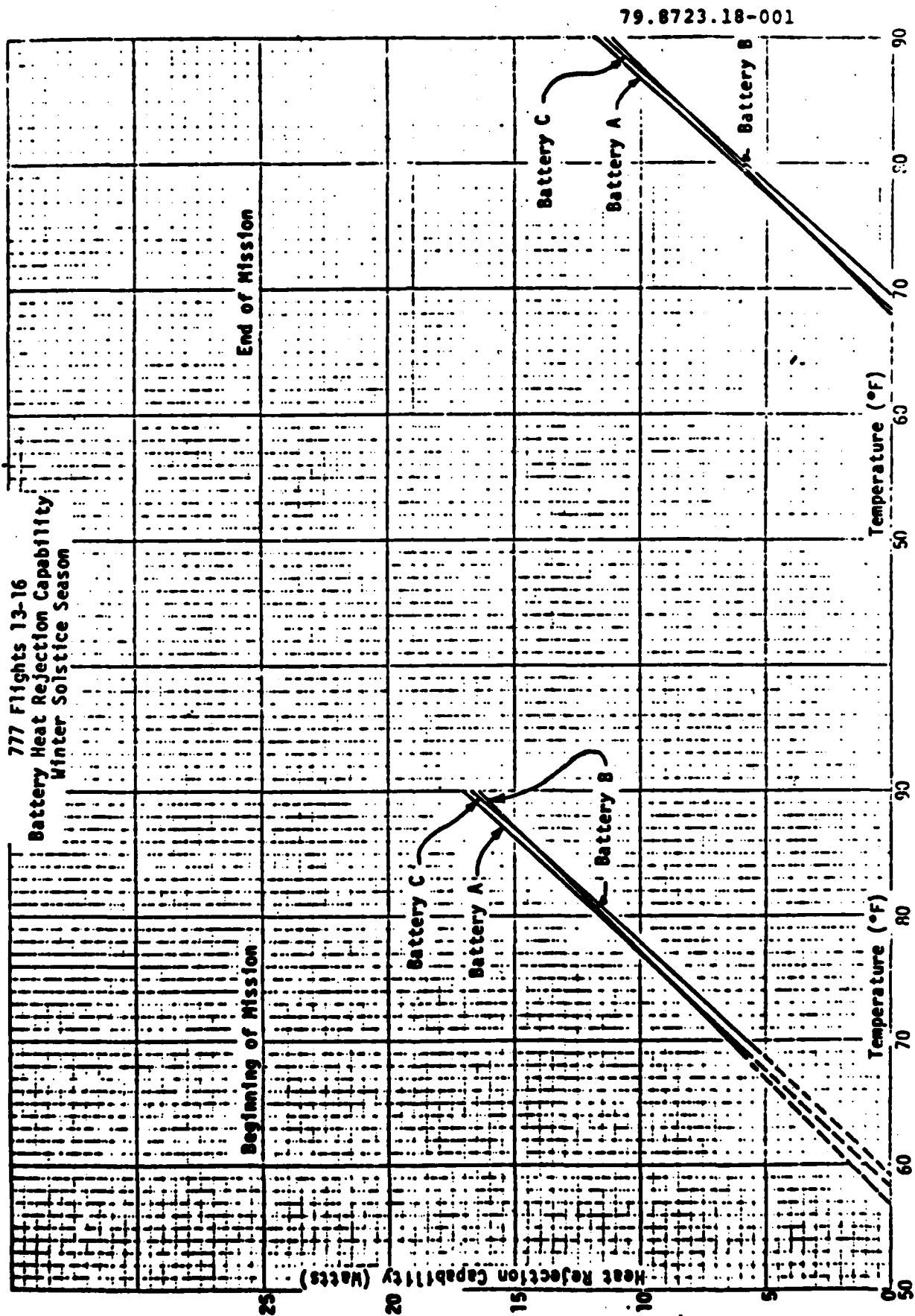
In order to have a general design that meets the requirement for all batteries, the value of 3.1 watts is used. This power is dissipated in the worst-case at EOM (cell voltage uncertainty is 0.000 volt relative to minimal Tafel overcharge data) when the current is 0.10712 ampere. The cell voltage and battery voltage at this current level are 1.378 and 28.938 volts. The constraint on isolation mode resistance is

$$R_{MT} \geq \frac{V_{BUS} - V_{BAT}}{I}$$

or, specifically

$$R_{MT} \geq \frac{V_{BUS} - 28.938}{0.10712} \quad (4.5-1)$$

FIGURE 4-9



4.5.3 Minimum Temperature of Battery With 22 Unshorted Cells During Isolation Mode

Current during battery isolation mode must be great enough that temperature of a 22 cell battery will not cool below a temperature of 42°F during solstice. The most demanding period for this requirement is summer solstice at beginning of mission.

Heat rejection capability during summer solstice is graphed in Figure 4-10 for beginning and end-of-mission (Reference 6). Extrapolation from this data yields minimum battery dissipation which will maintain temperature to at least 42°F of

0.2 watts for Battery 1,
1.3 watts for Battery 2, and
0.2 watts for Battery 3

For the general case, 1.3 watts dissipation in each battery will maintain its temperature at or greater than 42°F.

The cell current and voltage which will cause a battery to dissipate 1.3 watts at 42°F are 0.042A and 1.407 V ($\Delta V_{\text{cell}} = 0.000$ V/cell at worst case). The corresponding battery voltage is 30.957. The corresponding constraint on limiting resistance is

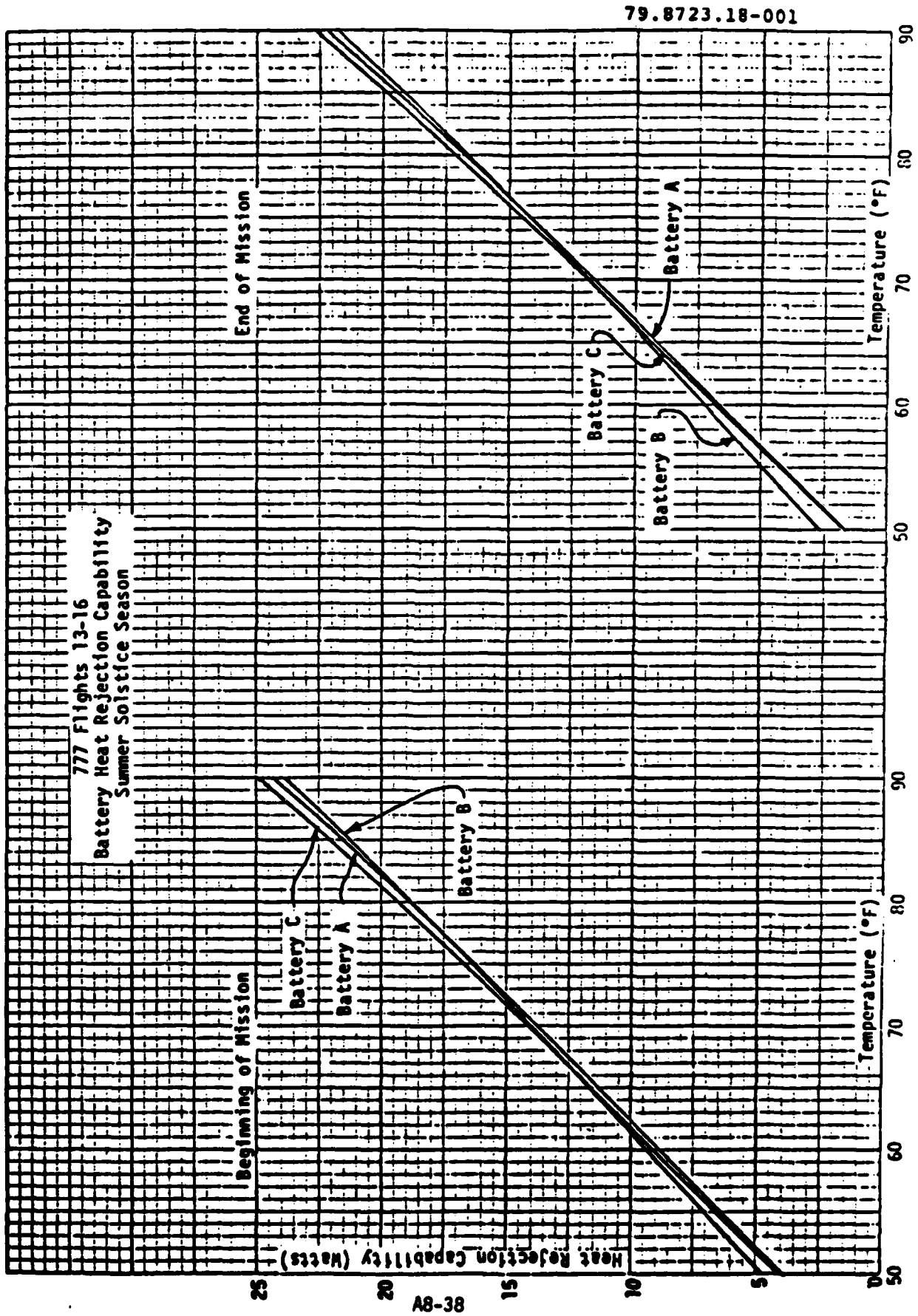
$$R_{\text{MT}} \leq \frac{V_{\text{BUS}} - 30.957}{0.04200} \quad (4.5-2)$$

4.5.4 Minimum Current During Battery Isolation

It is desired to maintain battery current at no less than C/200 (0.081A), according to Section 2.9. At the minimum temperature of 42°F (constrained by expression 4.5-2), cell and battery voltage are 1.420 and 31.237V. The constraint on limiting resistance to satisfy this goal is:

$$R_{\text{MT}} \leq \frac{V_{\text{BUS}} - 31.237}{0.081} \quad (4.5-3A)$$

FIGURE 4-10



For the upper temperature of 55°F (if the maximum temperature requirement of Sections 2.7 and 4.1.1 could be met), the constraint on limiting resistance would be

$$R_{MT} \leq \frac{V_{BUS} - 30.830}{0.081} \quad (4.5-3B)$$

4.5.5 Bus Voltage Limit

The bus voltage limit has been selected to be $33.8 \pm 0.2V$ (Section 4.1.6). The corresponding constraints for battery isolation mode are

$$V_{BUS} \leq 34.0 \quad (4.5-4A)$$

and

$$V_{BUS} \geq 33.6 \quad (4.5-4B)$$

4.5.6 Combined Requirements for Battery Isolation Mode

The combined constraints of expressions 4.5-1 and -2, 4.3-3A, and 4.5-4A and -4B are graphed on Figure 4-11. The acceptable region for each constraint is the unshaded side of the constraint line.

Examination of Figure 4-11 reveals incompatibility between the constraints; this means that the design requirements of Section 2.7 through 2.10 are themselves incompatible. The minimum-current constraint for 42°F (4.5-3A) would allow operation only in the upper left hand region of the graphed space, whereas the maximum temperature constraint for a 21 cell battery (4.5-1) would restrict the operating region to the right-hand side of the graphed space. Even if the minimum current constraint were relaxed from 42°F to the maximum desired temperature of 55°F for a 22 cell battery (expression 4.5-3B), the incompatibility between requirements would continue to exist. It should be remembered that the maximum temperature requirement for a

22 cell battery cannot be achieved with any limiting resistance (Section 4.5.1).

4.5.7 Back To The Drawing Board For Battery Isolation

The consequences of using two representative point designs are examined relative to the requirements of Sections 2.7 through 2.10. Specifically, values of 55 ohms and infinity (open-circuit) are examined.

4.5.7.1 Fifty-Five Ohm Battery Isolation Resistance

Battery dissipation is calculated as a function of battery temperature for current limiting resistance of 55 ohms, using the worst case bus voltage band of 33.8 ± 0.2 volts and the worst-case bands for cell voltage uncertainty of -0.015 to 0.000 V/Cell at BOM and 0.000 to $+0.015$ V/Cell at EOM. Plots of battery dissipation characteristics are overlaid on battery heat rejection characteristics to determine simultaneous solutions to the combinations of curves. These graphical solutions are given in Figures 4-12 through 4-14 for batteries with 21 unshorted cells during equinox, winter, and summer seasons and in Figures 4-15 through 4-17 for batteries with 22 unshorted cells during the same seasons.

The bands of operating temperatures are summarized in Table 4-1 for the aggregate of three batteries with combinations of worst-case cell voltage uncertainty, together with the associated overcharge current ranges.

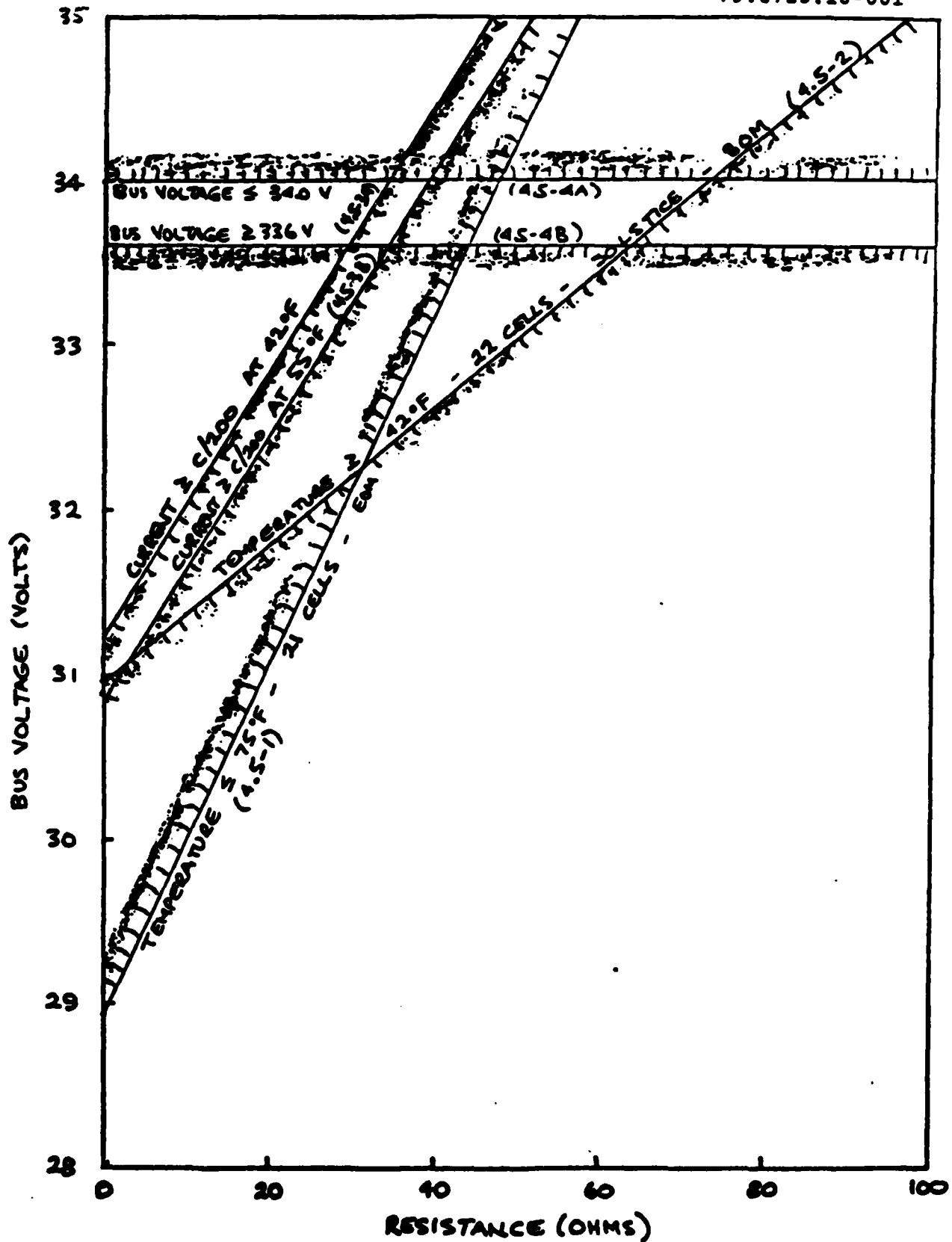


FIGURE 4-11. CONSTRAINTS ON BATTERY ISOLATION RESISTANCE

FIGURE 4-12

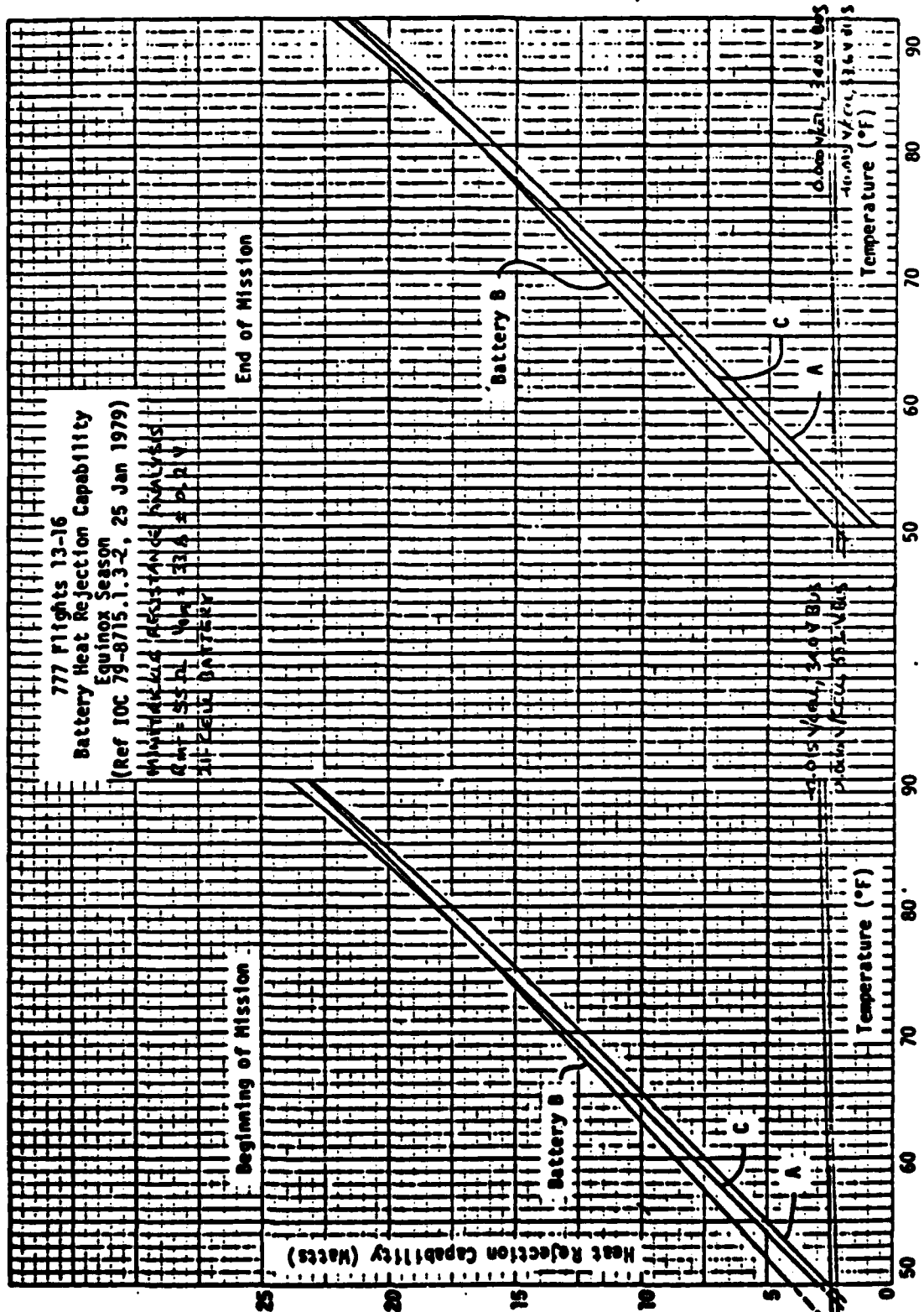


FIGURE 4-13

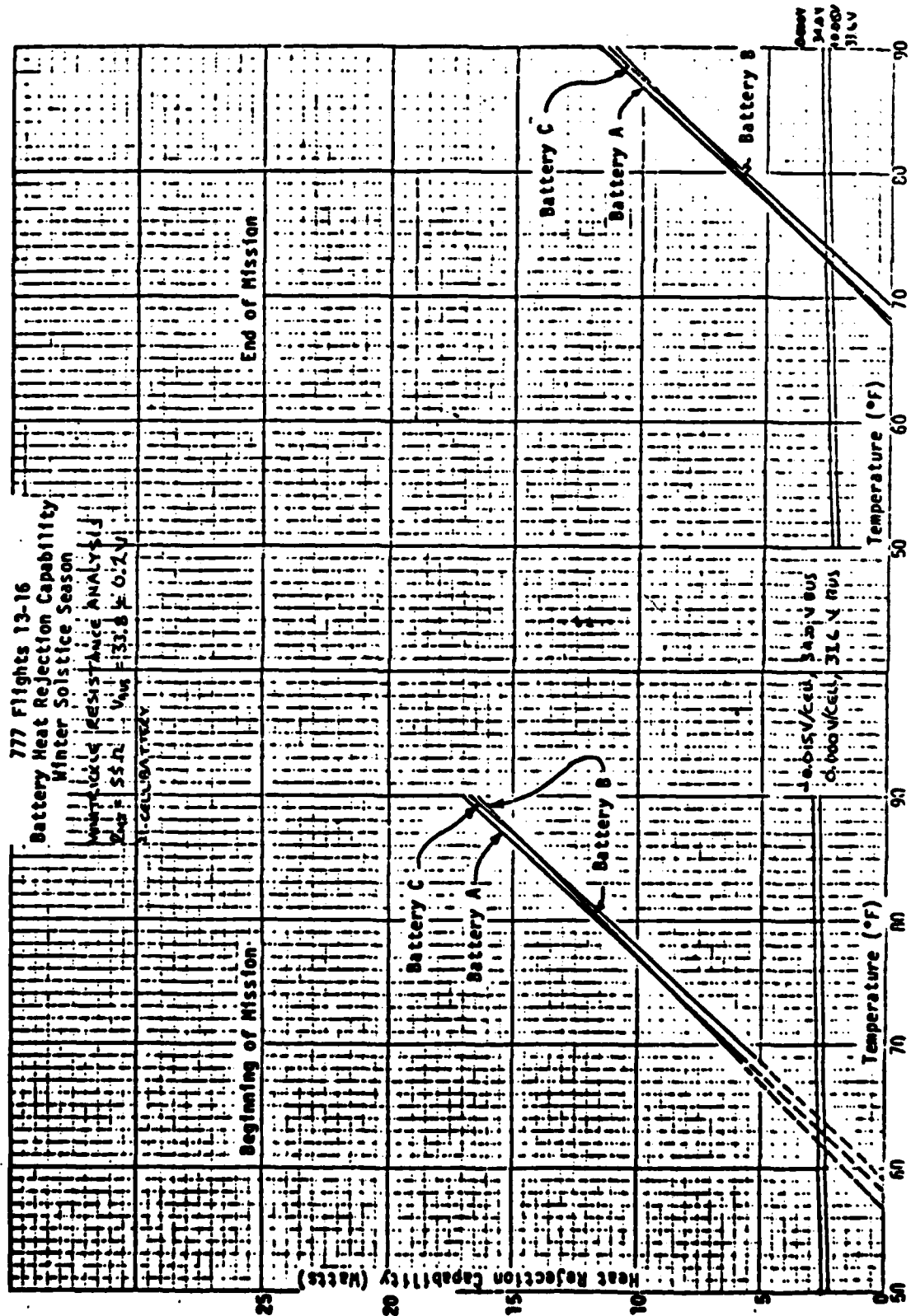


FIGURE 4-14

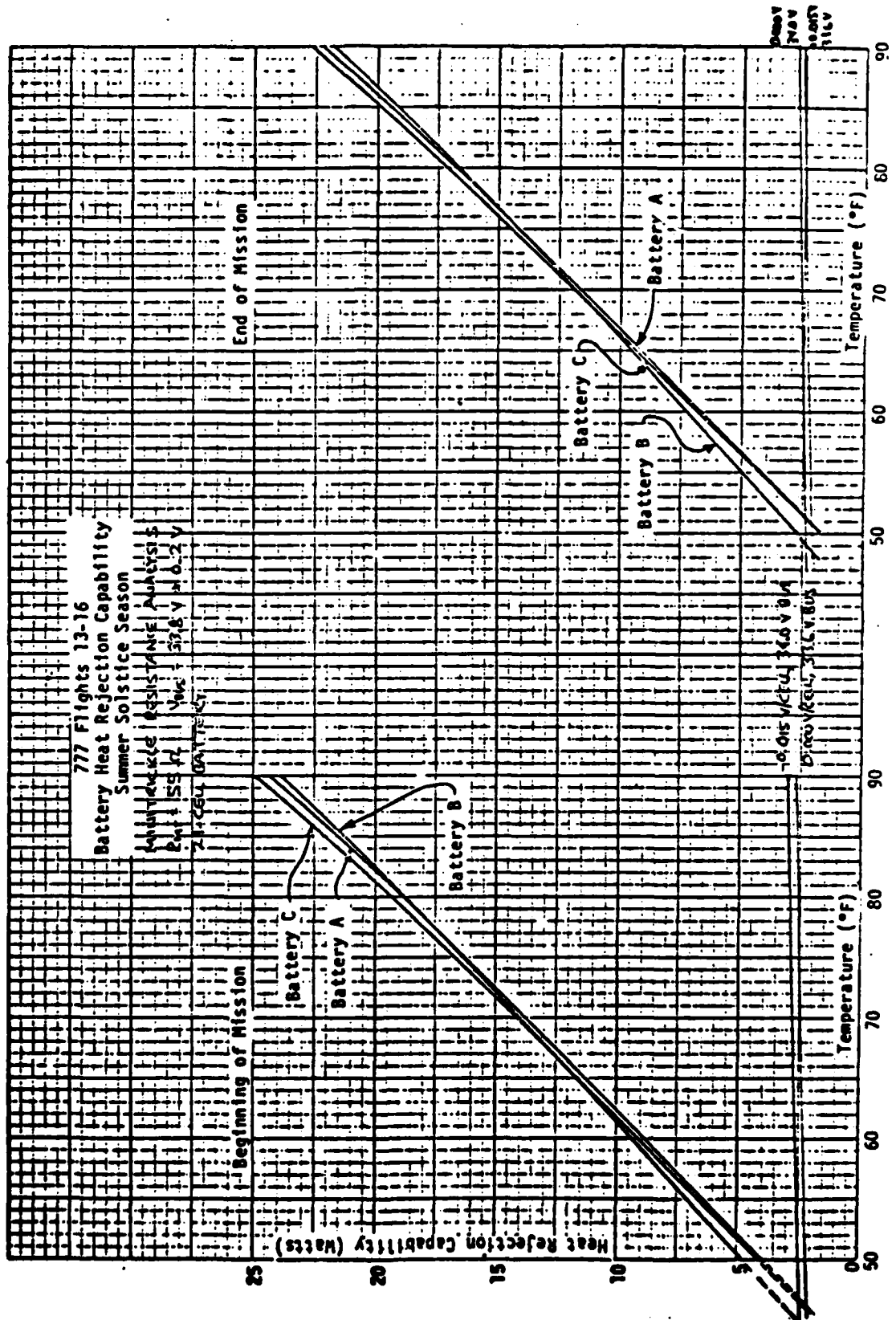


FIGURE 4-15

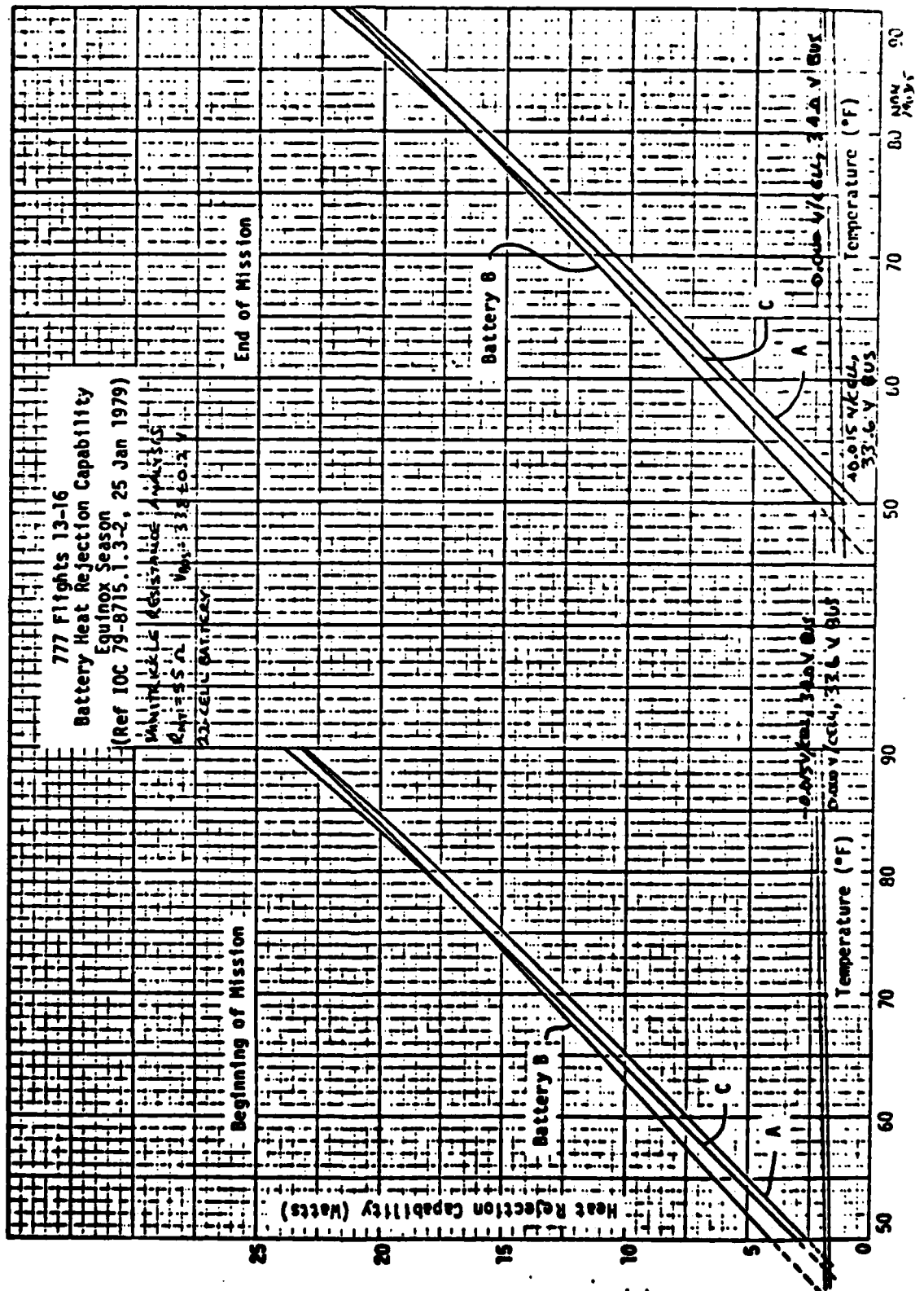


FIGURE 4-16

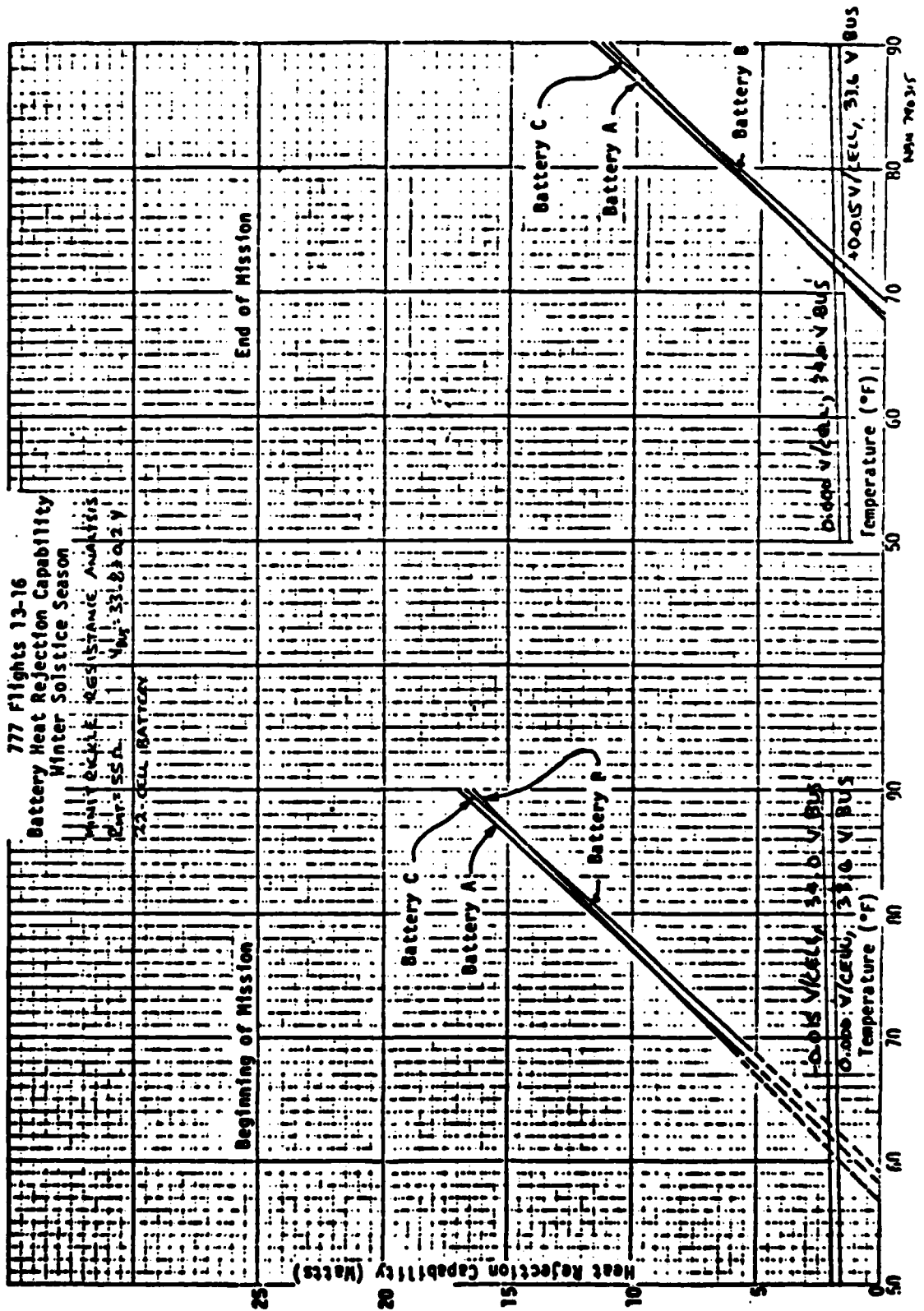


TABLE 4-1
CONSEQUENCES OF SELECTING 55 OHM VALUE FOR LIMITING RESISTANCE

<u>BATTERY ISOLATION MODE</u>			
<u>BATTERY TEMPERATURE</u>	<u>21 CELLS</u>	<u>22 CELLS</u>	
<u>STATED REQUIREMENT</u>	<u>T ≤ 75°F (All Seasons)</u>	<u>42°F (Solstice) ≤ T ≤ 55°F (All Seasons)</u>	
EQUINOX BOM EOM	45.5 to 49.8 49.2 to 53.3	45.6 to 48.6 47.5 to 52.2	
WINTER BOM EOM	61.6 to 64.3 72.5 to 74.3	60.1 to 63.1 71.1 to 73.2	
SUMMER BOM EOM	44.0 to 47.1 48.4 to 51.3	43.0 to 45.8 47.0 to 50.1	
● <u>OVERCHARGE CURRENT FOR 22-CELL BATTERY</u>			
<u>STATED REQUIREMENT</u>	<u>I ≥ C/200 (0.081A)</u>		
EQUINOX BOM EOM	C/268 to C/321 C/288 to C/345	(.061 to .050A) (.056 to .047A)	
WINTER BOM EOM	C/238 to C/281 C/237 to C/282	(.058 to .068A) (.058 to .068A)	
SUMMER BOM EOM	C/274 to C/330 C/290 to C/352	(.049 to .059A) (.046 to .056A)	

4.5.7.2 Open-Circuited Battery

Operating temperatures for batteries which are open-circuited in the charging direction are determined from the intersection of their heat rejection characteristics with the temperature axis (zero power). These temperatures are summarized in Table 4-2.

4.5.8 Evaluation of Alternate Battery Isolation Mode Approaches

Placement of batteries into isolation will not be a common occurrence during the spacecraft mission. Instead, it will be used only for the mode to which a battery switches following termination of recondition discharge or for abnormal, unanticipated events for which normal automode or manual low-rate trickle charging do not appear appropriate (including automatic switching to isolation mode in case of battery overtemperature). In the first case, isolation mode is of short duration to allow battery open-circuit voltage to reach a value high enough that automode charging can be used without excessive dissipation in the limiting resistors. In the second case, isolation mode can be used for short durations to give time for decision making regarding unanticipated events, or for longer durations to store a battery which has suffered worse degradation than what the power subsystem has been designed for.

Concern has been displayed by various parties and agencies about long-term storage of batteries in open-circuit, because of possible degradation within open-circuited cells. The point that is to be made here is that the only time which long-term storage of a battery would be used is when the battery has deteriorated so much that it is essentially abandoned for any further use. Long-term storage in open circuit is thus of no concern for the DSCS-II spacecraft application.

TABLE 4-2

CONSEQUENCES OF SELECTING INFINITE RESISTANCEBATTERY ISOLATION MODE● BATTERY TEMPERATURE

STATED REQUIREMENT	<u>21 CELLS</u>		<u>22 CELLS</u>	
	$T \leq 75^{\circ}\text{F}$ (All Seasons)	42°F (Solstice) $\leq T < 55^{\circ}\text{F}$ (All Seasons)		
EQUINOX BOM EOM	42 to 52 (with heater) 45 to 48		42 to 52 (with heater) 45 to 48	
WINTER BOM EOM	57 to 59 68 to 70		57 to 59 68 to 70	
SUMMER BOM EOM	42 to 52 (with heater) 44 to 47		42 to 52 (with heater) 44 to 47	

● OVERCHARGE CURRENT FOR 22-CELL BATTERYSTATED REQUIREMENT $I \geq C/200$ (0.081A)

EQUINOX BOM EOM	0 0
WINTER BOM EOM	0 0
SUMMER BOM EOM	0 0

Open circuit for isolation of a battery from the bus (in the charging direction only) thus becomes attractive. The stated requirement for minimum overcharge current of C/200 is abandoned because of lack of need or value.

Open-circuit mode allows a battery to operate as cool as is possible, because no dissipation from overcharging will occur. Thus the maximum temperature requirements of Sections 2.7 and 2.8 are met with the greatest margin (or, in the case of a 22 cell battery in winter solstice at end-of-mission, with the least negative margin).

Use of a 55 ohm resistance for battery isolation offers very little benefit relative to open-circuit. The 22-cell battery overcharge current is still not very close to the stated goal of C/200. The margin from the desired maximum battery temperature is not as great and the capability for disconnecting a really degraded battery from the bus does not exist (an extremely unlikely occurrence if the design is presumed to be correct, but remember Murphy and his laws).

The open-circuit mode is thus preferable to the old high-resistance minitrickle mode for isolation of a battery for either short or long duration.

4.6 EMC Considerations

Bus impedance is required to be less than 1 ohm for dc to 100 kHz when the bus is being supplied by the batteries. The circuit path for this operational mode is the same as for initial and replenishment satellites when all batteries are in low-rate trickle charge configuration (K1 and "K5" contacts open, current path through the PCU diodes).

The flight 13-16 circuit uses the same circuit path; since this represents no departure from earlier satellite series, and since the flight 13-16 batteries will offer lower source impedance than the flight 7-12 batteries (because of greater plate surface area), this operating mode is not reanalyzed in this study.

Bus impedance is required to be less than 1 ohm from dc to 100 kHz when the bus is being supplied by the solar array in the bus limiting mode and shunt current is greater than 1.2 amperes. Bus impedance in this mode is controlled primarily by the shunt regulator and PCU bus filter. The battery circuit itself provides shunting impedance across the bus of 0.89Ω or less when all K1 contacts are closed and the "K5" contacts are open and 6.67Ω or less when all K1 and K5 contacts are open.

This is in parallel with the shunts limiter and array circuit that feeds the bus. The combined bus impedance under a similar mode, charging two batteries in trickle charge through 7 ohm resistances, was analyzed, tested, and demonstrated to meet the specification of less than 1.0 ohm from dc to 100 kHz (Reference 7).

5. CONTINGENCY MODE OPERATION

Various contingencies must be analyzed to satisfy questions regarding operation under various abnormal conditions. These include such events as excessive load demand (because of potential failure of power using equipment) and loss of one or more batteries from useful operation. This contingency analysis is beyond the scope of this report, and is planned for presentation in a separate report.

6. CONCLUSIONS

The selected component values for the battery control network are given in Figure 6-1. This network will serve to provide a more benign setting for battery operation than the previous designs, and will offer flexibility in choice of operating mode to accommodate many prospective situations in order to gain the most useful life from the DSCS-II batteries.

7. ACKNOWLEDGEMENT

Great indebtedness is owed to Charles Sollo for providing the spark of inspiration to use the concept of linear constraints to bound the region of feasible solutions.

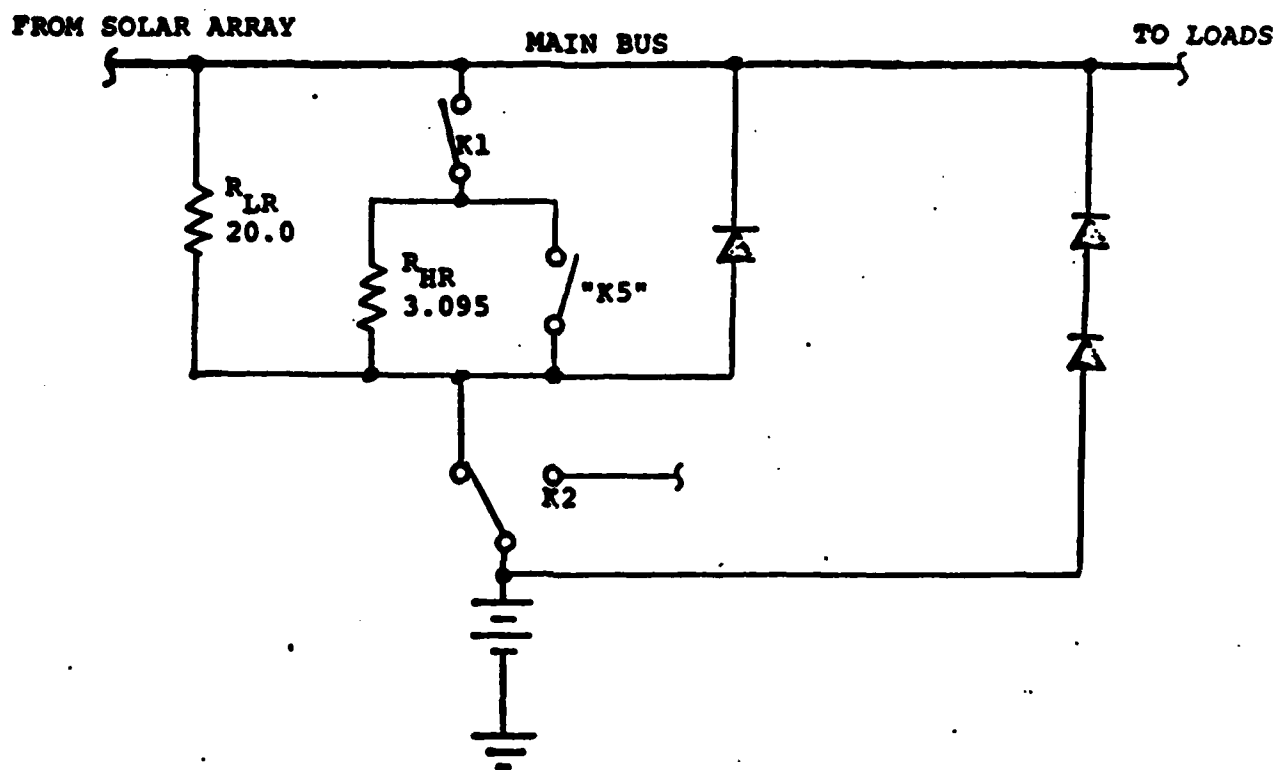


FIGURE 6-1. SELECTED COMPONENT VALUES FOR BATTERY CONTROL NETWORK (Typical of 3)

REFERENCES:

1. R. H. Sparks, 777 F13-16 Battery Control Design Requirements, TRW IOC 79.8723.0-021, 22 February 1979.
2. G. M. Reppucci, Prime Item Product Function Specification - Electric Power Subsystem - Program 777 - Flight 13 and subsequent, TRW Specification EC-SS14-41B, 14 April 1978.
3. H. M. Pan, 777 F13-16 Battery Heat Rejection Capability During Equinox Season, TRW IOC 79-8715.1.3-2, 25 January 1979.
4. C. Sollo, ECP 124 Preliminary Parts List; DSCS-II, TRW IOC DSCS-C3A-11-A, 28 February 1979.
5. H. M. Pan, Uncertainty of Prediction of Battery Heat Rejection Capability, private communication 5 March 1979
6. H. M. Pan, 777 F13-16 Battery Heat Rejection Capability During Solstice Season, Private communication, 1 March 1979.
7. M. Koslover, Analysis of Primary Bus Impedance for Program 777 Electric Power Subsystem, TRW Engineering Report 70-8215.5-015, 6 January 1970

DATE
FILMED
-8